AD NUMBER
AD371658
CLASSIFICATION CHANGES
TO: unclassified
FROM: confidential
LIMITATION CHANGES
TO: Approved for public release, distribution unlimited
FROM: Distribution authorized to U.S. Gov't. agencies and their contractors; Administrative/Operational Use; APR 1966. Other requests shall be referred to Air Force Rocket Propulsion Lab., AFSC, Edwards AFB, CA.
AUTHORITY
AFRPL ltr, 7 May 1973; AFRPL ltr, 7 May 1973

SECURITY MARKING

The classified or limited status of this report applies to each page, unless otherwise marked.
Separate page printouts MUST be marked accordingly.

THIS DOCUMENT CONTAINS INFORMATION AFFECTING THE NATIONAL DEFENSE OF THE UNITED STATES WITHIN THE MEANING OF THE ESPIONAGE LAWS, TITLE 18, U.S.C., SECTIONS 793 AND 794. THE TRANSMISSION OR THE REVELATION OF ITS CONTENTS IN ANY MANNER TO AN UNAUTHORIZED PERSON IS PROHIBITED BY LAW.

NOTICE: When government or other drawings, specifications or other data are used for any purpose other than in connection with a definitely related government procurement operation, the U. S. Government thereby incurs no responsibility, nor any obligation whatsoever; and the fact that the Government may have formulated, furnished, or in any way supplied the said drawings, specifications, or other data is not to be regarded by implication or otherwise as in any manner licensing the holder or any other person or corporation, or conveying any rights or permission to manufacture, use or sell any patented invention that may in any way be related thereto.

AFRPL-TR-66-82

April 1966

ADVANCED ROCKET ENGINE--STORABLE (u)

QUARTERLY TECHNICAL REPORT AFRPL-TR-66-82

January through March 1966

Prepared for

AIR FORCE ROCKET PROPULSION LABORATORY
RESEARCH AND TECHNOLOGY DIVISION
AIR FORCE SYSTEMS COMMAND
UNITED STATES AIR FORCE
EDWARDS, CALIFORNIA

0947
AGC Report 10830-Q-3

AFRPL-TR-66-82

April 1966

ADVANCED ROCKET ENGINE--STORABLE (u)

QUARTERLY TECHNICAL REPORT AFRPL-TR-66-82

January through March 1966

Prepared by

AEROJET-GENERAL CORPORATION
Advanced Storable Engine Program Division
Liquid Rocket Operations
Sacramento, California

Prepared for

AIR FORCE ROCKET PROPULSION LABORATORY
Research and Technology Division
Air Force Systems Command
United States Air Force
Edwards, California

AGC Report 10830-Q-3

2508T

FOREWORD

This is the third written progress report submitted under the ARES Program, Contract AF 04(611)-10830. It provides a summary of major accomplishments and discusses the technical aspects of the program. The period covered by this report is 1 January 1966 through 31 March 1966. The program structure number is 63409604; the project number is 3058.

This program is under the direction of Mr. R. Beichel, Manager of the Advanced Storable Engine Program Division, Liquid Rocket Operations, Aerojet-General Corporation, Sacramento, California.

The program is sponsored by the Air Force Rocket Propulsion Laboratory, Research and Technology Division, Edwards Air Force Base, California, under the direction of C. W. Hawk/RPRZ, Project Officer.

Publication of this report does not constitute Air Force approval of the report's findings or conclusions. It is published only for the exchange and stimulation of ideas.

UNCLASSIFIED ABSTRACT

The objective of the ARES (Advanced Rocket Engine, Storable) program is to demonstrate the engineering practicality and the performance characteristics of an advanced storable propellant modular engine embodying high chamber pressure and the staged-combustion cycle.

This third quarterly report describes the technical accomplishments of the reporting period. Generally, the period was characterized as one in which many analyses and designs were completed, fabrication of many components was completed and testing accelerated. The most noteworthy accomplishment was the successful hot firing of two different modular injectors using the intensifier test system.

TABLE OF CONTENTS

TABLE OF CONTENTS (Cont.)

TABLE OF CONTENTS (cont.)

TABLE OF CONTENTS (cont.)

FIGURE LIST

FIGURE LIST (cont.)

FIGURE LIST (cont.)

FIGURE LIST (cont.)

FIGURE LIST (cont.)

I.

INTRODUCTION

(u) The principal objective of the ARES (Advanced Rocket Engine-Storable) program is to demonstrate the engineering practicality and performance characteristics of a high-chamber-pressure staged-combustion engine module.

(u) The modular engine is a highly integrated assembly in which the turbopump assembly housing combines the fuel and oxidizer pumps, the turbine, the engine controls, and the primary combustor chamber into a single assembly. Turbine exhaust is ducted directly into the secondary combustion chamber, where additional fuel is added. The resulting combustion products are exhausted through a cooled 20:1 area ratio nozzle. Thrust from the rocket nozzle is transmitted through the turbopump assembly housing to the vehicle frame.

(c) The engine is designed to produce 100,000 lb of thrust at sea level and operates at a secondary combustion chamber pressure of 2800 psia using N_2O_4 and AeroZINE 50 as propellants. The engine module is designed to allow ready employment of the module single, in parallel axis clusters, or in forced-deflection nozzle or plus nozzle propulsion systems.

(c) The modular engine uses a staged combustion cycle in which all the oxidizer and 19% of the fuel are injected into the primary combustor at 4775 psia to produce a turbine working fluid at approximately 1240°F. This fluid passes through the turbine, which operates at a pressure ratio of approximately 1.5, and exhausts at 2800 psia into the secondary combustor, where the additional fuel required to achieve a mixture ratio of 2.1 lb ox/lb fuel is added. The resultant combustion products exhaust through the nozzle producing thrust.

(u) Engine control is achieved through the use of eyelid valves (located at pump suction) wherein the segment of a ball is rotated out of the flow stream and admits propellant to the engine. For the development engine, auxiliary fuel control valves are installed to govern fuel admittance to the primary and secondary combustion chambers during transient and steady-state operation. All valves are powered independently to achieve the flexibility desired during the program.

(c) The secondary combustor uses a flameholder injector consisting of a series of radial vanes from which fuel is injected into the oxidizer-rich turbine exhaust stream. The resulting mixture burns in the thrust chamber and is exhausted through the nozzle. Two cooling systems are under consideration for the modular engine. These employ regenerative and transpiration cooling. The regeneratively cooled design employs a two-pass system made up of oval tubes. The transpiration cooled system uses a considerable number of thin wafers that are chemically milled to produce the desired pressure-drop pattern required to control the coolant flow.

I, Introduction (cont.)

(u) Phase I of the two-phase program is devoted principally to the development of individual components such as cooled combustion chambers, injectors, turbopump housings, bearings and seals, suction valves, and engine fuel controls. The Phase II program is devoted to performance improvement of the thrust-chamber components, development of the turbopump system, and the integration of turbopump, thrust chamber, and controls into an engine module.

(u) This report, covering activity during the third quarter of the program, is organized into four groups of sections. The first group, Section III through V, covers the combustion system development effort. Sections VI through XI cover the turbopump design and development tasks. Controls are reported in Sections XII through XIV. The remaining sections, XV through XX, cover the activity associated with the propulsion system as well as a series of related analytical activities.

II.

SUMMARY

The third quarter of the program resulted in completion of a large body of critical analyses and designs, ordering of essentially all of the remaining material needed for Phase I of the program, and initiation of testing on ARES configuration hardware in many key areas. Several time-consuming fabrication problems were encountered and solved. These included development of fabrication technique for Inconel 718, and development of proper heat-treating methods for large complex castings. Problems were encountered in activation of new test facilities and auxiliary test equipment. Considerable effort was devoted to expediting subcontractors for delivery of critically needed components.

In the TCA area, conversion of Test Stand H-2 to intensifier-fed operation was completed. This was followed by an extensive checkout program with both water and propellants. Finally, four valid tests were achieved on two secondary injectors of the new ARES configuration. Engine operation was smooth and stable. It was demonstrated that sector-engine operation with the intensifiers will permit a much higher test frequency than has been possible in the past.

All of the technical problems which have caused delays in fabrication of the cooled combustion chambers were resolved, and maximum feasible expediting action was taken to speed up lagging production at tube and transpiration-wafer vendors. It now appears that the first transpiration-cooled chamber should be available for testing in May and that the first regeneratively cooled chamber should be available in early June.

The primary combustor program experienced a significant delay from a non-repairable crack which developed in the first workhorse primary combustor housing. Revised weld and heat-treat procedures were successfully developed for the second housing, which was two weeks behind the housing that cracked.

Three valid 40,000-rpm bearing tests in N_2O_4 revealed that this task should be successfully finished as soon as initial problems with test-stand auxiliary hardware are resolved. Testing was also initiated in the combustion-seal and wear-ring programs; however, startup problems were encountered with auxiliary hardware in both of these tasks. The first advanced housing (the plug-welded A-design) was received at Sacramento and was being instrumented at the end of the reporting period.

The detailed design of the three-walled housing of the B-configuration for the advanced TPA is 70% complete. Many design improvements were effected on both the advanced and the inline TPAs.

Testing was initiated on the turbine inlet flow models at the Naval Post Graduate School in Monterey and on the aerodynamic nozzle models at FluiDyne in Minneapolis.

All analytical and testing efforts to date continue to validate the feasibility of the ARES advanced engine concept.

III.

PRIMARY COMBUSTOR ASSEMBLY, DESIGN AND FABRICATION

A. GENERAL

Design activity continued at a reduced level of effort because numerous design tasks were already completed. Fabrication of all components continued and many were completed. A stress analysis was completed for all injectors fabricated and a new analysis was initiated on an advanced injector design. Gas-flow distribution vanes and primary combustor-turbulator designs were initiated and have proceeded into the layout stage. A major fabrication problem was encountered when severe cracks developed in the primary-combustor workhorse housing, SN-1. The outer workhorse housing will probably have to be scrapped. A five-week delay in the program schedule as well as additional costs were incurred. Fabrication of the second primary combustor workhorse housing, SN-2, was therefore immediately accelerated, and welding and heat-treating procedures were revised to eliminate any possibility of cracking. Housing SN-2 will probably be delivered to the test area (Test Stand H-3) in mid-April, 1966; the first test firing is currently scheduled for 28 April 1966.

B. INJECTORS

Fabrication continued on all three primary injectors. The oxidizer full-flow injector and the quadlet injector were completed; the pentad injector, which is 90% complete, will be ready early in April. The quadlet injector assembly and the oxidizer full-flow injector assembly are shown in Figures III-1 and -2, respectively.

A final report covering the stress analysis of all three types of injectors was completed. Since the two porous-face injectors (oxidizer full-flow and quadlet) are structurally similar, only two, the pentad and the oxidizer full-flow injector, were actually analyzed. Calculations show that neither configuration yields when subjected to the maximum operating pressure in the absence of thermally induced stresses. Also, proof-test conditions at ambient temperature are not critical because the properties of Inconel 718, from which all primary injectors are made, are significantly higher at ambient temperatures than at injector operating temperatures. Calculations show that the injectors do yield when subjected to the combined effect of pressurization and thermally induced stress; however, maximum displacement and permenent set are not excessive and are not expected to adversely affect the function or performance of the injectors.

A turbopump housing design layout with a modified injector body is being prepared. The backside of the injector body and the forward hub are modified to accommodate a retaining ring and a new turbine nozzle, respectively. This new injector configuration, which is compatible with the Mod-B turbopump housing, is currently being stress-analyzed.

III, Primary Combustor Assembly, Design and Fabrication (cont.)

C. WORKHORSE PRIMARY COMBUSTOR HOUSING (WPCH)

Fabrication of WPCH SN-1 continued on an accelerated basis (three shifts per day, six days per week) to permit initiation of the primary combustor test program at the earliest possible date. All work proceeded satisfactorily until a severe crack developed in the outer forged housing of the WPCH. The crack (Figure III-3) occurred, after all welding at Aerojet-General had been completed, during shipment of the WPCH to an outside vendor for solution heat-treating and hardening. A thorough investigation was initiated immediately to determine the cause of the cracking, to decide whether the cracked housing could be salvaged, and to institute corrective action. (WPCH SN-2 was about two weeks fabrication time behind WPCH SN-1.)

All fabrication procedures and processes in effect until the time of failure were reviewed by metallurgical, fabrication, welding, and design personnel. It was determined that the failure was most probably the results of a combination of two factors: (1) the low impact resistance of the 17-4PH outer housing (the housing was received, fabricated, machined, and welded in the solution heat-treated condition, i.e., at 1900°F followed by air cooling to 90°F), and (2) the very high stresses induced by weld shrinkage incurred when the oxidizer-coolant turn-around manifold was welded to the outer housing. Since the inner housing had already been installed into the outer housing, shrinkage of the outer housing during manifold welding may have been prevented, and the resulting extremely high stresses may have initiated the cracking.

To prevent a reccurrence of this problem during fabrication of WPCH SN-2, the following corrective action was implemented: (1) the inner and outer WPCH were hardened to Condition H-1100 (temperature soak at 1100°F for four hours, followed by air cooling to 90°F) prior to proceeding with further fabrication, (2) all welding was performed on preheated material (350 to 400°F preheat), (3) the oxidizer turn-around manifold and the oxidizer torus closure ring were welded to the outer housing prior to installation of the inner housing, (4) all critical welds were peened after welding on the outer housing followed by a 1100°F temperature soak for four hours, and (5) after installation of the inner housing into the outer housing, a planned welding sequence was adhered to, followed by critical-weld peening, and by additional temperature soak at 1100°F for four hours.

All above steps have been implemented as of the close of this reporting period and no further problems have occurred.

After detailed visual examination and ultrasonic inspection of the cracked outer housing it was decided that repair was not advisable (1) because satisfactory accomplishment could be established only after expenditure of considerable time and money, and (2) because it was considered too risky to begin an extensive new test program using workhorse hardware of questionable structural integrity even if the repair was satisfactory. Therefore, it was decided to remove

III, C, Workhorse Primary Combustor Housing (WPCH) (cont.)

the inner housing; the outer housing will probably have to be scrapped. The inner housing is salvageable and will be used on a third WPCH. A new outer housing was ordered and is expected to be delivered early in May 1966.

D. OTHER PRIMARY COMBUSTOR COMPONENTS

The burnoff chamber, the support frame, and the burnoff injector were fabricated. Flow tests on the burnoff injector were completed, and flow coefficients were obtained and recorded.

Fabrication of the oxidizer inlet line, fuel inlet line, and flow nozzle (Figures III-4 and -5) was completed.

Three combustion-chamber liner assemblies were received from the supplier (see Figure III-6). An analytical study to determine pressurization and venting capabilities of the liner was completed and showed that adequate ventilation was provided through the spring tab slits and through the holes in the liner. It was determined that the thirty-two 1/4-in.-dia holes for gas ventilation can be eliminated. The elimination of these holes would probably reduce the heat flux to the housing wall by reducing the gas velocity and the amount of gas flow behind the liner.

E. ADDITIONAL DESIGN ACTIVITY

The design of a primary combustor turbulator was begun late in this reporting period. The turbulator will assist in mixing the fuel and oxidizer propellants, thus permitting a homogenous gas to enter the turbine. Uniform mixing of the propellants wil also prevent high temperatures, thereby eliminating the possibility for erosion on the combustion-chamber walls. The turbulence device, shown in Figure III-7, consists of external and internal tabs when viewed axially. A row of turbulators is located on the inside diameter of the chamber as close to the injector face as possible, and the second row is located on the chamber outer diameter 1 in. downstream of the first turbulator row and alternately spaced with the tabs of the first row. Each turbulator ring is composed of 0.060-in.-thick Hastelloy X tabs inclined at an angle of 60° to the direction of gas flow. Each turbulator extends to the center of the gas stream. This design will cause turbulence at the tip and at the sides of each turbulator tab. Drawings will be released and fabrication will be initiated early in April. Material has already been ordered.

A flow-diversion vane design was initiated late in this reporting period; these vanes will distribute the primary-combustor exhaust gas uniformly over the entrance of the secondary injector. The mixture-ratio distribution between the fuel and the oxidizer-rich gas will be uniform when proper vanes are designed and adjusted. The vanes begin at the oblong opening of the cast WPCH insert and stop at the 8.50-in. diameter of the housing. Five vanes extend between the two areas and divide each area into six equal parts. It is assumed that the gas across the entrance areas of the vanes is uniform in pressure, velocity, and density. A second assumption is that the gas would not uniformly enter the secondary injector without the vanes. Fabrication of these vanes should be completed by 1 July 1966.

III, E, Additional Design Activity (cont.)

The design of inserts, plugs, and closures permitting the test firing of a primary injector in a Mod-A TPA housing has been delayed pending the decision whether to use the Mod-A or Mod-B TPA housing for this testing. This decision is expected to be made in April 1966.

Quadlet Injector Assembly

Figure III-1

Full-Flow Injector Assembly

Figure III-2

Cracked Workhorse Primary Combustor Housing

Figure III-3

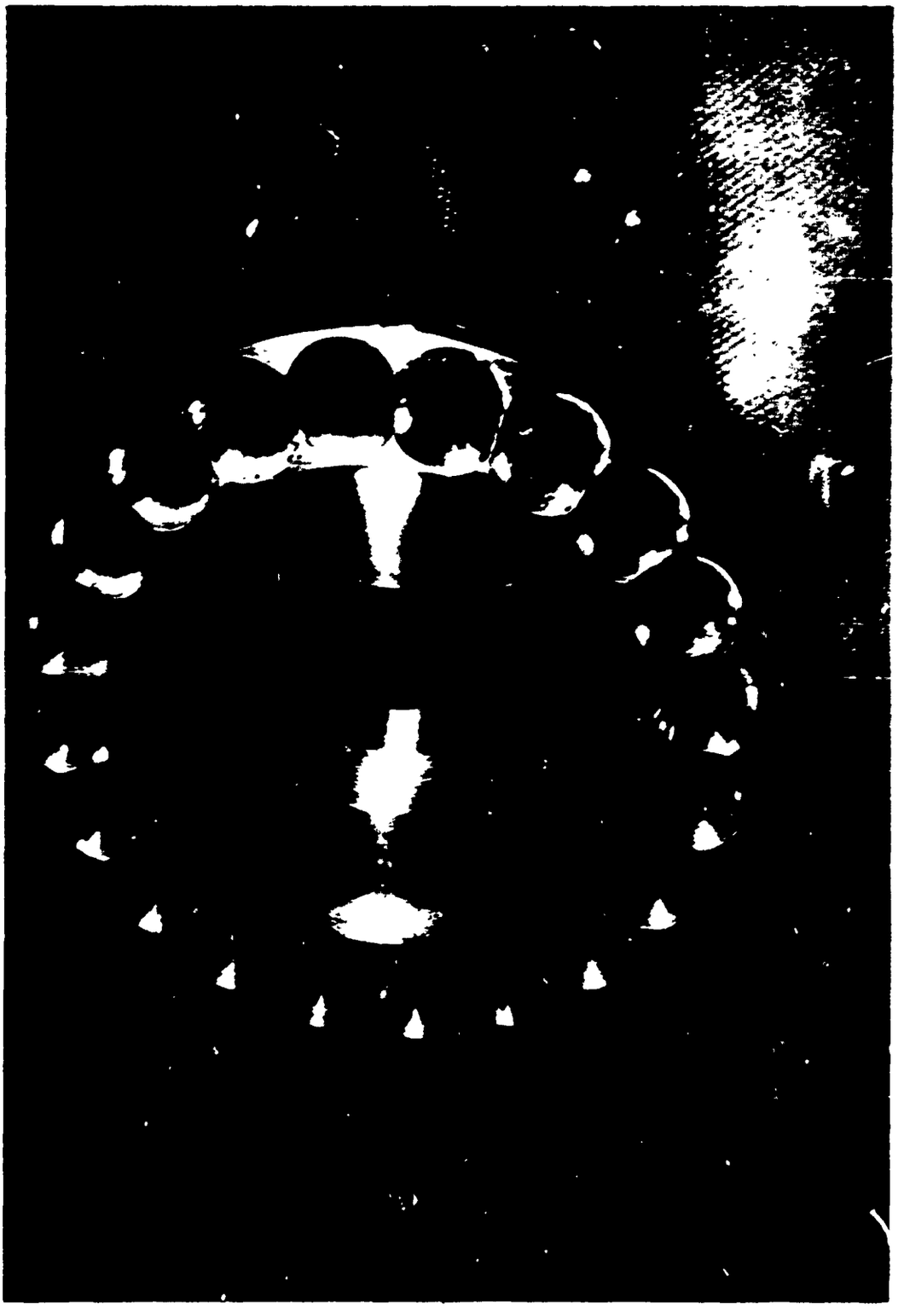

Flow Nozzle, Primary Combustor Entrance

Figure III-4

Flow Nozzle, Primary Combustor Exit

Figure III-5

Combustion Chamber Liner

Figure III-6

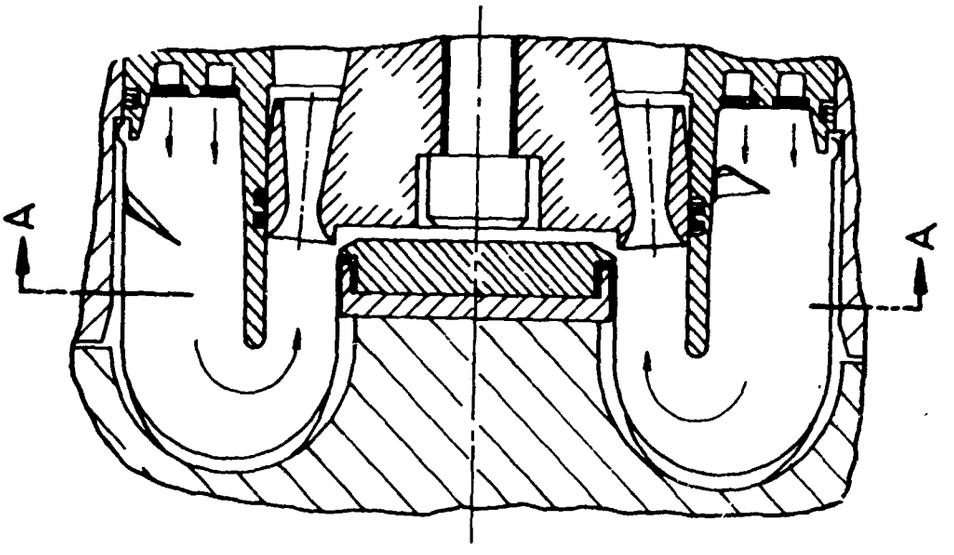

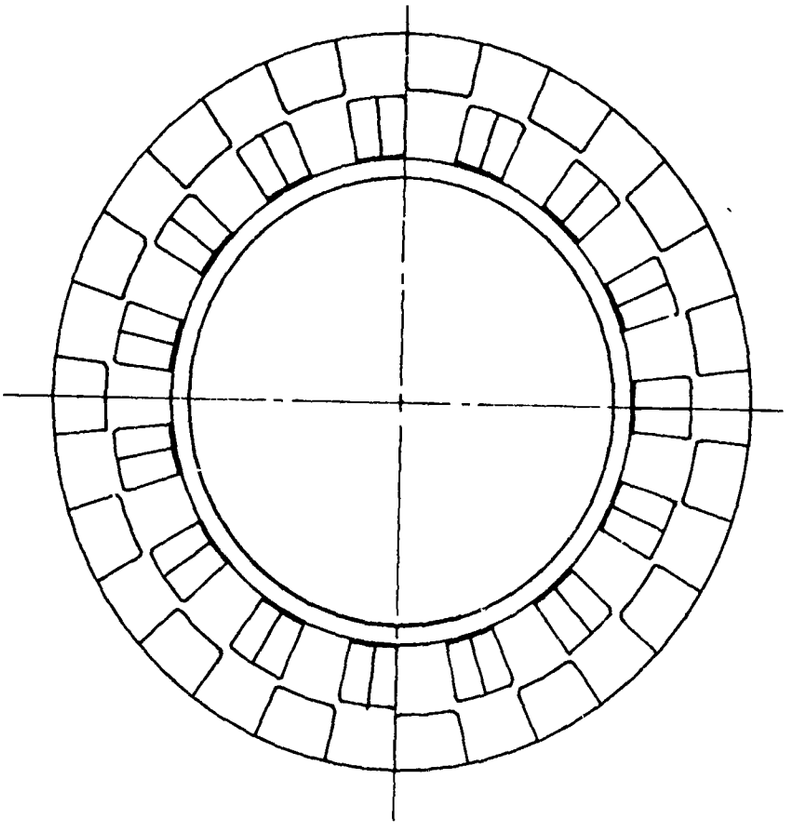

Turbulence Device, Primary Combustor

Figure III-7

IV.

SECONDARY COMBUSTOR ASSEMBLY, DESIGN AND FABRICATION

A. GENERAL

All component designs for the secondary combustor assembly were completed and released for fabrication. Design activity is currently limited to the redesign of details where necessary.

The first modular uncooled thrust-chamber assembly was completed and installed on Test Stand H-2. Fabrication of additional combustor components is continuing at a high level of effort.

Two separate task forces were created to accelerate the fabrication of the regeneratively cooled and the transpiration-cooled combustion chambers.

B. UNCOOLED COMBUSTION-CHAMBER COMPONENTS

1. Injectors

a. Mark 125

The first modular Mark 125 injector, SN-1, was fabricated, successfully hydrotested, and test fired (see Section V).

Fabrication of the second modular Mark 125 injector, SN-2, is 75% complete. The injector will be available for testing by mid-April. Injector SN-3 is approximately 50% complete.

b. Fuel Swirl-Rake Vane

The first fuel swirl-rake vane injector, SN-1, was received, hydrotested to determine its flow characteristics, and subsequently test fired. Receipt of the second injector, SN-2, is scheduled for 10 April 1966.

2. Ablative-Lined Combustion Chamber

Design drawings for ablatively lined combustion chambers with characteristic chamber lengths (L*) of 30, 40, and 50 in., were revised to include all the drawing-change notices (DCNs) necessitated by fabrication, quality-control, and instrumentation changes.

Four ablatively lined combustion chambers are being fabricated. The first chamber with a characteristic length of 50 in., has been completed, proof-tested assembled with the first modular Mark 125 injector, installed on Test Stand H-2, and recently test fired.

IV, B, Uncooled Combustion-Chamber Components (cont.)

The second ablatively lined combustion chamber ($L^* = 30$ in.) was also completed. The third and the fourth chamber ($L^* = 40$ in.) will be fabricated early in April. One of these two chambers will be instrumented and will incorporate a steel expansion liner. The other will be lined completely with ablative materials and will be instrumented as follows: with one Taber pressure transducer with a maximum recording range of 3500 psig; with eight 0.040- and three 1/8-in.-dia Chromel-alumel thermocouples; and with seven 3/8-in.-dia thermocouples, two having tungsten-tungsten rhodium and five having platinum-platinum rhodium junctions. Thermocouple locations are specified on Aerojet-General Dwg. 1121962.

The majority of all ordered ablative materials, together with inspection records and X-ray photographs, was received. The remainder is scheduled to be delivered in mid-April. The housings, bolts, and seals (with the exception of the backup-up Omni-seals) are also on hand.

3. Two-Dimensional Nozzle

Drawings for the two-dimensional nozzle were completed and have been released for fabrication. Two recent design changes, discussed below, have been incorporated to simplify their construction.

Theoretically, the internal expansion section is generated on a conical surface to match with the contour of a forced-deflection nozzle. Each base cone, nozzle, and internal expansion section contour is part of a specific propulsion system. (In the ARES proposal, 20 modules were clustered within a forced-deflection nozzle.)

The first change was recommended to simplify the basic design: a tilted cylinder was substituted for the base cone. A maximum deviation of 0.03 in. from the theoretical contour resulted from this change, which is considered insignificant.

The second change involves the substitution of a plane for the cylinder. Deviation from the basic contour is 0.65 in. at the end of the nozzle and is 0.15 in. at a point 4.76 in. downstream of the throat. Figure IV-1 shows the new contour of the two-dimensional nozzle.

The resultant flat contour will provide adequate heat-transfer information on the distribution of the film coolant and will greatly simplify the construction of the ablatively lined two-dimensional nozzle.

Quotes for fabrication of the nozzle are currently being solicited. A firm purchase order for a chamber is expected to be placed in late April 1966

IV, B, Uncooled Combustion-Chamber Components (cont.)

4. Adapter

Fabrication of both adapters was completed. Adapter SN-1 was hydrotested, installed on Test Stand H-2, and recently test fired. Adapter SN-2 is currently being hydrotested.

C. COOLED COMBUSTION CHAMBERS

1. Residual ICP Cooled-Combustion Chambers

The fabrication effort on regeneratively cooled Combustion Chamber SN R-6 was completed early in this reporting period. Chamber SN R-6 incorporates film cooling that is introduced through multiple holes on the crown of each of the coolant tubes. The film-coolant injection holes, made by electron-beam "drilling," were positioned to distribute the coolant over one half of the convergent section and over the throat section of the chamber.

Chamber SN R-6 was initially scheduled to be fired after the successful test of Chamber SN R-5; however, this firing has been postponed to permit the conversion of the test stand for use of the intensifier system, to check out the new system, and to commence testing of the modular secondary combustor at the earliest possible time.

Chamber SN R-6 was sent to the storage area and will be available for use, if required.

2. ARES Regeneratively Cooled Combustion Chambers

Extensive engineering, procurement, and fabrication effort was expended on the modular regeneratively cooled combustion chamber. A special task force was established to expedite completion of design, procurement, and fabrication activities on this critical component.

Initially, the task force concentrated on resolving a potentially serious problem concerning the Inconel 718 chamber-coolant tubes. This tubing was found to be of substandard quality. All tubing contained surface discontinuities, visible to the naked eye, which were suspected to be detrimental to the mechanical properties of the tubes. The flaws were circumferential depressions on the outside diameter of the tubes (Figures IV-2 through -5) and were present in varying degrees on all tubes. A very detailed metallurgical analysis, performed on random and on worst samples of tubing, established that all properties met the requirements to which the tubes had been procured. The surface depressions were found to have a depth of less than 0.001 in. Further, when typical depressions were sectioned, mounted, and examined at magnifications from 50 to 250 X the depressions were judged not to be cracks because their root radii were large. These surface flaws

IV, C. Cooled Combustion Chambers (cont.)

were probably introduced during a grinding operation. Based on the results of the metallurgical examinations, it was decided that forming operations on part of the tubing should be continued. The tubing was sorted into two groups: the best tubes were released for fabrication, and those with more numerous defects were rejected and returned to the supplier for rework.

Immediately at the beginning of forming operations the tubes were found to crack. This cracking was not caused by a propagation of the circumferential flaws, as might be expected, but from excessive cold working of the tubing. The vendor had been restricted to an anneal temperature of 1800°F. This low anneal temperature is desirable because it permits uniform elongation properties of the Inconel 718 tubing in the operating range of 1200 to 1400°F. If annealing temperatures exceed this 1800°F limit, the elongation properties at elevated temperatures are noticeably reduced, although still well within design requirements. After extensive attempts at fabricating formed tubes by repeating the annealing cycle and by forming them in multiple tapers, it was decided to increase the anneal temperature to 1925 $\pm$ 25°F. This higher temperature yields a softer material, which can be cold-worked to a much greater degree without cracking, and reduces the scrap rate considerably. About 40% of the material annealed to 1800°F had to be scrapped after the tapering operation.

Tube tapering, contouring, flattening, end swaging, penetrant inspection, and plating have been completed for two sets of tube bundles. These tubes will be induction-brazed and electron-beam-welded at two outside facilities early in April. The first set of tubes is currently scheduled to arrive at Sacramento on 15 April 1966, and the second set about one week later.

Tubes for the third chamber have been returned to the forming vendor after having been reworked at the mill. This set of tubes should be available in late May. Due to the large scrap rate encountered in fabricating the first two sets of tubes, tubes raw stock for the fourth chamber has been expended. Tube raw stock for Chambers SN 4 through 10 was therefore ordered and is expected to be received on 20 May 1966.

An Inconel 718 tubing specification (AGC 44204) was issued and then revised (AGC 44204A) to ensure that tubing of high quality and practical fabricability is obtained. Engineering, metallurgical, quality-control, and purchasing personnel at both Aerojet-General and the mill were actively involved with specification modifications, negotiations, and final placement of the purchase order. In addition, Aerojet-General top management has personally intervened to obtain and expedite delivery.

The task force also concentrated on completing the test hardware designs, the fabrication and hydrotest tooling designs, and the thermal-barrier coating tooling designs.

IV, C, Cooled Combustion Chambers (cont.)

All design on the non-capillary tube combustion chamber was completed, and all drawings have been released. A drawing change is being prepared to add capillary tubes to the chamber. These 0.005-in.-thick capillary tubes will have an OD of 0.055 in. A chamber with a characteristic length (L^*) of 40 in. was selected for fabrication. This chamber length offers the best combination of high performance (low film-coolant requirement), reasonable combustion-chamber volume, and minimum chamber weight. A complete discussion of factors relating to the selection of the characteristic length (L^*) is given in Section XIX.

All design work on combustion-chamber tooling was completed. Chamber lay-up mandrels, leak-check fixture, proof-test fixtures, and flow fixtures were completed and released. Fabrication of all tooling is in process and is expected to be completed by 15 April 1966.

All tooling required to apply a thermal-barrier coating to the regeneratively cooled chamber was designed. Fabrication of the new tooling and modifications to the coating machine are in process. All thermal-barrier coating tooling should be completed and checked out before mid-May 1966.

The stress analysis of the chamber was completed. A final report is expected to be available early in April.

Arrangements have been made to fabricate the metal chamber parts (except tubes) and to assemble and braze the chamber in Aerojet-General's Sacramento plant. Most of the chamber components are currently being fabricated, with the balance to enter fabrication in early April 1966. The chamber-brazing procedure was reviewed by engineering, quality-control, and manufacturing personnel; a satisfactory procedure was agreed upon and is being incorporated on the drawings. It is currently estimated that the first regeneratively cooled combustion chamber will be available for testing about 15 June 1966, the second chamber about two weeks later. The third chamber is scheduled for completion about 1 August 1966. Additional chambers should be available in early September 1966.

3. Transpiration-Cooled Combustion Chamber

Since the transpiration-cooled chamber is of equal importance as the regeneratively cooled chamber for meeting Phase-I objectives, special emphasis was placed on the timely completion of all tasks related to the successful completion of this chamber. A separate task force was assigned to resolve all problems and difficulties encountered in chamber design, fabrication, and assembly, and to support experimental and laboratory programs.

Procurement of individual washers from subcontractors (photo etchers) was the principal factor delaying the early completion of this chamber. Both subcontractors (suppliers of the flow-control and flow-diffusion washers) have only limited facilities and personnel. However, extensive coordination has

IV, C, Cooled Combustion Chambers (cont.)

yielded the best possible delivery dates. The fabrication of many special tools for handling and assembling the washers was completed. Several unique tools were designed and fabricated, and are now being checked out to permit accurate and rapid unitization of the washers.

Significant progress was made in fabrication experiments and hydraulic investigations. Numerous compartment-unitizing techniques were investigated and the most promising incorporated. Experiments to ID-contour the compartments were conducted successfully. In addition, all hydraulic investigations of subscale washers were completed, including surface-finish examinations, leakage tests, and flow tests. Full-scale washer flow tests will be performed during the next reporting period. The results of all hydraulic investigations will be reported in the next quarterly report.

4. Washer Assemblies

The 0.001-in.-thick flow-control washers and the 0.010- or 0.020-in.-thick flow-diffusion washers described and shown in Report 10830-Q-2 can be oriented with respect to each other in six possible combinations to achieve the desired flow rate or pressure drop at a given station within the 12 compartments of the transpiration-cooled combustion chamber.

To date, 600 flow-control and flow-diffusion washers have been received from the vendor. These washers have been properly oriented with respect to each other and have been spot-welded into unitized pairs using a specially designed washer-orienting tool and a micro-spot welder.

Laboratory tests were conducted concurrently to determine the best method of unitizing the spot-welded washers into unitized compartments. Each of these methods was to be limited to unitizing the washers on the outer periphery. Methods considered for unitizing the washers included brazing, electron-beam welding, soldering, and TIG welding. The first two methods were eliminated in favor of the last two because of the potential warpage that may be experienced with a high-temperature braze and the problem associated with keeping the braze out of the flow-control washer entrances and passages; electron-beam welding required a development program to achieve the proper length and intensity of the beam and posed further problems in possibly causing craters and weld spattering at the weld junctions.

Soldering and TIG welding appeared promising. Of the various solders investigated, Eutectic-157 exhibited the best characteristics. Two-inch-diameter sample washers were spot-welded into pairs and bolted between two 3/4-in.-thick plates. The assembly was preheated to about 400°F after which the Eutectic-157 was applied to the outer periphery. The solder was easily wiped on with an electric soldering iron. The location of the solder could be readily controlled. Further testing revealed that the Eutectic-157 solder and all other solders investigated

IV, C, Cooled Combustion Chambers (cont.)

were not compatible with nitric acid. All solder samples immersed in beakers of various concentrations of nitric acid were chemically attacked, leaving a heavy precipitate. Electroless gold plating of a solder sample proved unsatisfactory.

Although precautions could be taken to prevent moisture from contaminating the nitrogen tetroxide coolant, it was considered an unnecessary risk if a more reliable unitizing method could be developed.

TIG welding proved to be the final solution. Welds were located axially along the periphery of the sample compartment. Initially, weld shrinkage at the edge of the first and last washer of the compartment appeared to be a problem; however, it was later determined that a small weld bead (about 1/16 in. wide) could be obtained without appreciable shrinkage if the arc was struck on a copper plate located at the top and bottom of the compartment assembly and then moved toward the center of the stack using a minimum of current. It is anticipated that six axial welds, equally spaced around the periphery, are sufficient to unitize the compartment.

In addition to the 600 washers that have been micro-spot welded into pairs, about 30 rejected flow-control and flow-diffusion washers have been obtained to demonstrate the various unitizing and machining operations prior to using the actual hardware. Upon completing the compartment-unitizing operation, the compartment will be bolted into a washer-turning mandrel fixture in which the outside diameter of the locating tabs will be machined. After this operation, the compartment is bolted into a fixture in which the inside diameter will be machined to the proper contour. (Machining the inside diameter of three full-scale washers without visibly affecting the porosity of the flow-diffusion area has been demonstrated.) Upon completion of contour machining, the unitized washer compartment is scheduled to be flow-tested to determine its K-values.

At nominal operating conditions, laminar flow exists within the flow-control passages of the washers; thus, if water is to be used in obtaining the K-values, approximately three times the pressure drop is required to achieve the same weight flow at the proper Reynolds number. Therefore, fluids other than water have also been considered.

Trichloroethylene, a readily available degreasing fluid, is currently considered to offer the best compromise. The values of specific gravity and viscosity, listed below, illustrate the advantage of trichloroethylene over water:

	Trichlorethylene	Nitrogen Tetroxide	Water
Specific gravity at 77°F	1.46	1.43	1 nominally
Viscosity at 77°F, cp	0.55	0.393	1 nominally

IV, C, Cooled Combustion Chambers (cont.)

Trichloroethylene is bought per Specification O-T-0063A, which stipulates that the water content must not exceed 100 parts per million and that nonvolatile matter must not exceed 0.001 wt%. A final advantage of using this fluid is the fact that the compartment does not have to be dehydrated after flowing for K-values.

Curves have been prepared for specific gravity and viscosity of trichloroethylene at elevated pressures. A facility for flowing the compartments has been located at Aerojet-General's Control Systems Laboratory.

Upon completing the flow tests on all 12 compartments, the compartments will be assembled with instrumented washers on the weld-assembly mandrel where the exterior of the compartment retainers will be seal-welded.

Twelve instrumented washers will be installed in the fuel assembly, one downstream of each compartment. The heat-transfer characteristics of the transpiration-cooled chamber are discussed in Section XIX.

The entire assembly will be proof-tested prior to shipping the chamber to the test area.

All tooling required for completing the transpiration-cooled combustion chamber is available. Compartment retainers, forward and aft flanges, studs, nuts, and seals are either completed and available or will be completed early in the next reporting period. A purchase order for washers has been placed for a second transpiration-cooled combustion chamber.

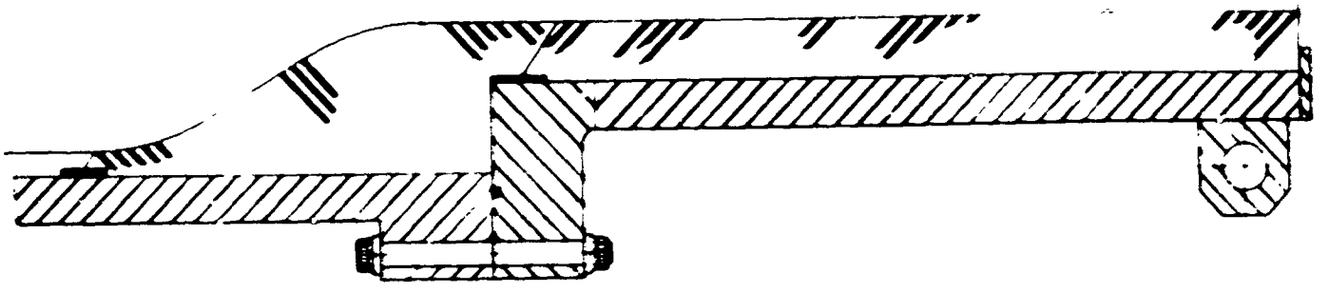

SECTION B-B

ROTATED 90° CLOCKWISE

℄ THROAT

X

Y

STA 0.000

STA 19.450

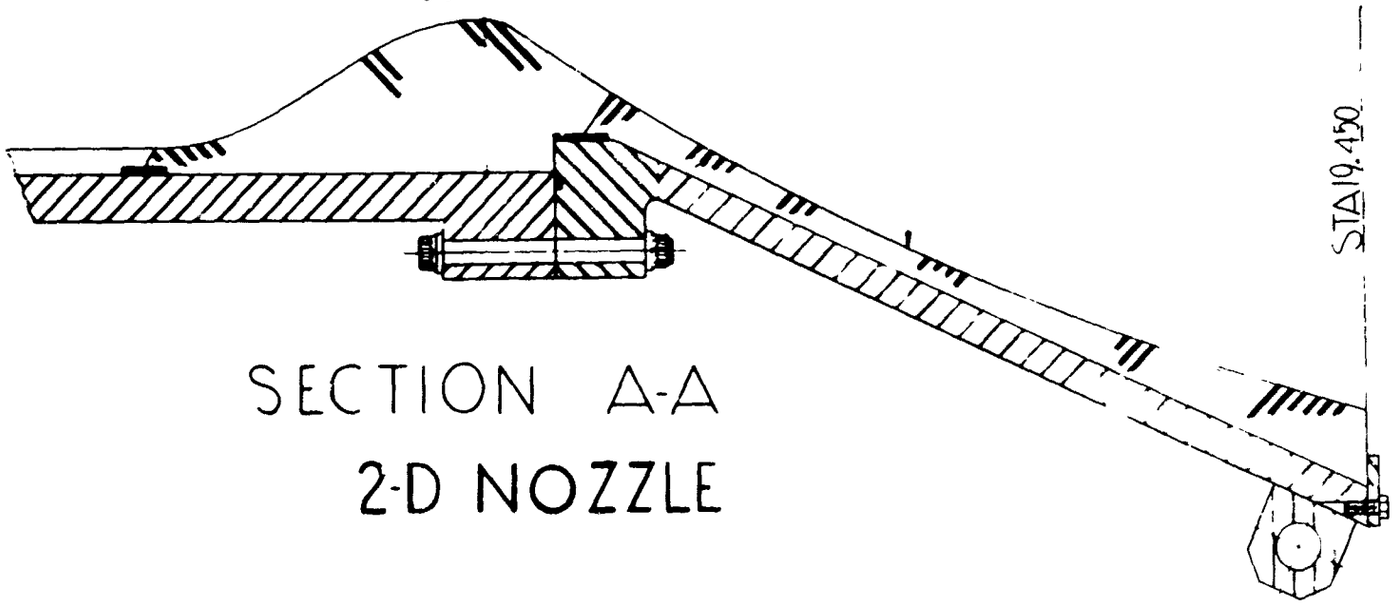

SECTION A-A

2-D NOZZLE

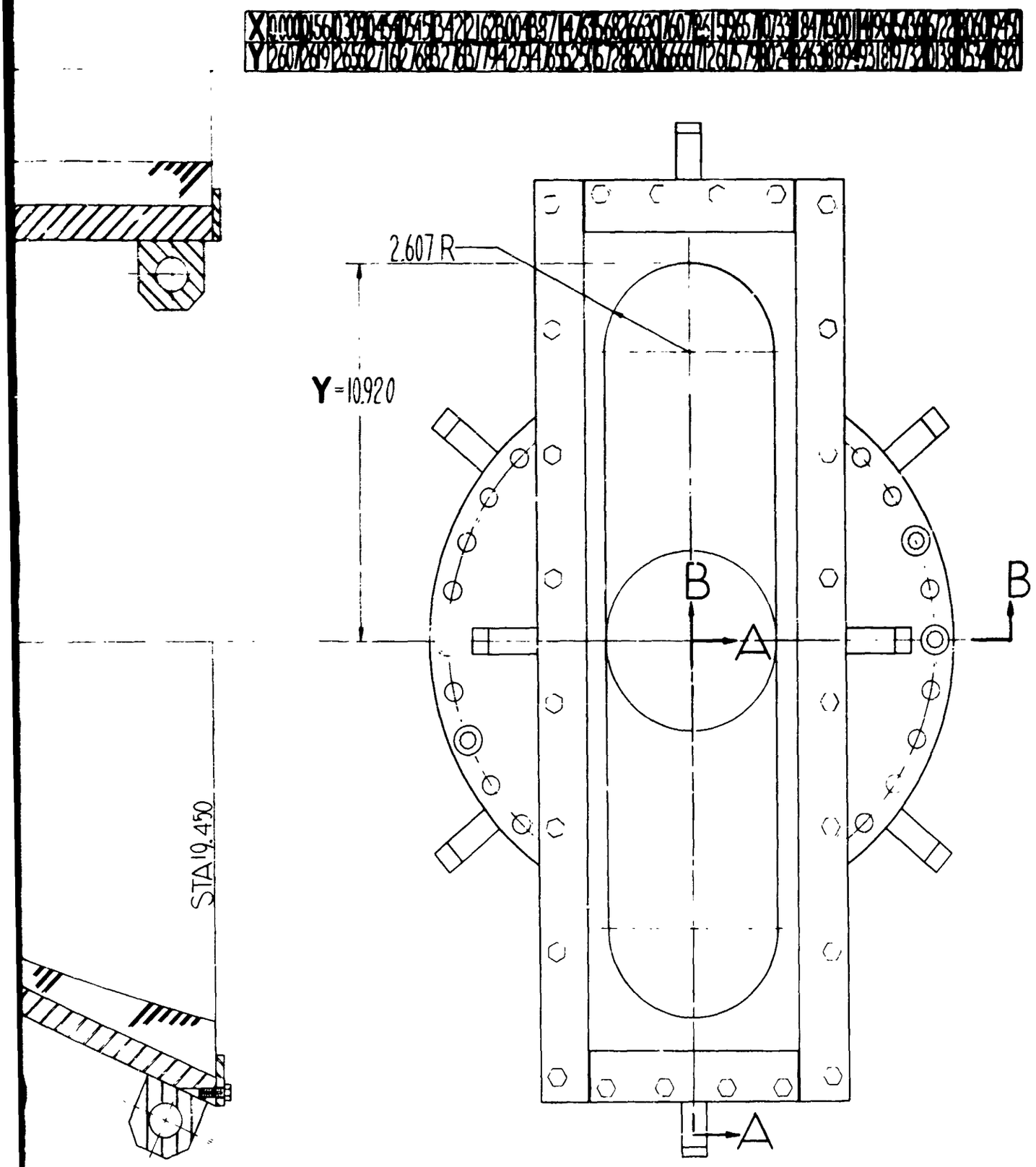

Two-Dimensional Nozzle

Figure IV-1

Figure IV-2. Macrostructure of 3/4-in.-dia Inconel-718 Tubing, 3X

Circumferential grinding marks are shown at higher magnification of 10X.
View with Figures IV-3 and IV-4.

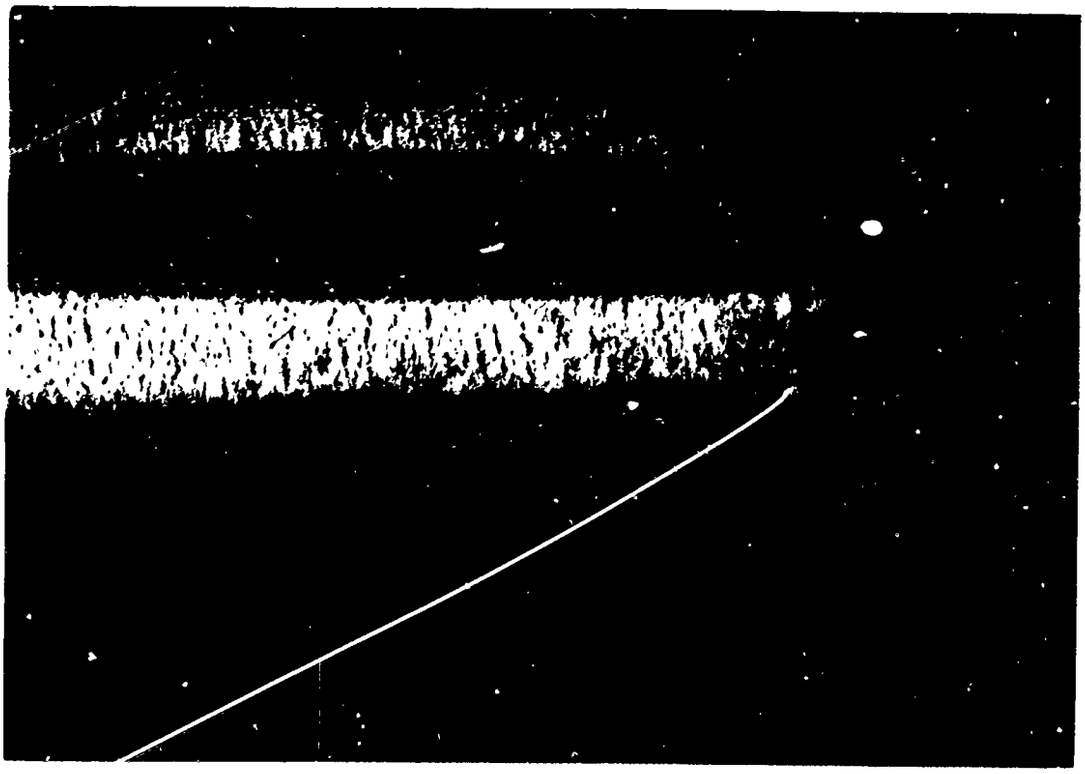

Figure IV-3. Macrostructure of 3/4-in.-dia Inconel-718 Tubing, 10X

Circumferential grinding marks are shown. Magnification is 3X.
View with Figures IV-3, IV-4 and IV-5.

Figure IV-2 and Figure IV-3

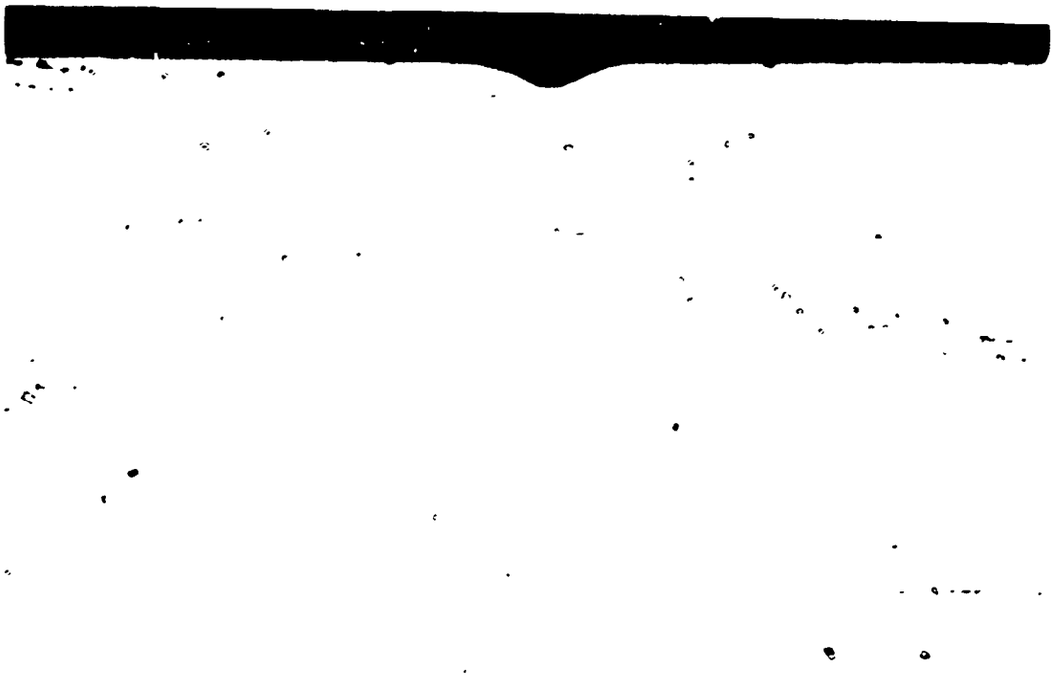

Cross-sectional view of circumferential grinding mark is shown. Magnification is 250X. Structure is unetched.

Figure IV-4. Microstructure of 3/4-in.-dia Inconel 718 Tubing

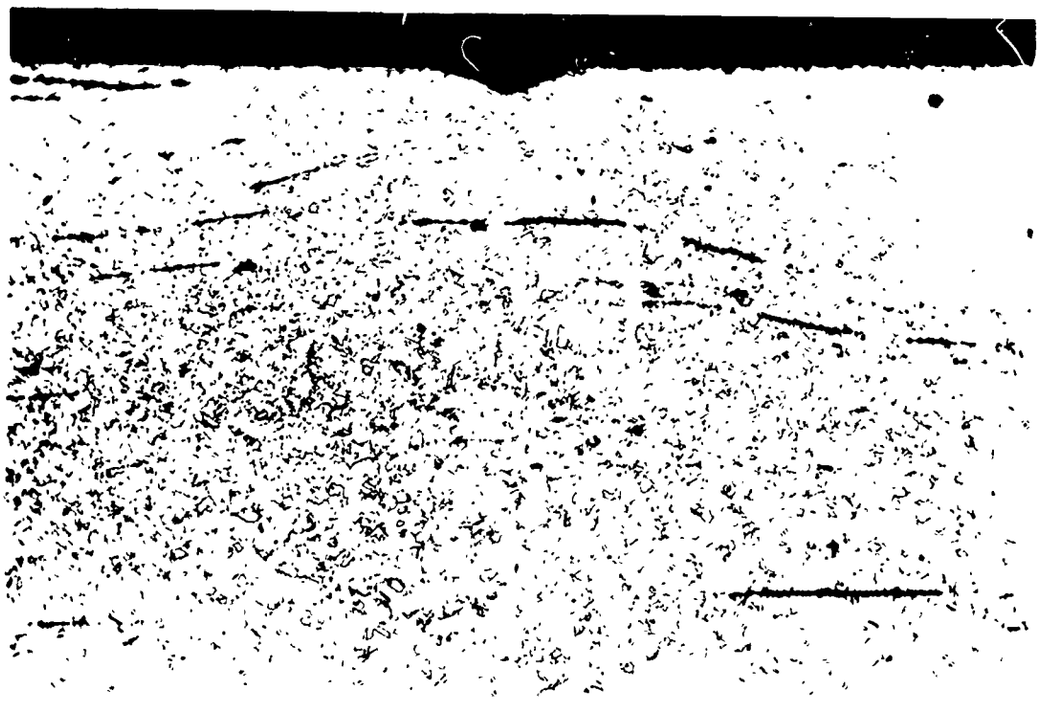

Cross-sectional view of circumferential grinding mark is shown. Magnification is 250X. Structure is etched. Stringers are also shown. Structure is fine-grained.

Figure IV-5. Microstructure of 3/4-in.-dia Inconel 718 Tubing

Figure IV-4 and Figure IV-5

V.

SECTOR-ENGINE TESTING

A. GENERAL

Three major mileposts were reached in the H-2 sector-engine test program: the activation and checkout of the intensifier propellant system, the conversion of the Sector Engine to accommodate modular-configuration secondary TCA hardware, and the initiation of the modular secondary injector test program. The following paragraphs summarize each of these events; detailed discussions follow in the subsequent sections.

The intensifier-fed propellant system was activated and checked out using residual hardware from the Integrated Components Program (ICP), Contract AF 04(611)-8548. Mathematical models simulating the intensifier controls, engine transients, and engine steady-state conditions were completed and verified by waterflow and hot firing tests. A series of 17 waterflow tests were conducted with the complete intensifier and engine feed system to establish the operational characteristics of the servocontrol system as well as the mechanical integrity of the system. These were followed by three hot firing tests. Completely satisfactory operation of the intensifier system was obtained.

Following the intensifier system checkout tests, the Sector Engine was modified to accommodate the modular-configuration hardware. This involved extensive plumbing changes as well as the installation of an adapter connecting the ICP-configuration primary combustor to the ARES-configuration secondary combustor. This effort was completed with the installation of the modular Mark 125 injector and of an uncooled 50-in. L* secondary combustor on the engine.

Modular-injector testing was initiated on 25 March 1966. Five tests were performed in this reporting period. Four of these tests yielded valid data. Both the Mark 125 and the Rake secondary injectors have been tested. Evaluation of these injectors will continue during the next quarter.

B. INTENSIFIER SYSTEM DESCRIPTION AND OPERATION

The fuel and oxidizer intensifiers are single-stroke, positive-displacement pumps capable of developing propellant pressures of 7500 psia. Each contains two pistons of different diameter on a common shaft operating in cylinders. The nitrogen-side piston has an area five times that of the propellant side. A gas pressure of 1500 psi yields propellant pressures of 7500 psi. The 5-ft-dia pistons are 20 ft long, and at ARES engine flow rates, can sustain engine operation for 4.5 sec. They are located on the second level of the H-1, H-2, and H-3 test-stand complex, and supply propellants to each test bay through a system of select valves. A schematic is shown in Figure V-1.

V, B, Intensifier System Description and Operation (cont.)

Intensifier transient and steady-state control is maintained by regulating the nitrogen gas supply with a closed-loop, electro-mechanical, hydraulic servo flow-control system. Nitrogen is admitted to the intensifier gas piston through parallel 2- and 4-in.-dia flow-control valves. The 2-in.-dia valve maintains pressure control at low flow demands, and the 4-in.-dia valve controls at larger flows. The position of the flow-control valve is established by the servo-controlled actuation system excited by an electrical signal generated through a computerized error system. An integral plus proportional network in the computer amplifier circuits determines the valve command based on a predetermined specified pressure-versus-time curve. The resulting command signal begins with a comparison of the gas-side intensifier pressure to the command curve. The resulting difference signal is fed, after amplification, into the integral and proportional portion of the control circuit. Here the signal is conditioned based on present and past time-control responses. This signal, in turn, is amplified and compared to the flow-control-valve position signal and a new required position is established. The resulting signal commands the actuation system of the hydraulic valve, which controls intensifier flows and pressures to the prescribed value.

The operating procedure is quite simple. Propellants are bled through the feed system to the thrust-chamber valves with the intensifier in the exhaust position (piston against the flow exit end). This condition is established by venting the liquid side prior to admitting propellants and by applying a slight gas-side pressure. Once the discharge flowmeters indicate a satisfactory system "bleed," the liquid vents are closed and the gas supply terminated. With the gas vents open and a slight liquid pressure, the piston is reversed until a position 5 in. from the gas inlet end is established. This procedure ensures that no ullage will be present in the liquid side of the intensifier. The units are now ready for test. Just prior to engine fire switch, the 2-in.-dia flow-control valves are energized to establish the required prepressure. At FS_1, the control program is initiated and the computerized system controls the pressure through the transient and steady-state operation. On Test Stand H-2, the 4-in.-dia flow-control valves are used during the pressure ramps and during steady-state operation. Shutdown is effected by de-energizing the flow-control valves with the gas vents open and closing the thrust-chamber valves rapidly. Any system water-hammer is either absorbed or minimized by the intensifier.

C. INTENSIFIER SYSTEM ANALYSIS

1. Analog

The objective of the analog analysis was the design of a stable system for control of oxidizer and fuel intensifiers on Test Stands H-2 and H-3.

Due to the nonlinearities involved in the overall system, an analog computer-modeling approach was employed. The study was initiated by compiling all available data relating to the physical configuration of the system (e.g., line lengths, types and quantities of fittings, bottle capacities, and booster characteristics). Simultaneously, a generalized mathematical model was

V, C, Intensifier System Analysis (cont.)

developed; the model was written in terms of 70 coupled nonlinear differential and algebraic equations that characterized the hydraulic and pneumatic flow dynamics, intensifier dynamics, and the approximate engine dynamics. In addition, the control system components (valves, servo valves, actuators, servo controller output stages and coupling dynamics) were ascertained by subjecting each control system to a series of transient response tests--the resulting response data were then equated to linear transfer functions that described the basic control-system hardware. The mathematical model, together with all required constants and parameters, and the description of the control system hardware were then programed for analog computer simulation.

Once the computer program was verified, an analysis of possible modes of control was initiated. Based upon these initial computer results (together with previous experience in intensifier control), it was concluded that a direct "booster gas-side" control mode offered the most promising compromise between control-system stability and propellant flow-rate control accuracy. Thus, the control system was designed to maintain a desired (predetermined) intensifier gas-piston pressure as a function of time.

A series of computer simulations was conducted to determine an optimum set of control-system gains, together with any required electrical shaping networks. Proportional-plus-integral equalization was ultimately selected to ensure a zero steady-state control error. In the steady state, the difference between set-point pressure and the achieved intensifier gas-side pressure decays to zero due to the action of the proportional-plus-integral compensator. The system gains were specified such that, for the nominal pressure-rise-rate conditions required, an adequate transient response was obtained consistent with steady-state stability. For a nominal 2.8-sec run (total duration including pressurization ramp), the resulting design ensured a minimum of steady-state duration of 1 sec at nominal environmental conditions (nominal initial booster gas ullage, gas-bottle pressure, and initial gas-side prepressurization levels). A parametricl study was then conducted to determine the variations in these parameters which will ensure reliable operation.

2. Steady State

The steady-state computer program, as previously described in past reports, was modified to simulate the pressure-fed engine. Engine balances for the three hot firings and 17 water-flow tests were established using the modified program. A special study was conducted to determine the effects of varying film-coolant flowrates on an existing engine balance. The results indicate that the injector flows varied only slightly when film coolant was reduced from 50 lb/sec to zero. The secondary combustor chamber pressure decreased 75 psi since the lower total weight flow was partially compensated by an increase in overall combustion efficiency. This study proved the feasibility of conducting a rapid-repeat film-coolant test series with the only change between tests being a predetermined film-coolant balance-orifice change.

V, C, Intensifier System Analysis (cont.)

3. Transient

An analytical model of the system was constructed to understand the dynamic behavior of the feed system on Test Stand H-2 during engine transients. All liquid lines were described using water-hammer equations which were solved on the digital computer. The model represents a detailed description of sector-engine feed-system hydraulics. This model was used to determine preliminary transient requirements, which were then evaluated by hydrotests. The test and model results agreed very well, with no major discrepancies apparent.

The model was used to conduct various sensitivity studies on the engine system. The studies include the effects of intensifier preset pressure, intensifier gas ramps, time delay between initiation of the oxidizer ramp and the fuel ramp, and engine valve sequences. From these studies, the valve sequences and the desired intensifier characteristics were specified for the hot-firing checkout tests.

Test 1.2-09-WAM-002 of the checkout series was simulated with the analytical model, as presented in Figure V-2, Pages 1, 2 and 3. Excellent correlation was obtained. All deviations between the data can be explained by individual component characteristics. As an example, chamber-pressure deviations are a result of changing combustion efficiencies during start rather than of the constant values used in the model. The verified model is now being used to determine control requirements for ARES thrust-chamber testing on Test Stand H-2.

D. INTENSIFIER SYSTEM CHECKOUT TESTS

1. Summary

Check-out of the intensifier feed system and of the control system was completed during February with engine Test 1.2-09-WAM-003. This fulfilled the primary objective of the test series. Prior to this test series, satisfactory operation using water as the pressurized fluid was demonstrated on 17 flow tests on 5 February 1966. The checkout demonstration consisted of:

a. Determining the integral and proportional gain settings of the servo-control system to give near-linear pressure rise rates.

b. Demonstrating the minimum pressure overshoot of 3%.

c. Verifying an electrical-mechanical control-system response of 65 millisec and its repeatability.

d. Determining the system sensitivity to initial gas-side piston position (ullage), nitrogen cascade pressure, and required pressure rise rate.

V, D, Intensifier System Checkout Tests (cont.)

(u) e. Developing a malfunction shutdown device to terminate engine testing because of (1) fuel or oxidizer overpressure, (2) oxidizer or fuel exhaustion, (3) greater fuel pressure than oxidizer pressure, and (4) fuel pressure not equal to a prescribed value at a given time.

(u) f. Determining of the resistances of the feed system.

(u) g. Defining the operating flow capability of the 2-in. and 4-in.-dia flow-control valves.

(c) Secondary objectives of the hot firing tests were to evaluate the performance of the Mark 20 primary injector, the Mark 32 secondary injector, and the Mark 125 AB secondary injector. This secondary objective was not achieved on the Mark 20 primary injector because of gross damage experienced during Test 1.2-09-WAM-002. Test 1.2-09-WAM-003 did demonstrate continued high performance of 89.5% vacuum specific impulse for the Mark 125 secondary injector in a 20.8-in. L* rough-wall ablative chamber.

2. Water-Flow Tests

(u) Seventeen water-flow tests were conducted with the complete intensifier and engine feed system to establish the operational characteristics of the closed-loop servo-control system as well as the mechanical integrity of the design. The testing was conducted in a manner to demonstrate satisfactory operation at all anticipated operating transients of the ARES thrust-chamber assembly. Upon completion of testing, the operating and control requirements for reliable component testing were demonstrated. Limitations of the design as well as flexibility of operation were also demonstrated. This minimized the number of hot firing checkout tests required.

3. Hot Firing Tests

a. Test 1.2-09-WAM-001

(1) Purpose

(u) The primary test objective was to check out the intensifier feed-system control characteristics at the hot firing level. Performance evaluation of the Mark 20 primary injector and of the Mark 32 secondary injector in an 18-in.-L* ablative thrust chamber was a secondary objective.

(2) Attempted

(c) The test was conducted on 15 February 1966, with an intended test duration of 2.3 sec at a chamber pressure of 2500 psia. Engine configuration was as shown in Figure V-3, with balance and sequence conditons as shown in Figures V-4 and V-5, respectively.

V, D, Intensifier System Checkout Tests (cont.)

(3) Obtained

The test was terminated prematurely at FS_1 + 1.543 sec due to opening of the second-motion microswitch of the primary fuel valve.

(4) Discussion

(a) Test Hardware

Posttest inspection revealed slight discoloration and erosion of the primary injector face, outer ring, and chamber wall (Figures V-6 and -7). The hardware was suitable for refiring.

(b) Test

Record analysis indicated a 4.2-cps fuel-system oscillation during the intensifier-pressurization ramp. The primary combustor responded to this feed-system oscillation by producing a 1400-cps oscillation in the primary and secondary injector parameters. The large-amplitude oscillations attenuated during the compression phase of the 4.2-cps oscillations.

Detailed investigation of the fuel servo-control system traced the 4.2-cps oscillation to overcontrol of the fuel intensifier. This overcontrol was due to a shift of 33% in the loop gain of the hydraulic system from values previously established during water-flow testing. The effect was produced by a fuel-system servo valve which had been replaced after water-flow tests and prior to the first hot firing.

The increased gain was to be compensated for by lowering the electrical gain in the servo-control system by 33% from the loop-gain value developed during water tests. (The loop gain is a multiple of the hydraulic and electrical gain.)

The maximum amplitudes of the 1400-cps primary oscillations occurred during the decompression phase of the 4.2-cps oscillations and during high primary mixture ratios (MRs) of 20 or greater. An earlier dynamic analysis indicated that attentuation of low-frequency oscillations is obtained at low primary MRs (high temperatures). Therefore, the next test was sequenced to ignite the primary combustor at a mixture ratio below 20, with a rapid reduction of mixture ratio to the balance value of 14.

An early (by 120 millisec) secondary fuel flow caused secondary ignition to occur at or before primary ignition. This early flow was traced to a misaligned secondary fuel valve. The valve-opening position was reset to the proper position for the next test.

V, D, Intensifier System Checkout Tests (cont.)

b. Test 1.2-09-WAM-002

(1) Purpose

Identical to Test 1.2-09-WAM-C .

(2) Attempted

Identical to Test 1.2-09-WAM-001. This test was made on 23 February 1966.

(3) Obtained

The second test ran for the scheduled duration of 2.3 sec with all intensifier-controls functioning satisfactorily.

(4) Discussion

(a) Test Hardware

Postfire inspection revealed severe erosion of the primary combustor barrels (Figure V-8), primary injector (Figure V-9), secondary injector (Figure V-10), and turbine-simulator orifices. The second barrel eroded through the wall at the location of the Photocon high-frequency transducer (Figure V-11).

(b) Test

Record review indicated that all engine parameters were as expected until FS_1 + 1.6 sec, at which time the primary-combustor temperatures rose sharply (Figure V-12). At FS_1 + 1.7 sec the turbine-simulator orifice-pressure drop increased, indicating either higher mass flow or higher temperature. No apparent change in upstream flow or pressure was noted. At FS_1 + 1.95 sec the primary combustor barrels eroded through, as indicated by decreasing engine pressures.

The sharp rise in temperature is attributed to local burning of the primary injector producing a reaction between the steel and the highly oxidizing primary gas products. Local burning raised a small portion of the metal to its ignition temperature (in excess of 2800°F); it burned exothermally, releasing large amounts of heat at high flame temperatures. The combustion continued to accelerate to destruction. Motion-picture analysis indicated the presence of brilliant chamber exhaust gases, just following secondary ignition, which verifies this exothermic reaction.

V, D, Intensifier System Checkout Tests (cont.)

c. Test 1.2-09-WAM-003

(1) Purpose

(u) The primary test objective was to check out the control characteristics of the intensifier feed system. Performance evaluation of the Mark 125 AB secondary injector in a 20.8-in.-L^* chamber was the secondary objective.

(2) Attempted

(c) This test was conducted with an intended duration of 2.5 sec at a chamber pressure of 2800 psia. Balance and control settings were as specified in Figures V-4 and -5. The tested configuration included the Mark 125 AB secondary injector, the Mod-H primary injector, two primary barrels (the first primary barrel included turbulators), and an uncooled ablative secondary chamber (see Figure V-13).

(3) (c) The test was conducted on 3 March 1966 and operated successfully for the prescribed test duration at a chamber pressure of 2850 psia. The specific-impulse efficiency was 89.5%. A complete listing of performance functions is presented in Figure V-14.

(4) Discussion

(a) Test Hardware

(c) Posttest evaluation revealed no hardware damage.

(b) Discussion

(u) Record analysis indicated excellent engine and thrust-chamber operation throughout start, steady state, and shutdown. The loop gain of the fuel servo-control system, which had been decreased on Test -002, was slightly increased to increase the responsiveness of the system. Indications of overcontrol were present, but not of the same magnitude as in Test -001. Test -003 therefore determined the upper limit for the fuel gain settings. No other abnormalities resulted.

E. CONVERSION OF TEST STAND H-2 TO MODULAR TCA CONFIGURATION

In converting Test Stand H-2 for ARES configuration hardware, the following modifications were made:

1. A test-stand adapter was installed. This adapter incorporates the ICP thrust takeout interface: the ICP primary combustor chamber at one end, and the ARES secondary injector at the other end. Since this adapter simulates the pump

V, E, Conversion of Test Stand E-2 to Modular TCA Configuration (cont.)

housing (from a secondary chamber fluid-flow standpoint), it is manifolded to carry the entire oxidizer flow. Orifice-plate recesses are provided at the oxidizer inlet and outlet flanges to enable metering orifices to detect any oxidizer loss at the adapter-injector or injector-chamber interfaces or from the regneratively cooled chamber itself.

2. An expansion bellows was incorporated in the primary oxidizer line. This line is needed for the pump-fed tests of 1 to 20 sec duration.

3. A common film-coolant supply-point interface was provided. The film-cooled ablative chamber, the externally supplied regeneratively film-cooled chamber, and the transpiration-cooled chamber are all supplied from this point.

4. All plumbing used with the ICP pump-fed configuration was saved for use in APES pump-fed tests. All existing propellant lines, actuation systems, etc., were used whenever possible.

A drawing of these modifications is shown in Figure V-15. The actual conversion was completed during the week of 25 March 1966.

F. MODULAR INJECTOR TESTING

Development testing of the modular secondary injector was initiated in March. Five tests were conducted, and valid data points were obtained in four of these tests. The first test was terminated prematurely due to an erroneous signal from a malfunction-detection device. The testing has progressed with performance evaluation of the Mark 125AE and Rake injectors in 50-in. L* chambers. No hardware damage has been experienced in any of the tests. Finalized performance data are not yet available. Detailed performance data and their analysis will be presented in the next quarterly report.

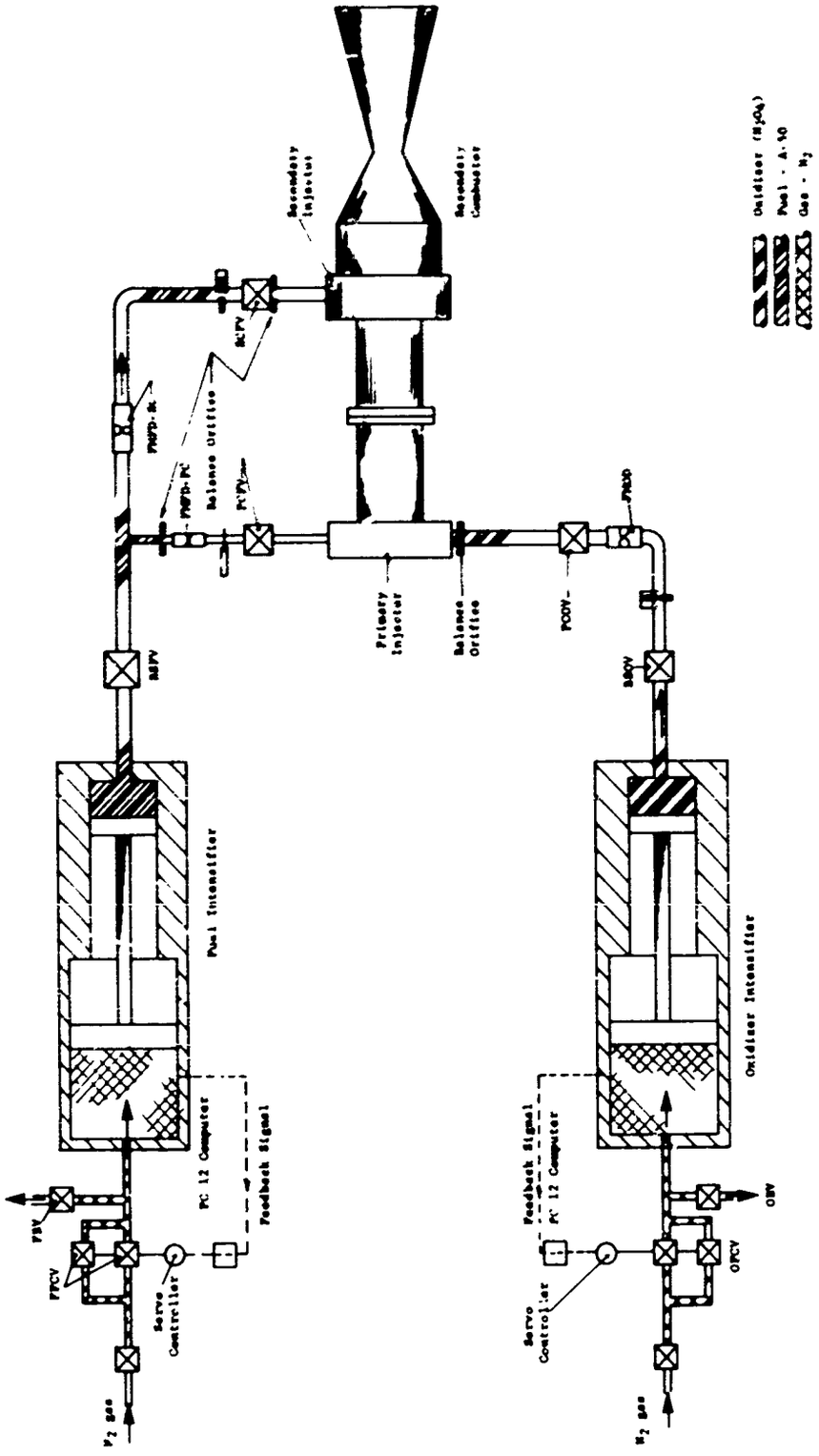

Intensifier Feed-System Schematic

Figure V-1

(This page is Unclassified)

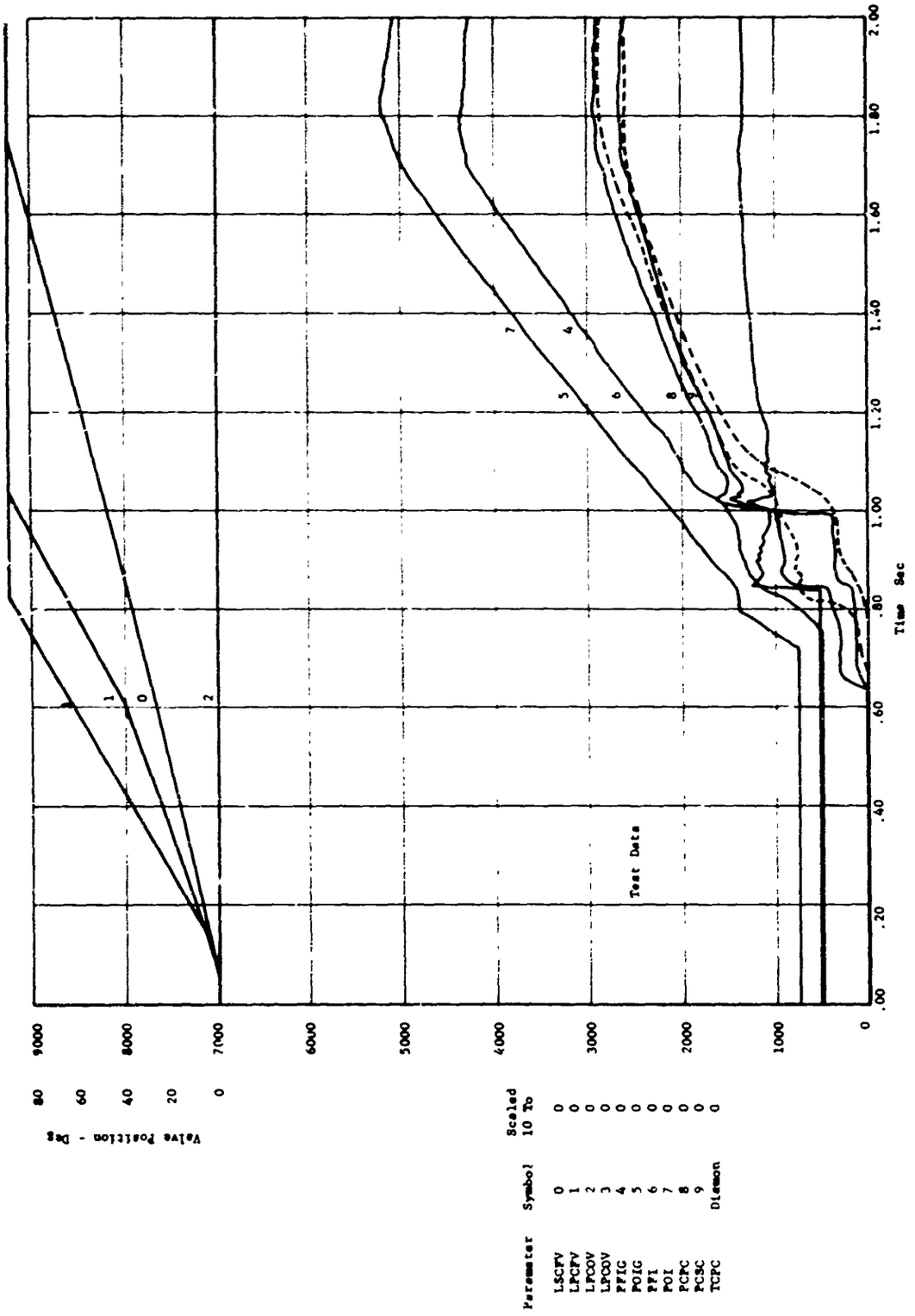

Transient Comparison, Test 1.2-09-WAM-002 (u)

Figure V-2, Sheet 1 of 3

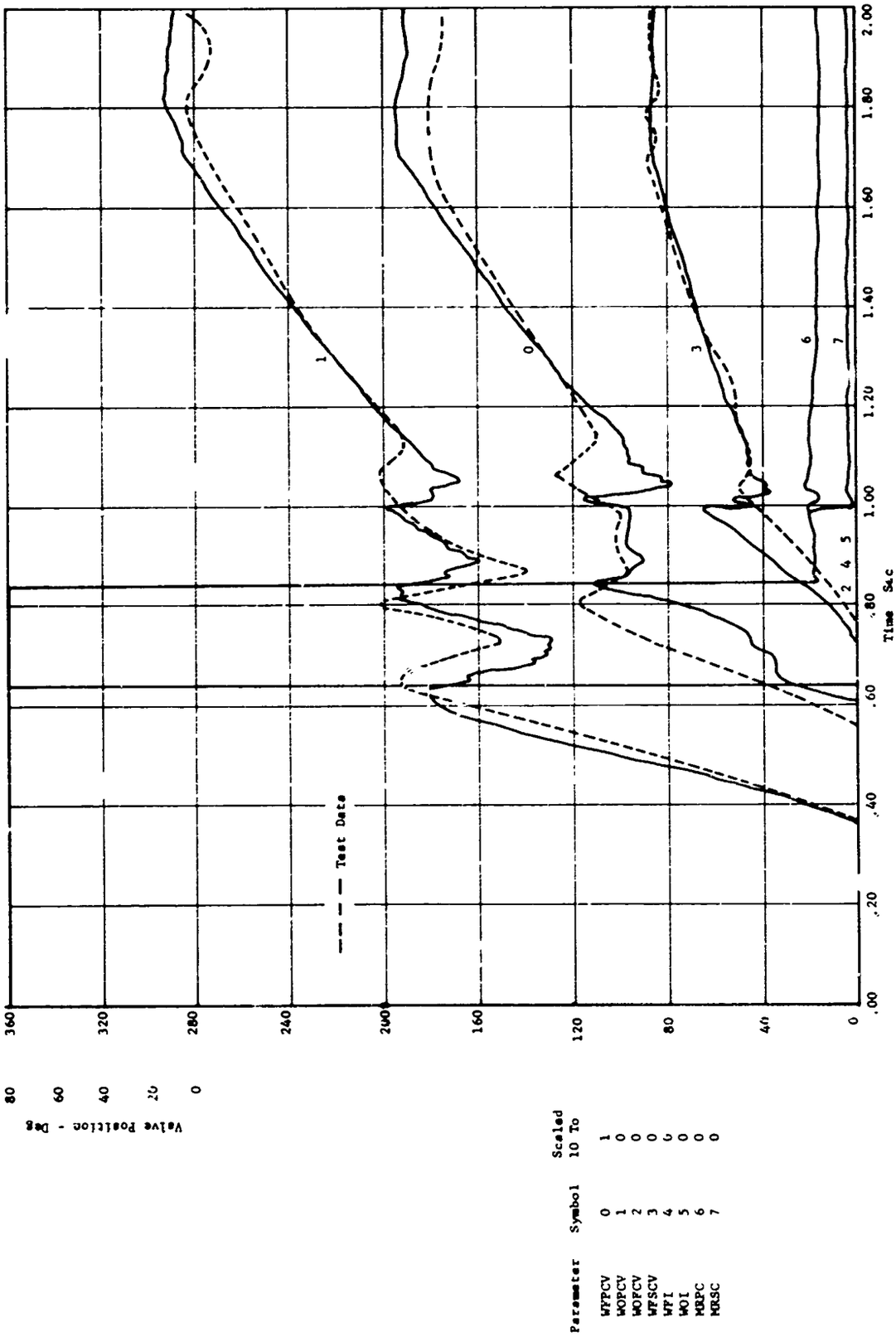

Transient Comparison, Test 1.2-09-WAM-002 (u)

Figure V-2, Sheet 2 of 3

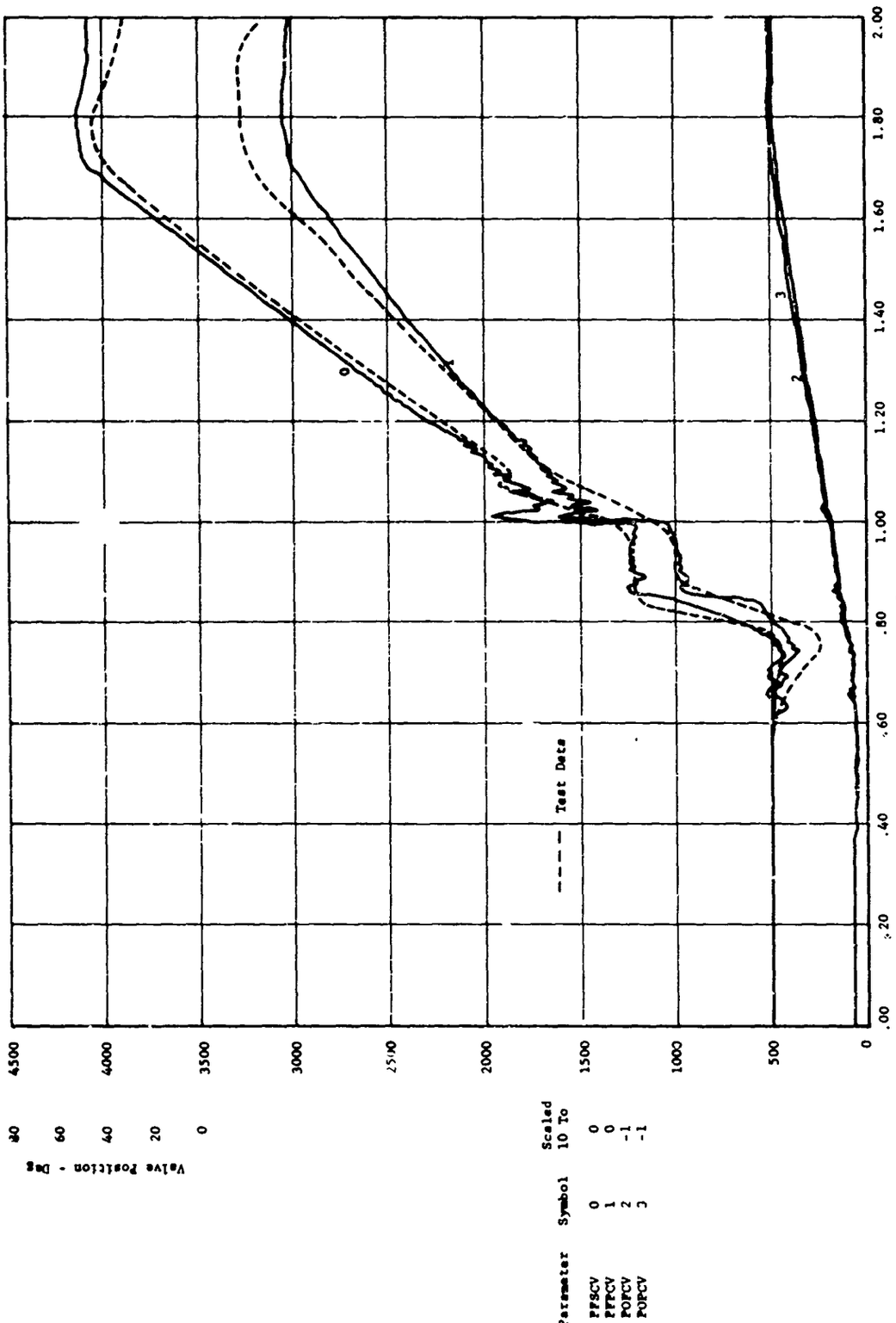

Figure V-2, Sheet 3 of 3

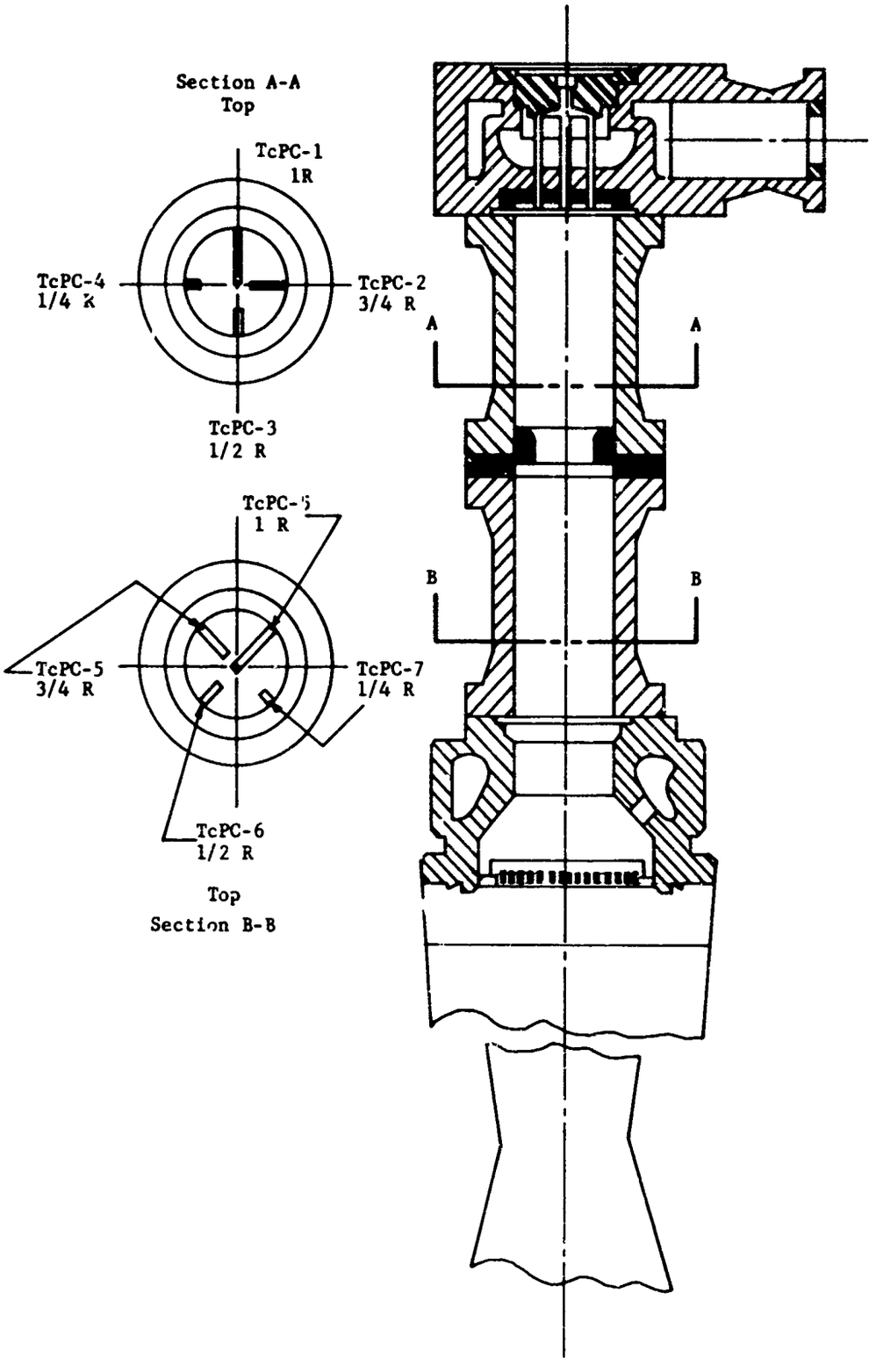

Primary Combustor Schematic, Tests 1.2-09-WAM-001 and 002

Figure V-3

(This page is Unclassified)

Summary of Engine Balance Requirements (u)

Test	Pre-Set Pressure, PSIA		Steady State Pressure, PSIA		Ramp Time, SEC		Chamber Pressure (Nom), PSIA	Secondary Mixture Ratio (Nom)	Primary Mixture Ratio (Nom)	Film Coolant, #	Ox. Inj. (Comb)	Ox. Inj. (Comb)	Fuel Orifice, Primary (Comb)	Fuel Inj., Primary (Comb)	Fuel Orifice, Primary (Comb)	Fuel Inj., Sec. (Comb)	Film Coolant (Comb)
	OX	FU	OX	FU	OX	FU											
1.2-09-xxxx-001	735	495	5002	4540	1.0	1.0	2800	2.8	14	N.A.	XXXX	1,540	.809	XXXX	XXXX	0.691	XXXX
1.2-09-xxxx-002	735	495	5002	4540	1.0	1.0	2800	2.8	14	N.A.	XXXX	1,540	.809	XXXX	XXXX	0.691	XXXX
1.2-09-xxxx-003	735	495	4988	4493	1.0	1.0	2800	2.8	14	N.A.	XXXX	1,540	.834	XXXX	XXXX	0.691	XXXX

Figure V-4

PVH	VALVE TIMER, SEC										PURGE SETTINGS				
	PSOV		PSOV		PSPV		SSPV		PSOV		PSSP, PSIG	PSSP, PSIG	PSPP, PSIG	SSPP, PSIG	PSSP, PSIG
	OPEN	CLOSE	OPEN	CLOSE	OPEN	CLOSE	OPEN	CLOSE	OPEN	CLOSE					
1.2-00-GAH-001	N.A.	N.A.	0.66 ± 0.03	0.48 ± 0.03	1.00 ± 0.03	0.16 ± 0.03	1.40 ± 0.03	0.30 ± 0.03	N.A.	N.A.	N.A.	400	400	400	N.A.
1.2-00-GAH-002	N.A.	N.A.	0.46 ± 0.03	0.46 ± 0.03	0.66 - 1.0	0.46 ± 0.03	1.6 - 1.7	0.30 ± 0.03	N.A.	N.A.	N.A.	400	400	400	N.A.
1.2-00-GAH-003	N.A.	N.A.	0.66 ± 0.03	0.4 ± 0.03	1.10 ± 0.03	0.46 ± 0.03	1.50 ± 0.06	0.30 ± 0.03	N.A.	N.A.	N.A.	300	400	400	N.A.

Figure V-5

Summary of Valve Times and Purge Settings

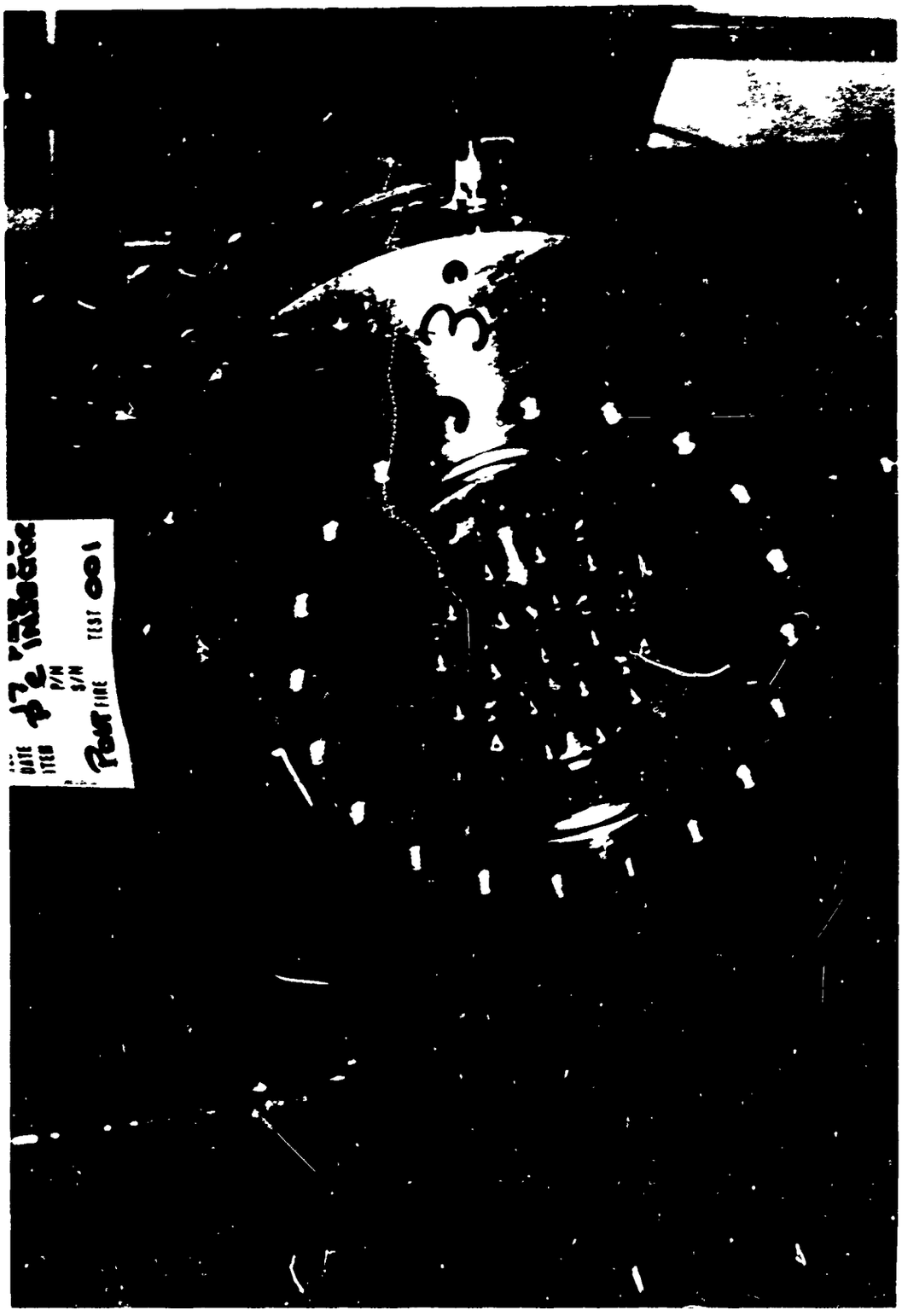

Primary Combustor Injector after Test 1.2-09-WAM-001

Figure V-6

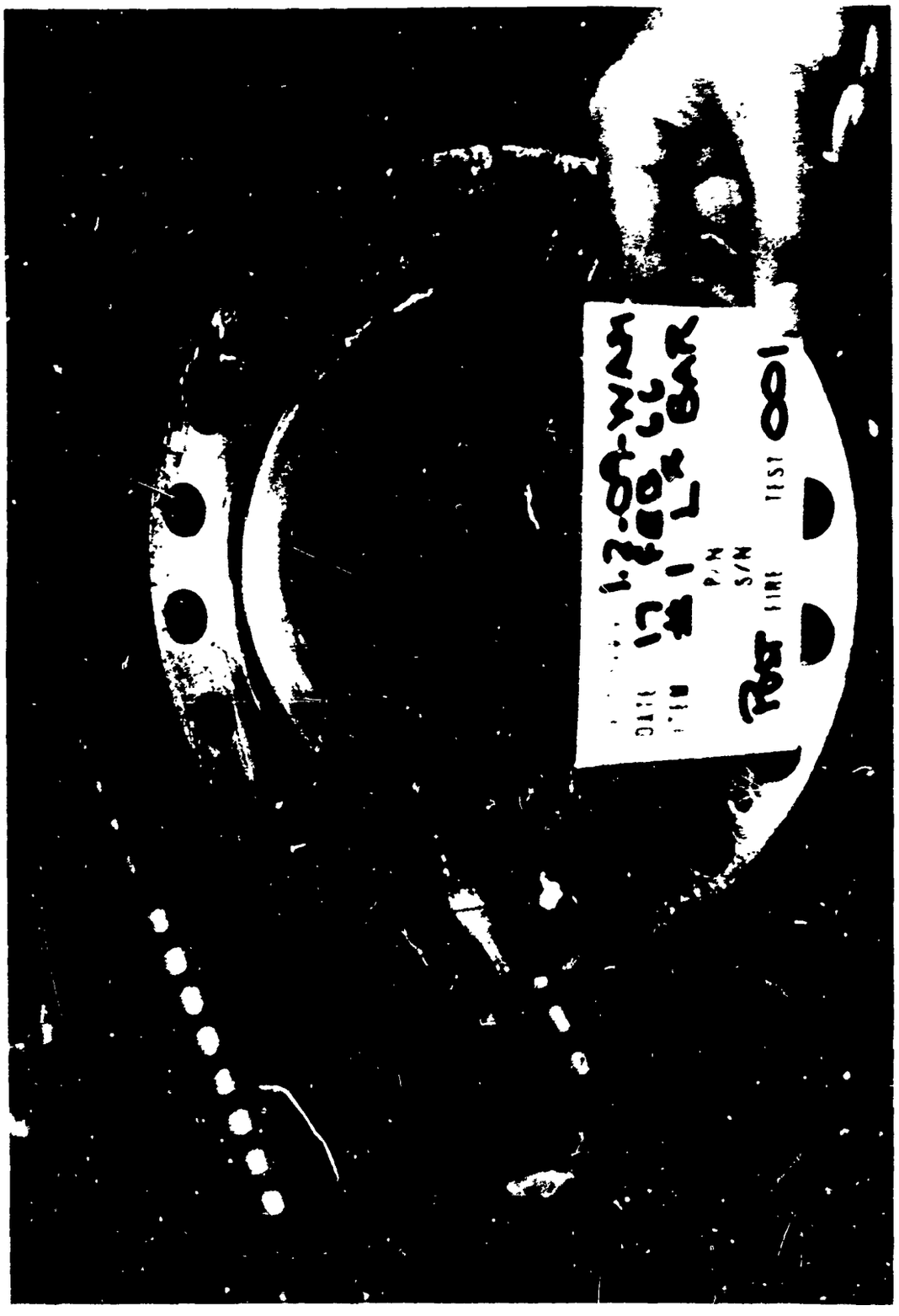

Primary Combustor Chamber after Test 1.2-09-WAM-001

Figure V-7

Primary Combustor Barrels after Test 1.2-09-WAM-002

Figure V-8

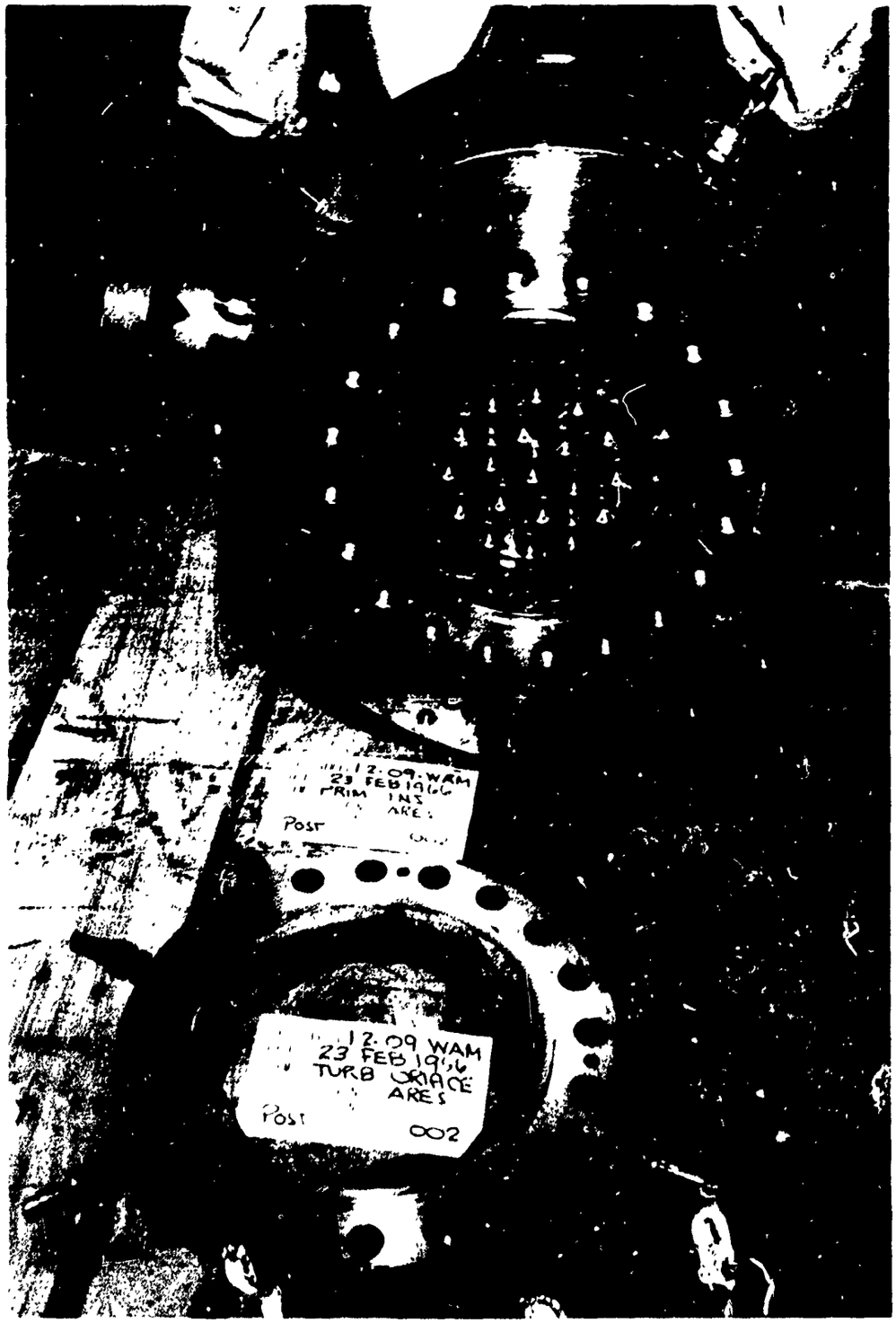

Primary Injector after Test 1.2-09-WAM-002

Figure V-9

Secondary Injector after Test 1.2-09-WAM-002

Figure V-10

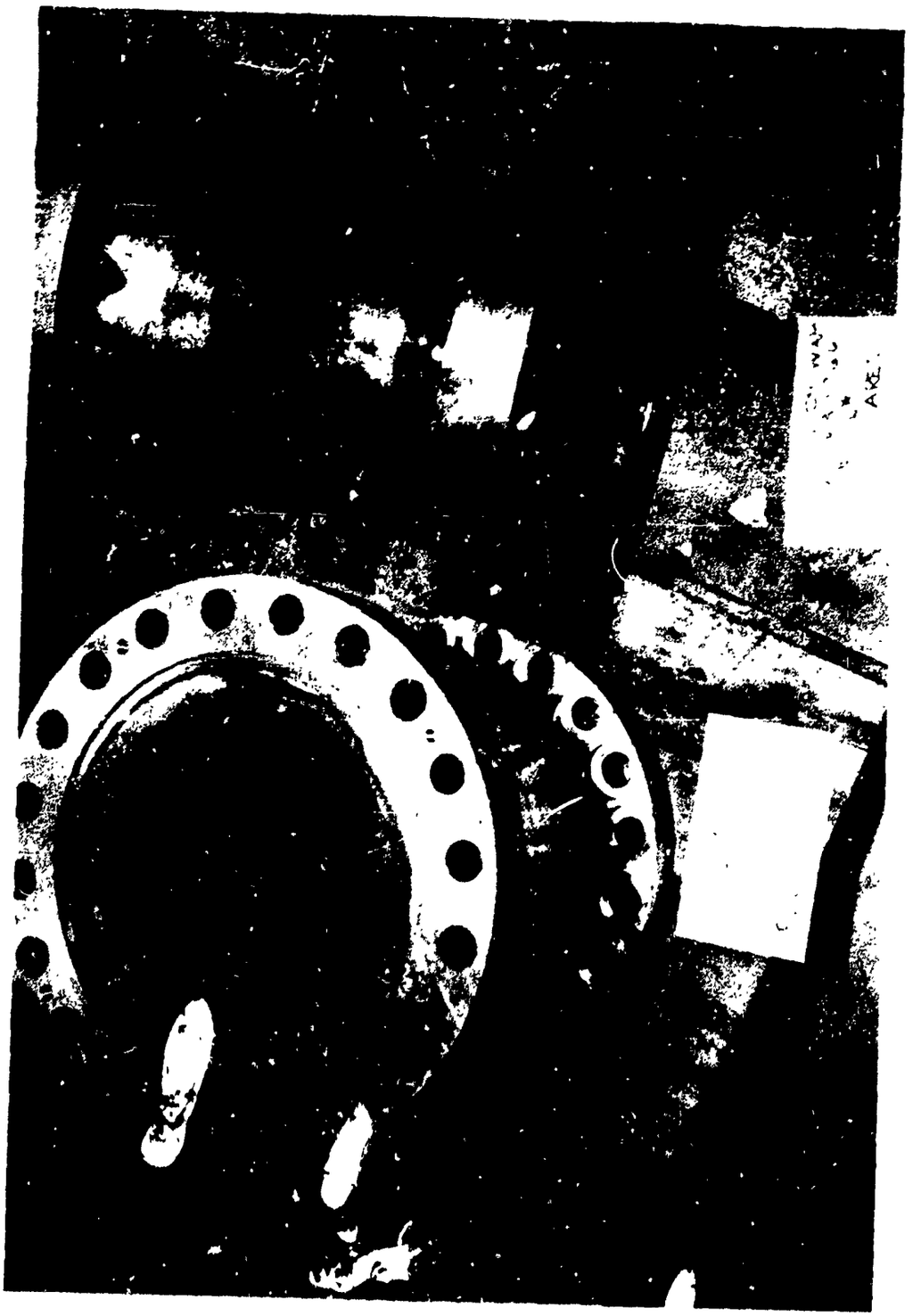

Primary Combustor Burnthrough after Test 1.2-09-WAM-002

Figure V-11

(This page is Unclassified)

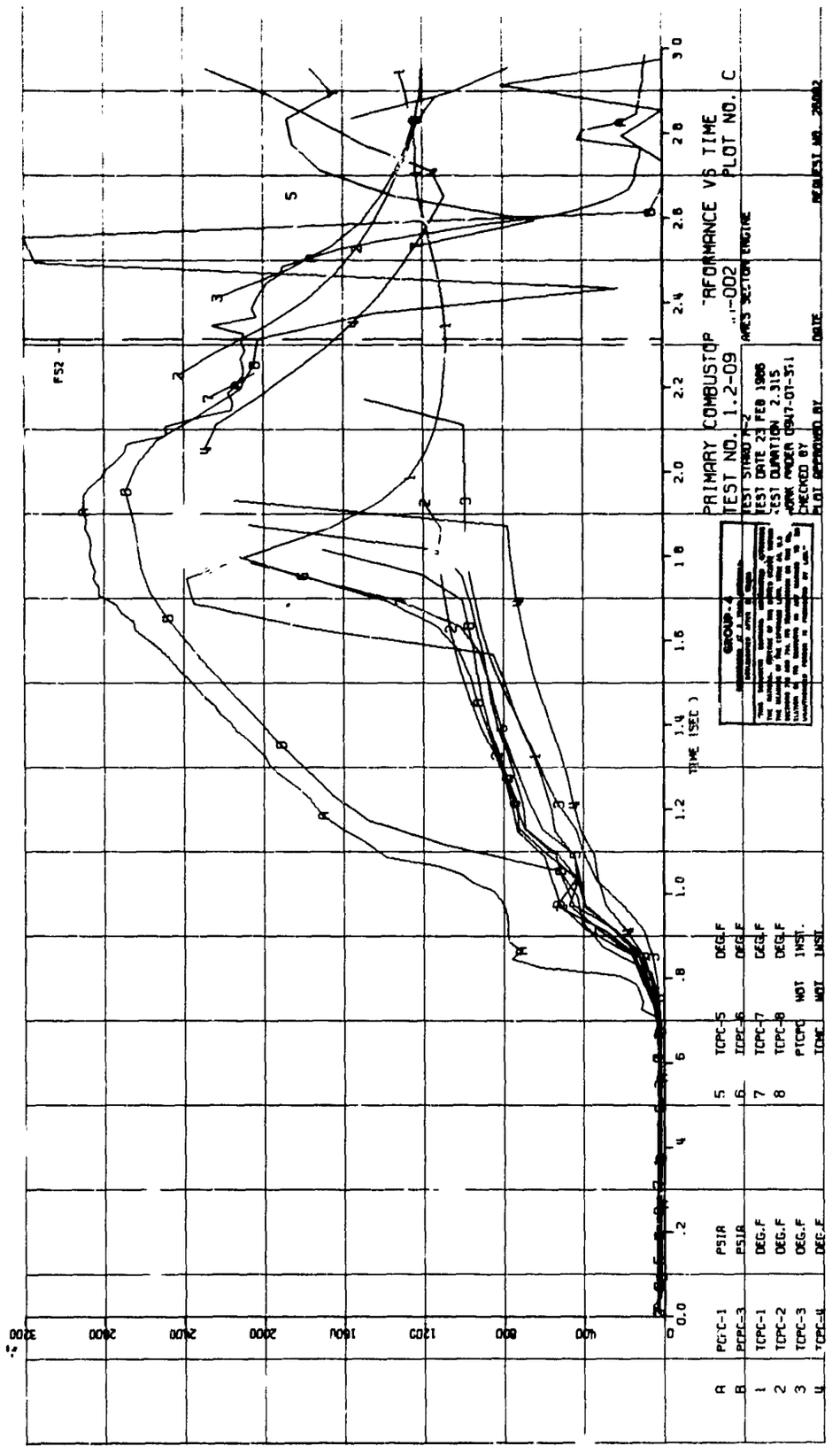

Figure V-12

Primary Combustor Performance vs Time, Test 1.2-09-WAM-002 (u)

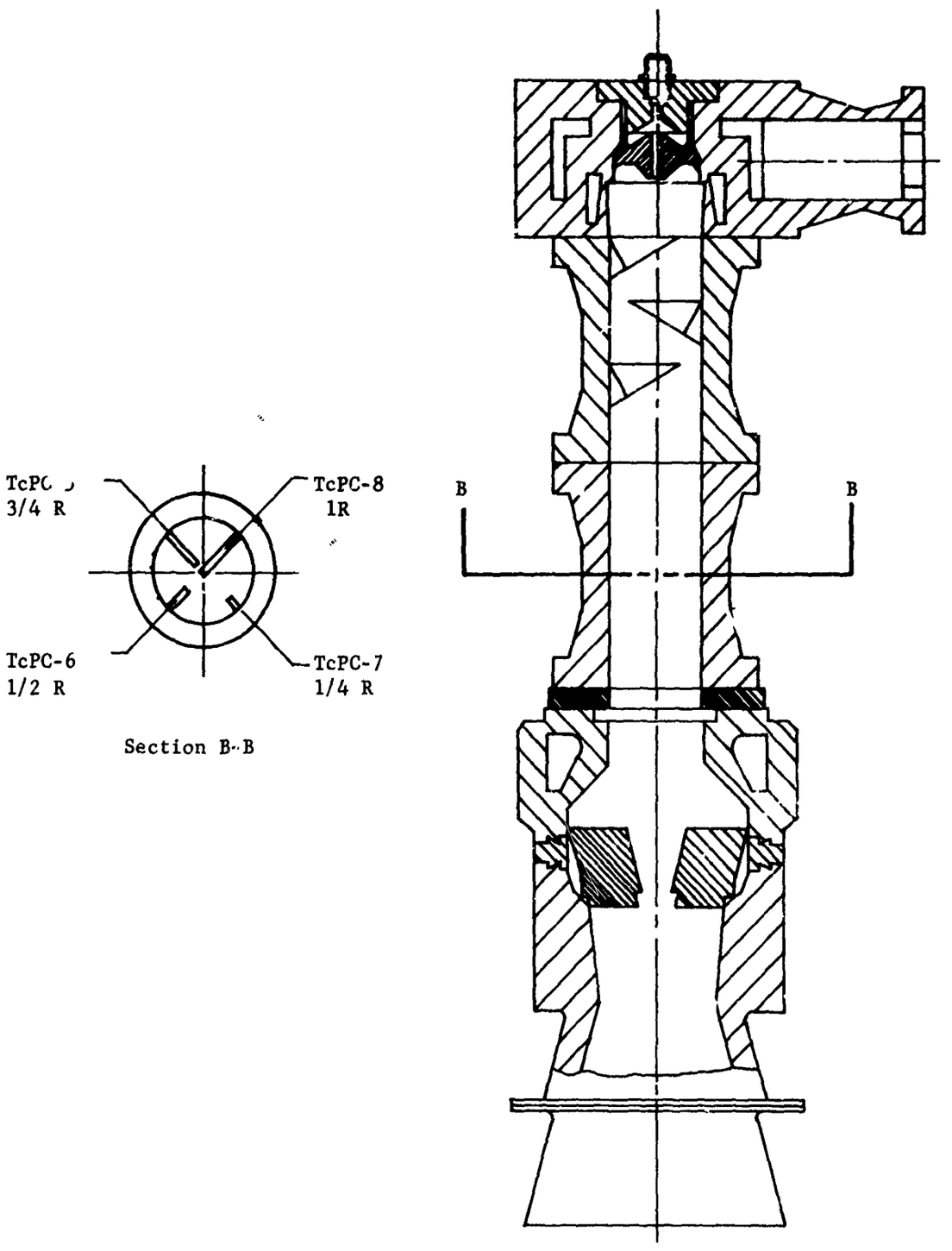

Section B-B

Primary Combustor Schematic, Test 1.2-09-WAM-003

Figure V-13

(This page is Unclassified)

	SYMBOL	UNITS	
TEST SERIES	--	--	1.2-09-WAM
TEST NUMBER	--	--	003
INJECTOR	--	--	MARK 12CA-8
DURATION	--	SECS	2.814
DATA PERIOD	--	SECS	1.960-1.460
NOZZLE TYPE	--	--	ABLATIVE
THROAT AREA	A_T	$IN.^2$	21.823
AREA RATIO	ϵ	--	17.31
CHARACTERISTIC LENGTH	L*	IN.	20.8
CHAMBER PRESSURE	P_C	PSIA	2845
INJECTOR MIXTURE RATIO	MR_J	--	2.592
ENGINE MIXTURE RATIO	MR_E	--	2.592
VACUUM THRUST	F_V	LB_F	106,558
ENGINE WEIGHT FLOW	$\dot{W}_E$	LB_M/SEC	377
CHARACTERISTIC EXHAUST VELOCITY $\frac{P_C A_T g}{\dot{W}}$	C*	FT/SEC	5,290
VACUUM SPECIFIC IMPULSE-MR_J (MEASURED)	I_{SV}	$\frac{LB_F\ SEC}{LB_M}$	283
MIXTURE RATIO DISTRIBUTION LOSS	--	$\frac{LB_F\ SEC}{LB_M}$	8.9
NOZZLE [illegible] LOSS	--	$\frac{LB_F\ SEC}{LB_M}$	2.7
NOZZLE FRICTION LOSS	--	$\frac{LB_F\ SEC}{LB_M}$	3.3
LOAD STREAM LOSS	--	$\frac{LB_F\ SEC}{LB_M}$	18.3
COOLING LOSS	--	$\frac{LB_F\ SEC}{LB_M}$	0
THEORETICAL VACUUM SPECIFIC IMPULSE	I_{SV-T}	$\frac{LB_F\ SEC}{LB_M}$	316
PERCENT COOLANT FLOW $\dot{W}_{FC}/\dot{W}_E$	% FC	%	0
PERCENT COOLING LOSS	% I_{SFC}	%	0
PERCENT COMBUSTION EFFICIENCY $\frac{P_C A_T g}{\dot{W}}$	% C*	%	95.68
PERCENT VACUUM SPECIFIC IMPULSE	% I_{SV}	%	89.49

Thrust-Chamber Performance Summary (u)

Figure V-14

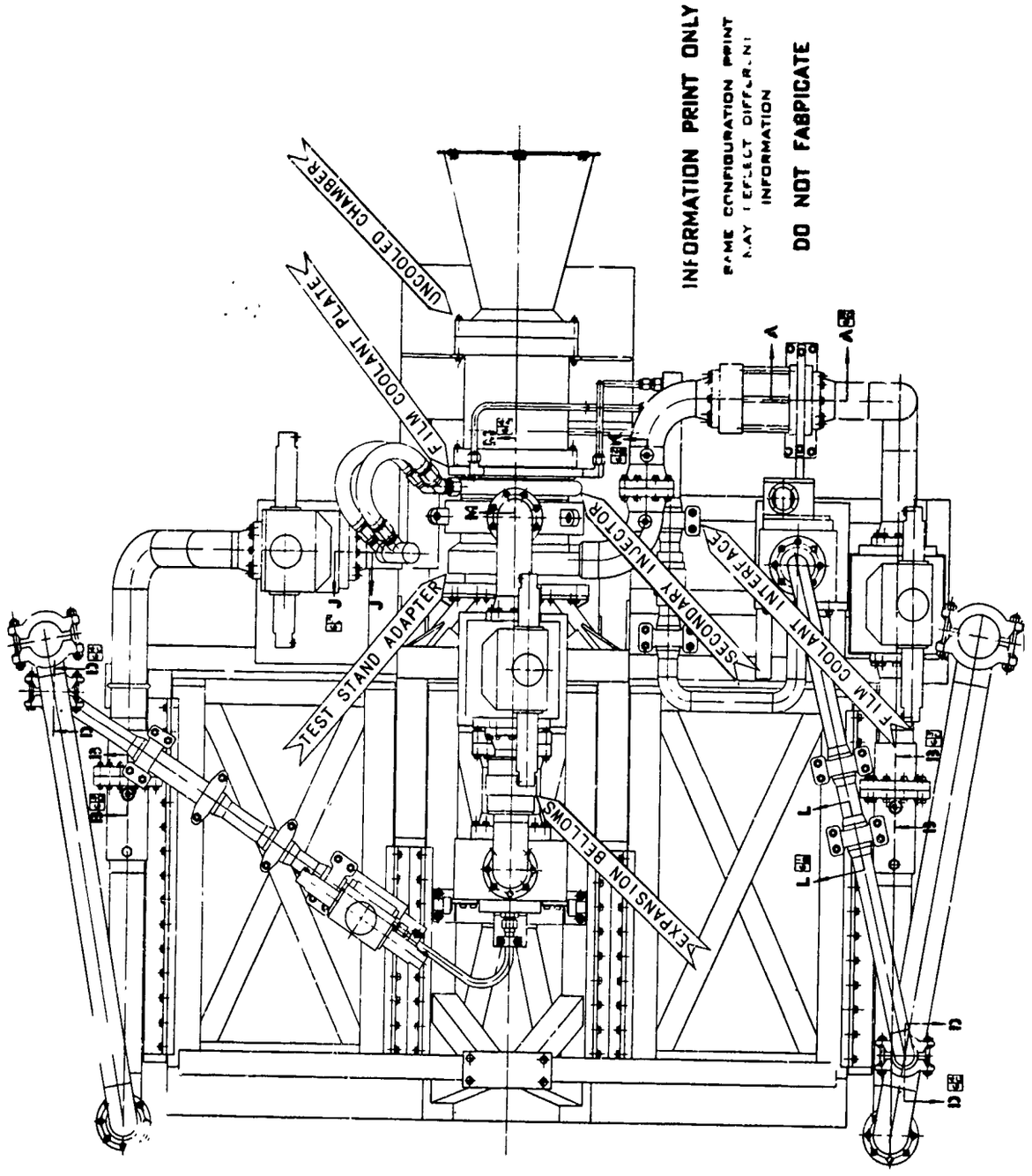

Modular Engine Configuration

Figure V-15

VI.

ADVANCED TPA

A. GENERAL

The major design effort was concentrated on finalizing the three-walled B-design TPA. Although an earlier study had indicated that the two-walled housing would be easier to fabricate, fabrication of the initial three-walled housings proceeded satisfactorily. It was therefore decided to continue with the three-walled design and to keep the two-walled design in reserve.

The configuration of the three-walled B-design TPA was changed only slightly (Figures VI-1 and -2). Heat-transfer, stress, critical-speed, and housing-deflection studies indicated no serious problems, although some areas are still undergoing detailed design analysis. The boost-pump designs were initiated, and a discussion of design concepts and preliminary design results is included in this report.

B. ADVANCED TPA DESIGN

The layout of the three-walled B-design TPA was completed and reviewed on 28 February 1966. The basic design was approved by Division Management, but several areas (e.g., cooling of the fuel bearing housing, the design of the primary valve-to-primary combustor feed-line bellows, turbine-shaft heat transfer and stress analysis, and turbine stator heat transfer and stress analysis) require some additional work.

Turbopump housing stresses and deflections were calculated and modifications made until acceptable values were obtained. The axial deflection of the housing between the bearings was given particular attention. To limit this elastic deflection to approximately 0.030 in. at proof conditions, the housing curvature and the wall thickness at the oxidizer end were increased slightly. A detailed discussion of these and other studies conducted on the TPA housing is included in Section VIII. The diameters of the rotating shaft and of the impeller labyrinth, the clearances, and the tooth configurations were also finalized and are shown in the TPA layout (Figure VI-2). The resulting axial thrust of the TPA rotating assembly is balanced when the first-stage fuel impeller (balancing piston) operates with an equal clearance of 0.010 at each land. The flows throughout the system remain essentially the same as those given in Report 10830-Q-2. A more detailed discussion of the axial-thrust studies is presented in Paragraph F, below.

Filters were incorporated for bearing-coolant and combustion-seal propellant flows. The locations selected are shown in Figure VI-2; the filter size considered for this application is about 10 microns. The oxidizer filter, shown in Figure VI-2, is self-cleaning and filters a total of 35 gpm. Of this total, 15 gpm flows through the oxidizer-end roller bearing and the remainder is divided equally between the upstream leakage at the turbine rotor and the required flow to the combustion seal. On the fuel-pump side, the entire flow of 187 gpm to the second-stage pump must be filtered to provide 19 gpm of filtered coolant to the fuel

VI, B, Advanced TPA Design (cont.)

roller bearing. The combustion seal requires 8 gpm of filtered fuel from the second-stage pump discharge. Two filter locations were considered: (1) a self-cleaning design in the first-stage fuel pump volute and (2) a nonself-cleaning design shown in Figure VI-2. The latter location was selected because the self-cleaning design located in the fuel-pump volute is not removable and is therefore considered undesirable for TPA development testing. However, for a production engine, this location would be preferred because a filter with a larger area could be incorporated.

On the basis of radial deflections of the fuel-pump housing and on the downstream temperature distributions in the combustion seal, cooling of the fuel bearing housing appears desirable to ensure proper bearing fits and to minimize potential hot spots on the turbine exhaust liner. The oxidizer flow (Figure VI-2) to be utilized for this cooling is tapped off behind the fuel-housing piston ring and flows at about 50 ft/sec along the outer wall of the fuel bearing housing to the downstream side of the combustion seal where it is mixed with fuel and burns with the turbine exhaust gases. Detail design of the cooling passages is now in process. Test data from the rotating-combustion-seal tests will be used to finalize the design.

The turbopump instrumentation layout was completed and is shown in Figure VI-3. Instrumentation includes sufficient static-pressure taps to calculate the TPA axial thrust and to compare these values with the measured balance-piston operating position. If necessary, the axial thrust will be corrected by changing the diameter of the labyrinth or by adjusting the flow-path resistances. In addition to monitoring these pressures and thrust-balance positions, the bearing temperatures and the strain-gage readout on the thrust bearing will also be monitored to obtain thrust-balance information. Pressures and temperatures will also be measured throughout the TPA assembly to determine pump, turbine, primary-combustor, and valve performance.

Turbopump stackup tolerances and shimming requirements were determined, and a summary of critical pump buildup and operating clearances is given in Figure VI-4. These dimensions will be incorporated on the master layout drawing. Also, the test-fixture layouts for the pumps (Figures VI-5 and -6) are nearing completion, and tester layouts for the inducer, the boost pump, and the hydraulic turbine will follow.

C PUMP DESIGN

The pump hydraulic analysis was completed. The pump wear-ring leakages resulting from the selected operating clearances and from the predicted pressure schedule are essentially the same as those given in Report 10830-Q-2. Alternative wear-ring designs considered for the oxidizer impeller are included as auxiliary views on the TPA layout (Figure VI-2); their effects on oxidizer pump efficiency for the various types of wear-ring designs are summarized in Figure VI-7. As shown,

VI, C, Pump Design (cont.)

oxidizer impeller wear-ring clearances for the straight labyrinths could be increased from their present nominal value of 0.007 to 0.015 in. without penalizing the overall TPA performance too severely. Wear ring development work is further discussed in Section X.

The final stress analysis on all main-stage impellers and inducers was completed, and a summary of the impeller materials and margins of safety at critical locations is given in Figure VI-8.

Cast Aluminum 356 was found to be inadequate for both main-stage impellers; the fuel impeller will therefore be made from titanium, 6Al-4Va alloy. This heavier fuel impeller reduced the critical speed from 51,800 to 51,600 rpm. The oxidizer impeller will be made from Aluminum 6061-T6. Although steel was considered, it was not selected because the critical speed would decrease 4,000 rpm and fall below the desired design value of 48,000 rpm. With these new materials, the margins of safety are very adequate for all impellers and inducers.

D. TURBINE

Parts for the air-testing of two designs were ordered. The highly twisted blade design described in Report 10830-Q-2 has been ordered, and delivery of hardware for air-testing is expected in mid July. In addition to this design, a less complex blade geometry (constant cross section from hub to tip) will also be fabricated and tested. The results of these tests will determine the efficiency that can be obtained with rotors having optimum and less-than-optimum blade angles.

A summary of turbine critical clearances and blade stresses is given in Figures VI-6 and VI-8, respectively; since the turbine blade root stresses are quite high at 44,000 rpm, extended overspeed operation at the maximum turbine inlet temperature of 1500°F will be limited to several minutes only. At 40,000 rpm, the turbine has an adequate margin of safety of 0.14.

E. SHAFT

The critical-speed analysis for the B-design turbopump was completed; the results are summarized in Figure VI-9. Case 1 (i.e., critical speed, 55,600 rpm, for the rotating assembly only) neglects the housing and thrust-chamber effects. Case 2 illustrates that the mass of the housing and the spring rates of the bearing support are sufficiently large to have little effect on the critical speed of the rotating assembly. Cases 3 through 15 show the effects of increased rotating component weights, various bearing spacings, and reduced bearing sizes on critical speed. These cases illustrate that changes on the oxidizer side greatly influence the critical speed, whereas changes on the fuel side have a much smaller effect. The combined influence of housing and thrust-chamber effects on critical speed is shown as Case 16; the resulting value of 51,800 rpm is more than 20% above the design speed of 40,000 rpm.

VI, E, Shaft (cont.)

A purchase order was placed for 3-in.-dia UDIMET 700 bar stock, and delivery is due in July. This material will be used to establish the tensile, notch-tensile, and fatigue properties of electron-beam-welded butt joints at room and elevated temperature. The 3-in. diameter was selected as being representative of the turbine-shaft weldment design. Heat-transfer results of the finalized turbine-shaft designs for slot depth of 0.31 and 0.56 in. between the turbine disc and the combustion seal are shown in Figures VI-10 and -11, respectively. As can be noted, a large temperature gradient exists at the root of the small slot, but this gradient is reduced considerably with the deeper slot. The heat-transfer analysis was based on a maximum absolute turbine inlet temperature of 1500°F; however, as noted on Figures VI-10 and -11, the maximum total temperature that the rotor can experience is 1360°F because the inlet relative velocity of the gas is considerably less than the absolute velocity and thus results in the lower relative total temperature.

F. AXIAL THRUST AND BEARING DESIGN

1. Axial Thrust Balance

The modifications to the axial-thrust-balance computer program (changing the mathematical model from the A- to the B-turbopump configuration with dual-acting thrust-balance piston) were completed. The steady-state analysis was also completed. This analysis investigated the effects of various parameters, i.e., wear-ring and shaft-labyrinth radial locations and clearances. It should be noted that the axial forces on this rotating system are very large (the summation in each direction is about 200,000 lb) and that the pressure distribution is based on a complex flow network which is subject to tolerances and deflections. Therefore, the dimensions predicted to give a thrust force of zero are not expected to be exact. However, the parameter-variance study permits the conclusion that thrust balance can be achieved by modifying certain component dimensions. The two dimensions which have the most significant effect upon axial thrust are the radii of the wear rings located on the inlet and on the backside of the oxidizer impeller.

Further analysis of the dual-acting balance-piston design resulted in the reduction of the maximum flow rate (at the zero-thrust position) from 200 to 140 gpm. This was accomplished by decreasing the radial clearances of the inlet labyrinths at the impeller shroud tips from 0.010 to 0.007 in. Figure VI-12 compares the total and the single-side flow rates for both radial clearances. Figure VI-13 shows the load-deflection curve as a function of this labyrinth clearance. The 0.007-in. labyrinth clearances result in a slightly lower spring rate under low axial loads, but the total load capacity would remain unchanged. Figure VI-14 is a plot of balance-piston stiffness versus axial-land clearance. In this case, the smaller clearance (0.006 in.) results in a much stiffer system, which is desirable; however, the combined effects of fuel-pump housing deflections, fuel-impeller deflections, and machining tolerances would make it difficult to maintain this small axial clearance.

VI, F, Axial Thrust and Bearing Design (cont.)

Based on this analysis and on expected operational conditions, an inlet labyrinth radial clearance of 0.007 in. and an axial land clearance of 0.010 in. appear to be the best selection.

Figure VI-15 is a plot of initial start-transient unbalance forces and axial displacements of the rotating assembly for the nominal computer steady-state mathematical model. This plot was based on the ARES engine start transient as presented in Report 10830-Q-2, Figure XV-1. The maximum deflection of the rotating assembly occurs at about 1.7 sec when pump discharge pressures are low in comparison with pump suction pressures. The maximum ball-bearing load is 370 lb and the force on the thrust balancer toward the oxidizer impeller is 645 lb. As the pressure levels throughout the turbopump rise, the thrust reverses, and the maximum ball-bearing and thrust-balancer forces are 370 and 3000 lb, respectively, in the direction of the fuel impeller. When steady-state conditions are reached, the axial position of the balancer is not at zero (nominal setting). Balance-piston operation at the zero position could be achieved by slightly changing the geometry of the wear ring or of the shaft labyrinth. However, this steady-state condition (i.e., an axial displacement of 0.0038 in. and an unbalance force of 2100 lb) is acceptable and would be within the expected allowable variation resulting from fabrication tolerances and pump performance variations.

Further analyses will be performed to determine the effects of the thrust-balance system on start transient and steady-state performance caused by variations in clearances, flow-passage resistances, and pump performance.

2. Bearing Design and Development

The spring rate of the diaphram which supports and allows axial movement of the duplex ball-bearing set was increased from 32,000 to 60,000 lb/in. With this spring rate, an axial load of 420 lb is required to bottom the diaphram out in either direction (the $\pm$ 0.007-in. allowable travel remains the same). This higher spring rate results in a stiffer shaft system during the start transient. The start transient, as plotted in Figure VI-15, was calculated considering this higher-spring-rate diaphram.

The roller-bearing cages are being modified as a result of a cage failure in the wear-ring Hydrolab test program. (This failure is discussed in Section X.) In this program, the bearing is water-lubricated. The lubricating properties of water appear to be very similar to those of AeroZINE 50, and, as a result, similar roller-end wear occurs. The design modification consists of riveting every web (only three webs are presently rivetted) for increased rigidity and of removing the pocket stickout of the aluminum shroud. The only function of this stickout is to retain the rollers in the cage when the outer race is removed.

It should be noted that the unmodified cage performed very well in 40,000-rpm tests with N_2O_4, as discussed in Section IX.

VI, F, Axial Thrust and Bearing Design (cont.)

Alternative cages of the design used in the successful 25,000-rpm tests are presently being fabricated and are scheduled to be available by the end of April.

Figure VI-16 is a tabulated comparison of ball- and roller-bearing contact stresses of the ARES bearing designs (at 40,000 rpm) with load requirements of the work statement and with the results of bearings successfully tested at 25,000 rpm. This tabulation shows that the ARES bearing stresses are essentially the same as those of the 25,000-rpm tests.

G. SEALS

A complete discussion of the seal development is given in Section XI.

H. TURBOPUMP HOUSING

A complete discussion of housing analysis and development is given in Section VIII.

I. BOOST PUMP

A design review of boost-pump concepts was held on 25 February 1966. Two concepts were presented: (1) an axial-flow design which requires a thrust-balance piston, and (2) a mixed-flow design (impeller discharge between radial and axial direction) which can be balanced without a piston (Figure VI-17). The mixed-flow design, although 5 lb heavier than the axial-flow design, was selected because of its simplicity. Also, it was decided that the oxidizer and fuel boost pumps should incorporate as many interchangeable parts as possible because the weight penalty thus incurred would be sm

The design specifications for the boost pump and hydraulic turbine remained unchanged from those given in Report 10830-Q-2 except for the fuel pump speed, which was reduced from 8000 to 7300 rpm to permit the use of the oxidizer hydraulic turbine rotor and nozzle vane on the fuel boost pump. The only difference in oxidizer and fuel turbines is the partial admission area, which is 3.4% for the oxidizer and 2.3% for the fuel.

The low arc of admission and the high turning loads on the turbine rotor blades require a high-strength blade material with good endurance properties. The selected material, AM-350, satisfies these requirements and results in a safety factor of 1.14 (preliminary analysis). The single-admission design was selected because of the small turbine-nozzle area, which, however, results in a radial bearing load of about 800 lb. Combined with this load, the bearings are required to carry an axial load of 1200 lb, which results in a predicted bearing life of 39 hr.

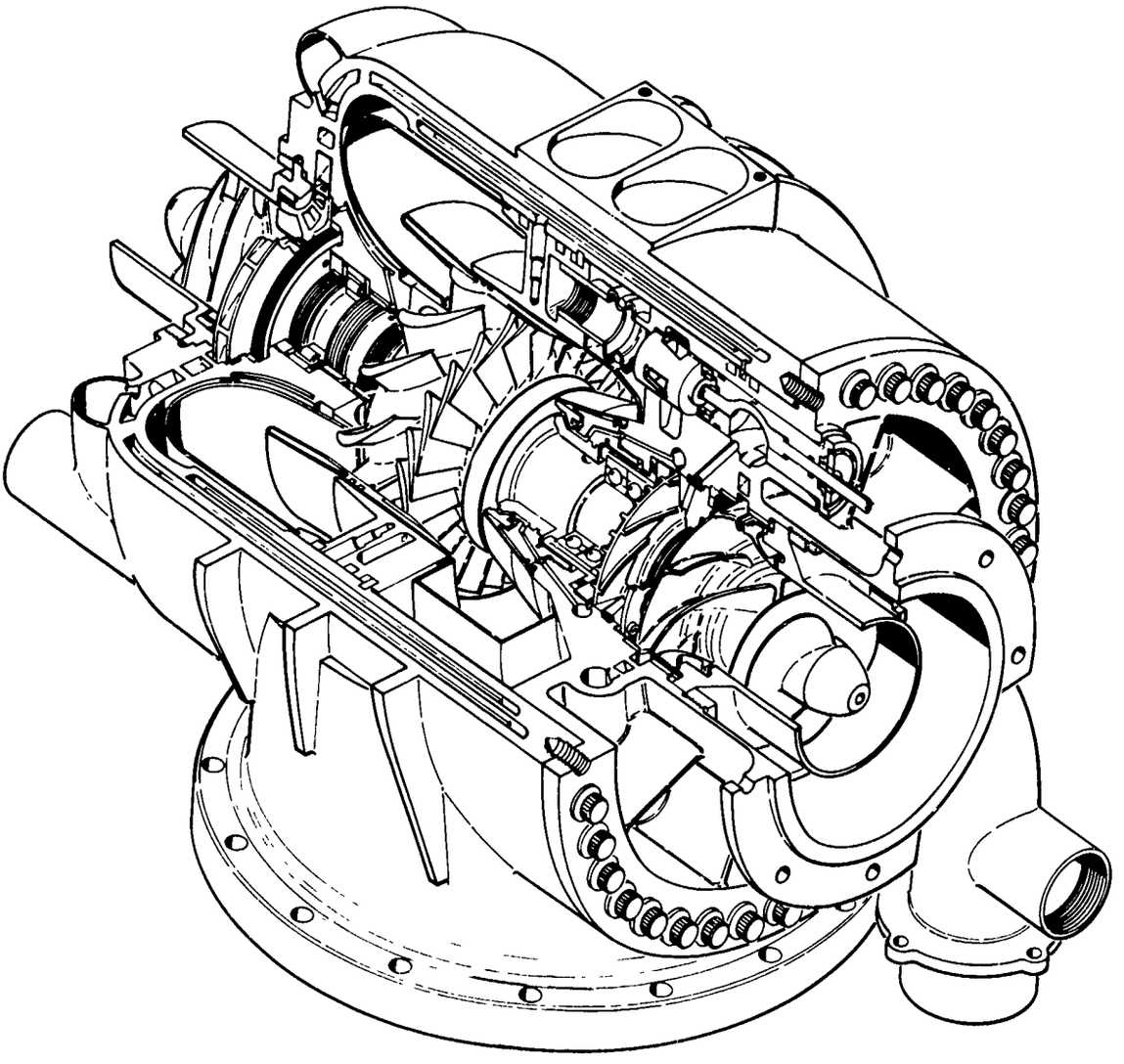

Turbopump Assembly, Isometric View (u)

Figure VI-1

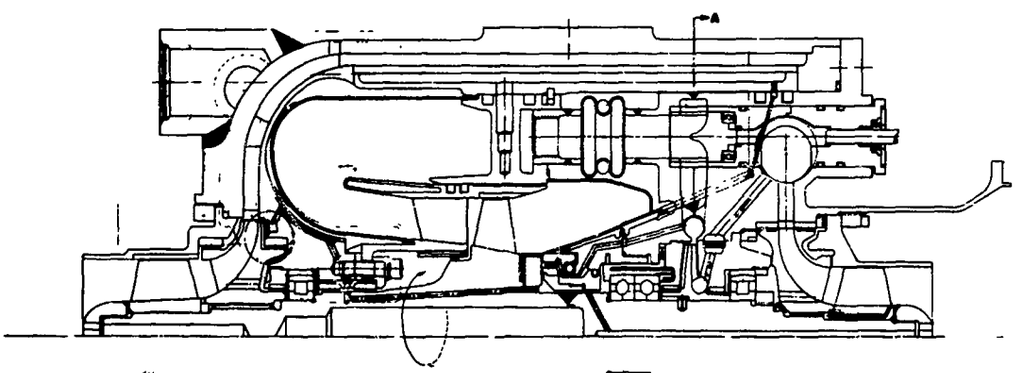

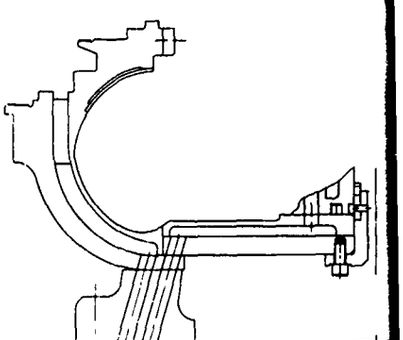

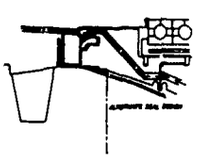

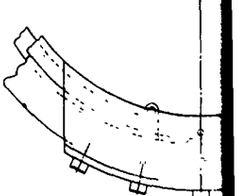

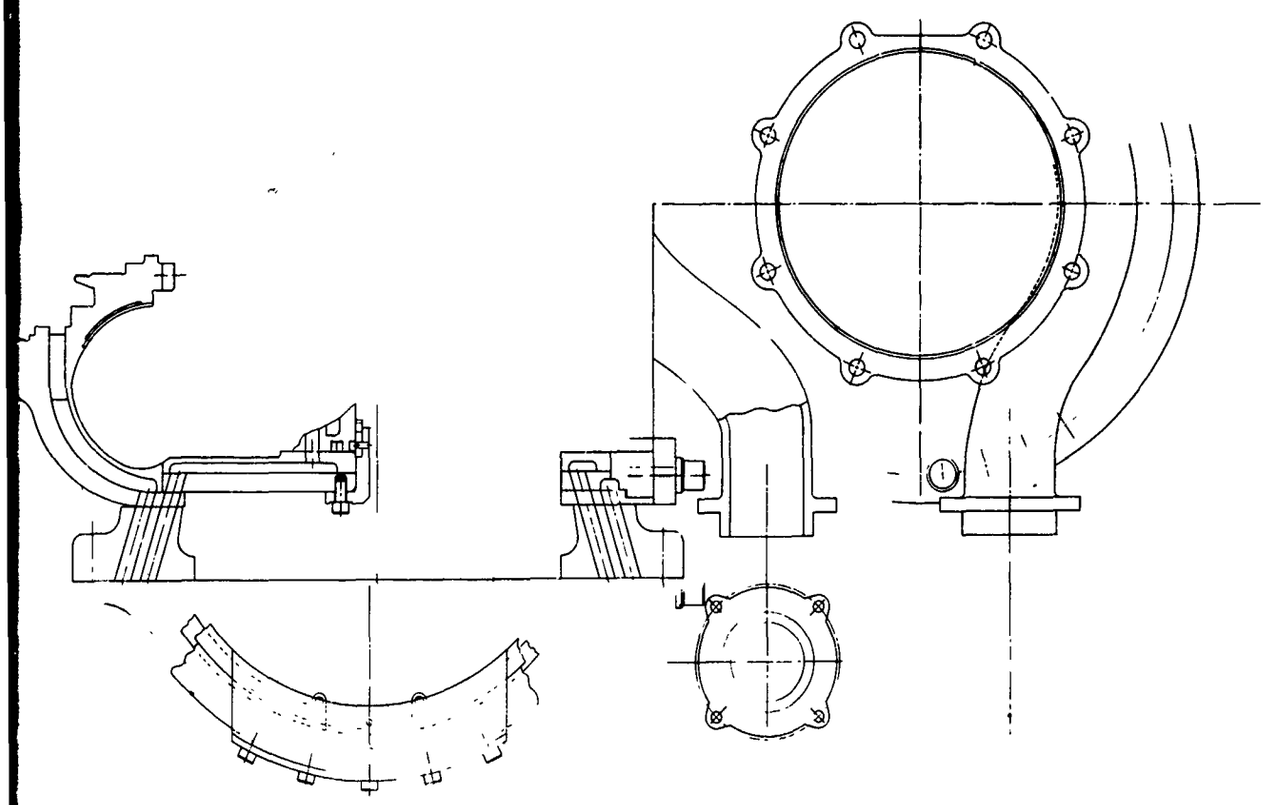

Turbopump Assembly Layout, B-Design (u)

Figure VI-2

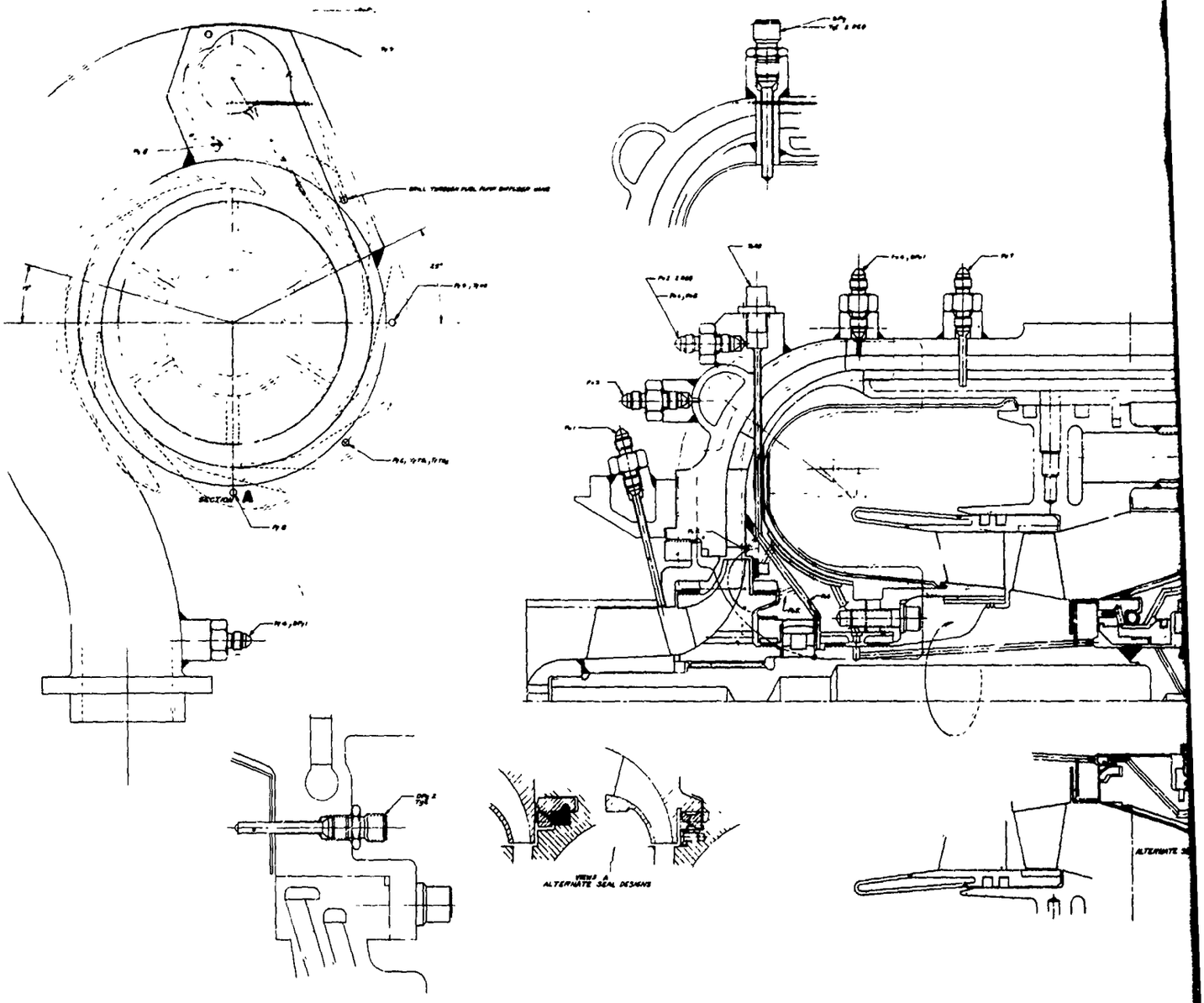
SECTION A-A
VIEWS A
ALTERNATE SEAL DESIGNS

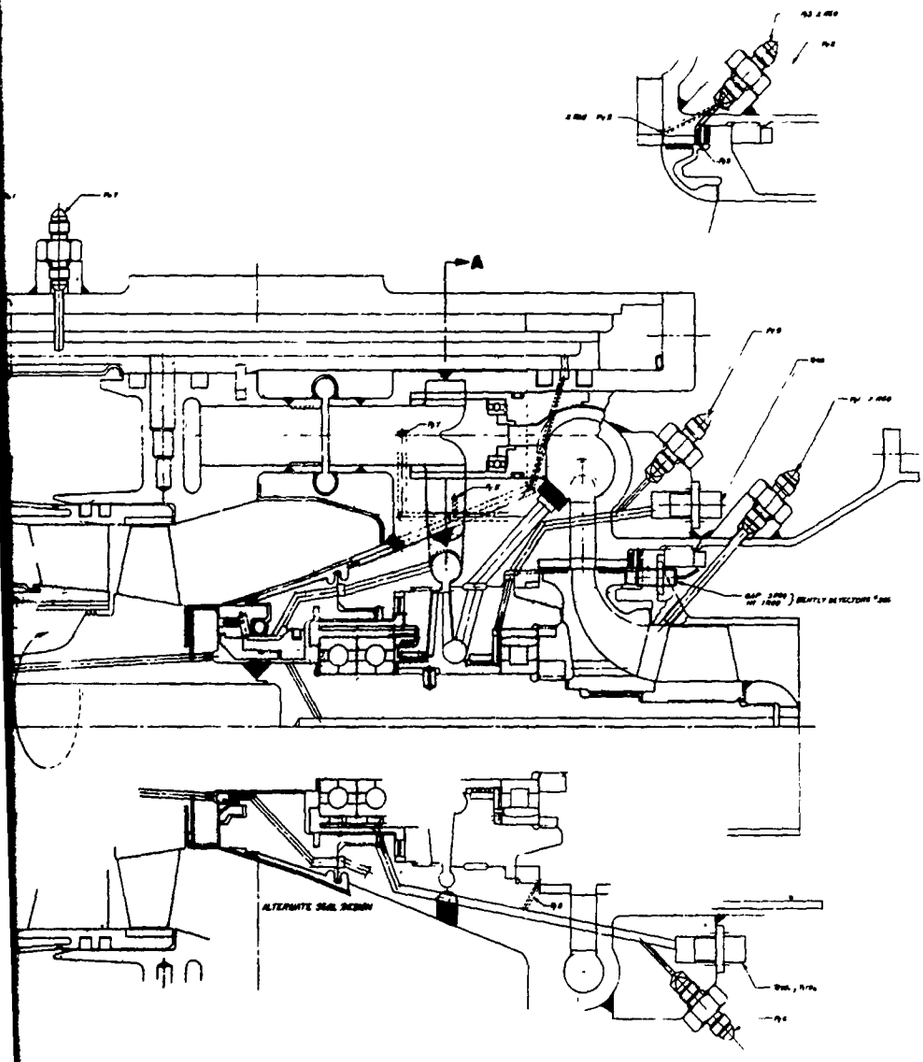

Turbopump Assembly Instrumentation (u)

Figure VI-3

	Critical Clearances, in.			
	Axial		Radial	
	Build Up	Hot Running	Build Up	Hot Running
Oxidizer impeller shrouded wear ring	0.050	0.028 cold* 0.040 hot**	0.006	0.007 (nom) 0.003 (min)
Oxidizer housing bearing fit	--	--	0.0001	0.00018 cold* 0.0007 hot**
Fuel housing bearing fit	--	--	0.0001	0.00049 cold* 0.0003 hot**
Fuel impeller shrouded wear ring			0.009	0.007 (nom) 0.004 (min)
Fuel impeller balance piston land	0.010	0.003 0.017	--	--
Primary combustor and oxidizer housing	--	--	0.0055	0.0016 (nom)
Turbine rotor tip	--	--	0.020	0.032 (nom)
Turbine stator - primary combustor	--	--	0.040	0.010 (nom)
Turbine stator-rotor	0.090	0.085	--	--

NOTE: Conditions considered include housing temperature (400°F oxid. side and 250°F fuel side), housing growth and misalignment, shaft deflections (critical speed, unbalanced loads), 0.0015 radial runout, and impeller growth.

* Cold--Initial start-up conditions
** Hot--Steady-state conditions

Critical Turbopump Clearances at Nominal Operating Conditions

Figure VI-4

(This page is Unclassified)

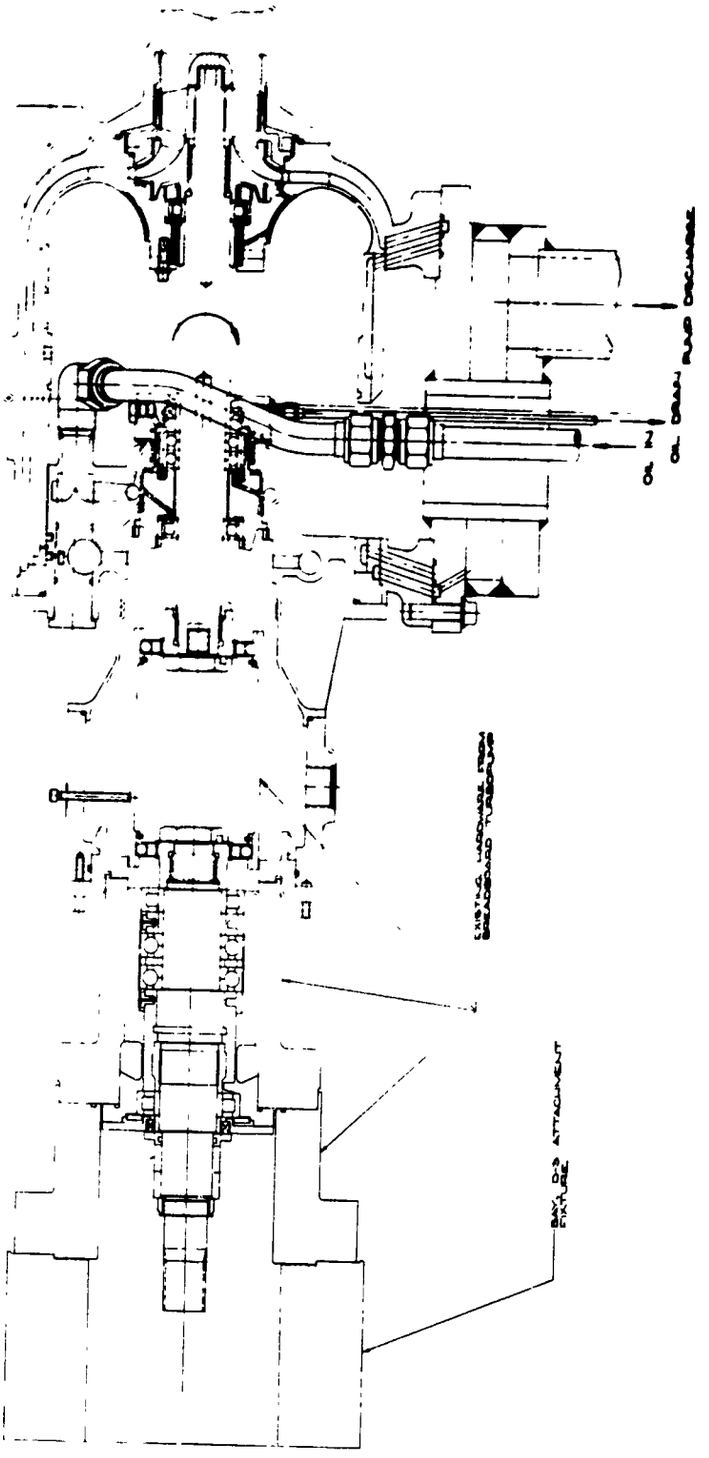

Test-Fixture Layout, Oxidizer Pump

Figure VI-5

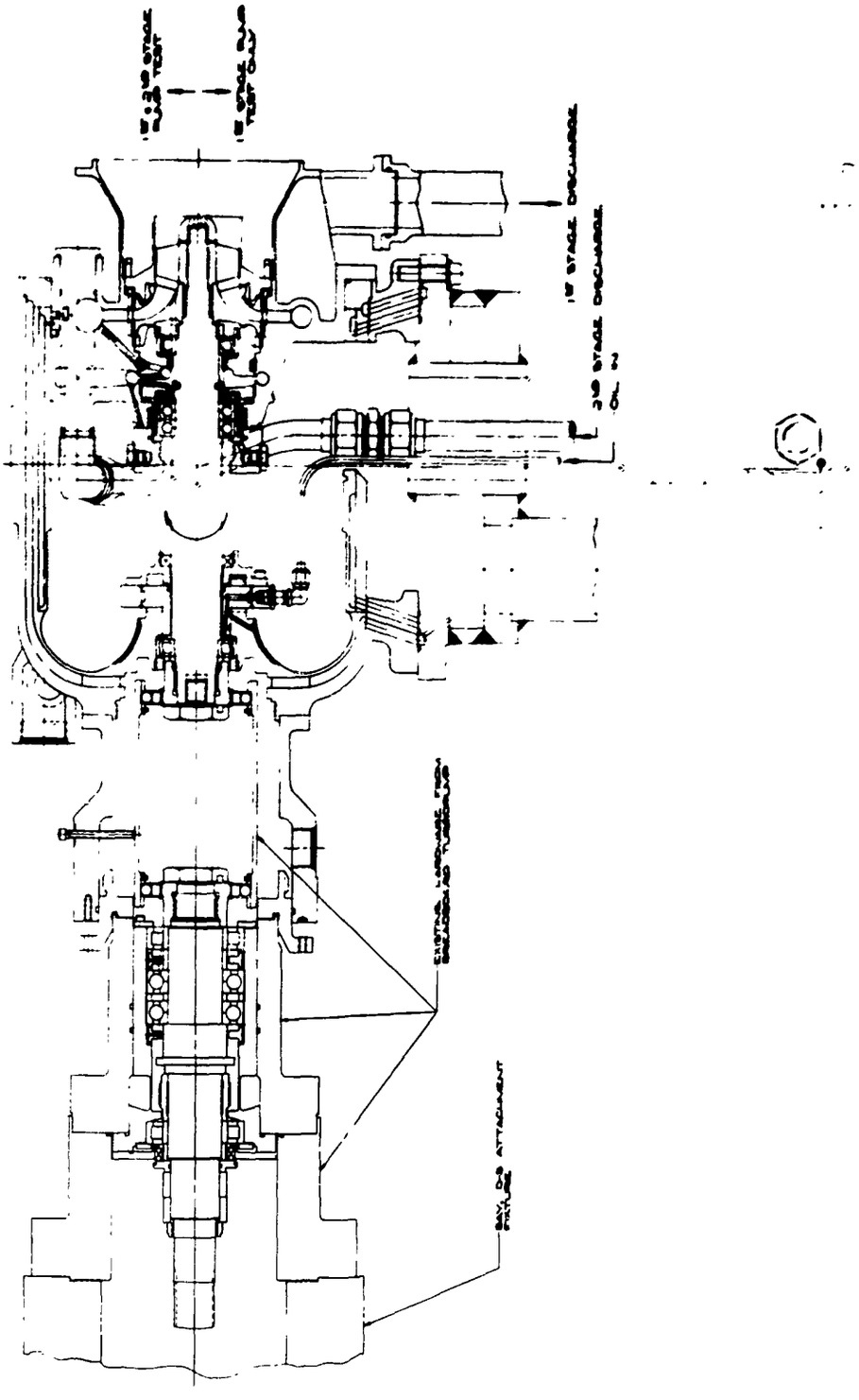

Test-Fixture Layout, Fuel Pump

Figure VI-6

TYPE OF WEAR RING	ESTIMATED LEAKAGE (GPM)	OX PUMP EFFICIENCY %	Δt ON TURBINE
1. STRAIGHT LABYRINTH 0.015-in. CLEARANCE	260	69.0	+35
2. STRAIGHT LABYRINTH 0.007-in. RADIAL CLEARANCE	121	75.0	-7°
3. STEPPED LABYRINTH 0.015-in. RADIAL CLEARANCE	206	71.5	+18
4. STEPPED LABYRINTH 0.007-in. RADIAL CLEARANCE	96	76.5	-18
5. RADIAL HYDROSTATIC 0.0014-in. CLEARANCE	49	79.0	-35°
6. AXIAL HYDROSTATIC 0.001-in. CLEARANCE	22	80.0	-42°

NOTES:

1. BASIC OX. PUMP EFFICIENCY HAS BEEN USED AS 74% FOR CYCLE ANALYSIS.
2. EACH PERCENT CHANGE IN OX. PUMP EFFICIENCY REQUIRES 7°F CHANGE IN TURBINE INLET TEMPERATURE TO BALANCE THE CYCLE.

Pump Wear-Ring Leakage vs Oxidizer-Pump Efficiency

Component	Material	Margin of Safety*
Inducers		
Oxidizer	A-286	0.26
Fuel	T_1-6_{Al}-4_{Va}	0.52
Mainstage Impeller		
Oxidizer, hub	Al-6061	0.52
Oxidizer, spline	Al-6061	0.21
First Stage, fuel, hub	T_1-6_{Al}-4_{Va}	0.65
First Stage, fuel, spline	T_1-6_{Al}-4_{Va}	2.99
Second Stage, fuel, hub	A-286	0.13
Turbine		
Rotor Blade	UDIMET 700	
Endurance, 10^8 cycles (40,000 rpm)		0.14
Endurance, 10^5 cycles (44,000 rpm)		0
Stator	UDIMET 700	400 cycles**

*Based on 1.1 Safety Factor
**Based on Low Cycle Fatigue Criteria

Pump and Turbine Stress Summary--Critical Areas

Figure VI-8

Case		Critical Speed		Brg Load @ 40,000 rpm	
		cps	rpm	Oxid, lb	Fuel, lb
1.	Rotating Assembly	928	55,600	465	365
2.	Rotating Assembly and Housing	945	56,600	360	220
3.	1 + Oxid. Ind. = 1/3 x Wt.	1020	61,200	420	275
4.	1 + Fuel Ind. = 2/3 x Wt.	930	55,700	460	260
5.	1 + Oxid. Imp. = 3 x Wt.	860	51,600	565	250
6.	1 + Fuel Imp. = 3 x Wt.	910	54,600	455	300
7.	1 + Turbine = 1.4 x Wt.	890	53,400	510	315
8.	1 + Turbine = 1.8 x Wt.	830	49,800	585	390
9.	1 + Brg. Span = 0.875 in.	950	57,000	465	215
10.	1 + Brg. Span = +0.875 in.	880	52,800	470	330
11.	1 + Riding Elements Removed	830	49,900	--	--
12.	1 with 35-mm Brg. on Oxid. End Only	808	48,500	449	253
13.	1 with 35-mm Brg. on Fuel End Only	910	54,600	465	246
14.	1 with Oxid. Imp. Overhang Extended 0.55 in.	809	48,500	523	235
15.	1 with Fuel Imp. Overhang Extended 0.50 in.	840	50,500	444	271
16.	1 with TPA Hsg & TCA Mass Effects TPA Mount Spring Rate Assumed as 0.5 (10^6) lb/in.	864	51,800	390	215

Advanced TPA B-Design Critical-Speed Summary

Figure VI-9

Report 10830-Q-3

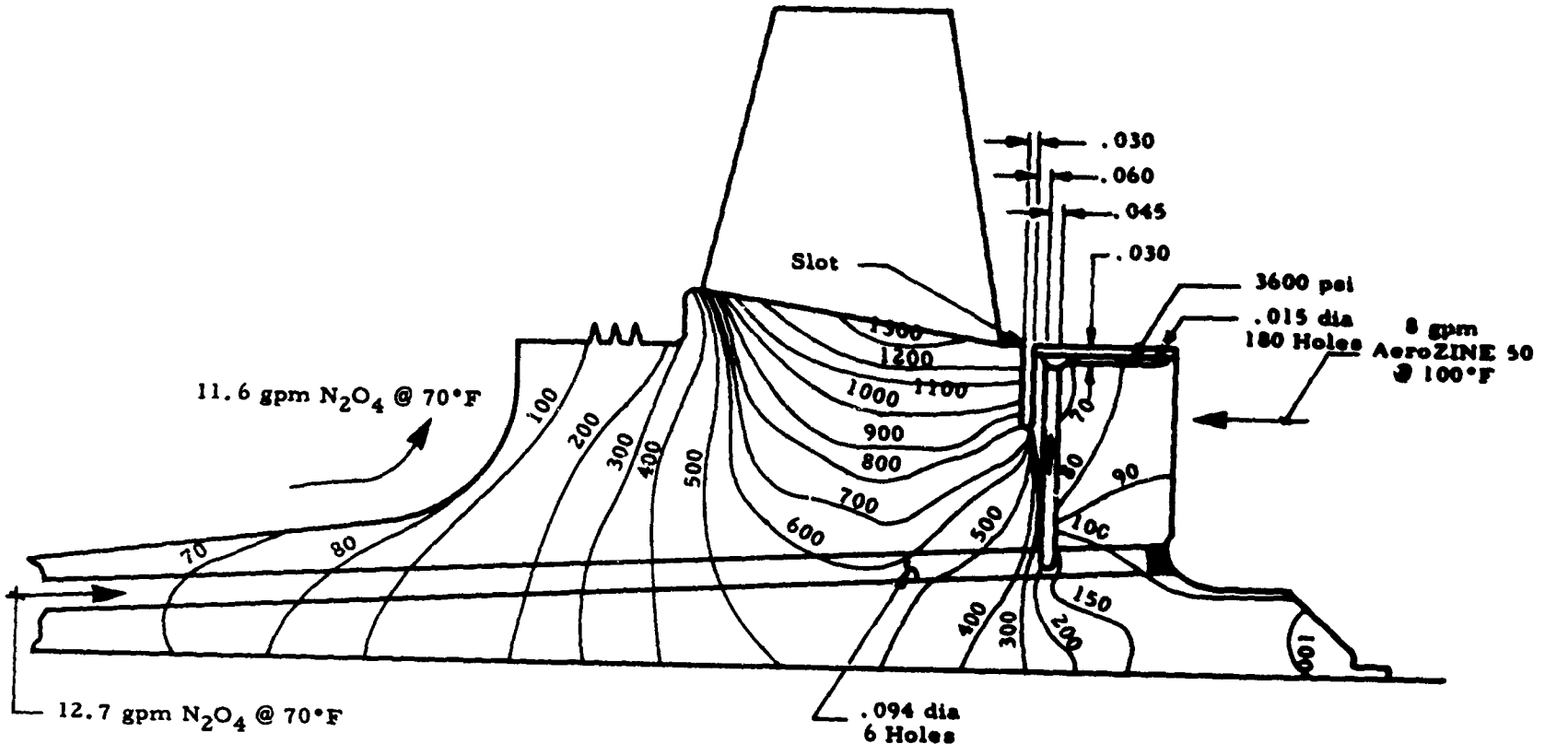

"B" DESIGN TURBINE
STEADY STATE TEMPERATURE
Slot Depth .310 inches
Total Temperature (Relative) = 1360° F
Scale 2:1

Figure VI-10

Turbine-Shaft Temperature Distribution, 0.31-in.-deep Slot

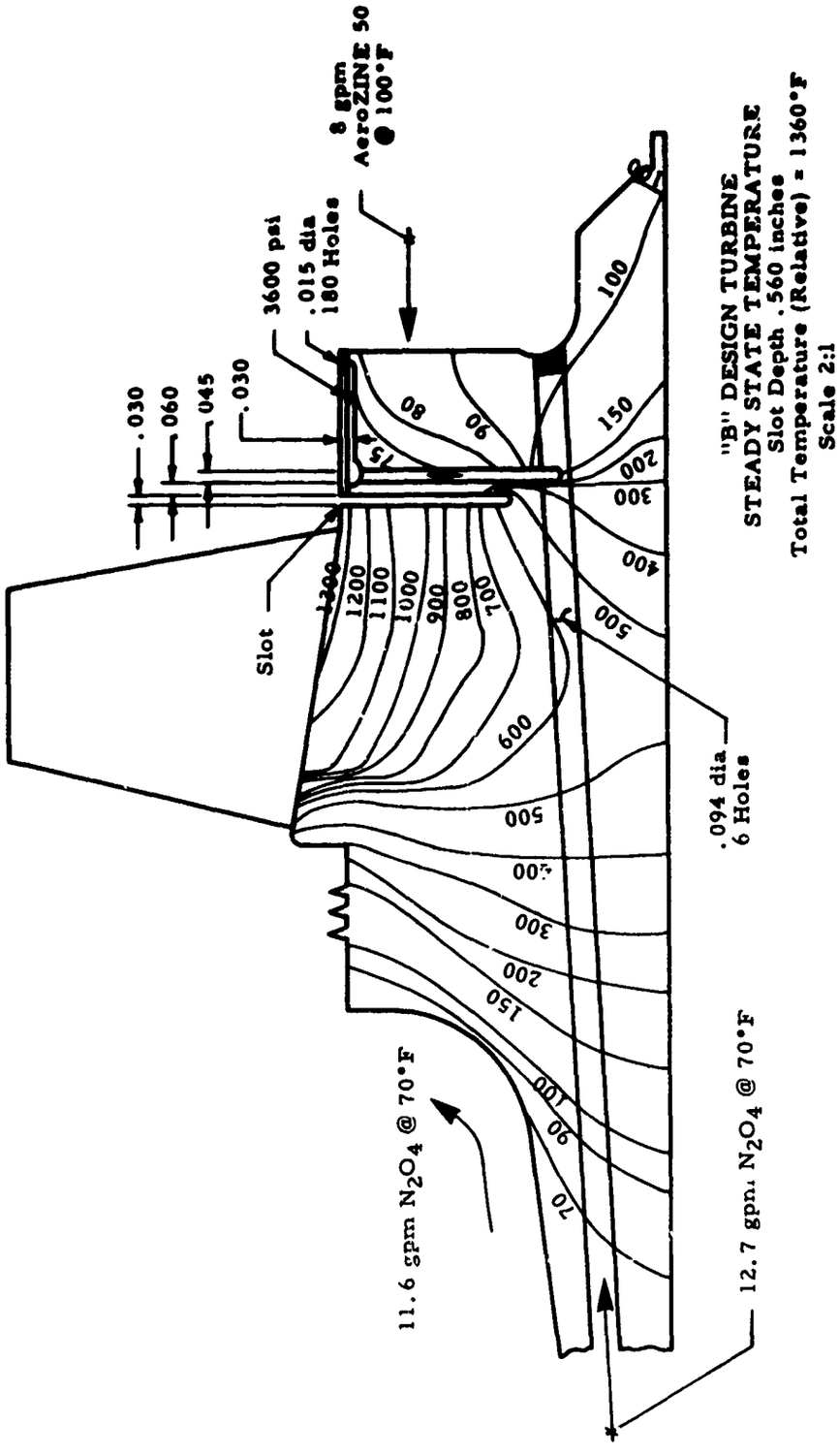

Turbine-Shaft Temperature Distribution, 0.56-in.-deep Slot

Figure VI-11

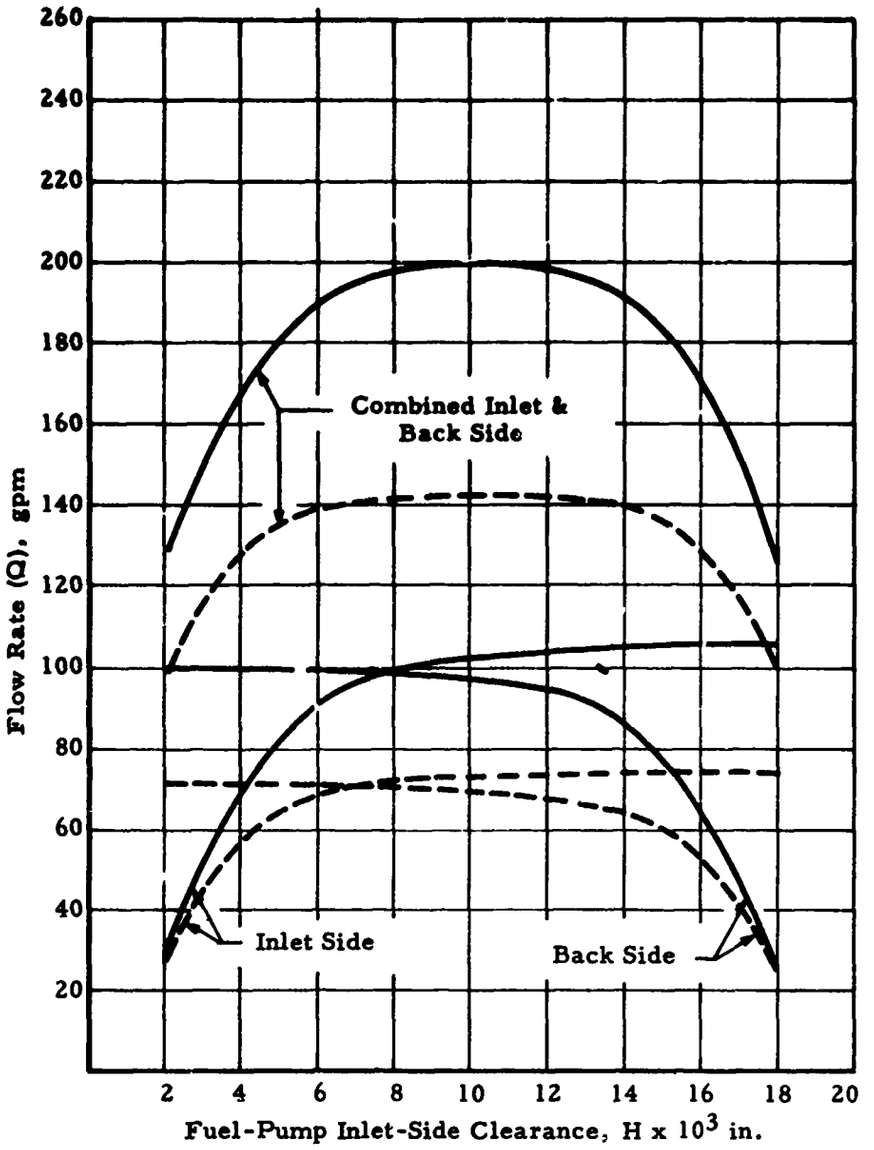

1. Speed 40,000 rpm
2. Nominal Land Clearance
   Inlet Side - 0.010 in.
   Back Side - 0.010 in.
3. Number of Labyrinth Teeth
   Inlet Side - 7
   Back Side - 7
4. Labyrinth Clearance
   Inlet Side-Back Side 0.010 ———
   0.007 - - - - - (Design)
5. Data per ARES Design-B Thrust-Balance Program GE 225, dated 21 Feb 1966

Thrust-Balance Flow Rate vs Position

Figure VI-12

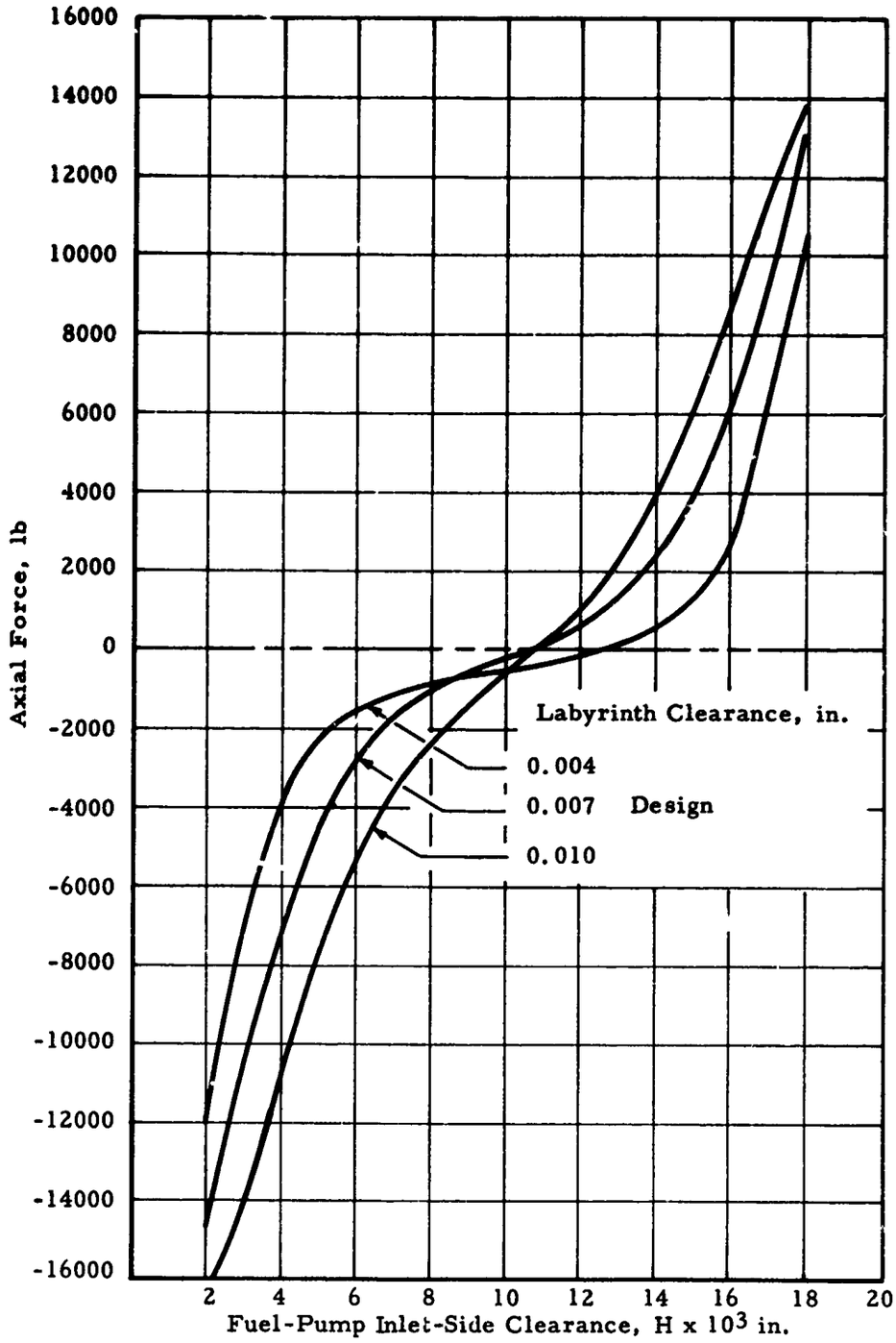

NOTES:
1. Speed, 40,000 rpm
2. Nominal Land Clearance (Inlet & Back-Side Land), 0.010 in.
3. Number of Labyrinth Teeth (Inlet & Back Side), 7
4. Positive Force Towards Fuel-Pump Inlet
5. Data per ARES-B Thrust-Balance Program GE-225, dated 21 February 1966

Summation of Axial Force vs Thrust-Balancer Position

Figure VI-13

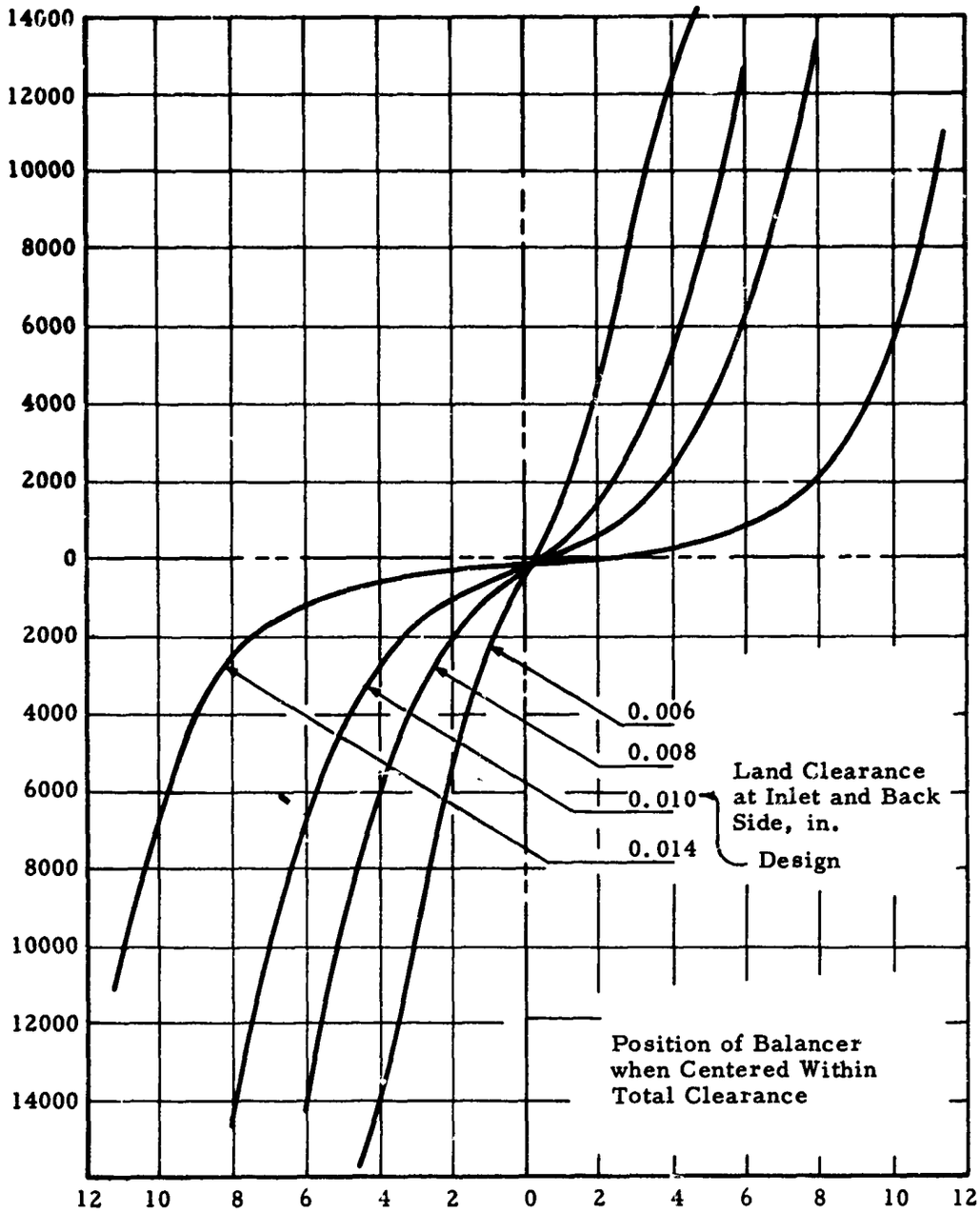

NOTES:
1. Speed, 40,000 rpm
2. Nominal Balancer Labyrinth Clearance, 0.007 in.
3. Positive Force Towards Fuel-Pump Inlet

Thrust-Balancer Load Deflection vs Axial-Land Clearances

Figure VI-14

NOTES:
1. Start-Transient Data per Figure XV-1 of Second Quarterly Report; Two-Stage Fuel Pump, Separate Fuel Valves.
2. Thrust-Bearing-Retainer Diaphragm Deflection, 0.007 in. @ 400 lb.

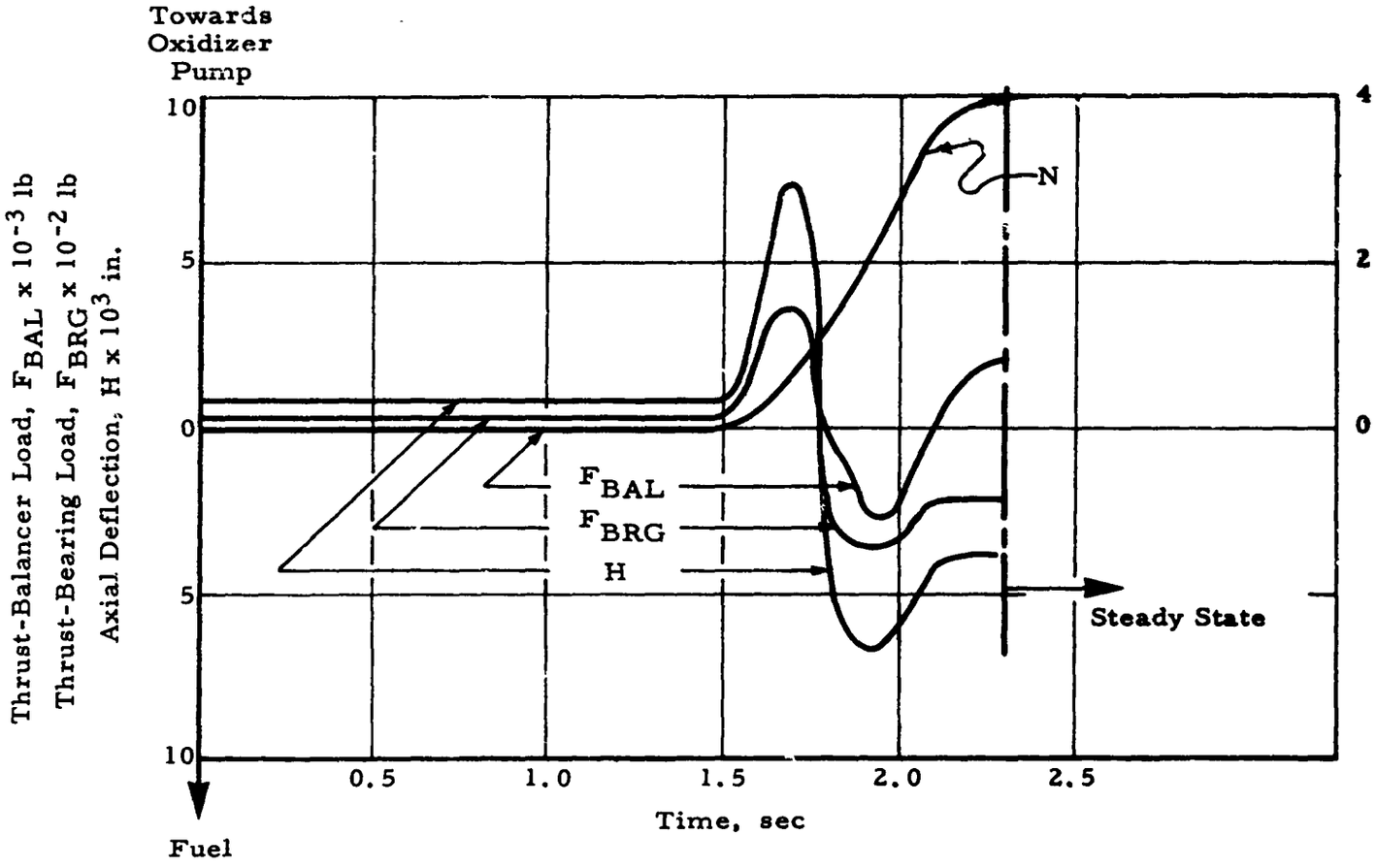

Thrust-Balancer Position and Load during TPA Start Transient

ARES BEARING (40,000 rpm)

A. 108 BALL BEARING

Thrust Load, lb	Stress, psi Outer Race	Inner Race
*1500 (2,500)	200,000	230,000
*900 (1,500)	175,876	194,407

B. 108 ROLLER BEARING

Radial Load, lb	Stress, psi Inner Race	Outer Race
1055	149,288	159,953
500	119,000	119,500

BEARINGS TEST UNDER CONTRACT AF 04(611)-8548) (25,000 rpm)

A. 210 BALL BEARING

Thrust Load, lb	Stress psi Outer Race	Inner Race
2,500	212,900	230,312

B. 210 ROLLER BEARING

Radial Load, lb	Stress, psi Outer Race	Inner Race
1095	135,242	147,084

*2,500- or 1500-lb thrust is applied to a tandem set of ball bearings, the highest loading bearing in the set is assumed to carry 60% of the load (1,500 or 900 lb, respectively).

Comparison of Bearing-Contact Stresses

Figure VI-16

Report 10830-Q-3

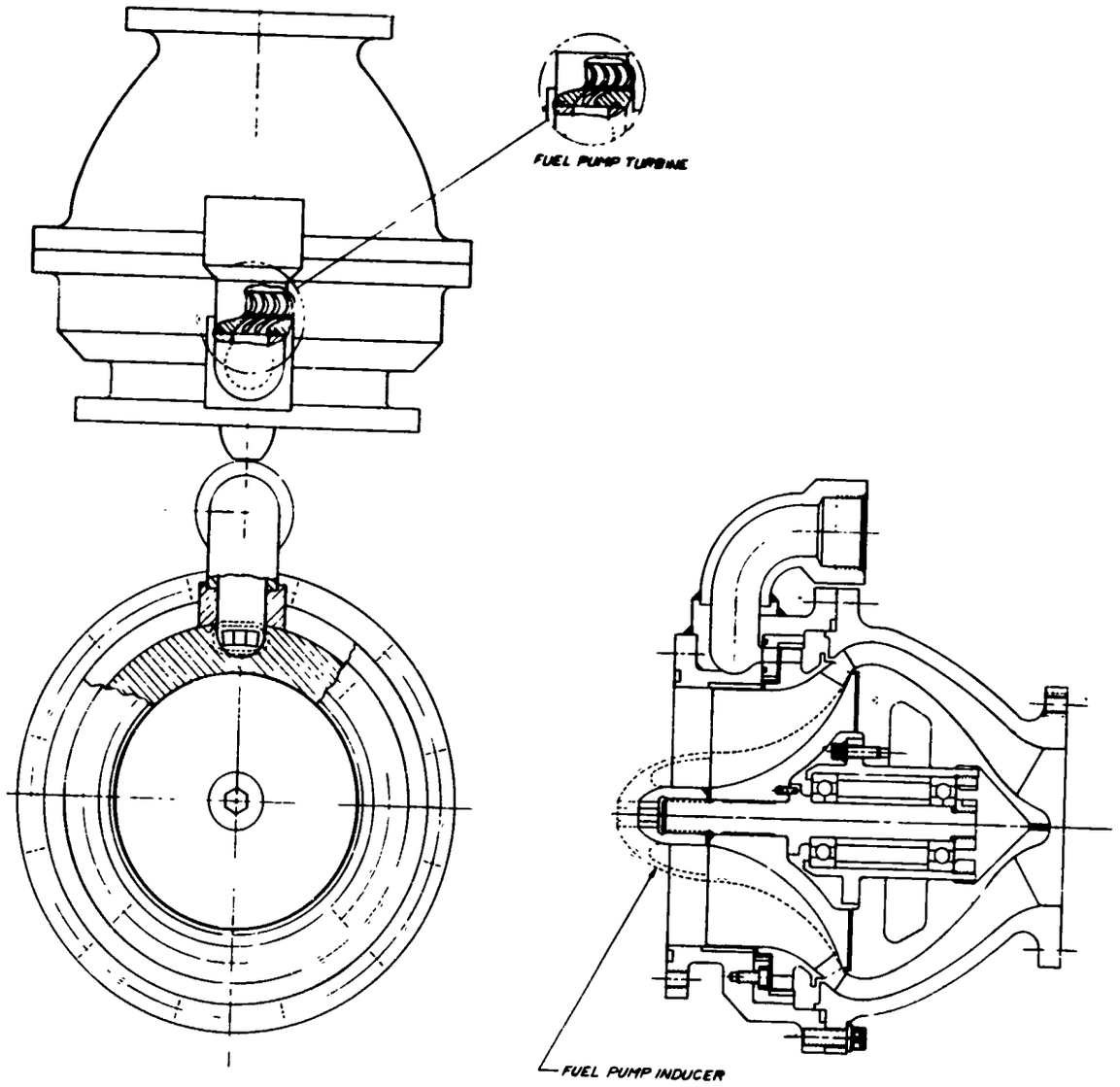

Boost-Pump Layout

Figure VI-17

VII.

BACKUP, OR INLINE, TURBOPUMP

A. GENERAL

A backup turbopump is being designed for the ARES Program and will be used if critical aspects of the advanced turbopump are not adequately proven in Phase I of the contract. The conservative design objective, together with other considerations, which were discussed in detail in the first quarterly report, resulted in the selection of a configuration with the shaft parallel to the line of thrust. This turbopump, consequently designated the "inline" design, has a nominal operating speed of 30,000 rpm. The design features include moderate bearing DN values, low pressure, ambient temperature, purged dynamic shaft seals, conventional housings, and an end-mounted axial flow turbine which confines the high-temperature elements to the thrust-chamber end of the TPA.

The design of the structural test housing was completed, all required forgings were delivered, and fabrication of the structural test housing was initiated. The final stress analysis of the housing, including the effects of thermal gradients, is nearing completion. The analytical design of pumps, turbine, bearings, seals, and thrust-balance system is continuing.

B. TPA DESIGN

1. Configuration Refinements

As the design analysis progresses, various areas of design improvements are disclosed. Detailed design of the second-stage fuel impeller indicated that, because it was open-faced, its head rise would be affected by changes in axial clearance associated with the normal operation of the thrust-balance system. To avoid this problem, a double-shrouded second-stage impeller was designed which also serves as the axial thrust-balance device. The new geometry eliminates the need for the second-stage diffuser, which provided structural support for the interstage thrust-balance orifices, and will thus permit the simplification of the housing. This conceptual revision under study, shown on the cross-section of the inline TPA in Figure VII-1, should be compared to Figure VII-1 of Report 10830-Q-2.

2. Performance Refinements

Detailed analyses of impeller and diffuser designs and of hydraulic losses indicate that specification values shown in Report 10830-Q-2, including predicted efficiencies, are sufficiently accurate; no performance adjustments are required at this time.

VII, Backup, or Inline, Turbopump (cont.)

C. PUMP DESIGN

1. Oxidizer Pump

Detailed analyses of diffuser and housing losses are nearing completion. The oxidizer impeller is being designed, and shroud and vane coordinates have been established.

The stress analysis of the inducer is nearing completion. Relatively high stress levels were found at the hub near the leading edge. The thickness of the hub and the blade taper from hub to tip will be increased to ensure adequate strength.

Initial analyses and layouts of the final oxidizer diffuser geometry indicate that a vane inlet angle of about 7° will be required. This shallow angle and the complex vane contours probably will not permit the "hogging out" of the vanes, as will be done on the simplified structural test unit. Thus, the fabrication approach for the final housing may have to be modified to permit the use of a revised method for milling the vane contours.

2. First-Stage Fuel Pump

Diffuser-vane layouts for the first-stage fuel pump were completed. As with the oxidizer diffuser, it may be necessary to revise the fabrication technique for the housing to improve producibility.

Impeller shroud profiles were established, and the vane geometry is currently being determined.

The stress analysis of the inducer is nearing completion. Preliminary results show unacceptable stress levels similar to those on the oxidizer inducer design, and a modification similar to that proposed for the oxidizer inducer will be used to achieve acceptable stresses.

3. Second-Stage Fuel Pump

Because of its dual role as impeller and thrust balancer, the second-stage fuel impeller has received considerable attention. In addition, the need to provide a significant negative slope to the H-Q curve for good engine-cycle "righting torque" requires careful investigation in an impeller design of such low specific speed ($\frac{600 \text{ rpm } \sqrt{\text{gpm}}}{\Delta H^{3/4}}$). Finally, the close proximity of the bearings presents special problems of mechanical positioning and support of components within the limited space. Figure VII-1 shows the revised concept of the second-stage pump. The second-stage impeller is circumferentially split and assembled in two halves to achieve the desired positioning of orifices.

VII, C, Pump Design (cont.)

(u) To achieve the sloping H-Q curve, the impeller uses unusually thick vanes. These vanes produce the required high discharge-flow coefficient and provide a rugged structure for bolting the two halves together.

D. TURBINE DESIGN

1. Performance

(c) The turbine has been designed to produce 10,500 bhp at a speed of 30,000 rpm. At an inlet temperature and pressure of 1222°F and 4475 psia, respectively, the turbine will flow about 239 lb/sec of oxidizer-rich gas at a pressure ratio of 1.5. Figures VII-2 and -3 show predicted turbine flow and torque characteristics not previously presented. The overall predicted performance map was included in Report 10830-Q-2.

2. Stress and Thermal Analysis

(u) The stress and thermal analyses on the turbine were completed. All stresses are acceptable. As indicated in Figure VII-4, showing combined stresses, some "first-cycle yielding" is expected to occur in the disc rim, which is acceptable. Figures VII-5 and -6 show the predicted disc thermal gradient and the centrifugal stress distribution, respectively. Figure VII-7 shows thermal stress only.

(u) Blade natural frequencies lie well above the exciting (nozzle-passing) frequency. Figure VII-8 illustrates the predicted values. The prediction method used has been verified by vibration-testing on other blading designs.

E. POWER TRANSMISSION

1. Critical Speed

(u) A detailed analysis of shaft critical speeds and deflections was completed, and a report is being prepared. Effects of housing stiffness were included in the analysis. The first critical speed is predicted to be between 40,000 and 42,000 rpm. This provides a critical-speed margin well in excess of 20% of the 30,000-rpm design speed. (These values are for the configuration shown in Figure VII-1 of Report 10830-Q-2.) The revised second-stage fuel-pump configuration has not been completely analyzed, but only minor critical-speed changes are anticipated.

2. Bearings

(u) A detailed design of the ball and roller bearings was completed. However, because of revisions to the axial thrust-balance system, the ball thrust-bearing design may require revision. The final design will be established in conjunction with the thrust-balancer analysis.

VII, E, Power Transmission (cont.)

3. Axial Thrust Balance

As mentioned previously, a revised axial-thrust-balance system is being investigated. The former geometry caused the oxidizer impeller to produce a net thrust of about 32,000 lbf, which was balanced against the net thrust of the first- and second-stage fuel impellers. Interstage orifices on the fuel pump provided position-sensitive thrust variation to achieve thrust balance. Figure VII-1 of Report 10830-Q-2 illustrates the original geometry. This system had the potential drawback of significant variations in axial thrust during engine cycle transients because of the relatively large and independent thrust vectors associated with each impeller and the turbine. In addition, the thrust-compensation system has relatively low response. The revised thrust-balance system is shown in Figure VII-1 of this report. Each first-stage pump impeller is essentially balanced, producing virtually no net thrust during steady-state or transient operation. The second-stage fuel impeller is also nearly balanced, but is position-sensitive to provide restoring force if moved from its center neutral position. This design, which results in approximately twice the recirculated flow of the former concept, is much less sensitive to system transients and has a maximum restoring force of about 18,000 lb compared to 10,000 lb of the original concept. It also has a higher response capability and is a fully double-acting system, i.e., increasing force on one side of the disc is accompanied by decreasing force on the opposite side. The axial-thrust-balance system analysis on the improved design will continue, although other configurations will also be investigated.

4. Dynamic Shaft Seal

In keeping with the conventional approach for the inline TPA, a low-pressure ambient-temperature seal location was selected between the two propellant inlets. This location and environment permits the use of conventional purged-seal concepts.

Several dynamic-seal concepts are under investigation. These include purged positive-contact face-riding seals; purged, hydrostatic lift-off seals; purged, controlled-gap shaft-riding seals; and purged, vented variations of the foregoing designs. Figure VII-9 illustrates the various concepts.

Controlled-gap shaft-riding seals have the significant disadvantage of not providing a positive static seal. Thus, they require extreme care in engine sequencing to ensure purge flow at all times during which propellant is in the system. Consequently, they are not favored for application in the dynamic shaft seal.

Positive-contact, face-riding seals provide the potential of lowest leakage and hence require the smallest purge-supply container. In turn, they may pose wear, cracking, and high heat-generation problems. However, extensive experience accumulated on Titan programs (including man-rated engines) and by industry in general, makes this seal concept a most promising choice.

VII, E, Power Transmission (cont.)

Hydrostatic lift-off seals also provide positive static sealing, but permit higher leakage rates than the positive-contact designs. However, since they do not rub during normal operation and do not use carbon nose pieces, they are expected to avoid the wear, fracture, and heat-generation problems of the rubbing-contact designs. Thus, they offer the possibility of longer life and improved reliability.

Purged, vented variations of the foregoing concepts are also being explored because of their potential for further increase in reliability. One potential failure mode consists of leakage of one seal into the inter-seal cavity during static conditions at startup, shutdown, or coasting. Re-admission of the purge fluid would then carry a portion of this propellant into the opposite pump inlet, precipitating an explosive failure. Vented systems would largely preclude this failure mode. Secondary Teflon wiper seals are being considered for added safety because of good results on the Titan IIA engines.

Two approaches are being considered for purge-supply systems: (1) independently actuated systems of the types schematically illustrated in Figure VII-9 of Report 10830-Q-2, and (2) integrated systems activated by inlet-valve and turbopump operation.

Independent systems require additional control circuitry for operation and monitoring, but their mechanical integration is relatively simple. Consequently, changes in valve, turbopump, and engine sequencing can be made without significant impact on the purge-supply system. However, improved adaptability to intermittent operation must be investigated for restart applications.

Integrated systems directly linked to the oxidizer inlet valve eliminate the need for additional control circuitry and can be adapted to intermittent operation. However, proper sequencing is of greatest importance to ensure that purge fluid reaches the seal before the propellant and continues to flow until all propellant has left the pumps. In addition, means of sealing the mechanical linkage must be provided. Because of the advanced status of design on the ARES inlet valves, it does not appear practical to consider mechanical modifications of these designs at this time. However, by virtue of its configuration, the in-line TPA can use less sophisticated butterfly-type inlet valves. These configurations are under investigation for their adaptability to purge-supply system control. A typical approach is shown in Figures VII-10 and -11.

Figure VII-10 illustrates a typical seal inert-purge supnply system. Oxidizer (the higher-pressure propellant) is tapped off the suction line between the boost pump and the inlet valve. It pressurizes the purge fluid container, augmenting the spring load of the bellows and increasing the purge pressure above the propellant pressure. Purge fluid flow is controlled by a cam-actuated plug valve, which is an integral part of the oxidizer suction valve. The cam-follower is contained in a bellows to provide positive separation of the purge fluid from the propellant. However, since the purge fluid is at a higher pressure than the propellant, leakage would not precipitate a catastrophic failure. Figure VII-11 shows the integrated oxidizer suction-valve/purge-valve detail.

VII, Backup, or Inline, Turbopump (cont.)

F. HOUSING

The in-line TPA housing is shown in Figure VII-12. The low-pressure inlet sections are formed of stainless steel 347, whereas the high-pressure sections are machined and welded from four Inconel-718 forgings. The outer shell consists of a formed Inconel-718 plate. One structural test unit will be fabricated.

1. Fabrication

Two sets of forgings were obtained, and fabrication was initiated. Initial machining operations are under way. The plaster molds for the pump-inlet forming dies have been prepared and are being inspected. Delivery of the housing is scheduled for mid-May 1966.

2. Design

The detailed stress and thermal analysis of the structural test housing is nearing completion. No areas of excessive stress were disclosed in the finalized design. The majority of the stresses range from 20,000 to 40,000 psi. Maximum indicated stress was 118,000 psi at the juncture of the radial-to-cylindrical sections of the oxidizer housing. This stress (which is outer fiber stress only) is acceptable for Inconel-718.

Results of the detailed stress analysis are being summarized. Stresses and deflections will be presented for hydrotest conditions, maximum expected operating point (MEOP) with maximum temperatures, and MEOP with ambient thermal conditions. The latter condition was investigated to determine the potential benefits of additional internal film cooling in the housing.

Predicted deflections were found to be low, in keeping with the intended conservatism of design. Axial deflection between the roller bearings is predicted to be from 0.002 in. (at ambient temperature) to 0.008 in. (at maximum temperature) which can be reduced, if required, depending on the amount of housing coolant (if any) supplied. Allowable deflection is on the order of 0.020 to 0.030 in.

Stresses for certain areas, e.g., the diffuser vanes, were not fully established. However, it is believed prudent to await preliminary results from actual testing of the structural test housing before proceeding further with the purely analytical approach.

Figure VII-13 summarizes predicted stress levels at pertinent housing locations. Figure VII-14 summarizes calculated housing deflections. The overall stress and deflection results are highly satisfactory and reflect, in general, the anticipated success of the conventional geometry and moderately sized high-pressure channels.

VII, F, Housing (cont.)

Only a limited thermal analysis of the housing was performed. A more detailed analysis was not considered necessary because of the ease and suitability of providing cooling if required.

The thermal analysis involved simplified one- and two-dimensional heat transfer into the housing surrounding the primary combustor. It was assumed that the combustor liner would be vented only near the injector. Pressure oscillations of the primary combustor were then estimated to create an average effective gas velocity of 1 ft/sec between the housing wall and the liner, except in the close vicinity of the liner vent ports where a velocity of 3 ft/sec was assumed. A conservatively high gas temperature of 1500°F was used in the analysis, compared to the 1220°F temperature required by the specification.

The calculated wall temperatures in the primary combustor area and the supporting heat-transfer analysis are presented in Section XIX. The temperature levels of the housing wall are acceptable, but could be reduced with virtually no cycle penalties by bleeding a small amount of oxidizer into the cavity between the primary combustor liner and the housing wall.

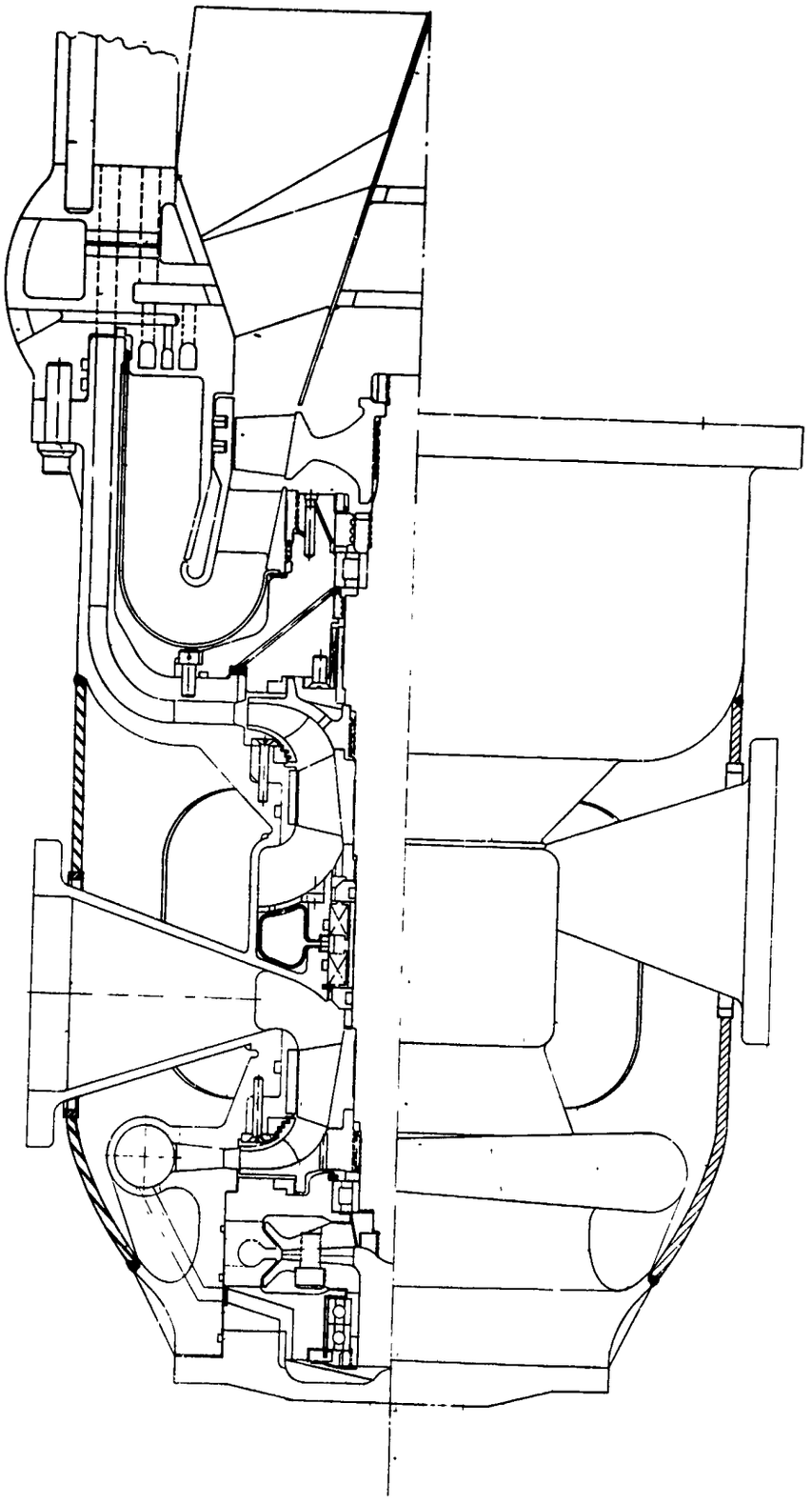

Inline TPA with Conceptual Modification of Second-Stage Fuel Pump (u)

Figure VII-1

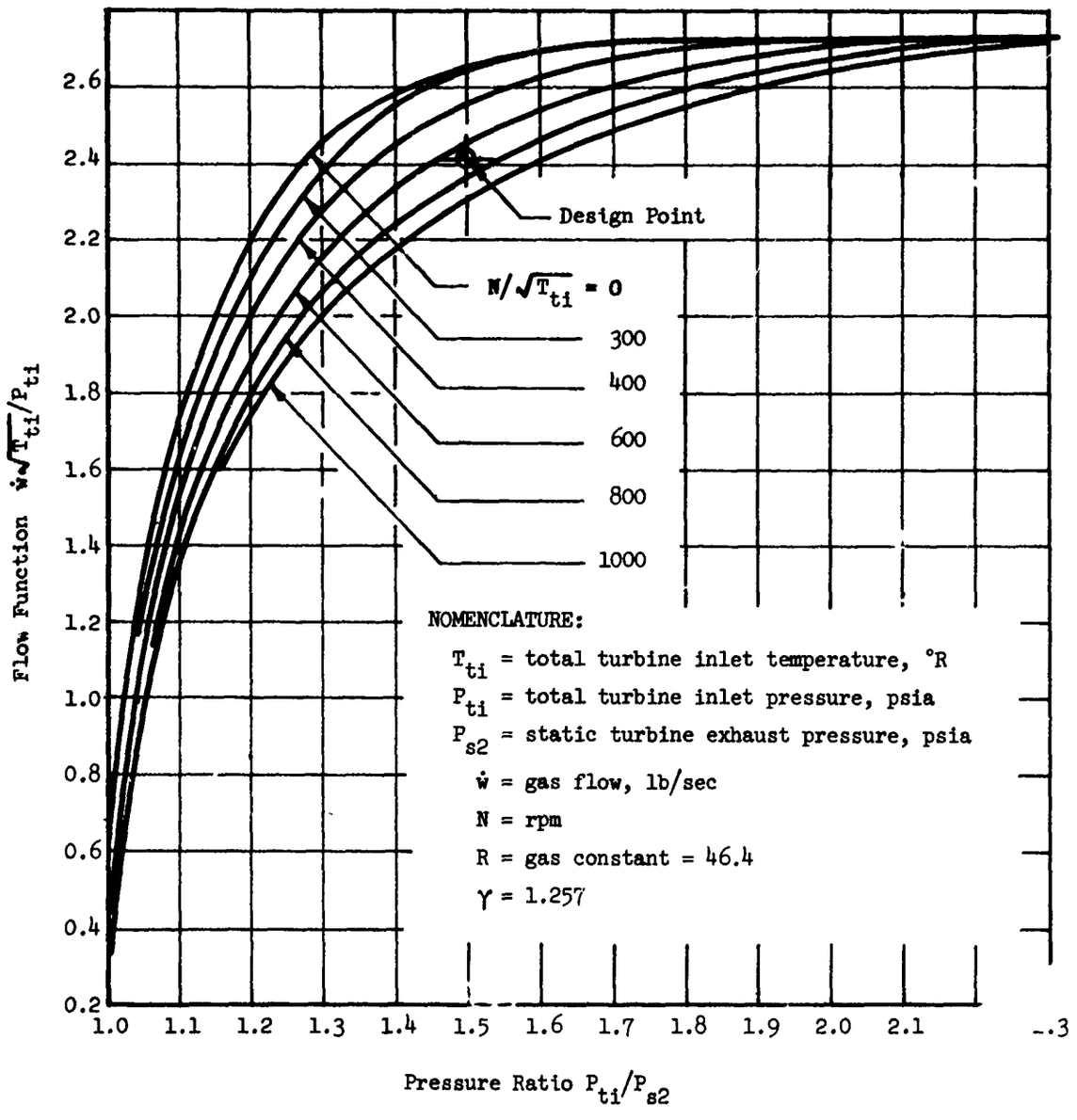

Turbine Flow Function vs Pressure Ratio

Figure VII-2

(This page is Unclassified)

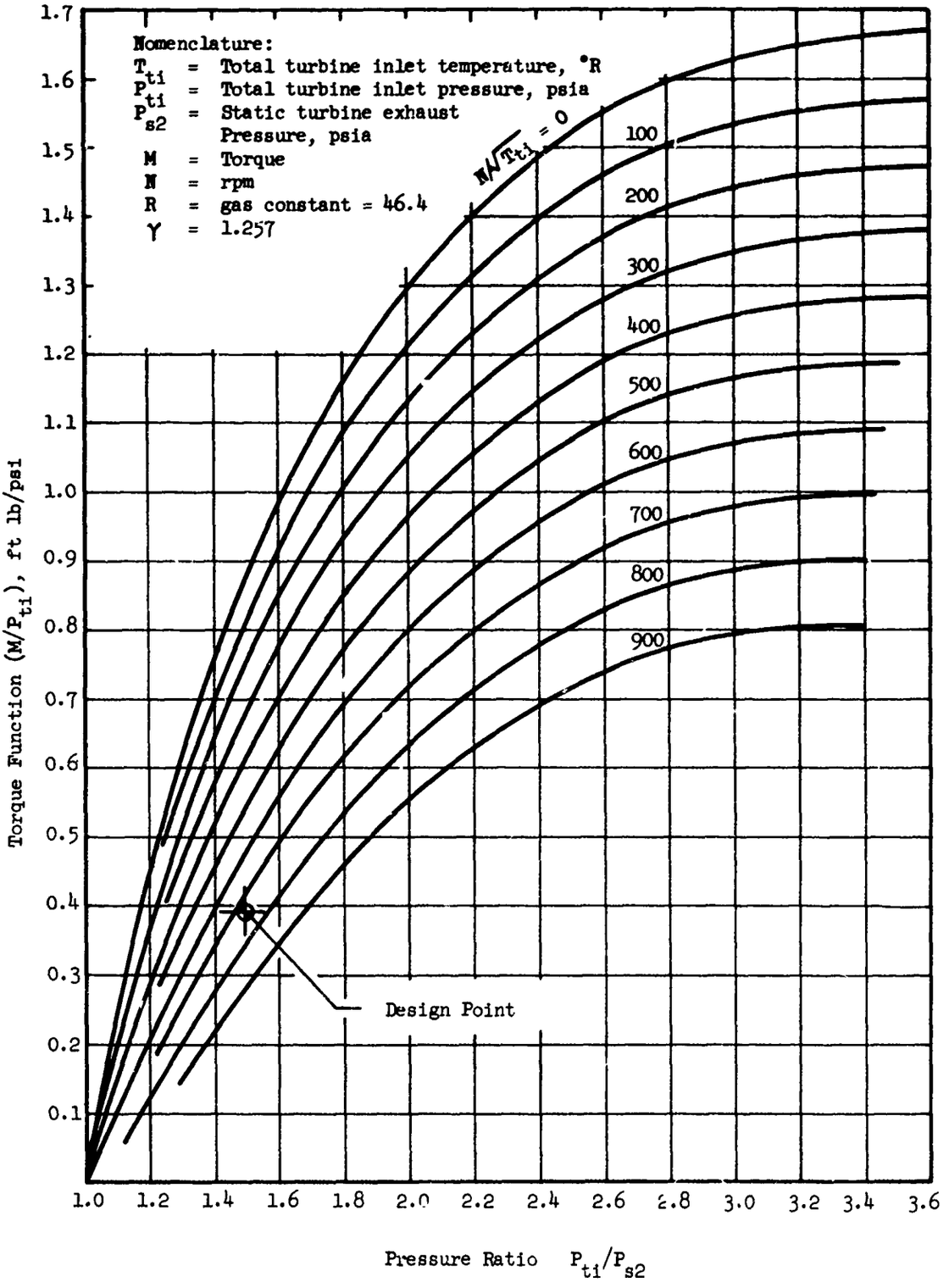

Turbine Torque Function

Figure VII-3

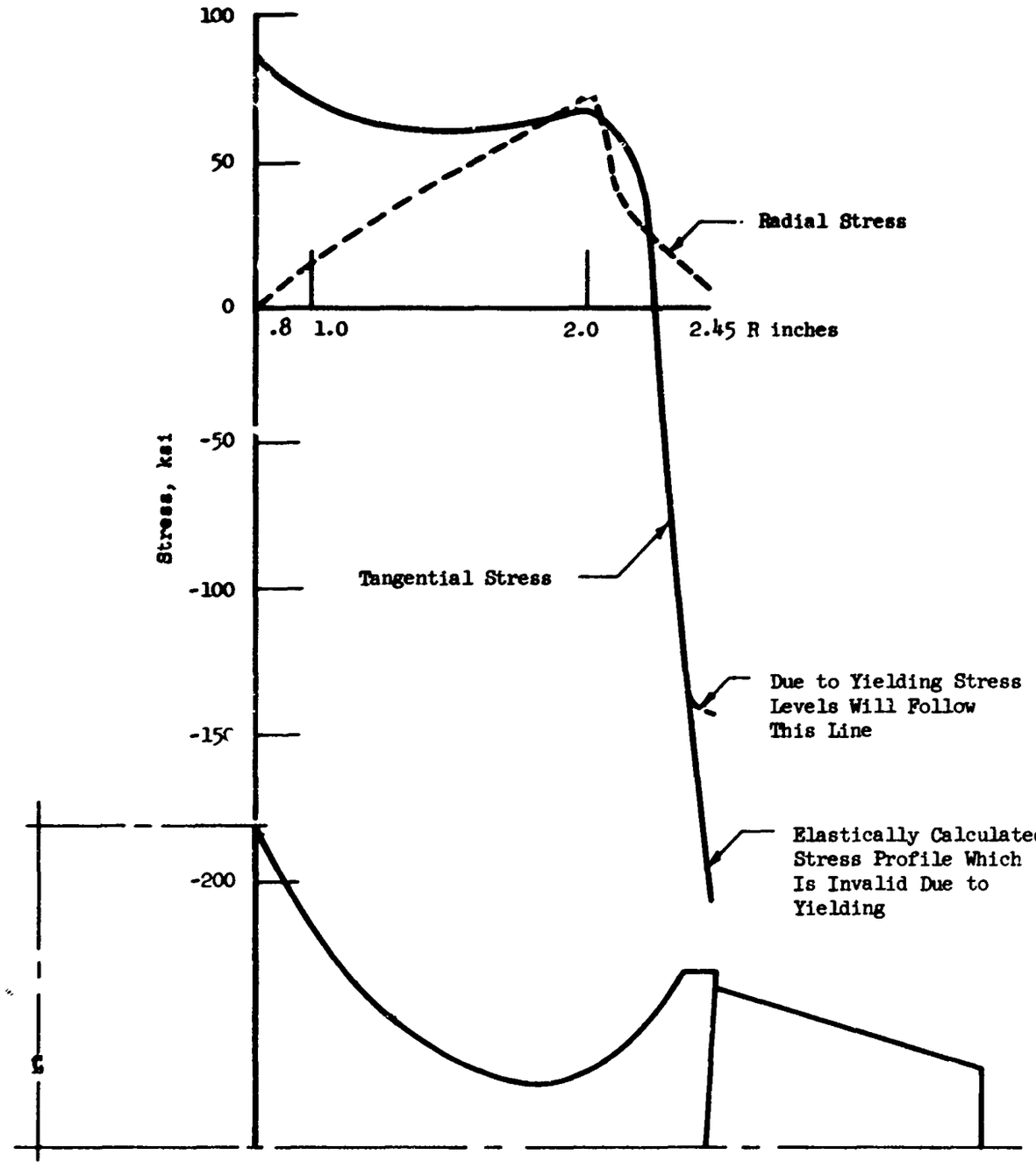

Stress Level @ 20 sec

Turbine Disc, Combined Stresses

Figure VII-4

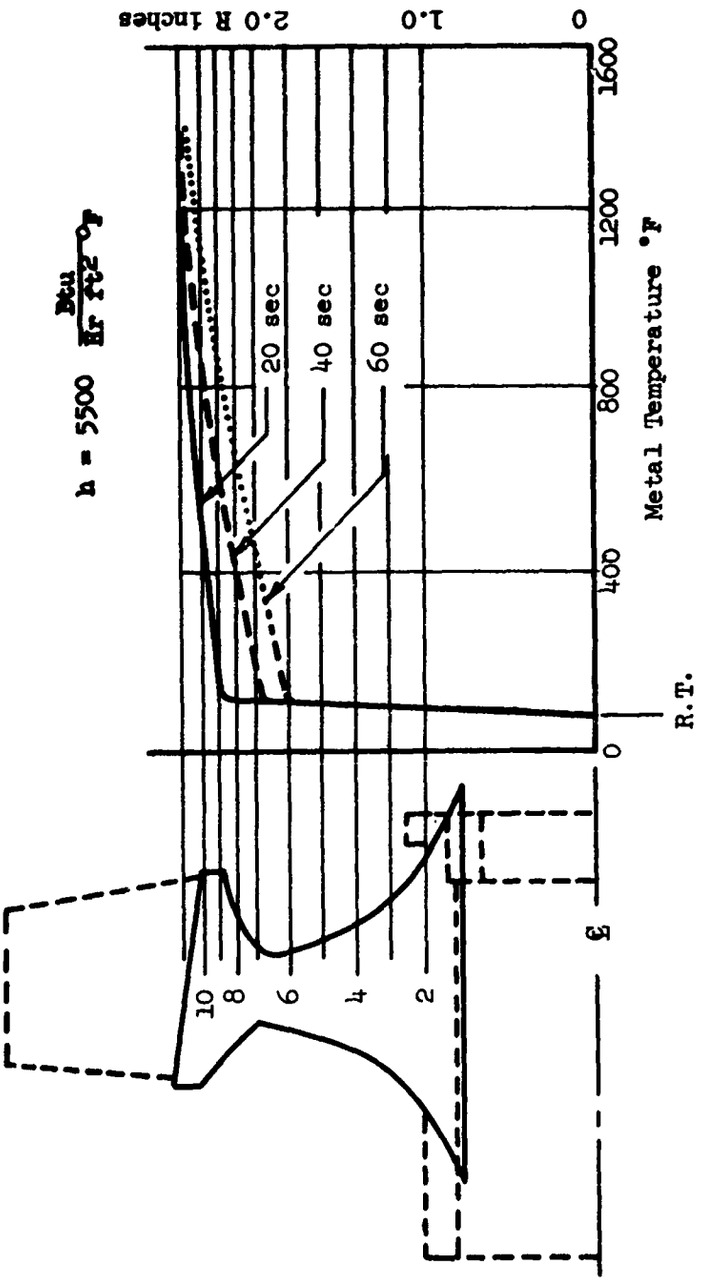

Turbine Disc, Thermal Gradients

Figure VII-5

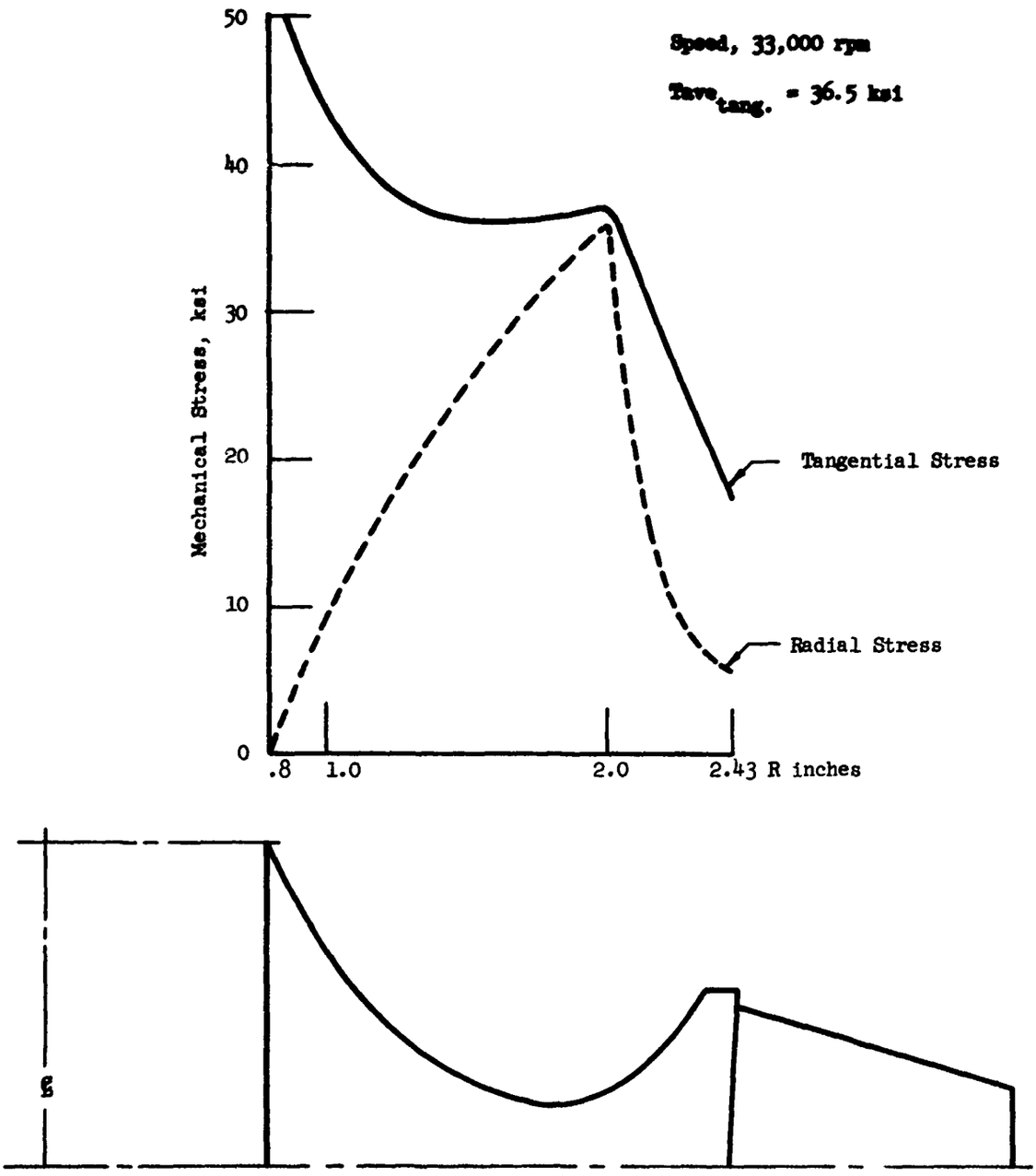

Turbine Disc, Mechanical Stress Only

Figure VII-6

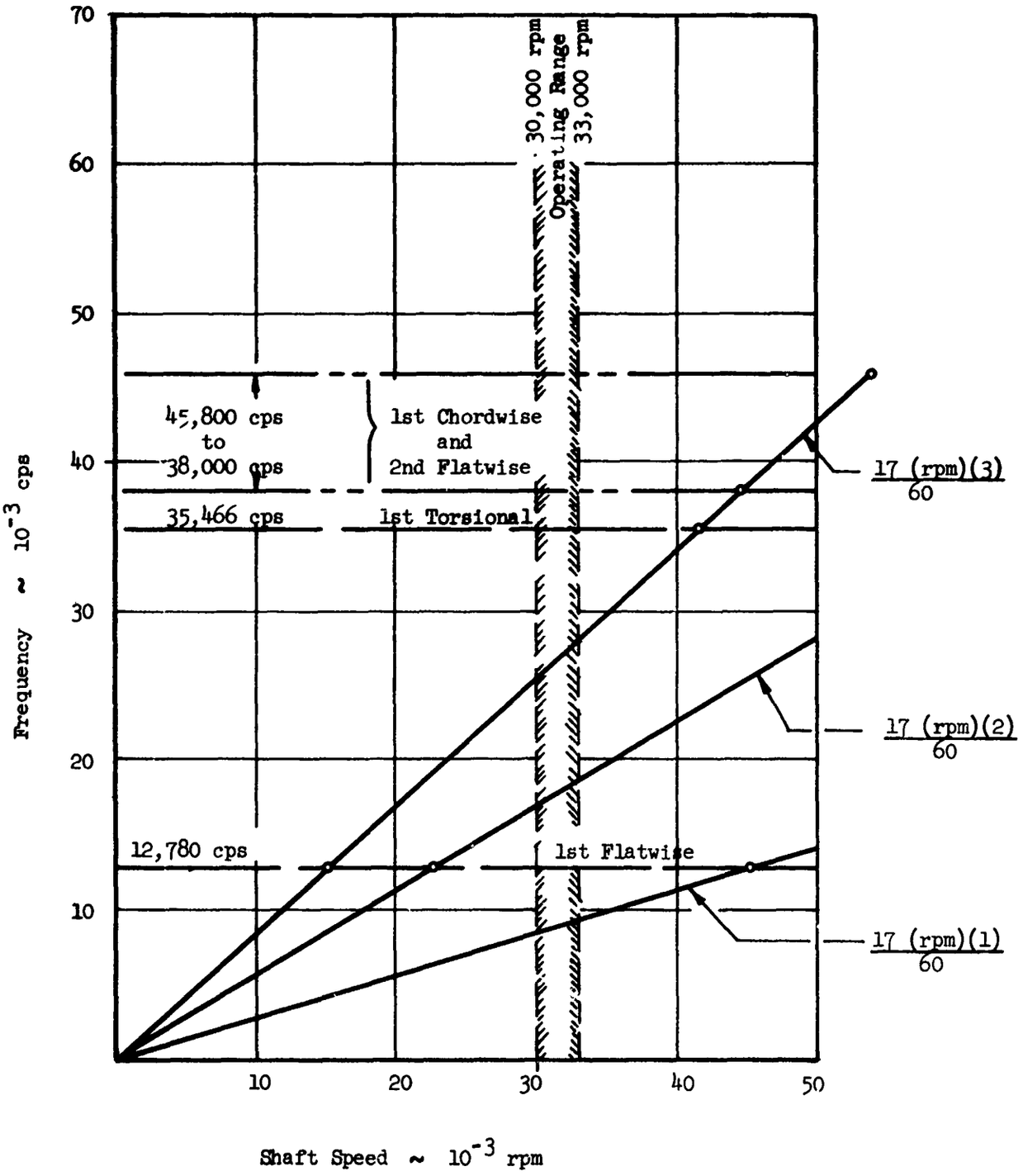

Turbine Disc, Thermal Stress Only

Figure VII-7

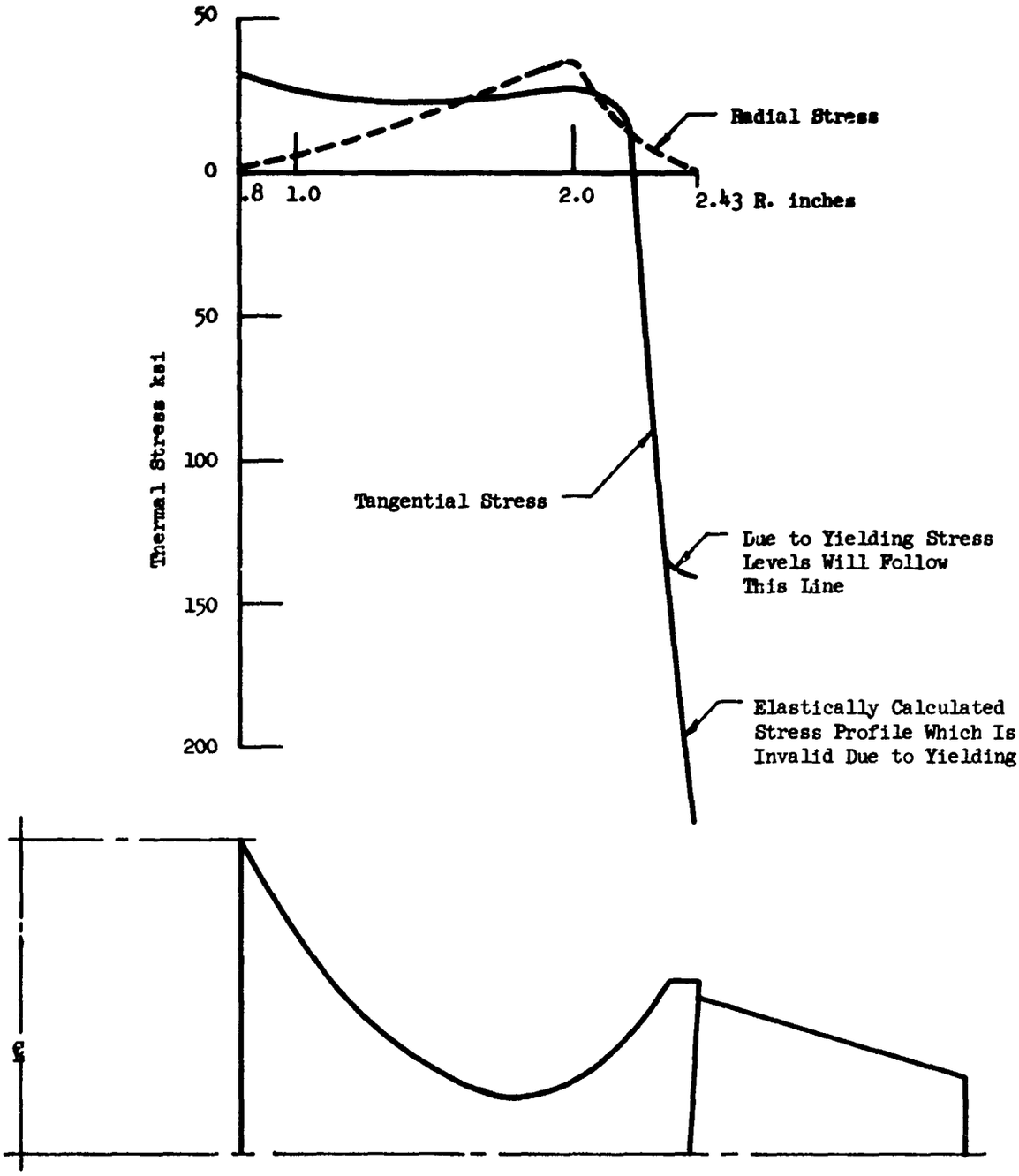

Thermal Stress at 20 sec

Turbine-Blade Resonant Frequencies

Figure VII-8

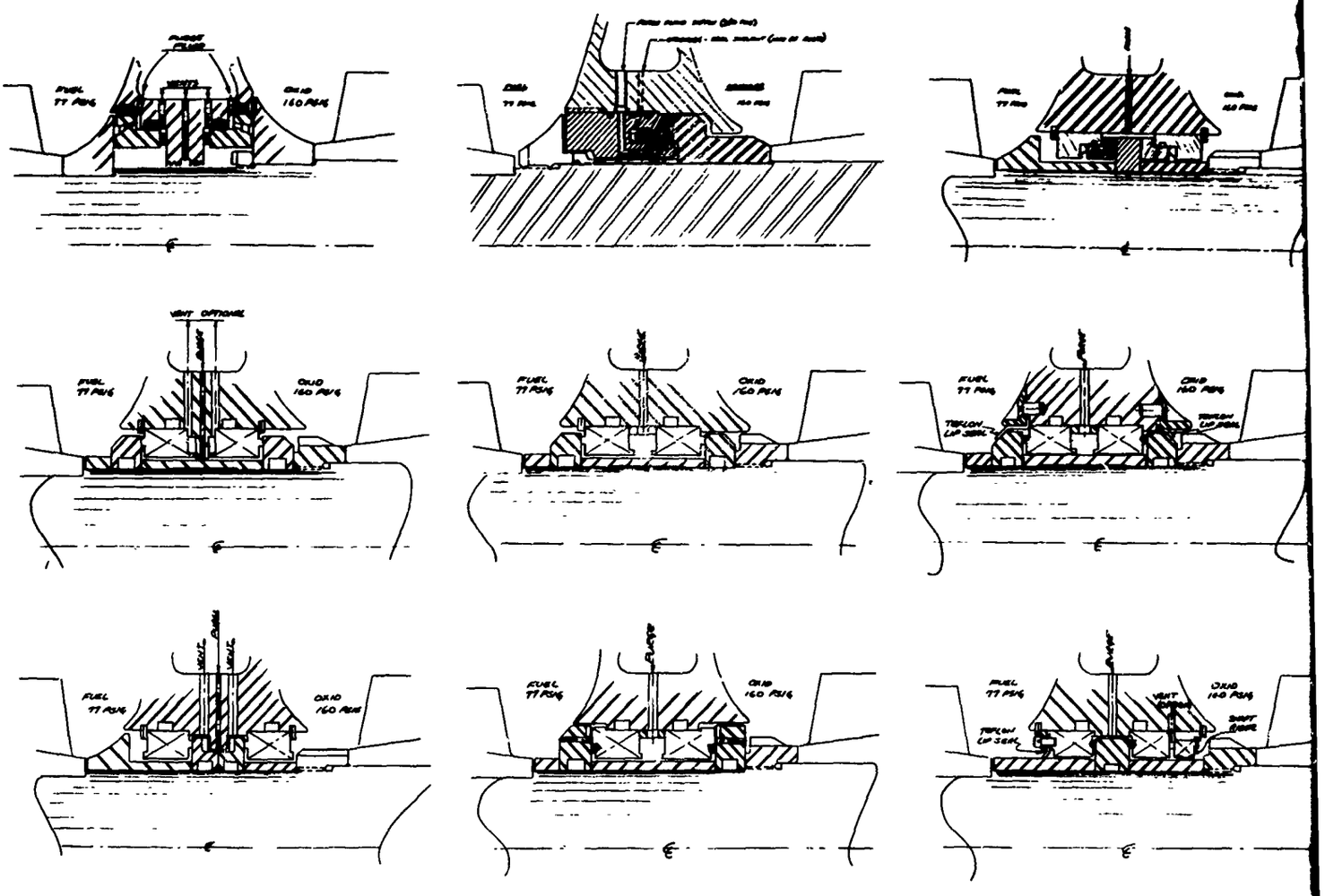

Purged-Seal Concepts

Figure VII-9

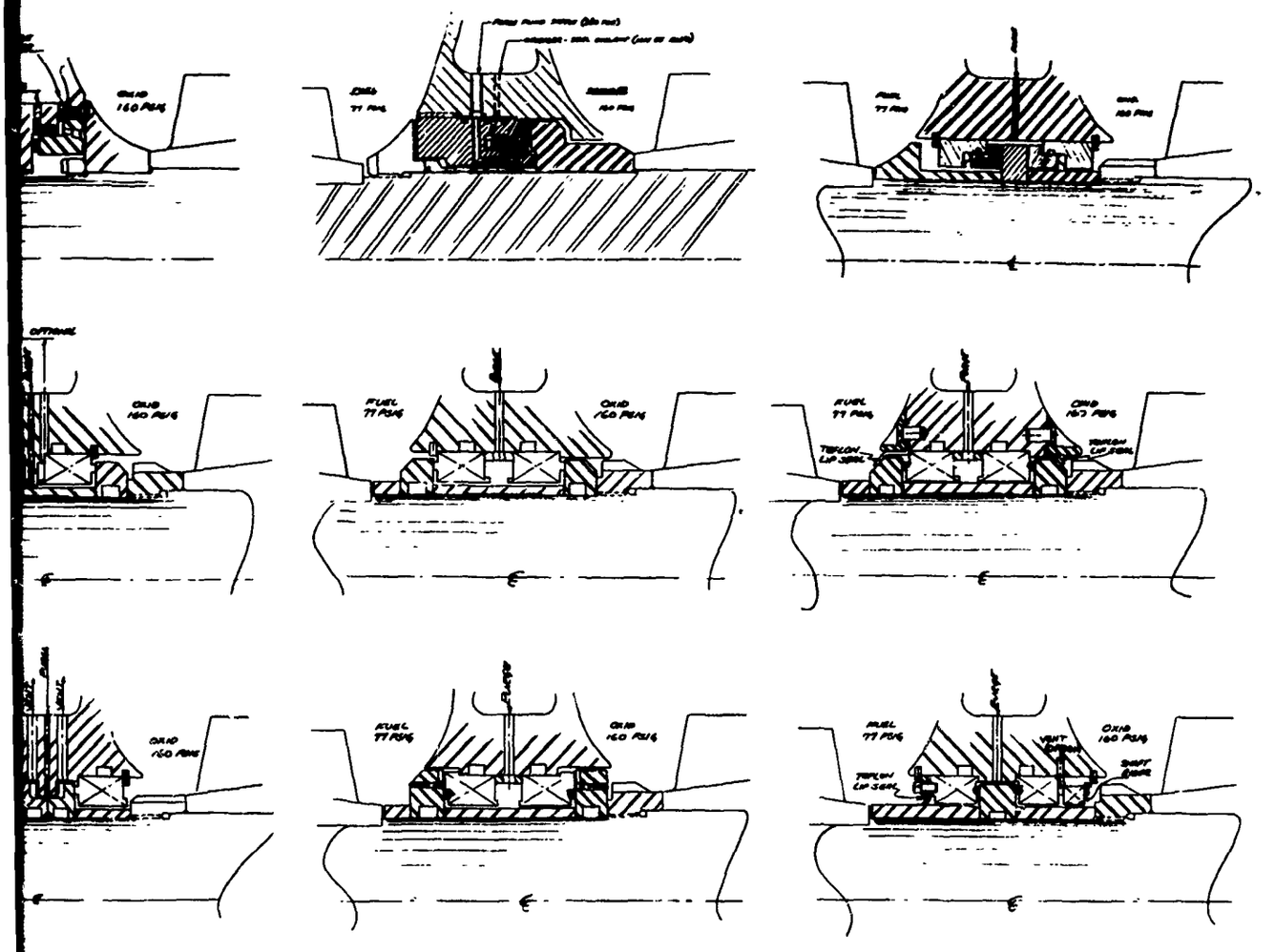

Purged-Seal Concepts

Figure VII-9

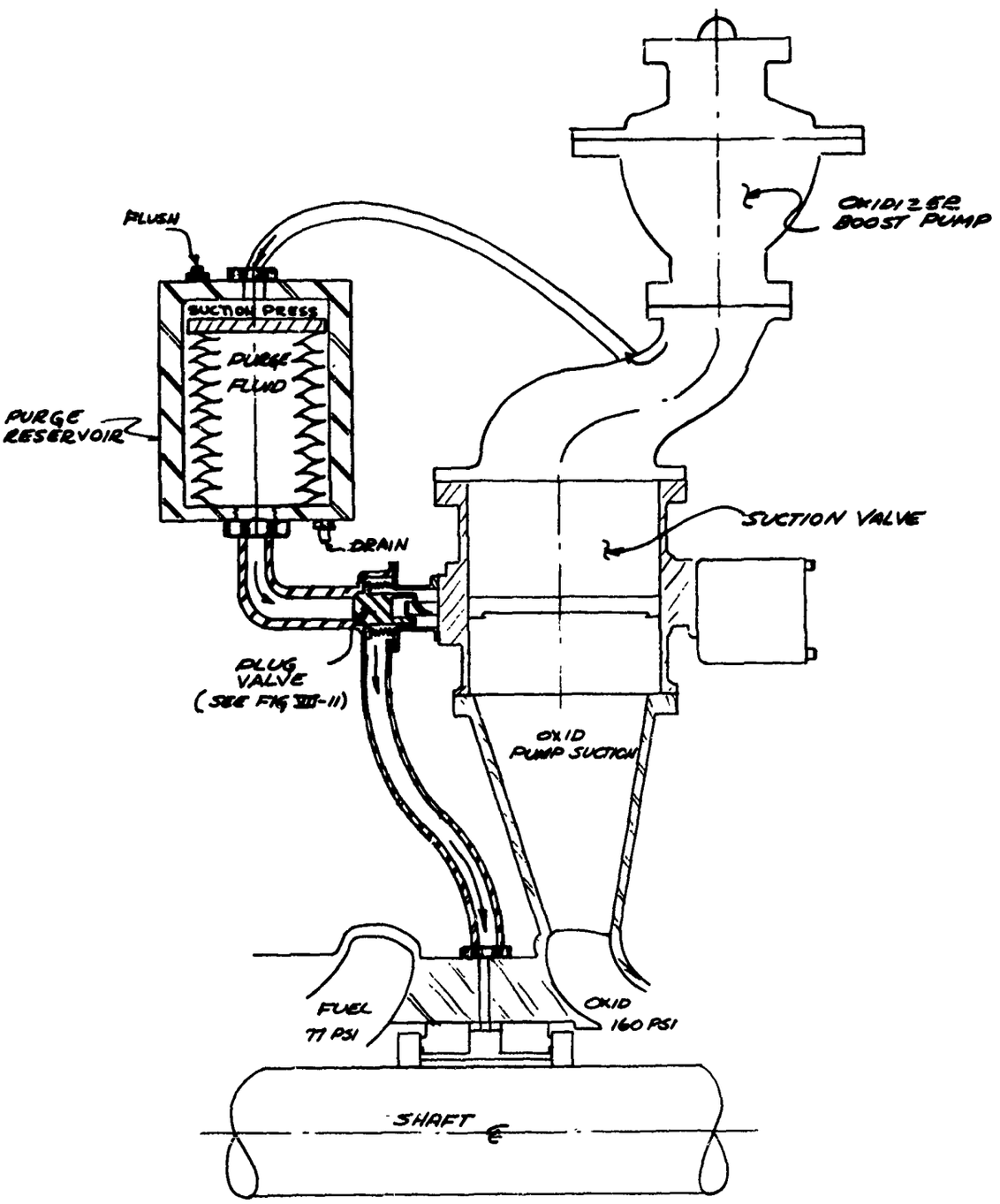

Purge Fluid Supply System Concept

Figure VII-10

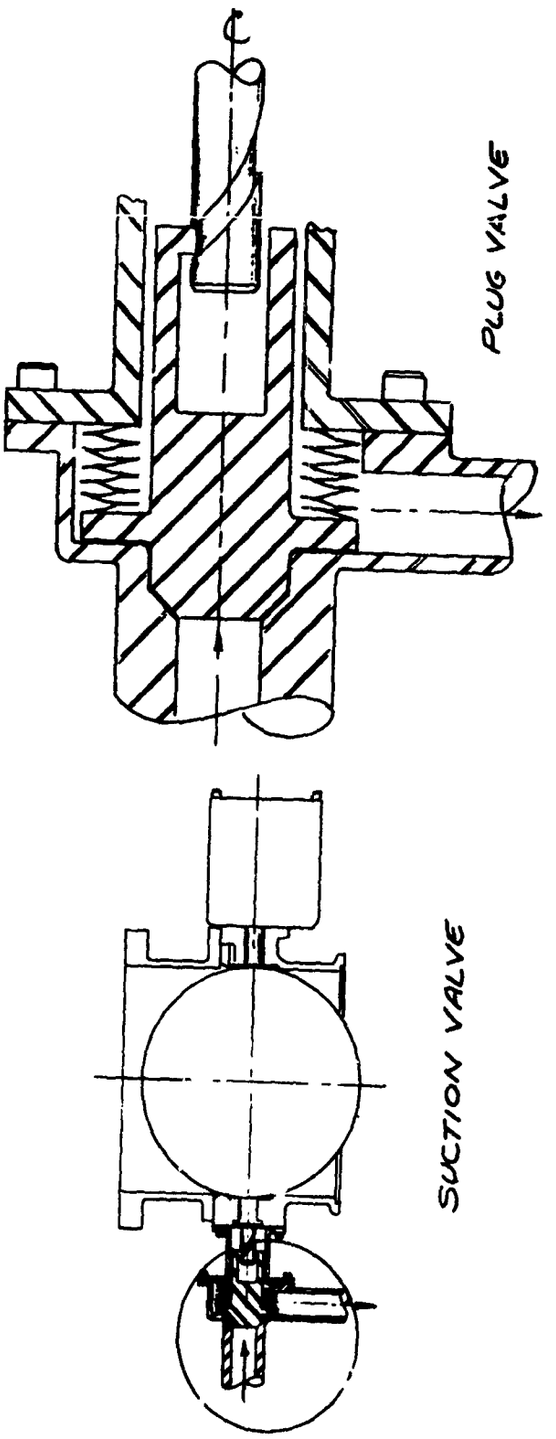

Butterfly Suction Valve Adapted to Purge Control

Figure VII-11

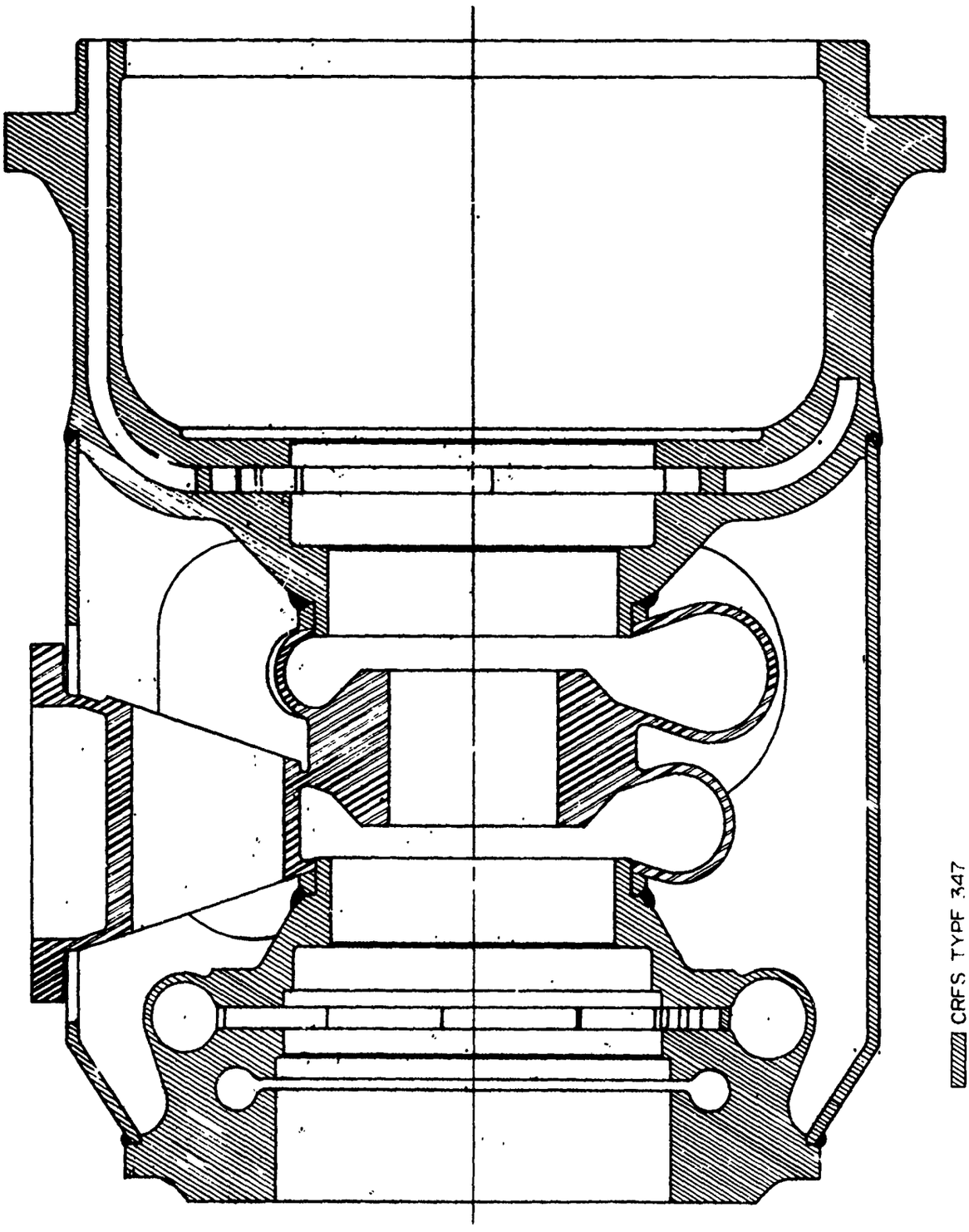

Figure VII-12

Station Element.	Item Description	Hydrotest Cond. Actual Stress, psi	Hydrotest Cond. Allow. Yld. Stress, psi	Hydrotest Cond. Min. M.S.	MEOP & Max. Temp. Actual Stress, psi	MEOP & Max. Temp. Allow. Yld. Stress, psi	MEOP & Max. Temp. Min. M.S.	ΔT = 0 MEOP Max. Temp. Matl. Prop. Actual Stress	ΔT = 0 MEOP Max. Temp. Matl. Prop. Allow. Yld. Stress	ΔT = 0 MEOP Max. Temp. Matl. Prop. Min. M.S.	Notes
1	Weld, Shroud to Fuel Pump Housing	13,000	144,500	+10.11	17,000	144,500	+7.5	13,000	144,500	+10.11	
2	Weld, Shroud to Turbine Housing	36,100	144,500	+3.0	36,500	144,500	+2.96	26,500	144,500	+4.45	
3	First Stage Fuel Pump Volute Wall	35,500	144,500	+3.06	25,900	144,500	+4.59	25,900	144,500	+4.59	
4	Weld, First Stage Fuel Pump Volute Wall	30,200	144,500	+3.79	17,900	144,500	+7.08	17,900	144,500	+7.08	
5	Weld, First Stage Fuel Pump Volute Wall	51,200	144,500	+1.82	27,700	144,500	+4.21	27,700	144,500	+4.21	
6	First Stage Fuel Pump Diffuser Vane	--	144,500	--	--	144,500	--	--	144,500	--	Not Available at this time
7	Bolt at Gimbal Mounting	--	--	--	--	--	--	--	--	--	Not Available at this time
8	Fuel Pump Housing	68,800	144,500	+1.1	12,300	144,500	+10.7	12,300	144,500	+1[illegible]	
9	Weld, Fuel Pump Housing to Inlet Volute	21,500	35,000	+0.63	10,800	35,000	+2.24	11,100	35,000	+2.15	
10	Inlet Volute Wall	3,500	35,000	+9.0	1,200	35,000	High	1,500	35,000	High	
11	Weld	7,900	35,000	+3.44	5,500	35,000	+5.36	6,900	35,000	+4.06	
12	Weld	7,400	35,000	+3.73	3,700	35,000	+8.45	4,800	35,000	+6.3	
13	Oxid. Inlet Volute Wall	8,000	35,000	+3.38	--	35,000	--	--	35,000	--	
14	Weld, Oxid. Inlet Volute to Oxid. Pump Housing	25,500	35,000	+0.37	--	35,000	--	--	35,000	--	
15	Oxid. Pump Housing	48,400	144,500	+1.99	--	144,500	--	--	144,500	--	
16	Oxid. Pump Diffuser Open Vane	--	144,500	--	--	144,500	--	--	144,500	--	Data being reduced. Stresses will be in final report.
17	Oxid. Pump Volute Wall	40,900	144,500	+2.53	48,700	143,700	+1.95	40,400	143,700	+2.56	
18	Bold, Oxid. Housing to Nozzle Support	--	--	--	--	--	--	--	--	--	Data being eval. Will be reported later.
19	Nozzle Support Wall	33,800	70,000	+1.07	71,500	139,100	+0.95	32,100	139,100	+3.35	
20	Nozzle (or Hydrotest Fixture at Nozzle)	7,700	70,000	+8.1	--	--	--	--	--	--	Data being evaluated.
21	Combustion Chamber Wall	119,600	144,500	+0.21	118,400	136,200	+0.15	105,500	136,200	+0.29	
22	Weld, Outer Wall	58,600	144,500	+1.46	75,200	144,100	+0.94	49,600	144,100	+1.91	
23	Oxid. Flow Channel	34,500	144,500	+3.19	16,800	144,100	+7.58	28,600	144,100	+4.04	
24	Flange	58,200	144,500	+1.48	63,300	144,400	+1.28	49,100	144,100	+1.94	
25	Bolt, TPA Housing to Injector	95,800	180,000	+0.88	78,800	180,000	+1.28	88,000	180,000	+1.05	
26	Hydotest Fixture	26,200	70,000	+1.67	--	--	--	--	--	--	
27	Bolt, Hydrotest Fixture	--	--	--	--	--	--	--	--	--	
28	Bolt, Hydrotest Fixture	--	--	--	--	--	--	--	--	--	

Housing, Predicted Stress Summary

Figure VII-13

Station Ident.	Item Description	Hydrotest Cond. Deflection, in. Radial	Hydrotest Cond. Deflection, in. Axial	Hydrotest Cond. Rotation, in.	MEOP & Max. Temp. Deflection, in. Radial	MEOP & Max. Temp. Deflection, in. Axial	MEOP & Max. Temp. Rotation, in.	ΔT = 0 MEOP Max. Temp. Mtl. Prop. Deflection, in. Radial	ΔT = 0 MEOP Max. Temp. Mtl. Prop. Deflection, in. Axial	ΔT = 0 MEOP Max. Temp. Mtl. Prop. Rotation, in.	Notes
A	Radial Brg. at Fuel Pump	-0.00074	+0.00461	--	-0.00023	+0.00185	+0.00057	-0.00023	+0.00185	+0.00057	
B	Radial Brg. at Oxid. Pump	+0.00016	+0.00629	--	+0.00291	-0.00564	+0.00057	-0.00025	+0.00862	-0.00026	
C	Thrust Brg. (Operating Design only)	--	--	--	-0.00005	+0.00268	-0.00009	-0.00005	+0.00268	-0.00009	
D	Seal between Fuel Pump & Oxid. Pump	+0.00001	+0.00461	-0.00001	+0.00002	+0.00172	-0.00002	-0.00002	+0.00275	-0.00002	
E	Bolt Joint at Gimbal Mounting	+0.00089	+0.00192	+0.00048	+0.00032	+0.00027	+0.00016	+0.00032	+0.00027	+0.00016	
F	Shroud Joint to Fuel Pump	+0.00062	+0.00182	+0.00060	+0.00038	+0.00062	+0.00132	+0.00038	+0.00062	+0.00132	
G	Shroud Joint to Oxid. Pump	+0.00458	+0.01850	+0.00111	+0.00425	+0.00615	+0.00300	+0.00384	+0.00601	+0.00200	
H	Bolt Joint, Housing to Injector	+0.00552	+0.00136	+0.00198	+0.00855	+0.00008	+0.00225	+0.00370	+0.00014	-0.00398	
I	Seal at Turbine Nozzle	-0.00145	--	--	+0.04354	-0.02380	--	-0.00272	-0.00342	--	
J	Seal between Fuel Flow Channel & Bolt Joint	+0.00052	--	--	+0.00026	+0.00023	--	+0.00026	+0.00023	--	
K	Seal between Fuel Flow Channel & Second Stage Fuel Pump	-0.00186	--	--	-0.00002	+0.00048	--	-0.00002	+0.00048	--	
L	Seal between First and Second Stage Fuel Pumps	-0.00030	--	--	+0.00026	-0.00040	--	+0.00026	-0.00040	--	
M	Seal at Second Stage Fuel Pump Inlet	-0.00108	--	--	-0.00063	+0.00033	-0.00320	-0.00063	+0.00033	-0.00320	
N	Seal at First Stage Fuel Pump Inducer (Hydrotest only)	+0.00216	--	--	--	--	--	--	--	--	
O	Mounting Face, TPA to Gimbal	+0.00149	+0.00235	--	0.0	0.0	0.0	0.0	0.0	0.0	Assumed Fixity for Oper. Cond. at this Station.
P	Seal between Fuel Inlet & First Stage Fuel Inducer	+.00145	--	--	+0.00025	-0.00062	--	+0.00084	-0.00061	--	
Q	Seal between Oxid. Inlet & Oxid. Inducer	+0.00164	--	--	+0.00116	+0.00269	--	+0.00184	+0.00507	--	
R	Seal between Inlet Volute & Thrust Chamber (Hydrotest only)	-0.00039	--	--	--	--	--	--	--	--	
S	Seal between Thrust Chamber & Oxid. Pump (Hydrotest only)	+0.00280	--	--	--	--	--	--	--	--	
T	Seal between Combustion Chamber & Oxid. Pump	+0.00022	--	--	+0.00203	+0.00268	--	-0.00046	+0.00430	--	
U	Seal between Oxid. Flow Channel & Combustion Chamber	+0.00130	--	--	+0.00735	+0.00161	--	+0.00100	+0.00271	--	
V	Seal between Oxid. Flow Channel & Bolt Joint	+0.00345	--	--	+0.00810	+0.00154	--	+0.00270	+0.00230	--	
W	Seal, Injector Simulator & Test Stand (Hydrotest only)	+0.00185	--	--	--	--	--	--	--	--	
N	Seal between First Stage Fuel Pump & Fuel Inducer	--	--	--	-0.00094	-0.00070	--	+0.00094	-0.00068	--	
P	Rubbing Seal at First Stage Fuel Pump Inducer	--	--	--	+0.00038	-0.00045	-0.00068	+0.00042	-0.00049	-0.00069	
Q	Rubbing Seal at Oxid. Pump Inducer	--	--	--	+0.00139	+0.00226	+0.00185	+0.00139	+0.00473	+0.00157	
S	Labyrinth Seal at Oxid. Fuel Pump	--	--	--	+0.00650	-0.00290	--	+0.00210	+0.00534	--	

Housing, Predicted Deflection Summary

Figure VII-14

VIII.

TPA HOUSING DEVELOPMENT

A. GENERAL

The objectives of the housing programs are the development of housings that will contain the required fluid and gas pressures, transmit the fluids and gases from station to station with minimum pressure drops, provide a stable base for the rotating components, and transmit the thrust load developed by the thrust chamber to the missile frame.

Model testing was accomplished with excellent results. The basic configuration of the housing was proven feasible. The design of the B-housing is proceeding on schedule. Fabrication of the first A-housing was completed on 31 March, and testing will begin early in April.

B. MODEL TEST RESULTS

1. Introduction and Summary

The testing programs for the advanced turbopump housing model were shown in Figure VIII-1 of Report 10830-Q-2. The results of Metal Model I testing were presented in Report 10830-Q-1. Preliminary test results from photoelastic models, from Metal Model II and from braze samples were presented in Report 10830-Q-2. The model testing programs have now been completed and the results analyzed. The test data from Metal Models I and II were analyzed and compared to those from Housing-A. The analysis shows that a thickening of the housing wall at the T-junction would be more effective than external ribs. The curvature of the oxidizer end dome is the major determinant of housing axial deflection. A comparison of dome curvatures versus axial displacement is shown in Figure VIII-1.

2. Braze-Sample Testing

Initial analysis of hydrotest results indicated a braze strength of 20,000 psi. Further evaluation of test results revealed that the strength of the braze joint, considering 100% area bond, was only 15,950 psi. A metallurgical examination of the brazed surfaces indicated that only 50% of the braze surface was bonded before testing. In addition, the braze material showed indications of poor amalgamation. The sample had been brazed with a 100-lb load on the specimen which was not sufficient to ensure a good bond. The metallurgist indicated that additional testing should be performed with cylindrical rather than flat samples. By using cylindrical shapes, a uniform pressure can be applied to the bond by interference-fitting of the two surfaces. Further braze-sample testing was discontinued until results of present fabrication methods have been evaluated.

3. Electron-Beam-Welded Sample

One sample was electron-beam welded and hydrotested early in the reporting period. Some difficulty was encountered during welding due to warpage

VIII, B, Model Test Results (cont.)

of the flat sample. As three weld passes were made on each rib and warpage occurred on the first pass, it was extremely difficult to follow the rib pattern on subsequent passes. This problem was not encountered in the actual part and could have been avoided in the sample with improved clamping.

The electron-beam welded sample was hydrotested in a manner similar to that used on the brazed sample. The sample was incrementally pressurized to 2000, 4000, and 6400 psig, returning to 0 psig after each increment. The specimen began to fail during the initial pressurization to 6400 psig when a loud crack was heard. The test was continued when the sample showed no leakage. The next cycle was terminated at 5100 psig and the last cycle at 3370 psig due to additional cracking sounds and subsequent burst.

A metallurgical examination of the weld joint showed improper weld width at the joint and insufficient penetration of the electron beam in some areas of the joint. These conditions were caused primarily by the warpage of the weld sample. To obtain proper penetration in the second Housing-A, weld samples were made immediately prior to welding on the housing to ensure proper machine operation. In addition, radiographic inspection was used to ascertain that a proper weld joint was attained.

An additional electron-beam-weld sample may be fabricated and tested at a later date; the sample will be either properly clamped during welding or a new specimen shape will be used.

4. Photoelastic Model Tests

The two photoelastic models were tested and the results were analyzed. The first model was subjected to pressure only, whereas the second model was subjected to pressure and thrust load. The results show that: (a) the maximum stress to be expected in the three-walled Housing-A is 75,000 psi; (b) some radii must be increased to avoid stress concentrations; (c) it is desirable to reduce the cylindrical projection into the outlet cylinder to reduce local stresses at the juncture; since this projection is required to hold the primary combustor, larger radii will be added at the juncture to reduce the stress level; (d) the thrust pad is well supported and should cause no serious problems; and (e) the bearing support areas should not rotate or misalign significantly under load to be detrimental to turbopump operation.

5. Metal Model II Tests

The hydrotests and thrust tests of Metal Model II were completed and the test results were analyzed. The results of pressure and thrust testing with the original large ribs are questionable due to a fixture slippage during testing. The large nut used to retain the fuel housing could not be torqued sufficiently during test setup, and test results show a large axial movement

VIII, B, Model Test Results (cont.)

between bearing centers in the first tests due to movement of the retaining nut. When the model was tested with ribs of reduced height, an additional measurement was made to ascertain the magnitude of the movement between the fuel housing and the oxidizer housing due to the inability to torque the retaining nut to the required value. This axial movement was 0.0082 in. which, when subtracted from the previously measured turbopump roller bearing center axial displacement of 0.0273 in., results in a true turbopump roller bearing axial displacement of 0.0191 in. inasmuch as Housing-A design replaces the retaining nut with a bolted flange. A final summary of results and a projection to Housing-A performance is shown in Figure VIII-2.

C. HOUSING FABRICATION

1. Housing A

The objectives of fabricating a Housing-A were to determine fabrication problems and solutions prior to the fabrication of Housing-B, to ascertain cost-reduction areas, to determine nondestructive test methods, and to provide a structurally stable housing that would meet Work Statement and rotating-element requirements.

Housing-A is fabricated in three separate parts: the oxidizer housing, the fuel housing, and the oxidizer bearing. Two each of these parts were ordered. Two versions of the three-walled oxidizer housing were designed and ordered. One version used plug-welding for attaching the internal passage ribs to the walls and the other used electron-beam welding for the rib-to-wall attachment. This allows an evaluation of the two fabrication methods on the basis of cost, fabrication time, and structural integrity.

a. Plug-Welded Oxidizer Housing

The plug-welded oxidizer housing, PN 1122522, shown in Figure VIII-20 of Report 10830-Q-2 was ordered on 21 December 1965 and work began immediately. During preliminary machining and forming, weld samples were being prepared to determine the slot length and shape of the plug weld. The final plug weld is a 1-in.-long slot, 0.210 in. wide, with a 30° taper from 0.030 in. above the inner surface to the outside surface. Root-weld passes are made to attach the ribs to the shell, and the weld is then dye-penetrant inspected for cracking. If the welds are satisfactory, the filler-weld passes are made to the desired surface level and are dye-penetrant-inspected again.

Assembly, machining, and welding of the housing proceeded on schedule until after the T-section was welded in place and the unit sent for solution annealling. After solution-annealling, the housing received a rough machine cut on the inner bore to remove excess material, and was then sent for stress relief and aging.

VIII, C, Housing Fabrication (cont.)

The heat-treat vendor erroneously decided to age the housing without stress relief because a solution-anneal had been performed two days earlier. The unit was rejected by Aerojet-General and returned to the heat-treat vendor with detailed instructions how to relieve the stresses of rough-cut machining that were locked-in by the aging cycle. The unit was to be placed in a furnace with a maximum temperature of 500°F, the temperature was to be increased at a rate of 100°F/hr to 1800°F and held at 1800°F for 1-1/2 hr. The unit was then to be cooled to 1350°F as rapidly as possible and the normal aging cycle performed. The vendor's furnace charts were requested. The furnace charts indicated that the heating cycle had been erroneously accomplished in 90 min. The two thermocouples on the part, as specified in Aerojet-General Specification 46604B, had not been used. This heat treatment was consequently rejected.

The heat-treat vendor was instructed to solution-anneal the unit with the required thermocouples attached. Aerojet-General personnel were sent to witness this heat treatment which was accomplished in accordance with the specification. Subsequent dye-penetrant inspection indicated over 150 cracks. Of these 150 indications, 40 were outside of Aerojet-General's specification and were repaired. Due to so much weld repair, the unit was returned for re-aging, which was again witnessed by Aerojet-General personnel. Dye-penetrant inspection after heat treatment revealed 26 major cracks. Aerojet-General's welding and materials experts immediately tried to determine the most feasible repair procedure. It was determined that the material had been subjected during previously described heat treatments to temperatures over 1950°F but less than 2200°F for a period of time sufficient to produce an excessive carbide film at the grain boundaries. This condition would produce a low elongation at elevated temperatures and seriously limit the weldability of the material in an aged condition.

The rapid heating and cooling of the three-walled structure had created high thermal stresses. A thermal-stress calculation showed that the inner complex of intermediate shell and ribs had lagged approximately 500°F behind the temperature of the inner and outer walls. The following corrective actions were taken. The housing was placed in a furnace at 400°F (max), and the temperature was raised from 400 to 1200°F at increments of 200°F/hr, with thermocouples installed on the three walls of the cylindrical portion. The unit was stabilized at 1200°F and then heated at a rate of 800°F/hr to 1500°F to pass rapidly through the age-hardening zone. After stabilizing at 1500°F, the unit was heated to 1800°F and held for two hours. The unit was then removed from the furnace, an adapter manifold was clamped to the thrust-chamber flange, and argon gas was blown through the passages at 5 ft^3/hr, increasing slowly to 25 ft^3/hr as the unit cooled. The hardness of the material on the Rockwell scale was Rc 7. The unit was then dye-penetrant inspected, and no additional cracks were evident.

The weld repairs were made by welding and peening each weld pass to accomplish an immediate stress relief. After all crack indications were removed, the unit was returned for aging. The aging cycle consisted of placing the unit in a 400°F furnace and heating to 1200°F at a rate of 200°F/hr, stabilizing at 1200°F, then raising to 1350°F at 200°F/hr and stabilizing at 1350°F. The part

VIII, C, Housing Fabrication (cont.)

was held at 1350°F for 10 hr, furnace-cooled to 1200°F, and held at 1200°F for a total aging time (1350° + furnace cool + 1200°F) of 20 hr. The part was then furnace-cooled by argon gas flow to room temperature. The final Rockwell hardness was Rc 44, and dye-penetrant inspection showed no further discrepancies. Final machining was accomplished, and the unit was received on 31 March. Figures VIII-3, -4, and -5 show the oxidizer end and thrust-chamber flange, the internal contour, and the thrust-support structure, respectively.

b. Electron-Beam-Welded Oxidizer Housing

The electron-beam-welding housing, PN 1121944 (similar to PN 1122522 as shown in Figure VIII-20 of Report 10830-Q-2), was ordered on 30 December 1965, and work has proceeded on schedule. The heat treatment of the three-walled structure was delayed by about one week to ascertain the effects of the new heat-treat cycle described above and to ensure that the problem was resolved. The T-section is being welded in place, and delivery of the housing is expected in April.

c. Fuel Housing

Two fuel housings, PN 1122426, as shown in Figure VIII-20 of Report 10830-Q-2, were ordered on 19 January 1966. Some difficulty was encountered in electron-discharge machining the integral diffuser vanes. On 23 February an Aerojet-General representative was sent to the vendor as an on-site observer to assist and accelerate the manufacture of the first housing. The housing was received on 16 March. The gamma-ray inspection methods used revealed two weld areas which could not be accurately resolved. This information was used to improve the Housing-B design. In addition, the difficulty of machining the integral vanes was resolved in the Housing-B design, as described in paragraph D,3, below.

d. Oxidizer Bearing Housing

The oxidizer bearing housings were completed (PN 1121915, as shown in Figure VIII-20 of Report 10830-Q-2) and shipped with the oxidizer housing. No problems were encountered in this unit.

2. Test Plans and Setup

The plan for hydrotesting and thrust-testing the Housing-A was completed. The test setup, Aerojet-General Drawing 1120346, was revised as shown in Figure VIII-6. The test tooling is shown in Figure VIII-7. Preliminary plans have been made for vibration-testing and will be finalized if the initial testing of Housing-A is successful.

VIII, TPA Housing Development (cont.)

D. HOUSING-B DESIGN

1. Design

Two housing designs for the B-version of the advanced turbopump were studied. The two-walled unwelded rib-to-shell design was completed and vendor quotations were solicited. The two-walled design, based on vendor quotations for two units, would cost approximately 40% less than the three-walled design. The main problem in the two-walled design is the requirement for complete redesign of the primary injector due to the addition of the return manifold. Further effort on the two-walled design was postponed unless serious fabrication or structural problems are encountered in Housing-A. The primary effort was therefore placed on the three-walled, welded rib-to-shell design similar to the Housing-A design.

The three-walled welded-rib Housing-B design is a refinement of the Housing-A design. The overall length of the housing between the fuel housing attachment flange and oxidizer inlet flange of the oxidizer housing, Figure VIII-8, has been reduced by 2.625 in. The center line of the thrust-chamber flange has been moved 1 in. towards the oxidizer inlet end. The T-section of the oxidizer housing is made from a solid-cone shaped forging, which is welded in place; the oxidizer passages are drilled holes. This will greatly reduce both time and cost of attaching the T-section. An orifice plate has been added to the face of the thrust-chamber flange which can be readily changed as required to ensure uniform entrance pressures to the tubes of the regeneratively cooled thrust chamber and uniform exit pressures from the tubes. The curved vanes in the oxidizer passages are designed for minimum pressure drop. A volute and boss have been added to the oxidizer dome for supplying high-pressure oxidizer to the boost-pump turbine. The oxidizer bearing housing has been made integral with the oxidizer housing. A boss is being designed for connecting the fuel-supply line to the boost-pump turbine. The weight of the housing has been reduced significantly.

2. Oxidizer Housing

The oxidizer-housing detail drawings are 70% complete. The curved rib patterns between shells have been submitted to the Housing-A vendors for study and comment. The major effort was concentrated on simplifying the manufacturing procedures. In addition, considerable effort has been expended to determine, by layout, the location for feed lines to the bearings and coolant passages, and the location of instrumentation.

3. Fuel Housing

The fuel housing, Figure VIII-9, has been designed based on using Inconel 718. The fuel housing for the Housing-A design was made from AISI 347, which resulted in a heavier unit and costly machining of diffuser vanes. AISI 347 is not suitable for electron-beam welding required in the new diffuser-vane

VIII, D, Housing-B Design (cont.)

manufacturing process. In the new process, the diffuser vanes are machined on the open face of the right-hand forging and inserted in holes in the left-hand face. The vanes are attached by several electron-beam-weld passes around the circumference of the left-hand forging, with sufficient penetration depth to ensure a strong bond. The use of Inconel 718 allows a reduction in wall thickness of the volute section and a reduction in the size of the outer flange. Cost estimates will be obtained before a decision is made to proceed with this design.

Provisions have been made for regeneratively cooling the hot-gas side of the fuel housing by bleeding oxidizer from the inner oxidizer passage across the fuel-housing face and discharging the oxidizer at the combustion seal. This will keep the fuel housing cool and avoid thermal-stress or distortion problems.

4. Stress and Deflection Analyses

The stress analysis for the Housing-B design is being made for two conditions: (a) proof pressure and thrust load at ambient temperature, and (b) maximum expected operating pressure and thrust load plus operating temperatures. The proof pressure and proof thrust loads are defined as 1.45 times nominal pressure and 1.4 times nominal thrust load, respectively. The maximum expected operating conditions are based on an allowable turbine overspeed of 10%, which raises the nominal pressures and the nominal thrust load by a factor of $(1.1)^2$ and 1.21, respectively.

The preliminary proof-pressure and thrust conditions at maximum stresses and deflections are shown in Figures VIII-10 and 11, respectively. The stresses and deflections were compiled from results of analyzing various areas through several design iterations as the final design was developed. An overall analysis is currently being set up to produce a final analysis of the entire Housing-B design for the two conditions. The axial and radial deflections are being compared with limiting values required by bearings, seals, pump impellers, and turbine to ensure that the housing has proper operational stability.

The turbine nozzle required special attention in the attachment to the housing and where contact is made with the primary combustor. The stresses and deflections, Figures VIII-12 and 13, are the results of several analyses conducted to establish the final design. The 180,000-psi stress at Point-B, Figure VIII-13, is a thermal stress and, when compared to fatigue strength, has a use life without failure exceeding 500 cycles. By comparing the radial deflections of Points 5, 6, 7, 8, and 9 of Figure VIII-13, a slight rotation is evident in this area. The rotation is not severe enough to affect the sealing of the piston rings or the turbine tip clearances and is therefore acceptable.

VIII, D, Housing-B Design (cont.)

5. Temperature

The housing inner-wall temperatures are dependent upon hot-gas velocity between the metal heat barrier and the housing wall, upon oxidizer coolant flow rates on the opposite side of the wall, and upon housing wall thickness. The interaction of these three variables is shown in Figure VIII-14. It can be readily seen that the hot-gas velocity at the housing wall is the primary determinant of housing wall temperature.

The hot-gas velocity at the housing wall is dependent on the effectivity of the metal heat barrier in reducing the main-gas-stream velocity. By reducing the number of hot-gas entrances and by their proper placing with respect to the cavity formed by the metal heat barrier and the housing wall, recirculation of hot gas and hot-gas velocity can be minimized (to less than 1 ft/sec). The hot-gas entrances must be of sufficient area to allow gas to pass to and from the cavity during start and shutdown transients without collapsing the metal heat barrier. The primary combustor in the workhorse housing will be used to additionally test various metal heat-barrier designs.

An analysis of thermal stresses in the oxidizer housing determined that the maximum inside temperature of the housing in the primary combustor region should not exceed about 400°F. Thus, the effective gas velocity between the shield and the housing should not exceed 5 ft/sec. In the oxidizer bearing region, the temperatures should be in the 250°F or lower temperature range. It appears this can be achieved with the proposed primary combustor liners. If the temperatures are higher than desired, a small quantity of cold oxidizer can be introduced to shield the area, as is being done on the face of the fuel housing.

6. Stress Model Development

Stress-model development consists of formulating a computer program capable of analyzing the complex shape of the T-section housing. This computer program will replace the empirical methods currently being used for stress and deflection analyses of the T-shape. Although the empirical methods have produced quite accurate results, as evidenced in the Metal Model testing, a more exact analysis is required for the final flight-weight housings.

The computer program for the stress model of the housing is undergoing final checkout. The user's manual has been written, reviewed, and is being reproduced. The final report on the development is being written. The computer program is being set up to analyze the photoelastic model. The results of this analysis will be compared with the final test results of the photoelastic models.

7. Fabrication

The Inconel 718 forgings required for the Housing-B oxidizer housing were ordered on 15 March. Delivery is expected early in May.

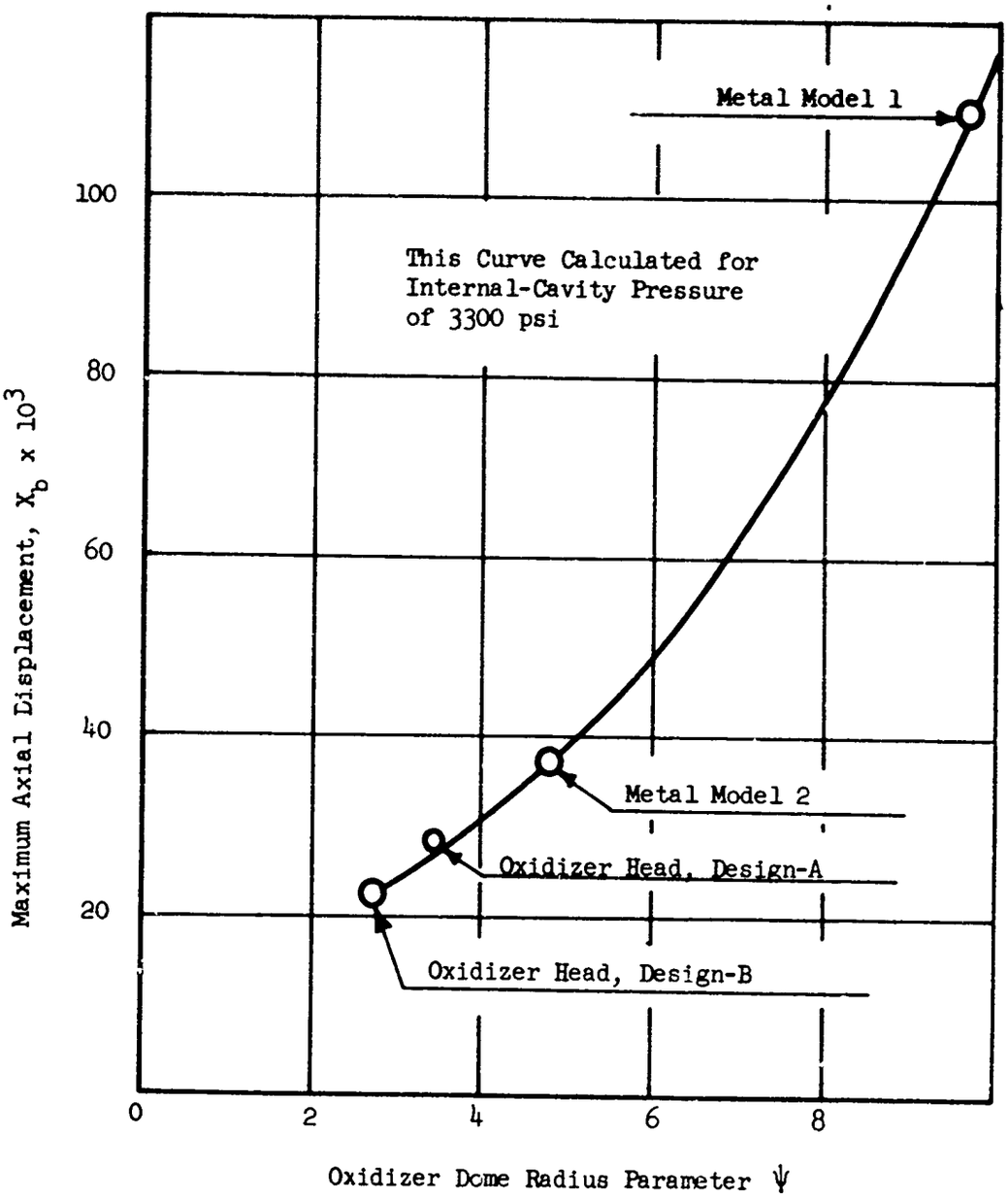

Axial Displacement vs Oxidizer Dome Radius Parameter

Figure VIII-1

(This page is Unclassified

	Metal Model I 1 Wall	Metal Model II 2 Wall	Housing A 3 Wall
Material	4130	4130	Inconel 718
Yield strength, psi	70,000	70,000	140,000
Design pressure, psig	2500 Inner	2500 Inner 3100 Ox passage	5000/3100 Inner 6025 Ox passage
Proof pressure, psig		3300 Inner 4300 Ox passage	7250/4500 Inner 8700 Ox passage
Design thrust load, lb		50,000	100,000
Proof thrust load, lb		70,000	140,000
Axial deflection between bearings at proof conditions, in.	.0171 Elastic .000 Permanent	.0195 Elastic .008* Permanent	<.030 Elastic Expected <.005** Permanent Expected
Rotation between bearings at proof conditions, in.	.0022 Elastic .000 Permanent	.008 Elastic .000 Permanent	<.010 Elastic Expected <.005** Permanent Expected
Status	Checks satisfactorily	Pressure & thrust loads contained satisfactorily. *Deflection retested satisfactorily.	Expect Phase II go-ahead

*Original tests showed excessive deflection at fuel end nut. Since this nut will not be used in Housing "A" Metal Model II was retested to check deflection for revised design. 0.008 in. was movement due to lack of nut preload.

**Work statement requires less than 0.020 in. permanent axial deflection and less than 0.008 in. permanent radial deflection at proof pressure.

TPA Housing Structural Testing (u)

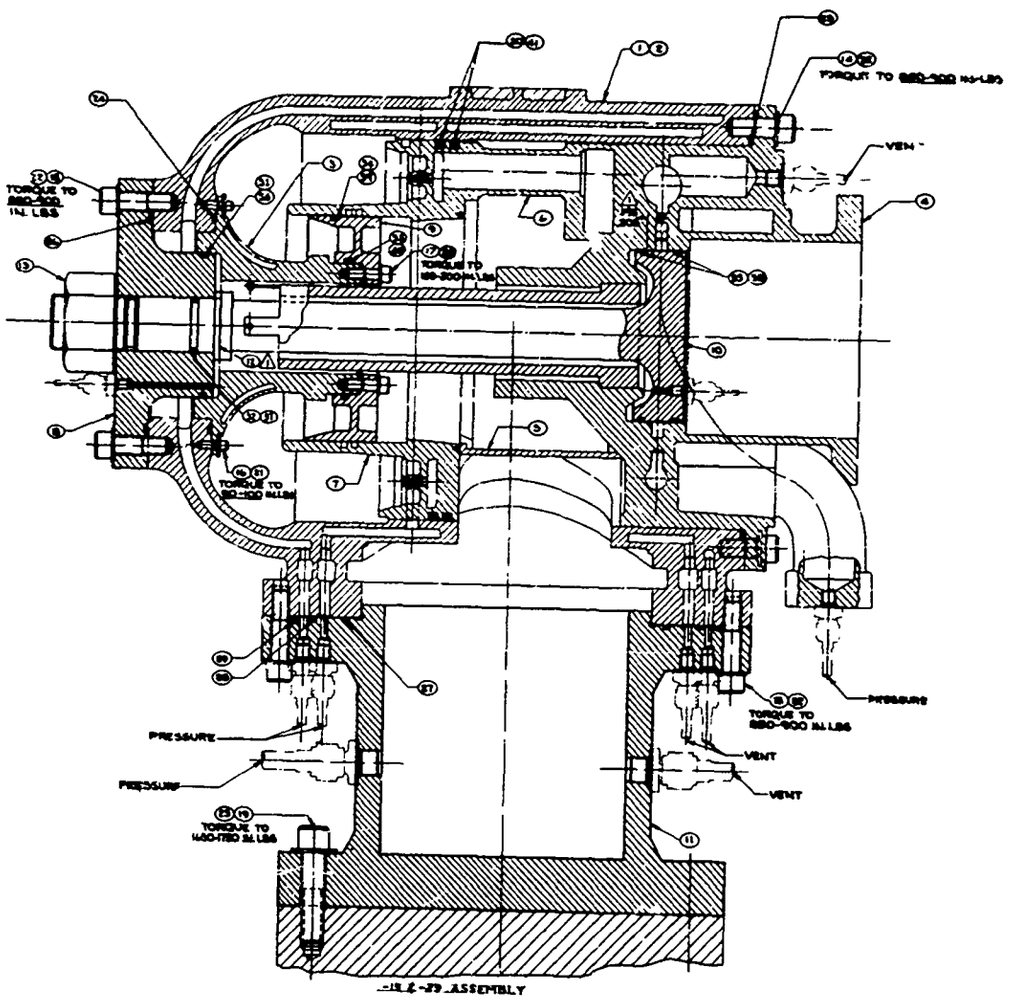

Housing-A Oxidizer-End and Thrust-Chamber Flange

Figure VIII-3

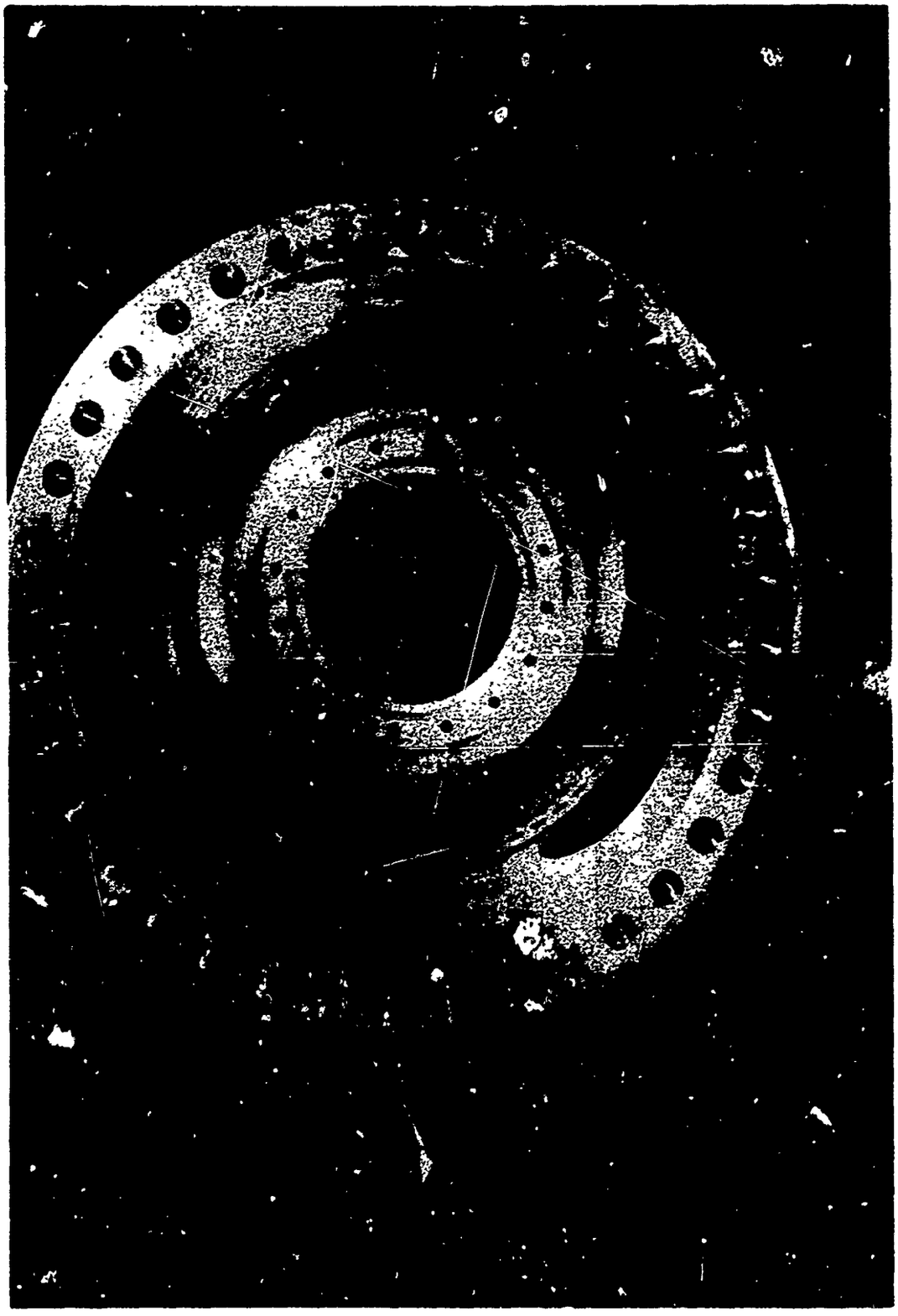

Housing-A Internal Contour

Figure VIII-4

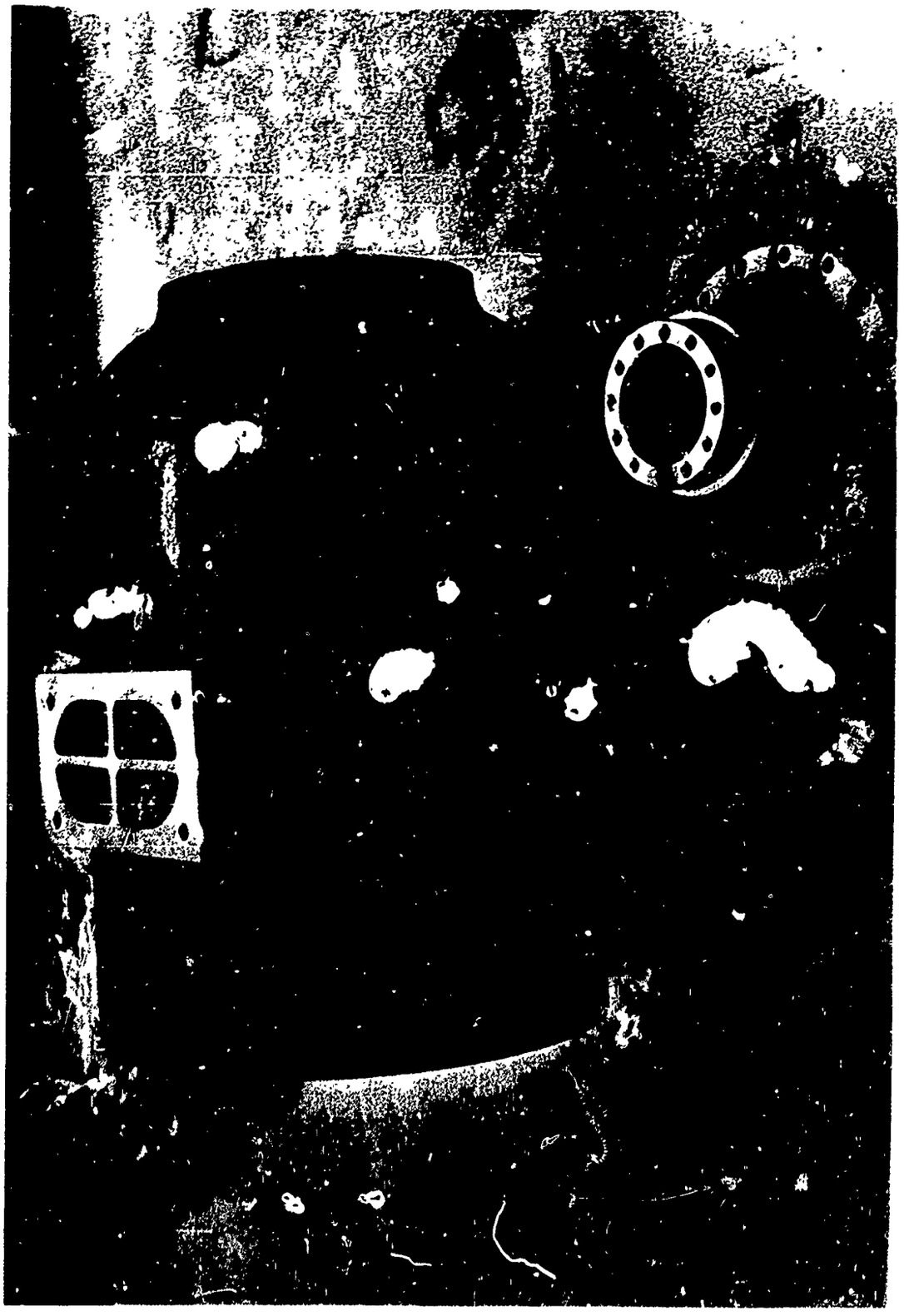

Housing-A Thrust-Support Structure

Figure VIII-5

Housing-A Test Setup

Figure VIII-6

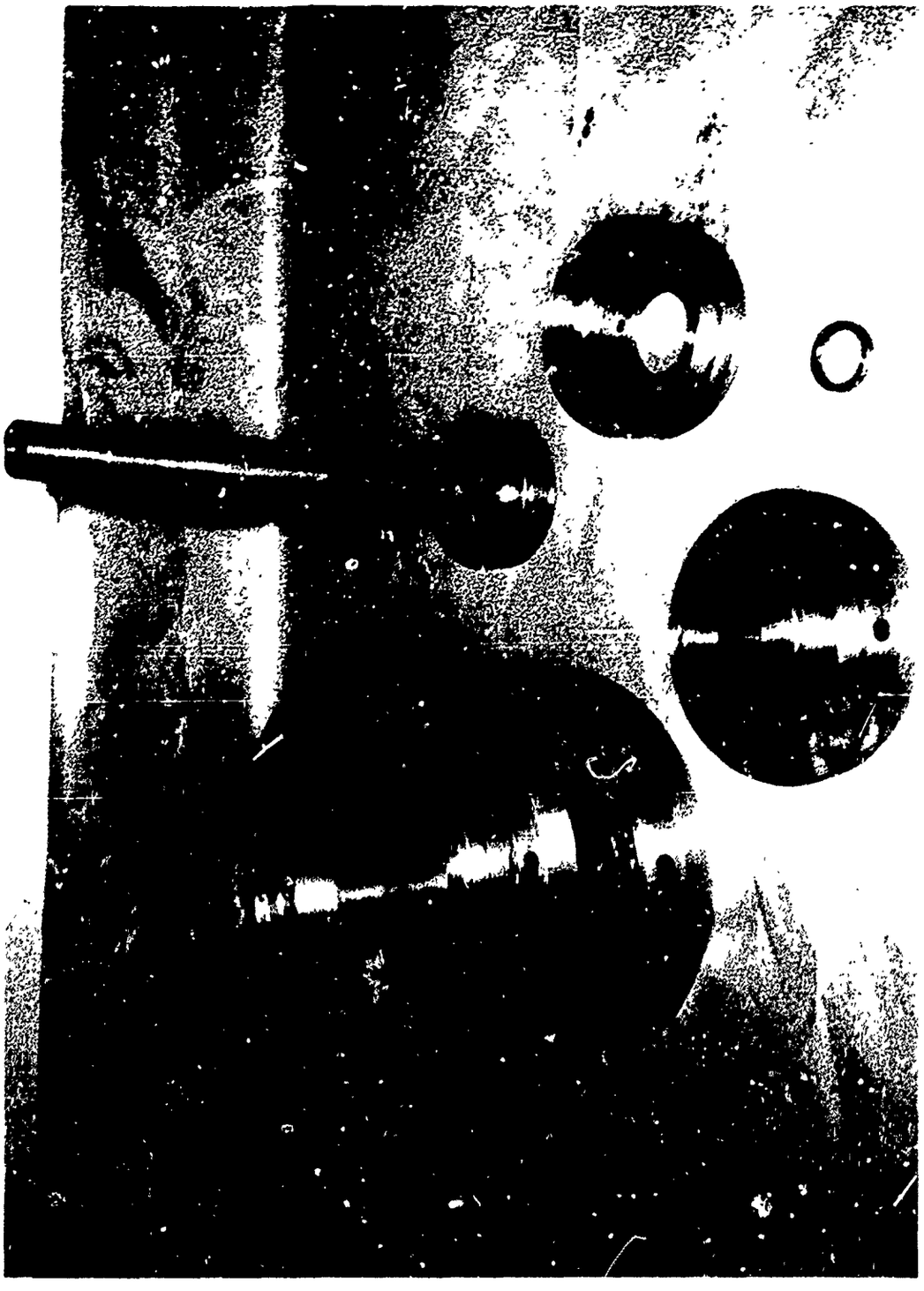

Housing-A Test Tooling

F ure VIII-7

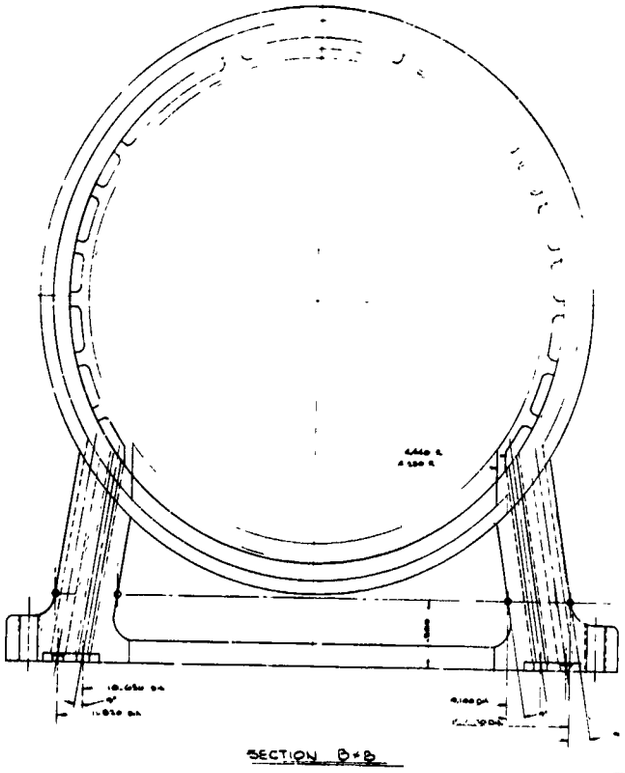

SECTION B-B

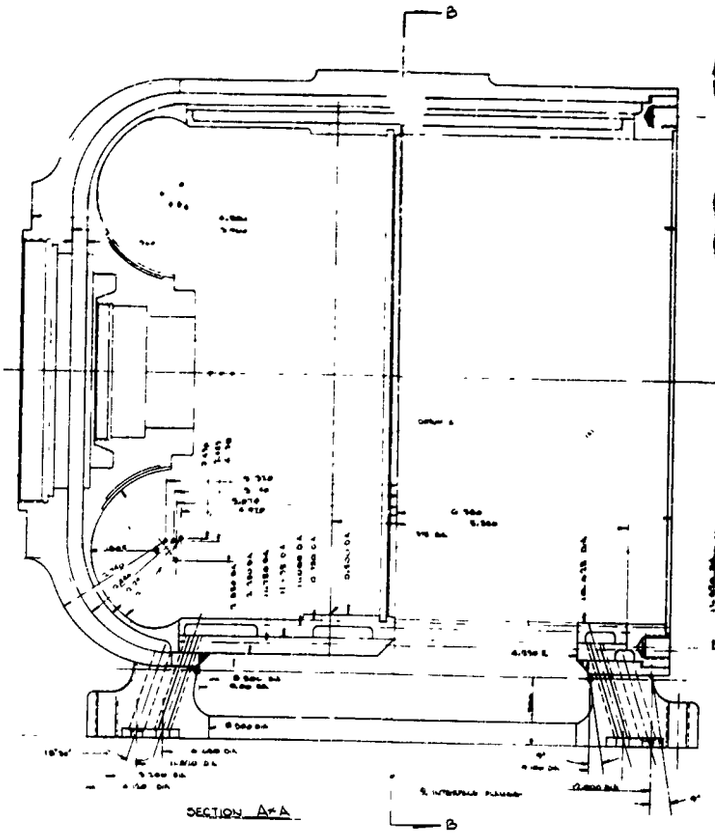

SECTION A-A

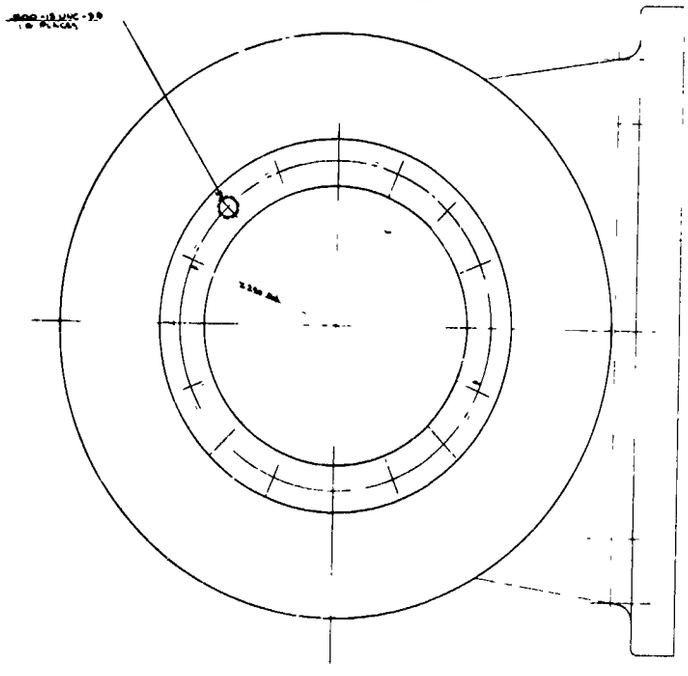

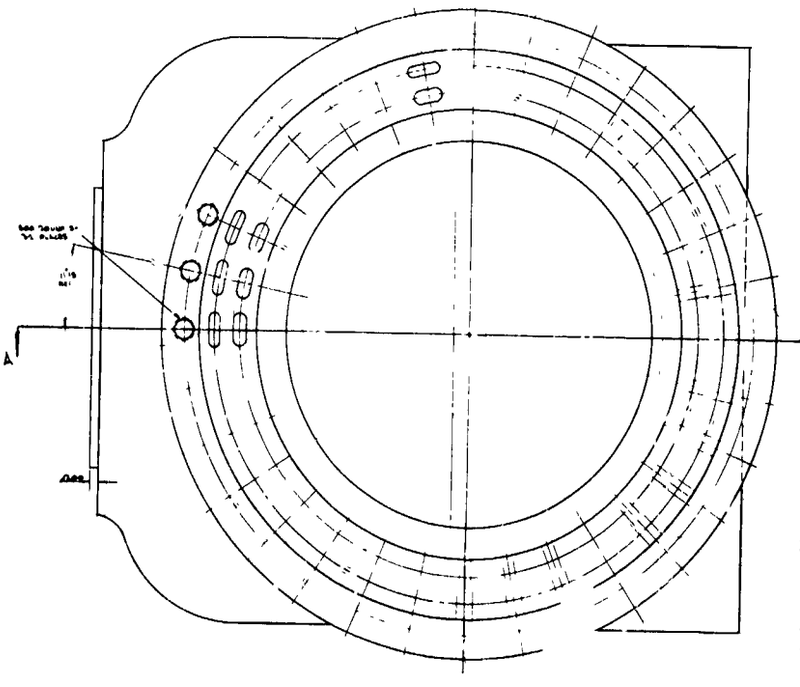

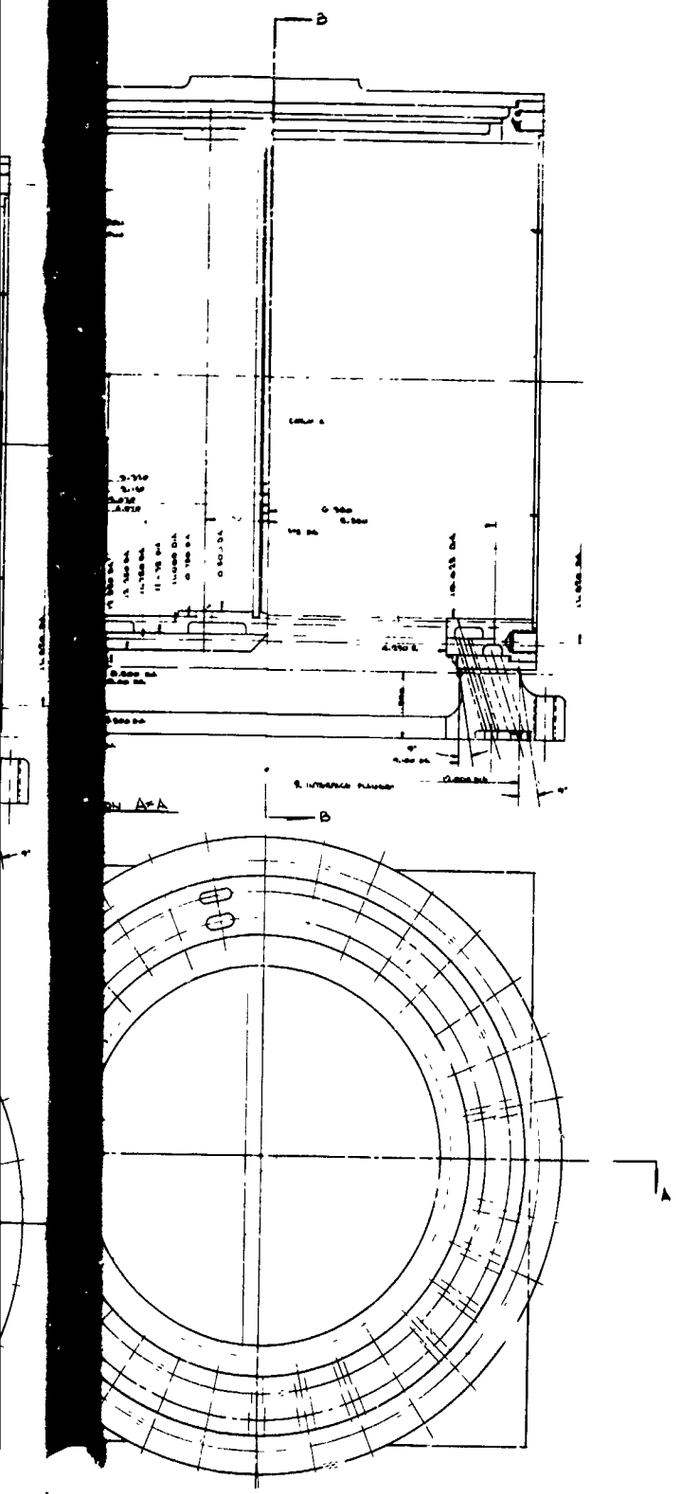

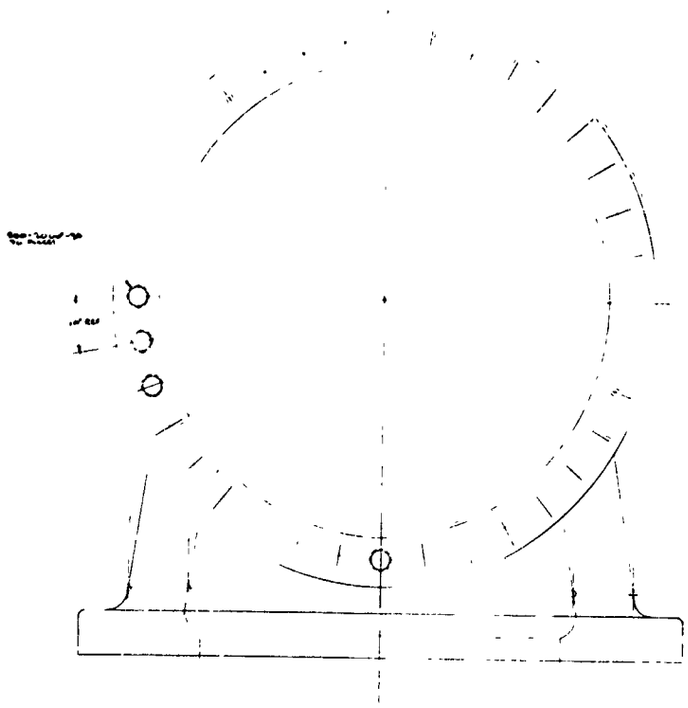

)sing-B Oxidizer Housing Layout

Figure VIII-8

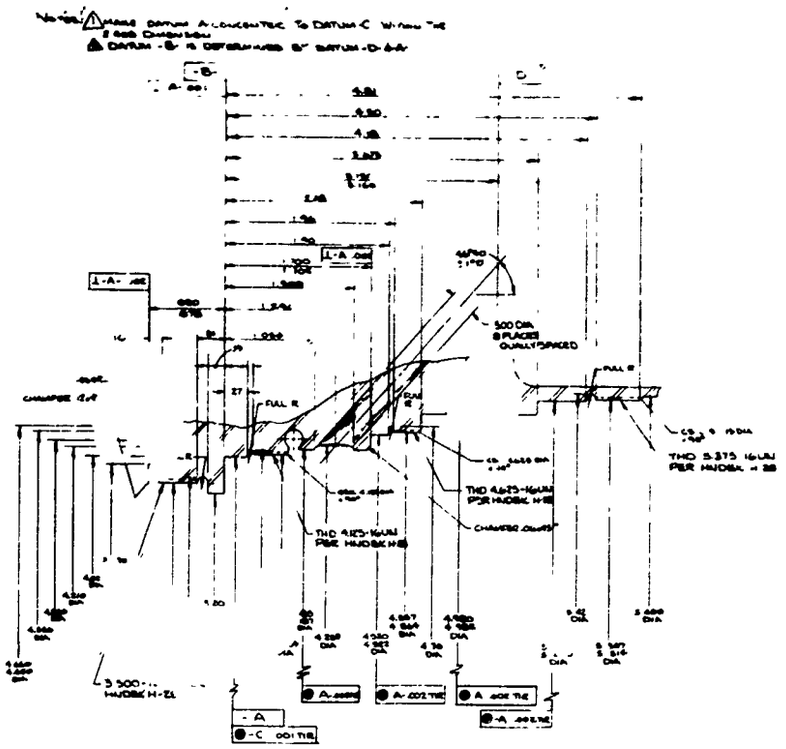

DETAIL A
SCALE 2/1

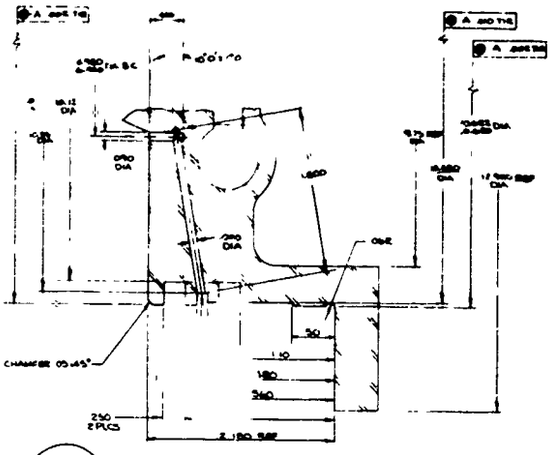

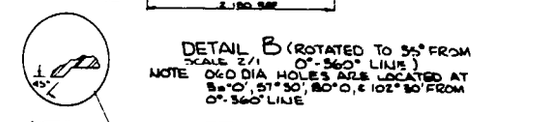

DETAIL B (ROTATED TO 35° FROM 0°-360° LINE)
SCALE 2/1
NOTE Ø60 DIA HOLES ARE LOCATED AT 5±°0', 51°30', 80°0', & 102°30' FROM 0°-360° LINE

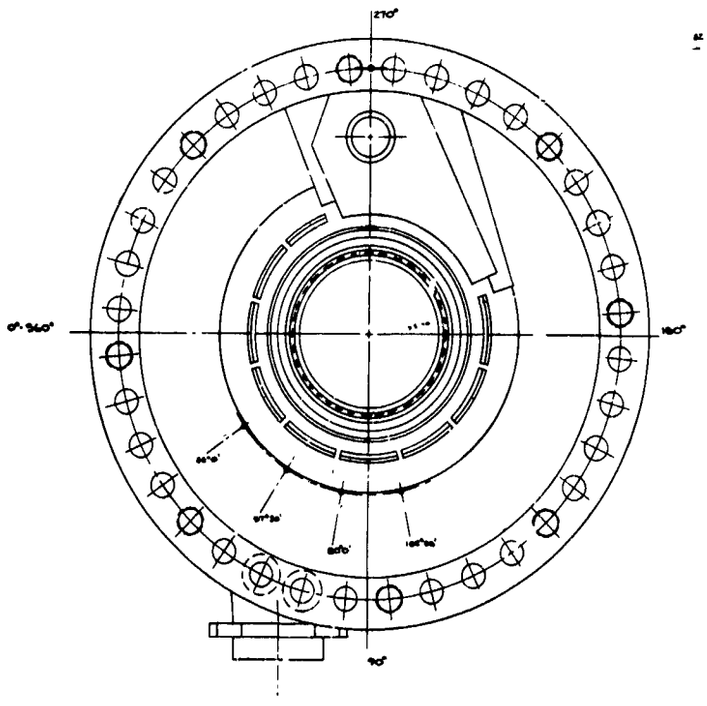

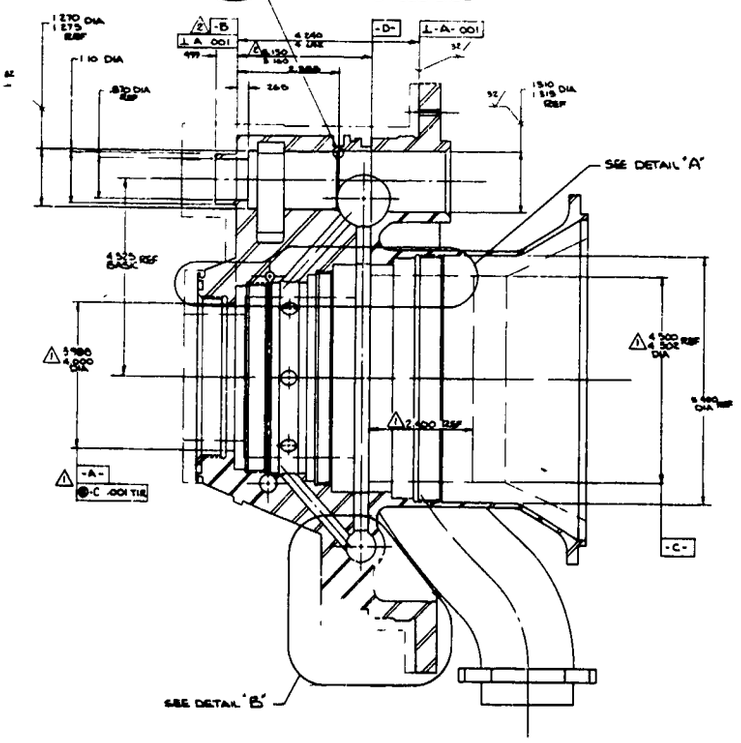

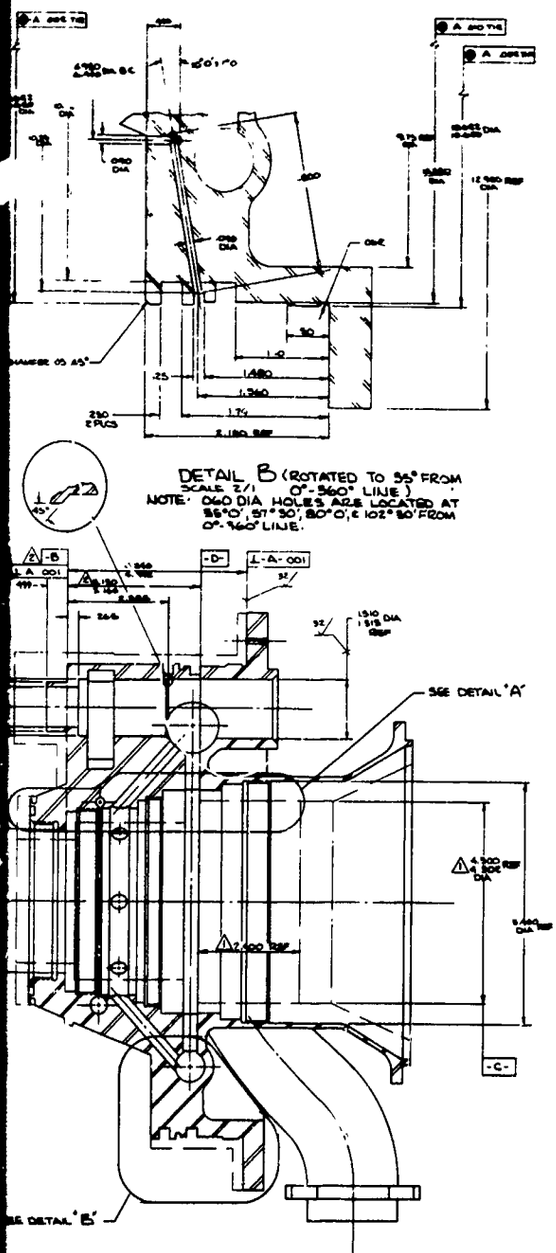

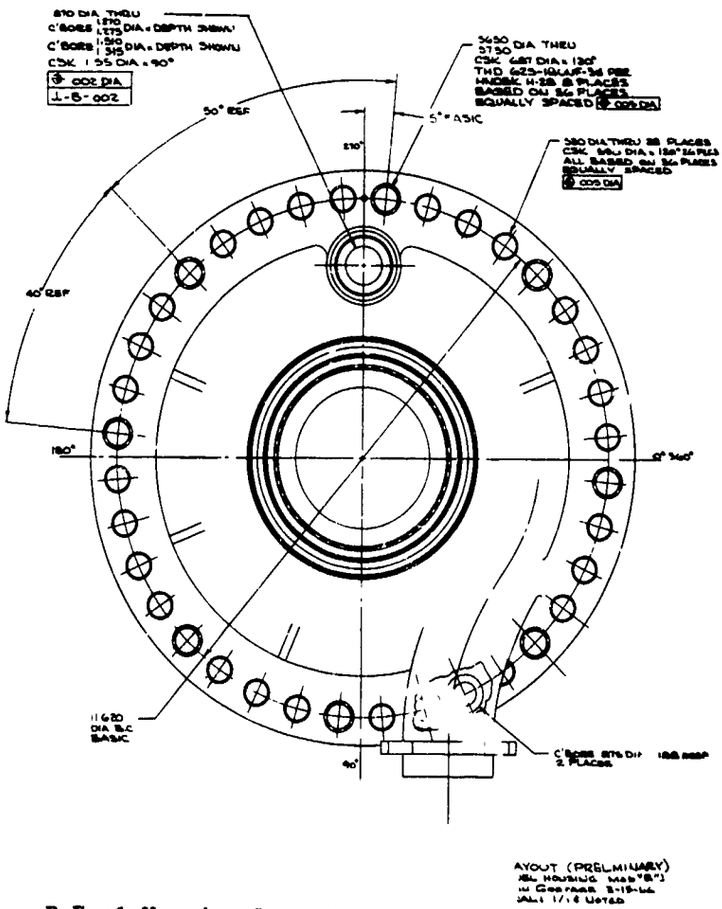

Housi _-B Fuel Housing Layout

Figure VIII-9

2

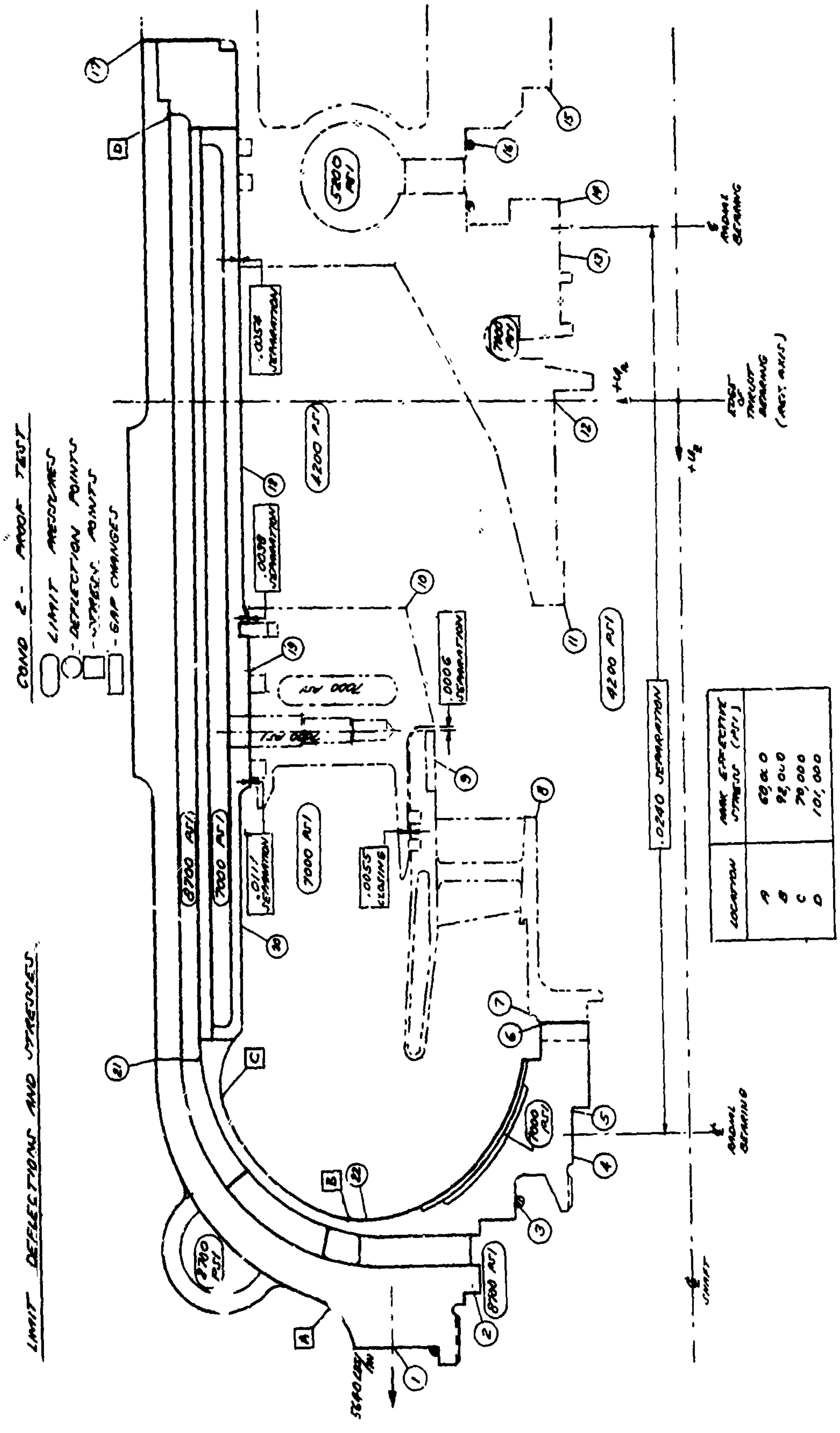

Housing-B Maximum Stresses and Deflections at Proof Conditions

Figure VIII-10

Limit Deflections - Proof Test Conditions

Location (Fig VIII-9)	U_r in.	U_z in.
1	0.00813	0.01356
2	0.00540	0.01919
3	0.00085	0.01683
4	0.00014	0.01669
5	-0.00008	0.01671
6	-0.00105	0.01580
7	-0.00014	0.01510
8	-0.00228	0.01462
9	-0.00081	---
10	0.00388	-0.01191
11	-0.00007	-0.00714
12	-0.00020	-0.00689
13	-0.00033	-0.00724
14	-0.00028	-0.00725
15	0.00017	-0.00783
16	-0.00011	-0.00743
17	0.00144	-0.00061
18	0.00697	---
19	0.00723	0.00030
20	0.00954	---
21	0.00529	0.00349
22	0.00133	0.01169

Deflections of Housing-B

Figure VIII-11

Location (Fig VIII-13)	Displacements Under Max. Operating Cond.			
	Pressure Plus Temperature		Pressure Only	
	U_r in.	U_z in.	U_r in.	U_z in.
1	-0.00018	0	-0.00073	0
2	0.00003	-	0.00005	-
3	0.02414	0.00730	-0.00009	0.00087
4	0.02555	0.02179	-0.00182	0.00075
5	0.03780	0.00503	0.00061	0.00370
6	0.03820	0.02128	-0.00148	0.00340
7	0.04739	-0.01336	0.00258	0.00476
8	0.04202	0.01830	-0.00120	0.00379
9	0.04287	0.03327	-0.00030	0.00313

Location (Fig VIII-7)	Effective Stress Under Max Oper. Cond, psi	
	Pressure Plus Temperature	Pressure Only
A	- 70,000	80,000
B	180,000	30,000

Housing-B Turbine Nozzle Stresses and Deflections at Maximum Expected Operating Conditions

Figure VIII-12

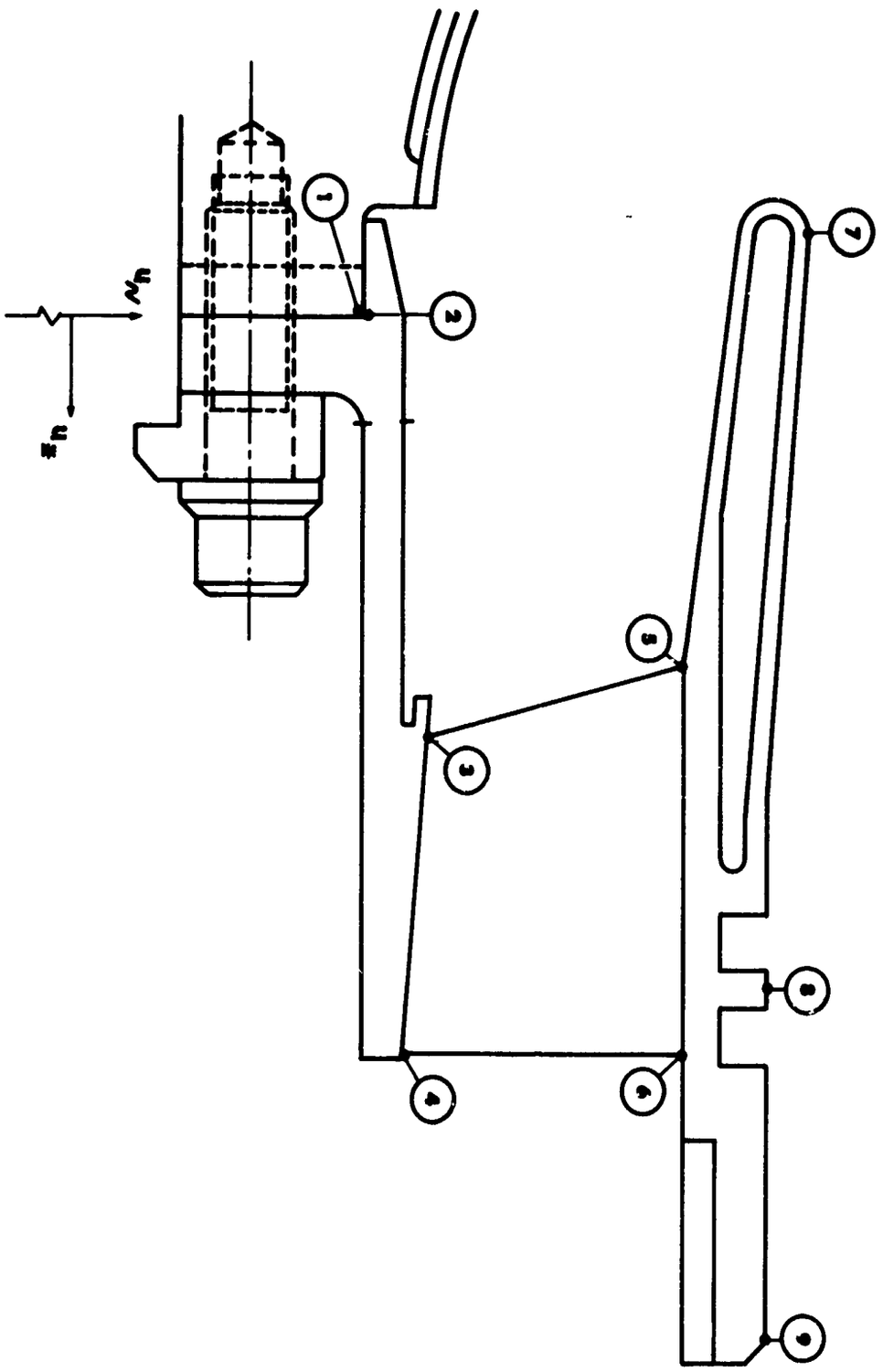

Housing-B Turbine Nozzle

Figure VIII-13

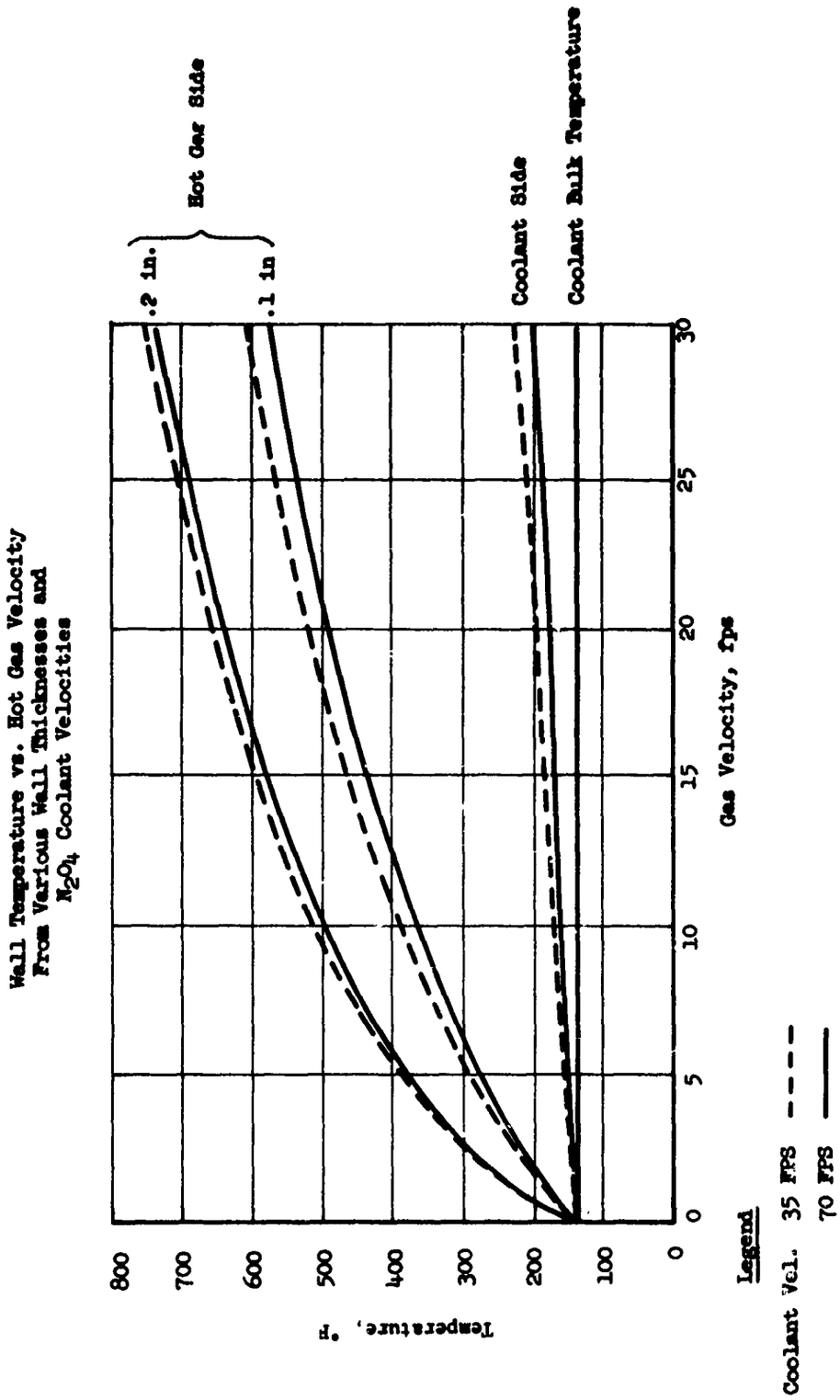

Temperature vs Gas Velocity

Figure VIII-14

IX.

TURBOPUMP BEARING DEVELOPMENT

A. GENERAL

Bearing development testing at 40,000 rpm with N_2O_4 as a lubricant began on 25 February 1966. Eight tests were attempted; significant data were obtained in three tests. Although no bearing problems were encountered, difficulties with the new tester design and the new test setup prevented the attainment of Work Statement objectives. The severity of this testing and the excellent post-test appearance of the bearings indicate that the N_2O_4 test objectives will be achieved without further difficulties. On 16 March 1966, the program was temporarily stopped when the hydrostatic thrust-bearing collar of the tester drive failed. The location of this collar is shown in Figure IX-1 of Report 10830-Q-1. Testing is scheduled to resume the first week of April.

B. BEARING TESTING AT 40,000 RPM IN N_2O_4

Three significant tests were conducted. Figure IX-1 tabulates steady-state data points for these tests, whereas Figure IX-2 shows the test-bearing installation and the parameters. In addition to these three tests, five test attempts were made which, however, did not generate significant data because of difficulties encountered. These attempts have been designated by letter subscripts to the test numbering system; for example, Test 1 consisted of two attempts, 1a and 1b, and of the significant test, 1c. Instrumentation difficulties with the recording of rotational speed were experienced on Test Attempts 1a and 1b. After correcting this instrumentation problem it was determined on Test 1c that a rotational speed of 40,000 rpm could not be attained. Total duration of this test was 197 sec, with about 60 sec of operation each at 10,000 and 25,000 rpm. The remainder of the duration was in transient conditions. Maximum speed obtained was 26,850 rpm. Axial and radial test bearing loads were 1250 and 480 lb, respectively. The temperature rises of the test bearings were 5 to 9°F. At shutdown, the propellant flow to the test bearings was terminated prior to turbine shutdown. This sudden flow interruption increased turbine speed to 34,350 rpm and caused an axial load peak of 4110 lb for about 10 sec. The outer-race temperature on the test bearings increased by about 60°F. Post-test inspection revealed no damage from this no-flow condition. The N_2O_4 was not filtered during the first three tests, and dirt dents in the ball and roller races were evident; however, the bearings were still serviceable.

A new ball-bearing tandem set and an aligning type roller bearing were installed for Test 2. The roller bearing was installed in the aligned position. Prior to this test, the exit areas of the two turbine nozzles were increased and a back shroud was installed behind the turbine wheel to reduce windage losses. No difficulty was experienced in obtaining 40,000 rpm. However, erratic recording caused an overspeed indication which, in turn, resulted in a trip shutdown after a duration of 152 sec.

IX, B, Bearing Testing at 40,000 rpm in N_2O_4 (cont.)

The turbine speed trip setting was increased to 50,000 rpm for Test 3. Prior to this test, the turbine inlet pressure (as established in the previous test to obtain 40,000 rpm) was set at the turbine shutoff valve. Due to a faulty regulating system, this setting had increased by the time the turbine supply valve opened. An overspeed exceeding 50,000 rpm occurred. The acceleration ratio was about 50,000 rpm/sec. Since no significant data were obtained, this test attempt was designated Attempt 3a.

After review of data and examination of the turbine wheel, Test 3b was conducted. This test had a duration of 216 sec, with axial and radial load peaks of 2500 and 955 lb, respectively, for 10 sec. The remainder of the time was at axial and radial load settings of 1550 and 520 lb, respectively. The test was terminated early because of fluctuating and decaying turbine supply pressures.

Post-test inspection revealed no bearing problems. However, one bearing of the ball-bearing set was damaged on disassembly (the puller groove broke). Consequently, a new tandem ball-bearing set was installed with the same aligning roller bearing. Figure IX-3 shows this ball-bearing set, which had accrued a total time of six minutes and 10 sec. Figure IX-4 shows the roller bearing, which accrued a total time of six minutes and 20 sec (four minutes of these operating times were at approximately 40,000 rpm).

Prior to the next test attempt, the dome-loading valve of the turbine-spin regulator was replaced and a line restriction was removed. This test attempt, designated Test 3c, was terminated prior to rotation when the motor pumping the oil lubricant failed.

The hydrostatic thrust-bearing collar of the tester drive failed during the next test attempt (Test 3d) at 35,600 rpm after a duration of 10 sec. Figure IX-5 illustrates this failure. (The location of this thrust bearing is shown in Figure IX-1 of Report 10830-Q-1.) This failure caused significant damage to the tester and resulted in a temporary suspension of the test program. A spare tester will be assembled with a new thrust disc, as discussed in Paragraph C, below, and testing is planned to resume in the first week of April.

Even though Work Statement objectives were not yet met, the following significant design information was obtained:

1. Operation without filters in the N_2O_4 supply line is feasible (with normal contamination); however, life would be decreased as evidenced by dirt dents on the bearing races (Tests 1a, 1b, and 1c).

2. High axial load (4100 lb) caused no problems during a temporary flow interruption (Test 1c).

3. Acceleration rates up to 50,000 rpm/sec appear to be attainable (Test 3a).

IX, B, Bearing Testing at 40,000 rpm in N_2O_4 (cont.)

4. Bearing designs (tandem ball-bearing set and aligning roller bearing) appear to be capable of withstanding Work Statement loads and durations in the aligned position (misaligned operation has not yet been attempted). Durations of over six minutes have been accrued on ball-bearing Set R-007 (Figure IX-3) and on aligning Roller Bearing R-001 (Figure IX-4) at speeds up to 40,000 rpm. Axial and radial peak loads of 2500 and 1000 lb, respectively, have been applied for 10 sec.

C. HYDROSTATIC THRUST-COLLAR FAILURE INVESTIGATION

A second thrust-collar disc failure occurred in the first wear-ring Hydrolab test at 5000 rpm. This low-speed failure demonstrated that overspeed was not the primary cause of the first failure. In further checking of these discs it was found that two new discs were cracked. These parts had been made from ultrasonically sound material, were dye-penetrant inspected, and were certified sound after completion. All four of these discs, purchased on the same order, failed or were cracked in the center of the keyway. Three out of four other new discs purchased on an earlier order were inspected and found free of cracks. The fourth disc was used for about six hours at speeds up to 28,000 rpm during hydrostatic combustion-seal testing. During this testing, an axial rub was experienced on the first test. Inspection of this disc revealed some heat-check cracks in the area of the rub and a small hairline crack in the keyway corner. Considering the length of service, the different crack location, and the appearance of this disc, this cracking is not related to the cracking of the disk purchased on a different order.

All these discs were fabricated from 440C material and were heat-treated to a minimum Rockwell hardness (Rc) of 55. The ultimate and yield stresses at this hardness are about 250,000 and 200,000 psi, respectively, but the elongation is low (about 2%). Since the maximum calculated operating stresses (without stress-concentration factors) were about 55,000 psi at 40,000 rpm and 76,000 psi at 50,000 rpm, it would appear that the material has more than sufficient strength. However, heat-treating to an elongation of only 2% may pose a problem because brittle material is prone to unpredictable failures. From this design consideration and from the failure pattern established in the four discs (two failed during testing and two cracked prior to installation) it is concluded (1) that the 440C material if heat-treated to a minimum hardness of Rc 55 could cause difficulties and (2) that the four parts from the second purchase order are of questionable quality.

The immediate solution to the problem was to temper the three uncracked new discs to a hardness of about Rc 40 to 44, which results in lower ultimate and yield stresses (about 180,000 and 150,000 psi, respectively) but increases the elongation to 7 or 8%. Two of these discs are ready and will be assembled in the bearing and seal testers. The third disc will be available soon and will be installed in the wear-ring tester.

IX, C, Hydrostatic Thrust-Collar Failure Investigation (cont.)

The ultimate solution to the cracking problem is the fabrication of new parts from a more ductile material. Four replacement parts are being fabricated from AM 350 steel with chrome-plated surfaces and will be completed in two weeks. Four additional parts will be fabricated from AM 355 with LW-1 flame-sprayed surfaces and will be available in four weeks.

DATE	RUN NO	DURATION	RPM	F_A Ⓑ	F_R	Q_P	T_{PI}	RISE OF OUTER RACE TEMPERATUPE ΔT_{TB-1}	ΔT_{TB-2}	ΔT_{TB-3}	
		SEC		LB	LB	GPM	°F	°F	°F	°F	
2-25	1A	30	Ⓐ	1500	434	8	Ⓐ	6	5	7	No speed indication, shutdown
2-25	1B	100	Ⓐ	1500	453	10.8	18	15	17	26	Low speed indicated (3000 rpm) hash, significant bearing temp, rise shutdown
3-1	1C	197	26,850	1500	483	10.8	44	5	5	9	Low level lube lite on shutdown
		FS_2 + 10	34,350	4110	465	0	44	59	62	60	@ FS_2, rpm continued to rise, propellant to test bearings was off, bearing temp. spike
3-8	2	152	42,750	1500	448	9.4	Ⓐ	9	9	14	OST @ 42,750 after 14 sec @ 40,000 rpm
		@ FS_1		1260							
3-8	3A	≈ 2	60/65000	2000	466						OST @ 50,000 rpm, estimated overshoot 60/6500 rpm. Acceleration was 50,000 rpm/sec. OST @ FS_1
3-8	3B	@ 94	38,000	1550	930	9.4	80	7	8	12	N-speed trace very "hashie" decay of rpm at end of run held high radial load for 20 sec. Held high axial load for 12 sec.
		@ 189	41,940	2500	520	9.4	81	8	8	13	
		@ 216	33,570	1500	515	9.4	81	9	9	12	
3-10	3C										Lube press quit after being on about 15 sec. Motor Burnout. Test not actually initiated.
3-16	3D	10	35,600	970	590	A					Normal start up to 35,600 rpm, shutdown due to failure of thrust disc.
		@ FS_1		1490	590	A					

Ⓐ Instrumentation malfunction

Ⓑ 1500 lbs, pre-test setting, instrumentation problems, problems being resolved

Figure IX-1

Report 10830-Q-3

Tabulation of Steady-State Data Points of 40,000-rpm Bearing Tests in N_2O_4

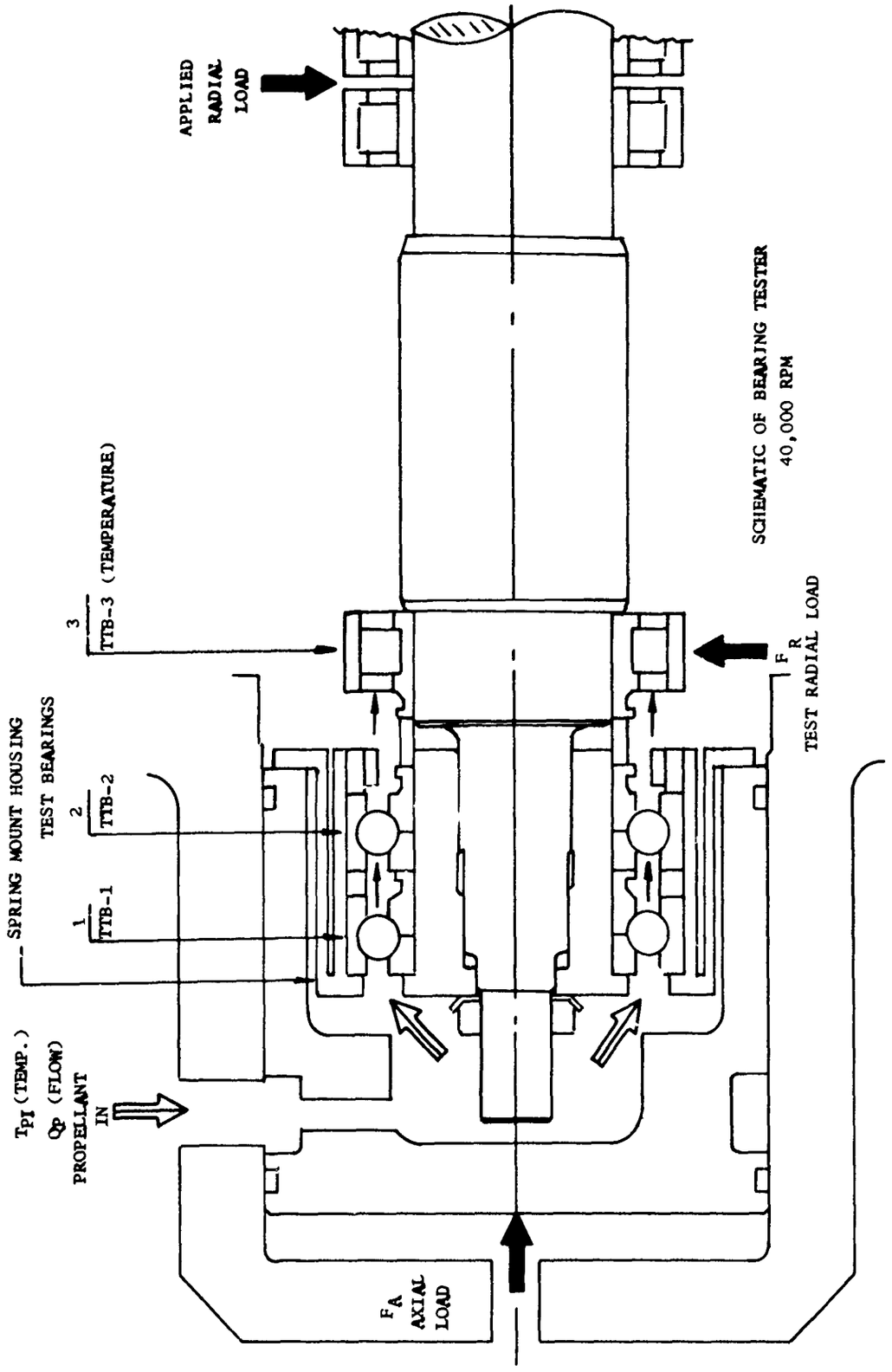

Schematic of Test-Bearing Installation Showing Parameter Location

Figure IX-2

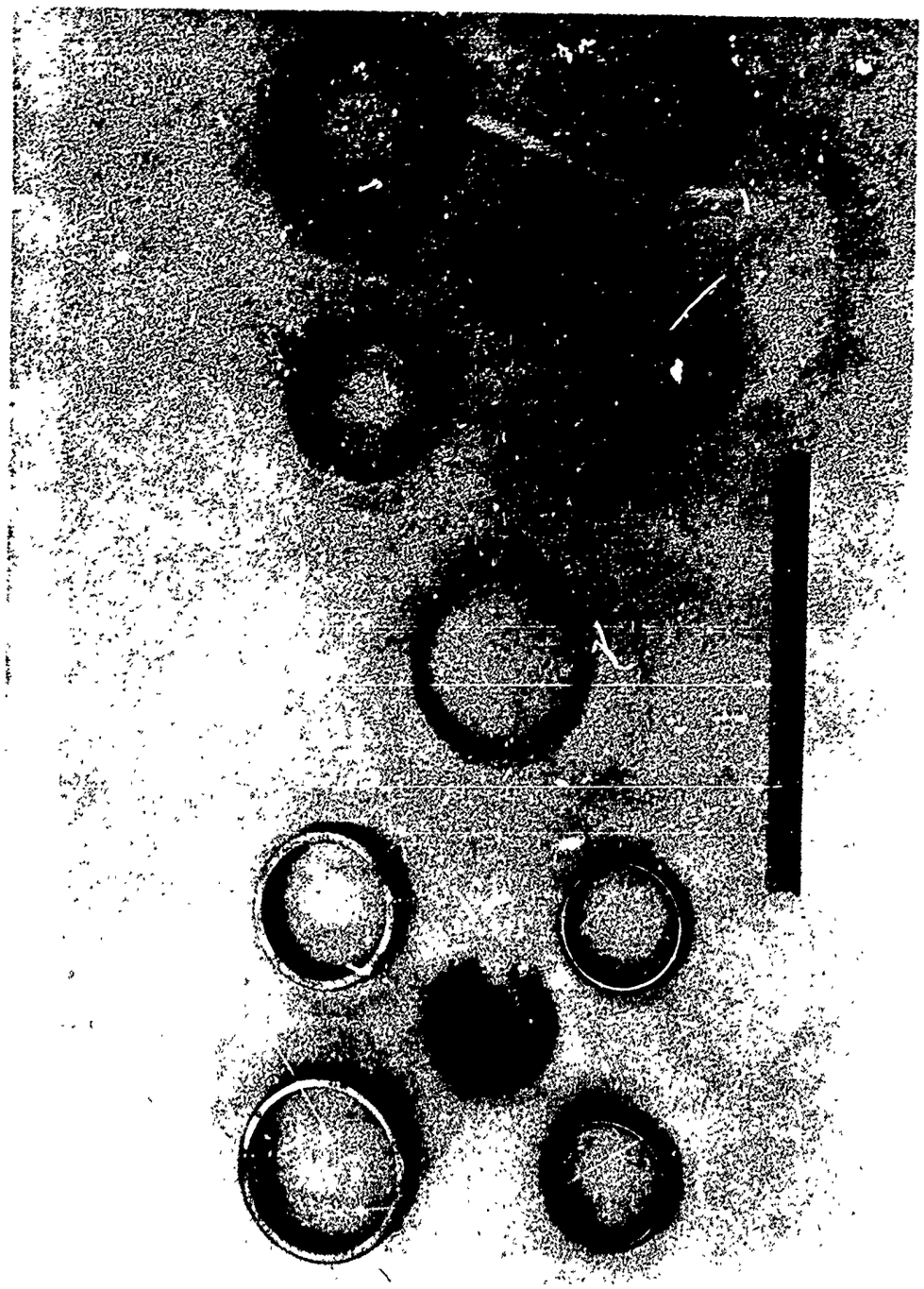

Ball-Bearing Tandem Set SN R-007 after Test 3b (6 min, 10 sec Total Accrued Time)

Figure IX-3

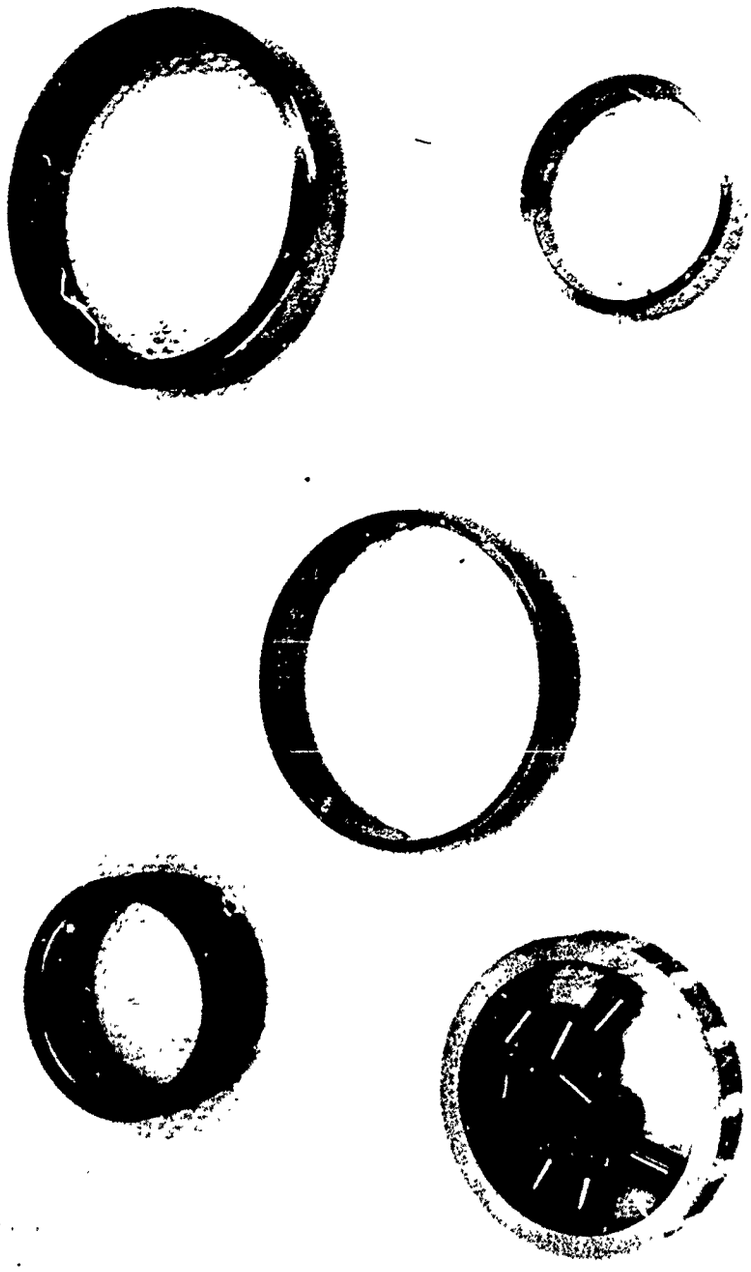

Aligning Roller Bearing SN R-001 after Test 3d (6 min, 20 sec Total Accrued Time)

Figure IX-4

Failed Hydrostatic Thrust-Bearing Collar after Test 3d

Figure IX-5

X.

TURBOPUMP WEAR-RING PROGRAM

A. GENERAL

To obtain shaft axial thrust balance and to allow relative growth between the shaft and the housing during operation, the ARES pump impellers are fully shrouded and incorporate wear rings to restrict the internal leakage of the pump. High-pressure differentials exist across the wear rings, along with high surface velocities. Because of high pump discharge pressures, running clearances (less than 0.010 in.) must be close if leakage is to be limited to an amount consistent with pump-efficiency requirements. These close clearances must be accommodated in the design to prevent impeller damage or a catastrophic failure if impeller rubbing occurs.

The objectives of this program are to develop a wear ring that will (1) satisfactorily limit the pump internal leakage and (2) operate safely and reliably at close running clearances in both N_2O_4 and AeroZINE 50.

The results of the seal-design techniques, materials investigations, and concept-testing programs will be applicable to the advanced B-turbopump design as well as to the incline turbopump design. The results will also be usable on other turbopump components such as the inducer housing, the shaft labyrinth seals, the axial thrust compensator, and the boost pumps.

Four wear-ring seal concepts have been selected:

1. The straight-labyrinth seal,
2. The stepped-labyrinth seal,
3. The axial hydrostatic face seal, and
4. The radial hydrostatic journal seal.

Two approaches are being taken in solving the wear-ring sealing and explosion-hazard problems. The first approach is to allow intermittent rubbing of the impeller wear ring on inert, compatible material inserts; both the straight and stepped-labyrinth seals have been designed with this philosophy in mind. The second approach is to allow low-speed transient rubbing, but to prevent high-speed contact by maintaining a fluid film between the impeller wear ring and the seal itself. The axial and radial hydrostatic seals are based on this concept. Experience with seals and bearings, obtained on Contracts AF 04(611)-8548, AF 04(611)-7439, and AF 04(611)-10784, indicates that this approach is feasible and will result in low and repeatable leakage flows. Analysis and design of the selected concepts were discussed in Report 10830-Q-2. Fabrication on most tester and test hardware was completed during this report period, and testing was initiated.

X, Turbopump Wear-Ring Program (cont.)

B. DESIGN

The four wear-ring concepts were examined to determine whether the advanced B-turbopump imposed any envelope constraints on the designs. All four concepts fit the turbopump with a minimum of rework.

A detailed stress analysis of the oxidizer impeller shows that the wear-ring sealing surfaces distort in a conical fashion due to the combined effects of speed and pressure. These distortions will not materially affect operation of the labyrinth seal concepts; they will, however, have a significant effect upon the operation of the hydrostatic wear rings. To utilize the hydrostatic concepts, it will be necessary to do two things:

1. Reduce the distortion of the running surfaces by design of the shroud cross-section.

2. Design the seal to distort sympathetically to the running surface distortions.

Additional analysis of these distortions is required.

C. FABRICATION

The tester drive unit was assembled. All test hardware is now available for testing with the exception of two of the hydrostatic seals and the Hystl insert. The two hydrostatic seals were completed, but had chipped flame-plated surfaces which required replating, requiring about one week. Problems were encountered in the bonding of the Hystl insert to the stainless-steel flange; efforts are continuing to obtain a satisfactory bond.

D. TESTING

1. Setup

Figure X-1 shows the wear-ring tester as designed for the 40,000 rpm tests. For the 30,000 rpm hydrotests, a geared electric-motor drive unit replaces the turbine drive illustrated. In addition to the wear-ring tests pieces, Figure X-1 shows the actuation cylinders whereby the test head may be displaced radially to induce rubbing of the test pieces. Figure X-2 shows a typical hydrotest setup. The inlet flow, Q_1, of high-pressure water is pumped through a 5-micron filter and hence into the test head where it is divided between the outboard seal, Q_3, and the inboard seal, Q_2. The inlet pressure, P_1, and the outlet pressures, P_2 and P_3, are monitored so that the pressure drops across the seals are known. An oil-supply pump feeds the oil-lubricated bearings and the hydrostatic thrust-bearing collar.

X, D, Testing (cont.)

All bearing temperatures as well as oil temperatures in and out of the tester are recorded. Tester vibration is monitored in two directions. In the hydrostatic-seal test series, the shaft displacement will be determined. An air-pressure supply is provided to load the bearings in order to minimize skidding during high-acceleration tests. Gaseous nitrogen is used for purging to minimize oil contamination, and for a test-head actuation to displace the test head during rubbing tests.

2. Test Results

The first water test, conducted on 18 March 1966, was made to check out the tester and the test setup, and to verify the leakage rate of the stepped labyrinth at a pressure differential of 2500 psi and varying speeds. The inlet pressure to the seals was increased as planned to 2500 psi (0 rpm). Visual inspection of the tester and a check of instrumentation showed all parameters working satisfactorily. Speed was increased from zero to 2500 rpm, and then to 5000 rpm. Speed was held at 5000 rpm for 2.5 min while the tester was inspected and the instrumentation checked. The water test bearing bound when the speed was increased, shearing the coupling which connects the drive motor and setup gears to the wear-ring tester. Disassembly of the tester indicated that:

(1) the hydrostatic thrust-bearing collar had cracked across a half-area of a diametral section through one of the keyways. This failure is related to the first thrust collar failure as discussed under bearing development (Section IX).

(2) The aluminum ring, which provides OD support to the Teflon cage, became lodged between the rollers and the outer race, causing the bearing to seize.

Analysis of the failed roller bearing and review of previous experience with water-lubricated bearings (i.e., combustion seal hydrotests, Contract AF 04(611)-10784) led to the following observations:

(1) The aluminum ring, which provides OD support for the Teflon bearing cage, overhangs the Teflon cage into the slots that guide the rollers (see Figure IX-4 where these overhung sections are shown).

(2) These overhung sections of the aluminum ring were deformed (probably by a combined rolling and sliding action of the rollers) and wedged between the rollers and the outer race.

(3) Roller end wear occurred on both ends of the roller but was most severe on the downstream side.

(4) The Teflon cage shows a high amount of burnishing from roller contact at the pitch diameter of the cage.

X, D, Testing (cont.)

The subject cage design was compared with the 30-mm bearing that was run successfully during combustion seal hydrotesting for a cumulative time of 6 hr at speeds up to 28,000 rpm. It was found that the 30-mm bearing cages had about twice the roller and land clearances that the 40-mm bearing had; the cage clearances for the two bearings are:

	Cage Clearance, in.	
	30-mm Bearing	40-mm Bearing
Land	0.035 to 0.040	0.015 to 0.020
Roller axial	0.035 to 0.040	0.015 to 0.020
Roller diametral	0.035 to 0.040	0.015 to 0.020

From the facts stated above, the following conclusions were drawn:

(1) Flow through the bearing causes sufficient end contact between the roller and the guiding-race land to momentarily skew and stop the rollers, which results in the moving rollers forcing the cage into the sliding rollers (Figure X-3). It should be noted that this type of action is probably always present, but its effect can be diminished by (a) lower through flows, (b) better lubrication (e.g., N_2O_4), and (c) large roller-to-cage clearances.

(2) The movement of the cage into the skewed and sliding rollers causes the overhung parts of the aluminum cage shroud to initially contact either the roller or the outer race, and ultimately both.

(3) This contact progressively deforms the shroud in the direction of rotation until the aluminum is jammed between the roller and the outer race, causing seizure of the bearing (Figure X-3).

The most reliable corrective action would be to replace the present cage with a cage of revised design having thicker webs and increased roller-to-cage clearances as proven on Contract AF 04(611)-10830 (25,000-rpm cage-development tests; see Report 10830-Q-2 for discussion and photographs). These parts are now in fabrication and are due 28 April 1966.

Because of the long lead time required for the revised cages, the immediate approach will be to mill-off the aluminum overhang. To ensure adequate support between the aluminum shroud and the Teflon cage, rivets will be added through each web (the part now has three rivets equally spaced). Provisions will be made to ensure that the major portion of the flow goes around the bearing instead of through it; this will reduce roller-end wear. Testing will be resumed in mid-April.

X, D, Testing (cont.)

3. Data

The first test was conducted with stepped labyrinths. The labyrinth parts were made of steel since no rubbing was intended. The outboard seal had diametral and axial clearance of 0.0195 and 0.050 in., respectively. The outboard flow rate was 53.8 gpm at a differential pressure of 2310 psi. The inboard seal had diametral and axial clearances of 0.011 and 0.050 in., respectively, and the inboard flow rate was 35.8 gpm at a differential pressure of 2350 psi. As anticipated, speed had no effect on flow rate.

4. Data Analysis

The calculated flow rates were based upon the orifice equation and assume that the labyrinth steps prevent any carryover of velocity from one tooth to the other. The equation used and a sample calculation are presented in Figure X-4.

For the inboard labyrinth, the calculated flow is 35.3 gpm at 2350 psi (Figure X-4); since the actual flow was 35.8 gpm, the correlation is excellent.

For the outboard labyrinth, a similar calculation yields 61.7 gpm at 2310 psi. Since the actual flow measured was 53.8 gpm, the overall resistance to flow is greater than assumed. This increased resistance is most likely derived from the restrictions formed by the steps and/or the turning losses caused by the steps. This factor is designated as K in Figure X-4. It is expected that subsequent tests and further data analysis will clarify this point.

Using the data obtained on Test 1, it is possible to check the predicted leakage rate (Figure VI-7) for the ARES oxidizer pump when stepped labyrinths are used. This check is carried out in Figure X-5; it is seen that for the case of small clearances, i.e., 0.007 in. radial (0.014 in. diametral), the flows check very well: 96 gpm predicted versus 99 gpm for corrected hydrotest data. For larger clearances, i.e., 0.015 in. radial (0.030 in. diametral), the corrected hydrotest data give somewhat lower flows than predicted: 180 versus 206 gpm.

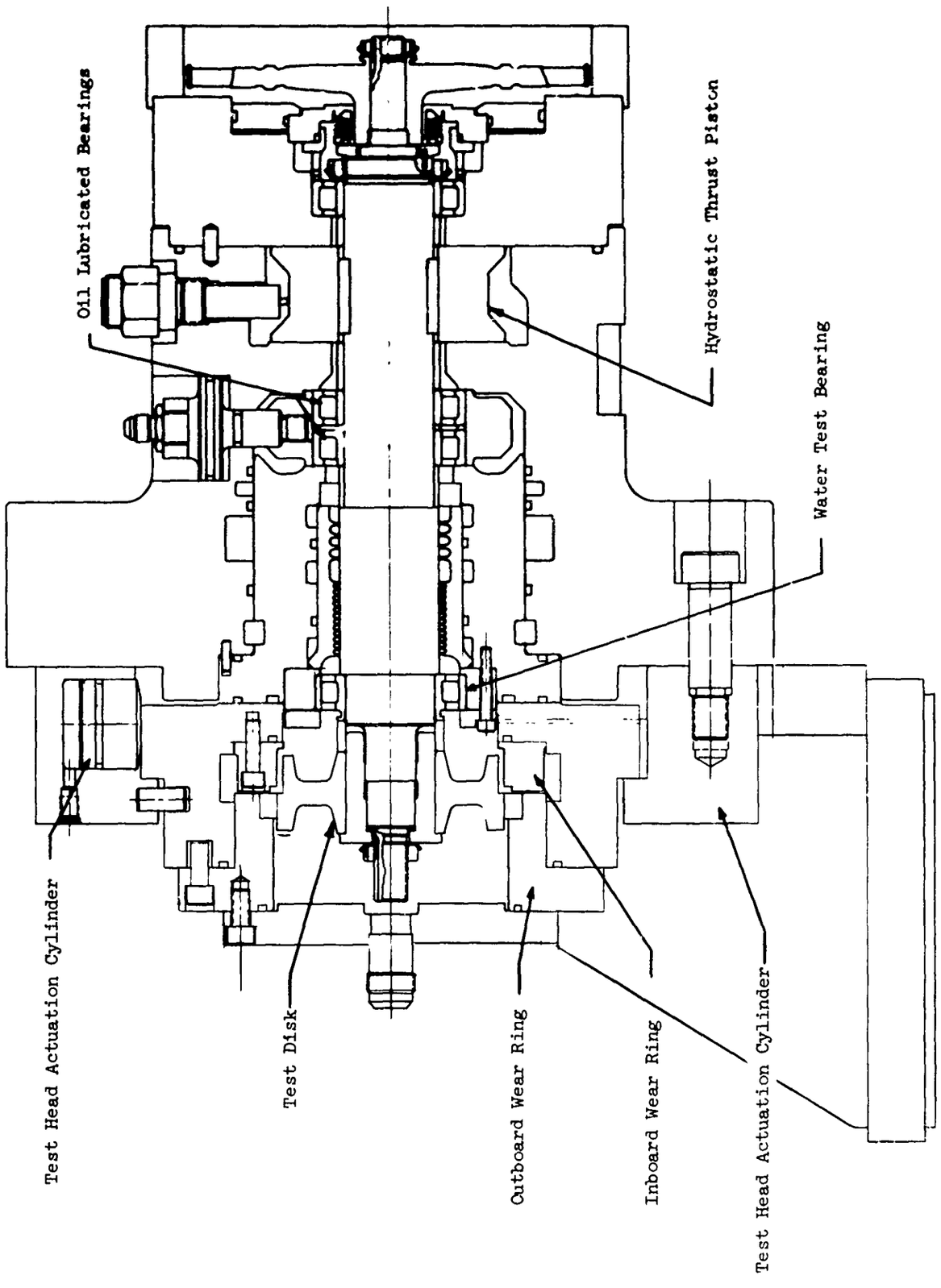

Wear-Ring Tester

Figure X-1

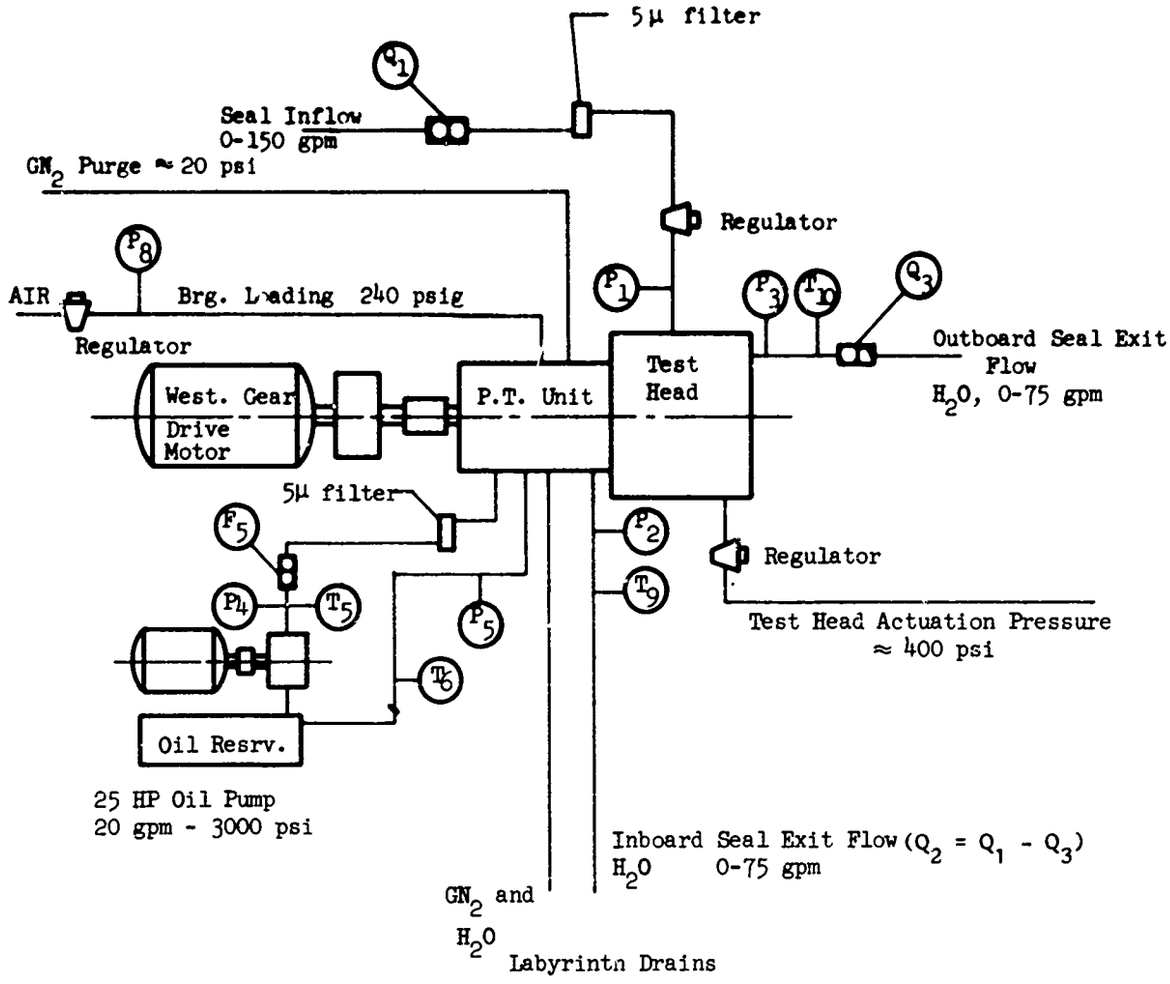

Typical Hydrotest Setup for Wear Rings

Figure X-2

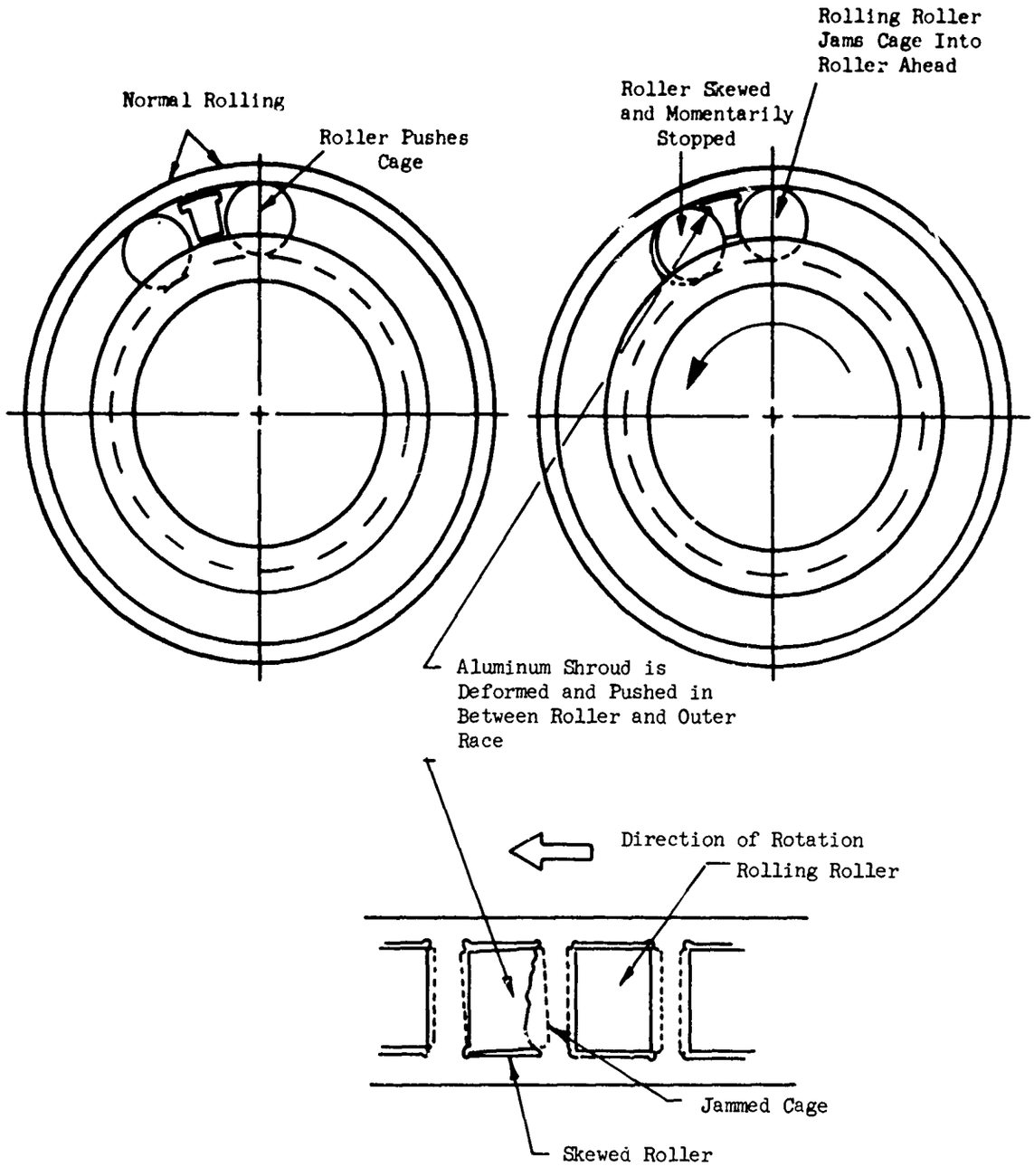

Mode of Failure of Wear-Ring Water-Test Bearing

Figure X-3

Sample Calculation of Leakage Rates Through Stepped Labyrinth. The orifice equation as applied to a labyrinth is:

$$Q = AC_D k \sqrt{\frac{2g}{\gamma} \frac{\Delta P}{N}} \times 0.26$$

where:

Q = flow rate, gpm

A = Annular area of labyrinth, $in.^2$

C_D = Discharge coefficient

g = gravitational constant, $in./sec^2$

γ = fluid density, $lb/in.^3$

P = differential pressure across the labyrinth, psi

N = number of labyrinth teeth = 5 (both inboard and outboard)

0.26 = conversion constant from flow rate in $in.^3/sec$ to flow rate in gpm

k = geometry factor - assumed to be equal to 1.0 until test data obtained

The annular area, A, has been taken to be the average of the five teeth, and is for the inboard labyrinth

$$A = \pi Dh = \frac{\pi \times 3.750 \times 0.011}{2} = 0.065 \text{ in.}^2$$

where:

D = annulus diameter, in.

h = radial clearance, (diametral clearance/2) in.

The discharge coefficient, C_D depends upon the shape of the tooth. For the test labyrinth, the teeth were ground to final dimension and should have a discharge coefficient of about 0.66. (Reference X-1b).

Hence, for the inboard labyrinth

$$Q = 0.065 \times 0.66 \sqrt{\frac{2 \times 386}{0.0361} \times \frac{2350}{5}} \times 0.26$$

$$Q = 35.3 \text{ gpm @ } 2350 \text{ psi}$$

Sample Calculation of Leakage Rate through the Stepped Labyrinth

Figure X-4

Case No.	Seal Location	Diametral Clearance, in.	Axial Clearance, in.	Seal Mean Diameter, in.	Diff. Press. psi	Fluid Density, lb/in.^{3}	Flow Rate, gpm	Remarks
1	Hydrotest inboard	0.011	0.050	3.375	2350	0.0361	35.8	Data from inboard seal, test #1 (3/18/66) K = 1
2	Oxidizer pump inboard	0.014	0.050	4.000	3443	0.052	49	Flow rate is computed according to the equation of Figure X-4, with K = 1 as per inboard seal data, Test 1
3	Oxidizer pump outboard	0.014	0.050	4.000	3623	0.052	50	
4							99	Overall leakage rate for the oxidizer pump. Compares with 96 gpm previously calculated (cf. Figure VI-7
5	Hydrotest outboard	0.0195	0.050	3.375	2310	0.0361	53.8	Data from outboard seals, Test 1 (3/18/66), K = 0.87
6	Oxidizer pump inboard	0.030	0.050	4.000	3443	0.052	89	Flow rate is computed according to the equation of Figure X-4, with K = 0.87 as per outboard seal data, Test 1
7	Oxidizer pump outboard	0.030	0.050	4.000	3623	0.052	91	
8							180	Overall leakage rate for the oxidizer pump compares with 206 gpm previously calculated (cf. Figure VI-7)

Figure X-5

Verification of Predicted Leakage Rates for ARES Oxidizer Pump When Stepped-Labyrinth Seals Are Used

XI.

TPA SEAL DEVELOPMENT

A. GENERAL

1. Background

The ARES engine, in which a single turbine drives both the fuel and the oxidizer pumps, requires a seal to separate the flows of fuel and oxidizer. Two sealing concepts are being developed: (a) the hydrostatic combustion seal (Figure XI-1) wherein fuel is allowed to leak at a regulated rate into the oxidizer-rich combustion gases downstream of the turbine, and (b) the purge seal (Figure XI-2) in which an inert fluid is introduced as the barrier between the fuel and the oxidizer-rich combustion gases.

The hydrostatic combustion seal was designed and its feasibility established on Contract AF 04(611)-10784, "Hydrostatic Combustion Seal Feasibility Demonstration Program." Details of this program are presented in the final report.*

Work completed on Contract AF 04(611)-10784 included the following:

a. Design of a hydrostatic combustion seal.

b. Fabrication of test hardware for testing in water.

c. Design and fabrication of testers for use in water (Hydrolab) and hot tests.

d. Design of a preburner and burnoff stack for hot testing.

e. Hydrolab seal tests under reduced pressures and at speeds up to 30,000 rpm.

f. Combustion tests at reduced pressures, of a small segment of the seal (2D tests, Figure XI-3) using a tester with a quartz window to permit motion-picture recordings of the combustion pattern.

Test results from Contract AF 04(611)-10784 established the following:

a. Hydrolab Tests

(1) The seal can be successfully operated at a clearance of 0.0009 in., at speeds up to 28,000 rpm.

*Aerojet-General Report 10784-F, "Hydrostatic Combustion Seal Demonstration Feasibility Program," Final Progress Report, presently being reviewed by the Air Force.

XI, A, General (cont.)

(c) (2) Flow from the seal is predictable (0.324 lb/sec of fuel to combustion and 0.605 lb/sec inward to the bearing cavity), and rotative speed produces negligible changes in flow.

(u) (3) The seal will follow an axial runout of the shaft face of 0.0025 in. without damage.

(u) (4) Rubbing actually experienced during start and stop transients does not abrade the sealing surfaces.

(u) (5) When static, the seal will positively shut off the fuel.

b. 2D Combustion Tests

(u) (1) The combustion and cooling concepts were demonstrated repeatedly without damage to the seal surfaces.

(u) (2) At design mixture ratios, the seal surface temperatures will remain within design limits.

(u) (3) The design of the seal provides oxidizer coolant in adequate quantities and at the proper location to prevent damage to the hardware.

(c) (4) The combustion pattern maintains a small flame over the burnoff area, adequately isolated from the adjacent surface.

(u) (5) The seal has survived combustion at rates and mixture ratios substantially more severe than design values without surface damage.

2. Summary

(u) The findings outlined above indicate that this sealing concept has high potential for meeting ARES requirements. Consequently, the hydrostatic combustion seal concept will be investigated under the ARES contract in the following test program:

a. Two-Dimensional (2D) Tests

(u) These tests are an extension of the 2D tests completed on Contract AF 04(611)-10784, and will consist of tests of a seal segment exactly duplicating the ARES seal cross-section (with reduced fuel gap), so that the effect of variations in flow, possible dimensional changes from distortion, and slight transient malfunctions can be examined. The comparatively low cost of 2D tests, the much less expensive hardware, and the possibility of photographic coverage during testing enhance this approach. It is desirable that information from these tests be gained before hot rotating seal tests be started.

XI, A, General (cont.)

b. Preburner Checkout

This effort, which consists of testing the test facility and the preburner gas generator has been completed.

c. Cold AeroZINE 50 Tests

These tests, in which the tester is operated in AeroZINE 50 without combustion, will provide data necessary before hot testing is started. Two tests have been completed.

d. Hot Rotating Tests

These tests are made under conditions simulating those of the ARES engine, with the goal of successful operation for 60 sec.

An additional effort on the ARES program is the design, fabrication, and testing of a purge seal under conditions simulating those of the ARES engine.

Work completed during this reporting period includes:

a. The design and fabrication of 2D test segments,
b. The installation and checkout of the burnoff stack,
c. Seven preburner tests,
d. Two cold seal tests with AeroZINE 50 and
e. The design of a purge seal and tester.

B. TWO DIMENSIONAL (2D) SEAL TESTS

Seal segments were designed and fabricated which duplicate the final profile of the hydrostatic combustion seal (Figure IX-4). The formation of a 0.001-in.-wide slot for fuel admission presented the greatest technical problem. A shim, 0.001 in. thick, was diffusion-bonded between two halves of the seal segment, with a portion of the shim cut away to form the fuel slot. Tests with this segment will be described in the next quarterly report.

C. HYDROSTATIC COMBUSTION SEAL

1. Preburner Checkout

a. Equipment

The preburner is used to generate oxidizer-rich gas at conditions simulating those of the ARES engine turbine discharge. The preburner is mounted on the test chamber (Figure XI-5) so that the hot gas is directed toward the seal. Pressure within the tester is controlled by means of an orifice in the chamber discharge.

XI, C, Hydrostatic Combustion Seal (cont.)

(u) The preburner injector head (Figure XI-6) consists of four coaxial injectors. Fuel emerges in a conical swirl, and is formed into discrete streams by grooves cut in the face of the exit cone. Oxidizer is admitted through an annulus around the fuel cone; the fuel impinges on, and penetrates, the oxidizer stream, which provides a well-mixed combustion zone.

b. Installation

(u) The tester and preburner were installed on Test Stand H-1 as shown in the flow diagram (Figure XI-7).

c. Tests

Seven tests were conducted:

(u) (1) Test 1 was performed to determine oxidizer-fill and ramping conditions and to check calibration of the Fox cavitating venturi meter. An orifice was installed in the injector inlet to simulate chamber pressure. Ramp (rapid pressure increase) was accomplished in 0.7 sec. All parameters were met. The cavitating-venturi flow was found to be lower than vendor data indicated, and data from this test were used to correct the venturi setting.

(u) (2) Test 2 was conducted to determine fuel fill and ramping conditions and to check calibration of the Fox cavitating venturi meter. An orifice was installed in the fuel line to simulate chamber and injector pressures. Fuel was discharged to a catch tank. A leak in the fuel line required that the test be repeated.

(u) (3) Test 3 duplicated Test 2. Ramping was accomplished in 0.7 sec. All test objectives were attained. The cavitating-venturi flow was found to be 14% lower than vendor data indicated.

(c) (4) Test 4, the first hot test, was started at 600 psi (fuel and oxidizer supply) and ramped to operating conditions in 0.7 sec. Run duration was 4 sec. All parameters were met, except chamber pressure which was 3600 instead of 3100 psi. Preburner temperatures averaged 1125°F and were purposely conservative. Figure XI-5 indicates the location of the test instrumentation. Posttest examination of hardware revealed no damage.

(c) (5) Test 5 was intended for a duration of 10 sec at a start pressure of 300 psi, with the chamber outlet orifice and the mixture ratio adjusted for target conditions of 3100 psig at 1175°F. An incorrectly set temperature limit caused a premature shutdown.

XI, C, Hydrostatic Combustion Seal (cont.)

(u) (6) Test 6 was run immediately after the malfunction on Test 5 was corrected. The test was concluded after full duration. Chamber pressure and temperature were low (2000 psi and 600°F), as was fuel flow. After the test, a shaving of metal was found to have lodged in the fuel cavitating venturi, reducing the flow. Although expected operating conditions were not reached, it was established that the starting pressure of 300 psi caused no problems. Therefore, this test was not repeated.

(c) (7) Test 7 was started at 60 psi, ramping in 0.7 sec to full test conditions of 3100 psi and 1175°F, and lasted for a duration of 15 sec. All parameters were met or exceeded (3200 psi and 1300°F). Figure XI-8 depicts operating conditions versus time. Posttest examination of hardware revealed no damage. This test concluded the preburner checkout series.

d. Test Results

(u) The specific objectives of the preburner tests were to check out operating equipment and to simulate engine pressure rises as closely as possible.

(u) All equipment functioned properly during the combustion tests. On Test 5, the ability of the computer to shut down the test during a rapid temperature rise was demonstrated. The theoretical engine start pressure transient was closely duplicated. Figure XI-9 compares the anticipated engine startup pressure with the actual pressure rise of Test 7. If desired, the computer-controlled ramping rate used in the test area can be adjusted and ramp time decreased to match more closely the theoretical rise rate.

(c) The ability of the preburner to function properly at the engine nominal fill pressure (60 psi) was demonstrated.

(u) The data derived from the preburner tests will permit seal hot rotating tests under conditions closely simulating those of the ARES engine; therefore, test data derived will be directly applicable to the ARES engine design.

2. Cold Tests in AeroZINE 50

(u) This series of tests is designed to investigate fill time, seal flow, acceleration and deceleration characteristics of the seal tester, and to study the fuel flow rates while operating at speeds and flows simulating those to be expected in the ARES engine.

(u) The tester (Figure XI-10) is the same as used for hot testing except for the internal shielding and combustion-gas velocity control equipment. Installation is in accordance with the flow diagram (Figure XI-11). Since combustion gas is not used in these tests, pressurization is accomplished by gaseous nitrogen. AeroZINE 50 is separated from the gas in a high-pressure float-actuated commercial separator. All flows are monitored.

XI, C, Hydrostatic Combustion Seal (cont.)

The test objectives are: (a) determine fill times and pressurization rates, and monitor flows and duplicate as nearly as possible engine start and stop transients with seals under various flows, face pressures, and differential pressures.

Two cold tests with AeroZINE 50 were conducted. Before rotating tests could be conducted, the chamber pressurizing rate and the labyrinth flow coefficient had to be determined to obtain a correct pressure setting of the seal inside cavity.

Test 1 was conducted without rotation, at a fuel pressure of 3000 psi, for a duration of 45 sec. To avoid pressurizing the convex side of the seal bellows during transient tests, it was necessary to determine the chamber pressurizing rate. It was also necessary to determine the tester labyrinth discharge coefficient so that pressures within the seal can be maintained at 2800 to 2900 psi. Pressurizing rates, flow rates, and system performance were determined, but the data were inadequate for establishing the proper seal internal pressure at the tester labyrinth.

Test 2 was conducted to obtain data for determining the tester labyrinth flow coefficient. Test duration was 45 sec, and all parameters were reached. From the data obtained, the labyrinth flow coefficient (K_L) was determined to be 1.73

$$(K_L = \frac{\text{Flow, in.}^3/\text{sec}}{\sqrt{\text{Differential Pressure, psi}}}).$$

Posttest examination of hardware revealed that the bellows between the seal face and the seal flange had failed at the weld to the seal flange.

Data from Tests 1 and 2 indicate that the seal functioned normally throughout Test 1 and until the end of Test 2. When the chamber pressure in Test 2 was decreased, seal flow increased disproportionately, indicating that failure occurred at that instant. Analysis of Test 1 revealed a brief pressure reversal of about 200 psi which occurred during shutdown. This was sufficient to initiate a failure at the junction of the bellows to the seal. Although test data show that failure did not actually occur until the end of Test 2, it is felt that the pressure reversal contributed to the failure, which was found to be along the weld between the bellows and the seal flange. The failed part was returned to the vendor for analysis and recommendations. The bellows failure indicates that proof and leak tests are not sufficient to ensure reliability and that corrective action is necessary.

Corrective action includes the following:

a. All test seals will be given a mass-spectrometer leak test.

b. The possibility of redesigning the bellows attachment is being studied to place the joint within the internal circumference of the seal rather than along the faces of the mating parts. This will reduce weld stress and facilitate inspection of the weld.

XI, C, Hydrostatic Combustion Seal (cont.)

c. The desirability of and the problems resulting from increasing the thickness of the bellows at the attachment point are being studied.

d. The use of concentric double bellows is being investigated.

e. The use of heat-treatable parts, with heat treat after assembly, is being studied.

A detailed discussion will be given in the next quarterly report.

D. PURGE SEAL

The design of the purge seal was completed. The purge seal (Figure XI-2) is similar to the hydrostatic combustion seal because a purge fluid (instead of fuel) is introduced at high pressure into six orificed pockets. The seal dimensions were selected to give an optimum balance of minimum flow rate without excessive temperature rise of the purge fluid, due to viscous friction. For the fluid selected (PR 143-AB), the optimum width of the seal land is about 0.1 in. which results in a fluid temperature rise of about 450°F at a total flowrate of 0.26 gpm. This temperature rise and flowrate correspond to a seal running clearance of approximately 0.0006 in. Heat-transfer and distortion studies were made which show this running clearance is feasible if the seal face is fabricated from a material having a low coefficient of thermal expansion (e.g., Invar). The face and the inside (bore) of the seal will be coated with a hard material to prevent galling caused by rubbing and foreign particles carried in the purge fluid. Three-piece piston-ring type seals were designed for use as secondary seals in this application (these seals are subjected to axial motion only) because minimum leakage is desirable. The stability aspects of the seal have been investigated to ensure that the seal will not be excited into axial vibration by wobble of the rotating ring. The natural frequency of axial vibration is 534,000 cpm or thirteen times the shaft speed; therefore the seal cannot be excited by the shaft rotation frequence. In addition, viscous damping due to squeeze-film effects and friction damping caused by the piston-ring secondary seals ensure a stable system.

At the expected design flowrate of 0.26 gpm of purge fluid (PR 143 AB), the weight of purge fluid plus spherical pressure-vessel container of a size required for a 3-min run duration is about 17 lb. This weight does not include valves, lines, and other auxiliary equipment that may be required.

HYDROSTATIC COMBUSTION SEAL

PROPELLANT FLOWS & COMBUSTION

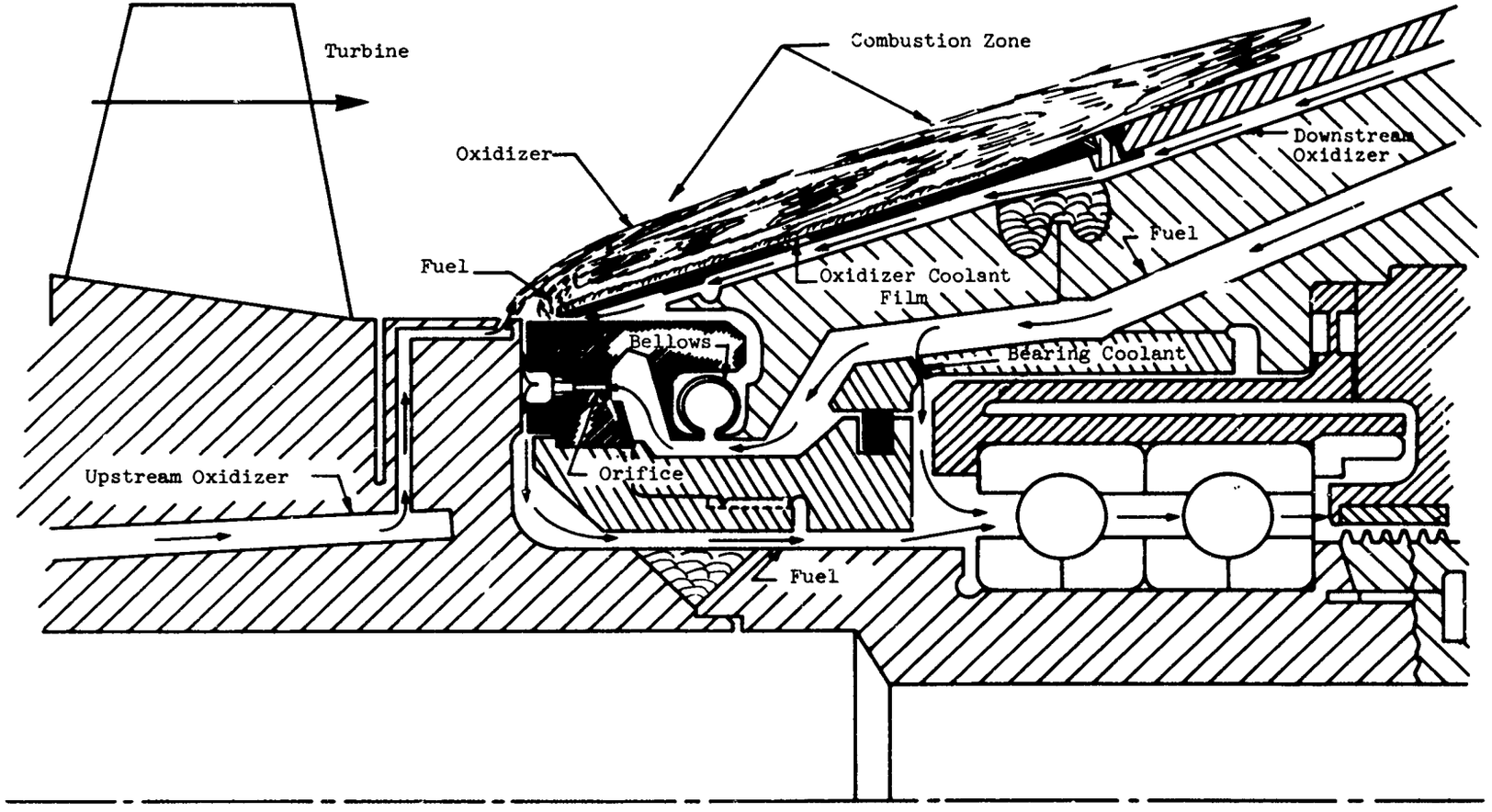

Figure XI-1

Combustion Concept of Seal (u)

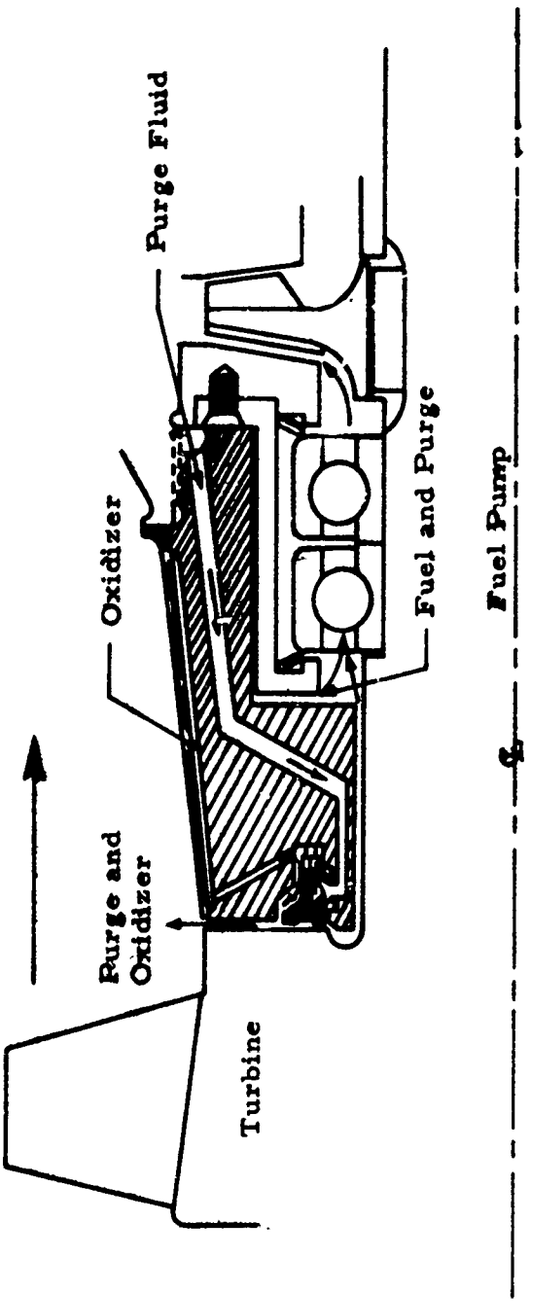

Figure XI-2

(This page is Unclassified)

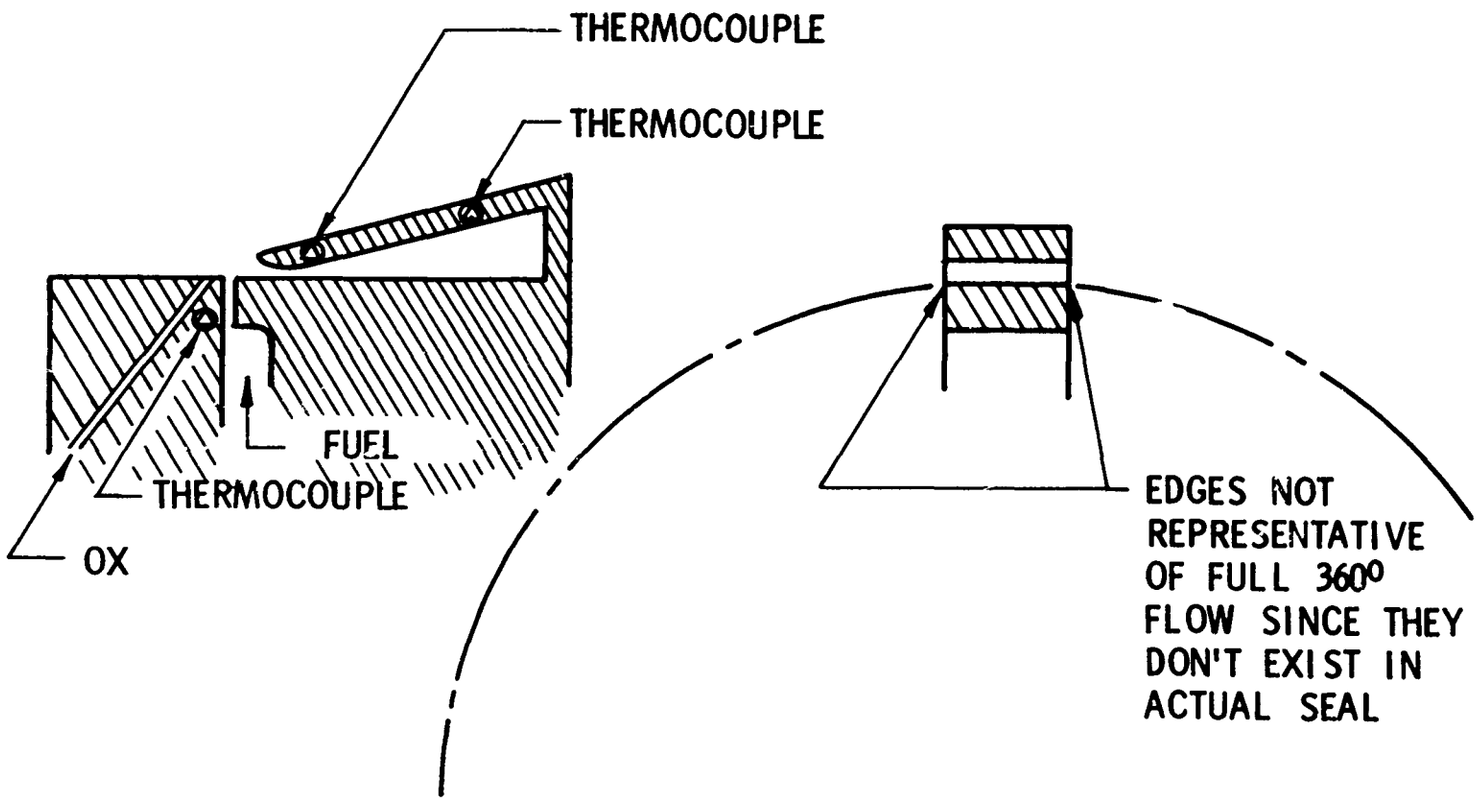

2D Test-Segment Concept

Figure XI-3

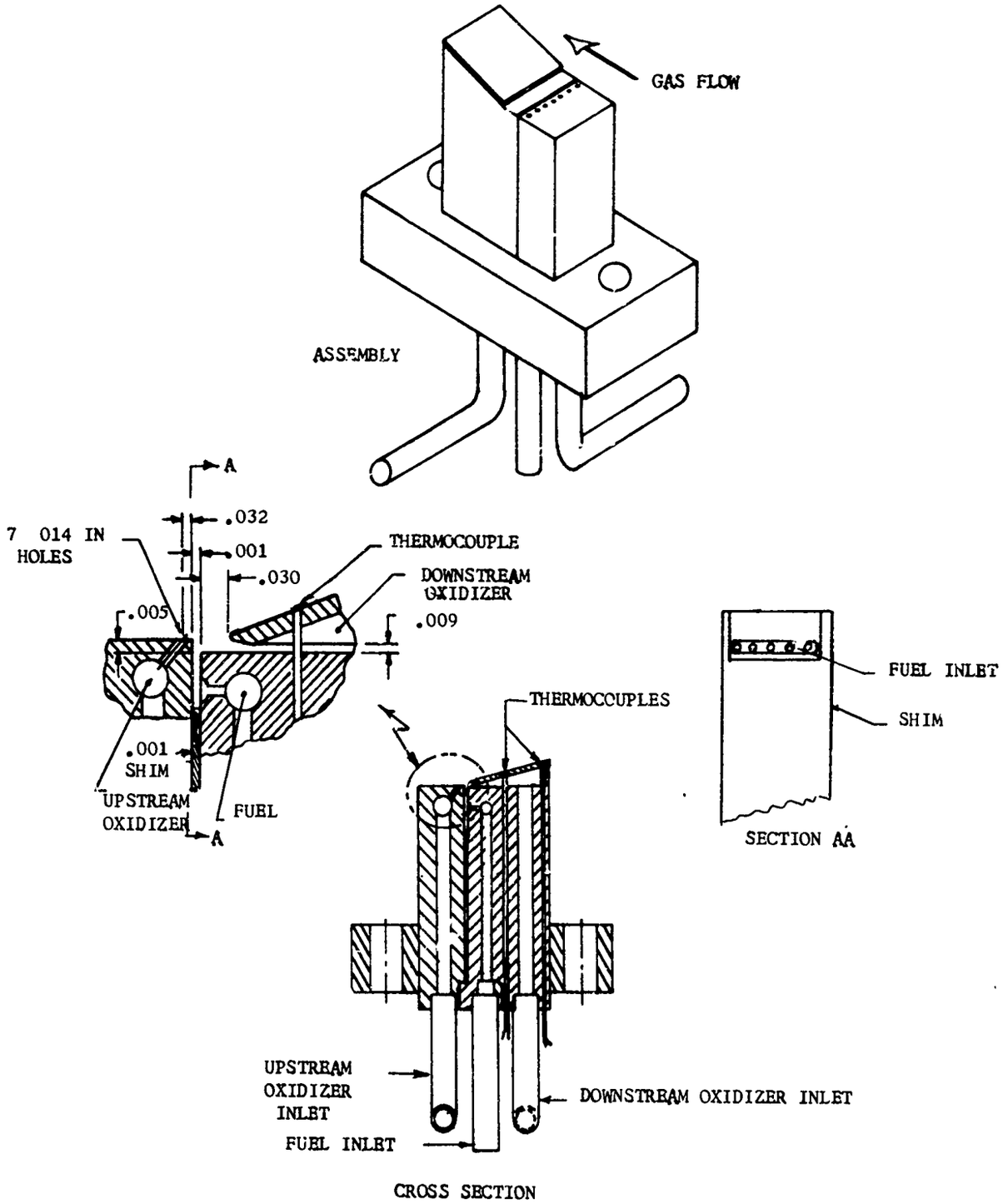

2D Test Segment

Figure XI-4

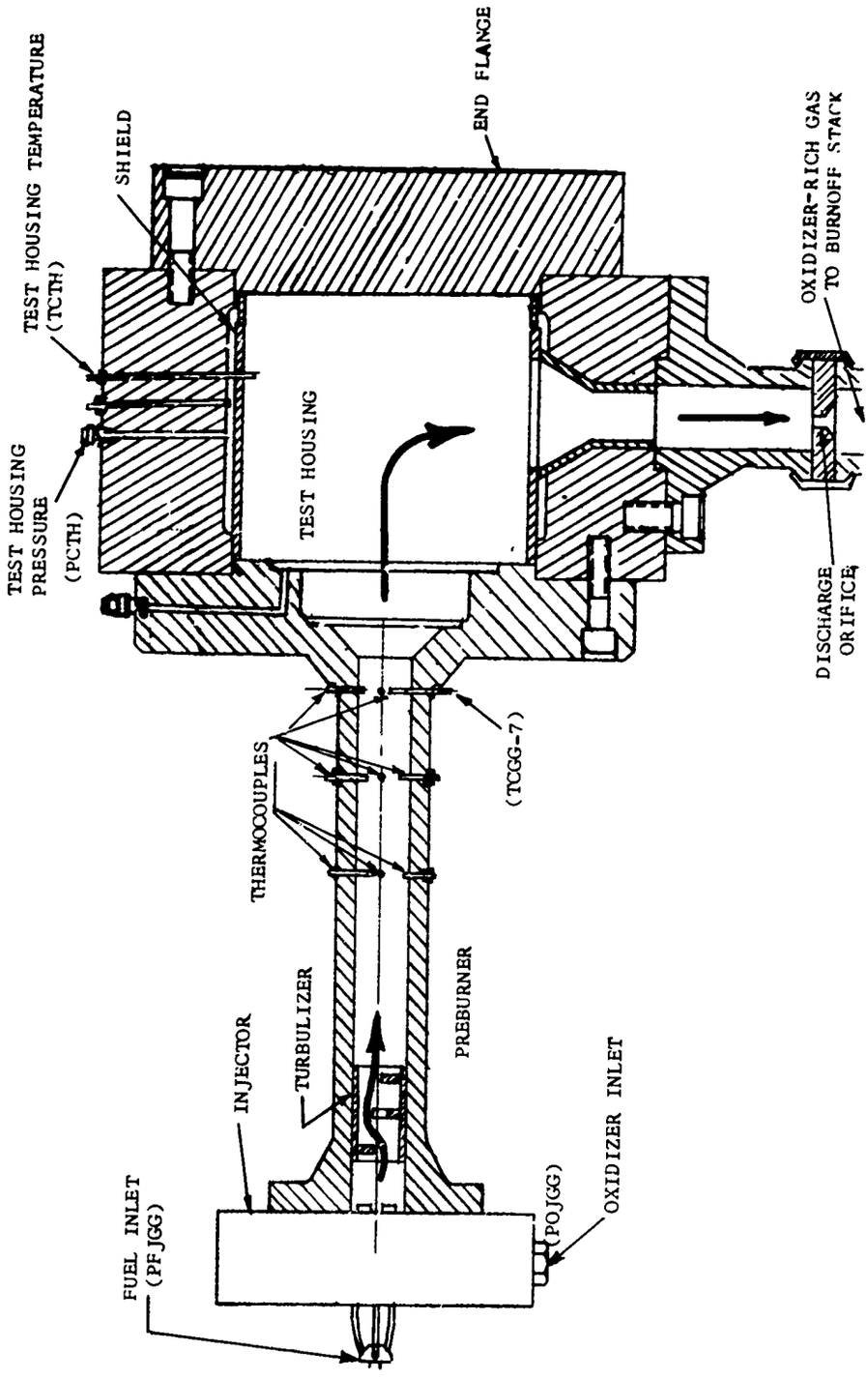

Figure XI-5

Hydrostatic Combustion-Seal Tester, Preburner Checkout

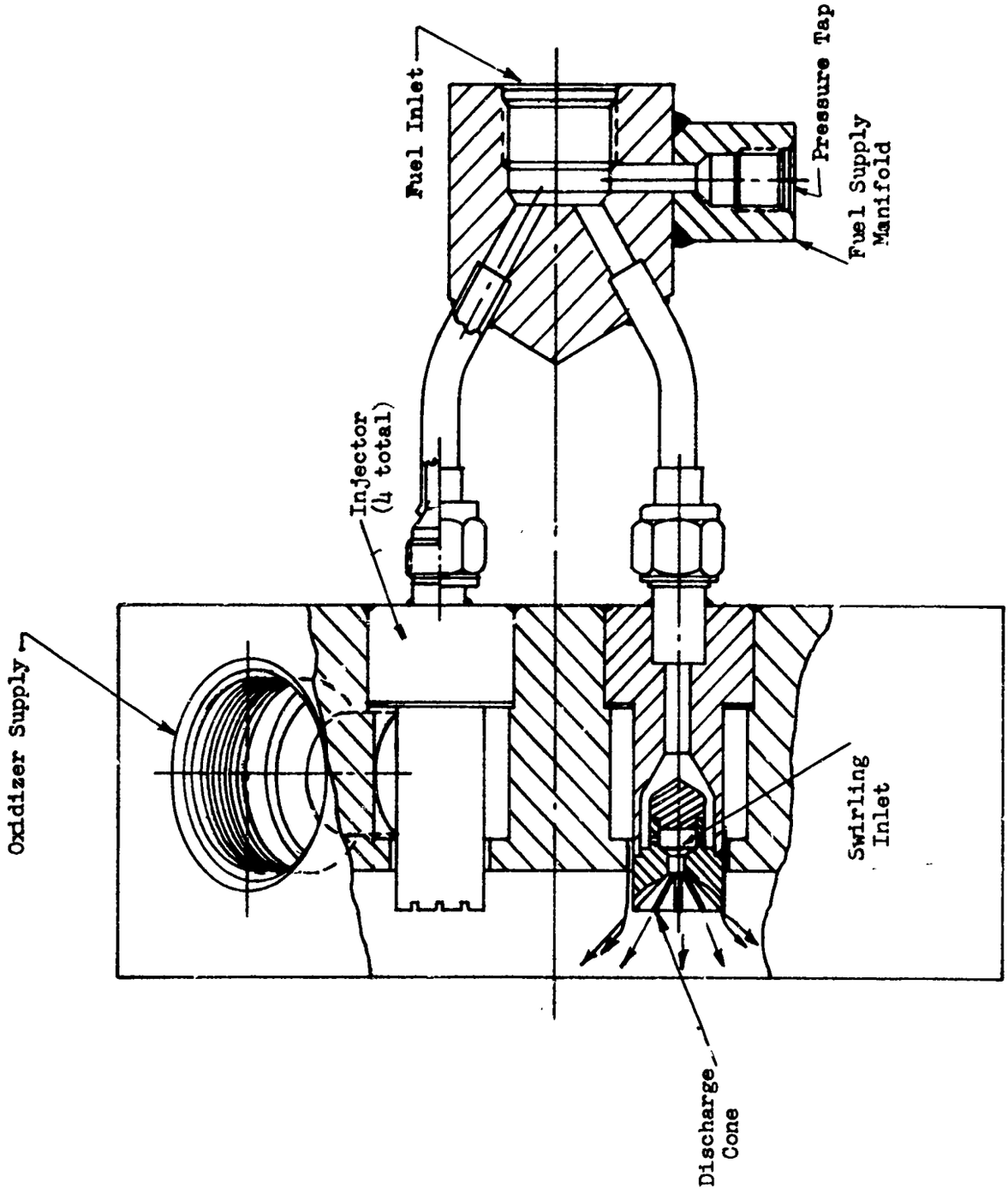

Injector for Seal Tester

Figure XI-6

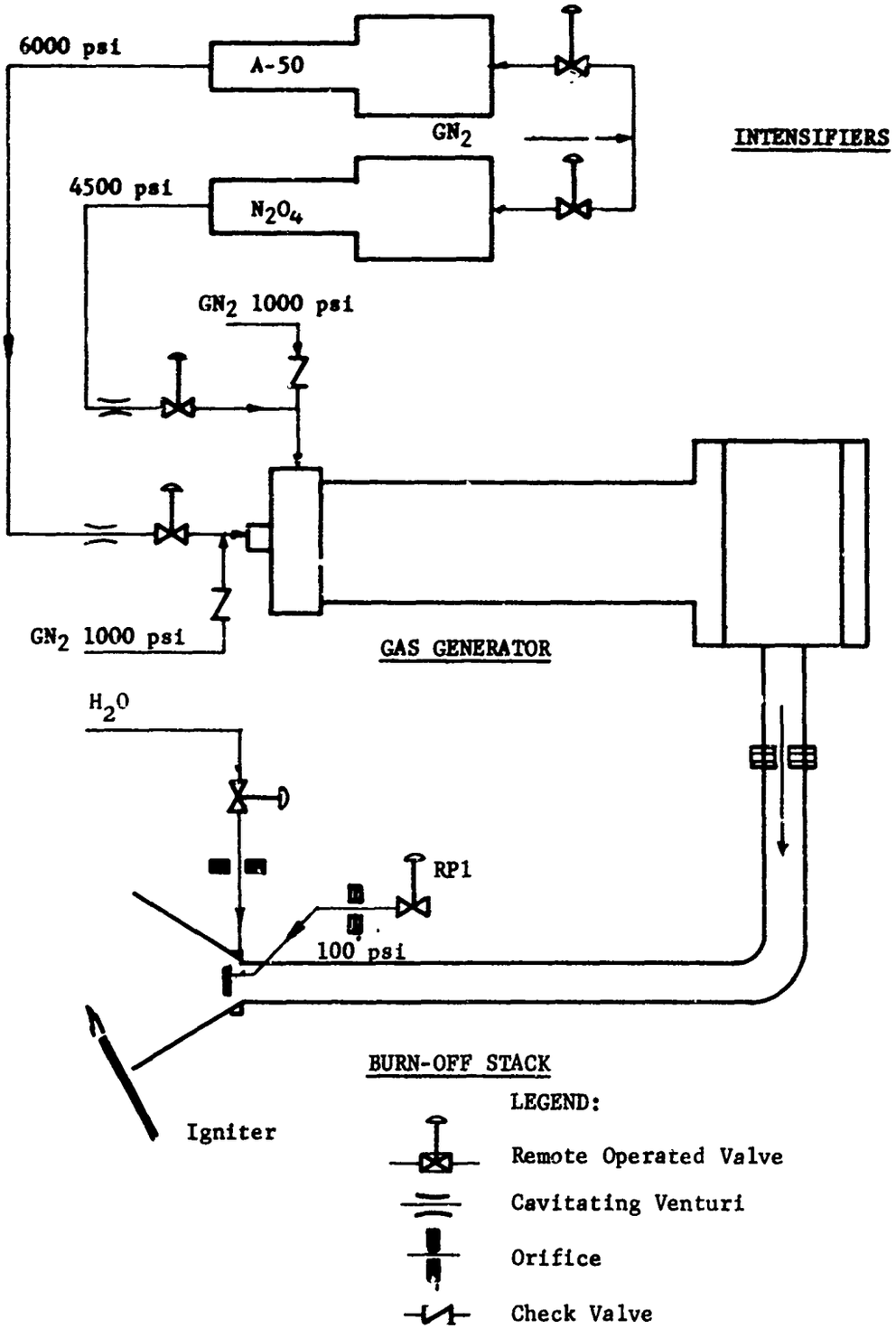

Flow Diagram--Preburner (Gas Generator) and Burnoff Stack Checkout Tests

Figure XI-7

(This page is Unclassified)

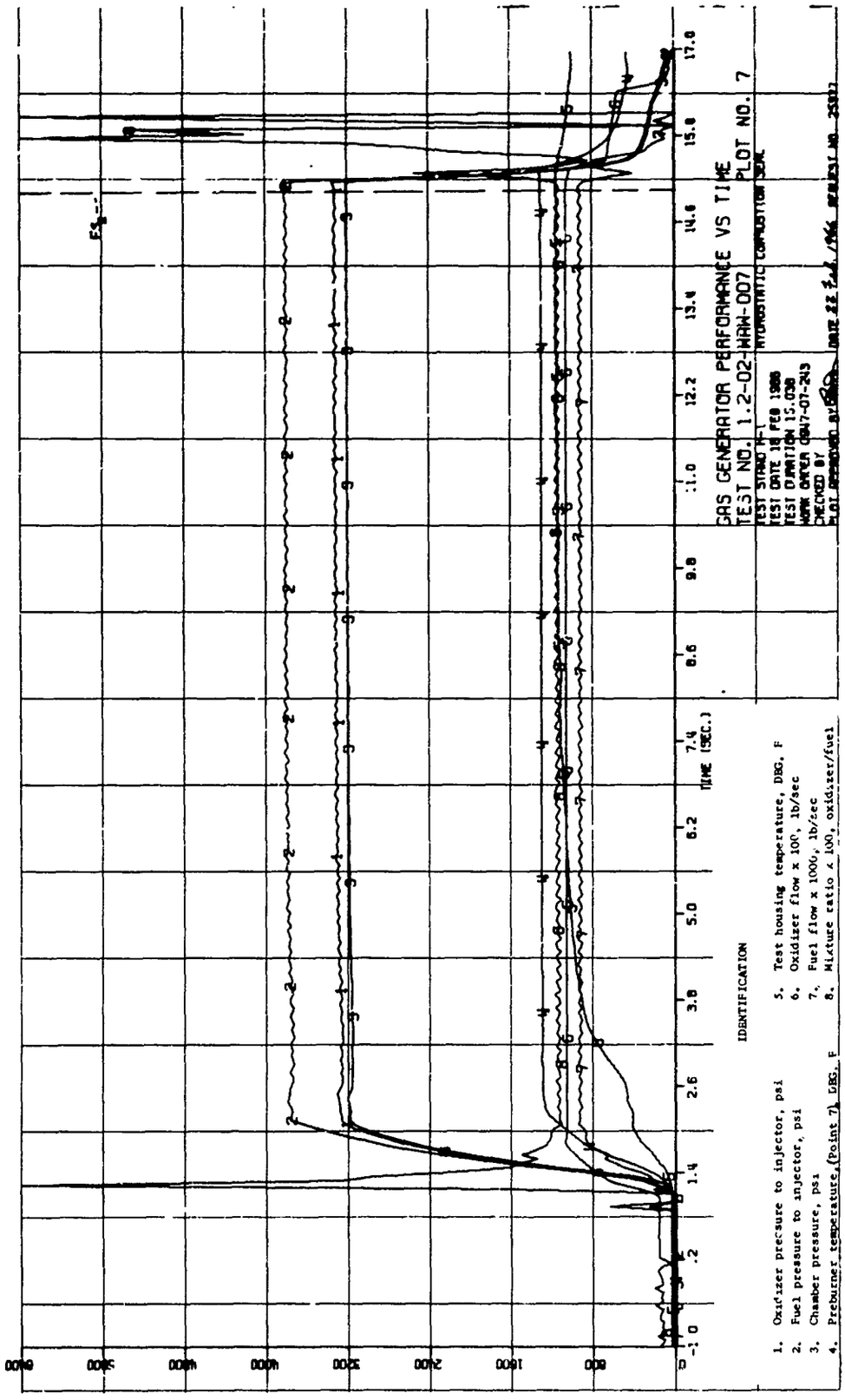

Gas-Generator Performance vs Time, Test 1.2-02-WAM-007 (u)

Figure XI-8

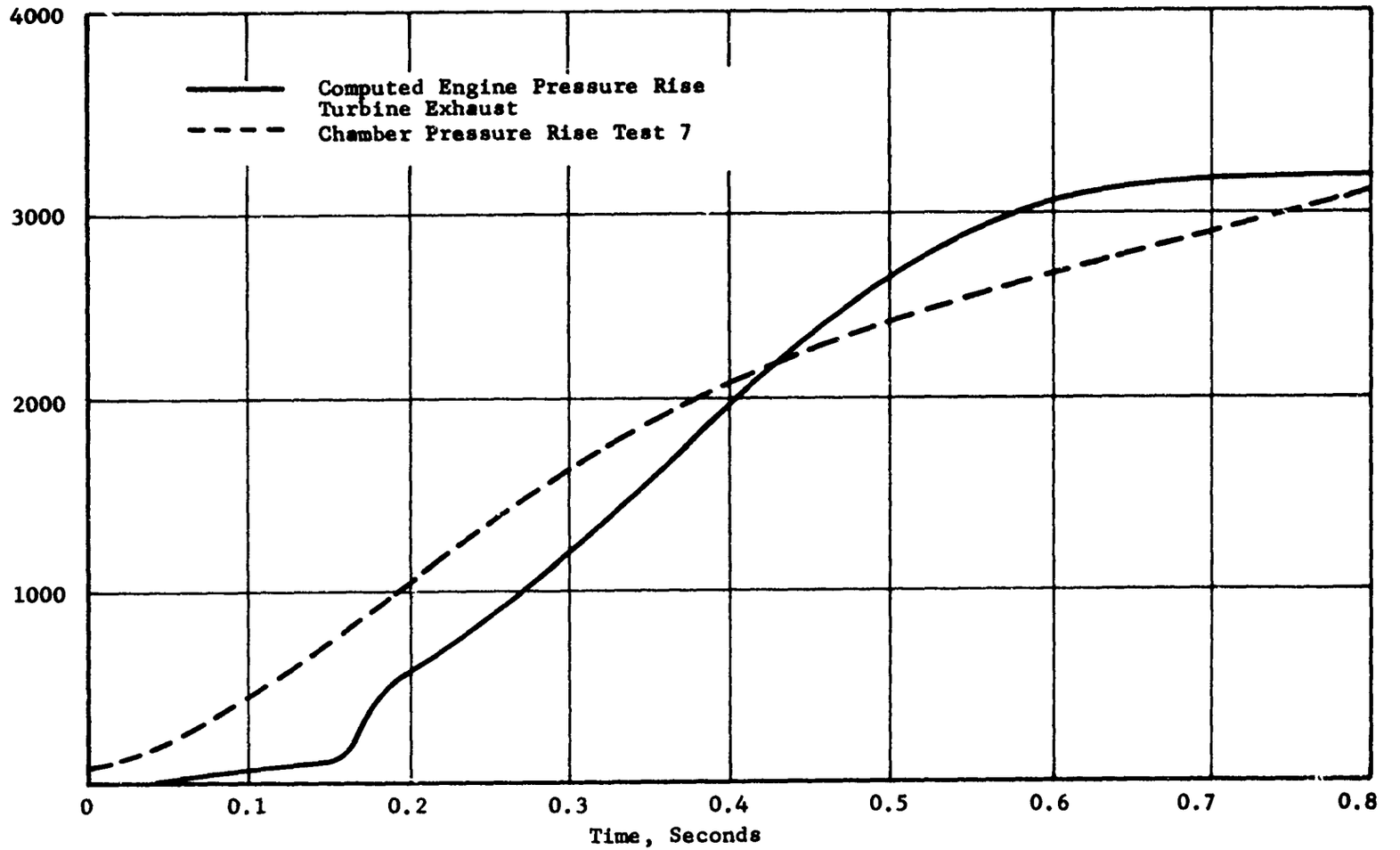

Figure XI-9

Chamber Pressure vs Time (u)

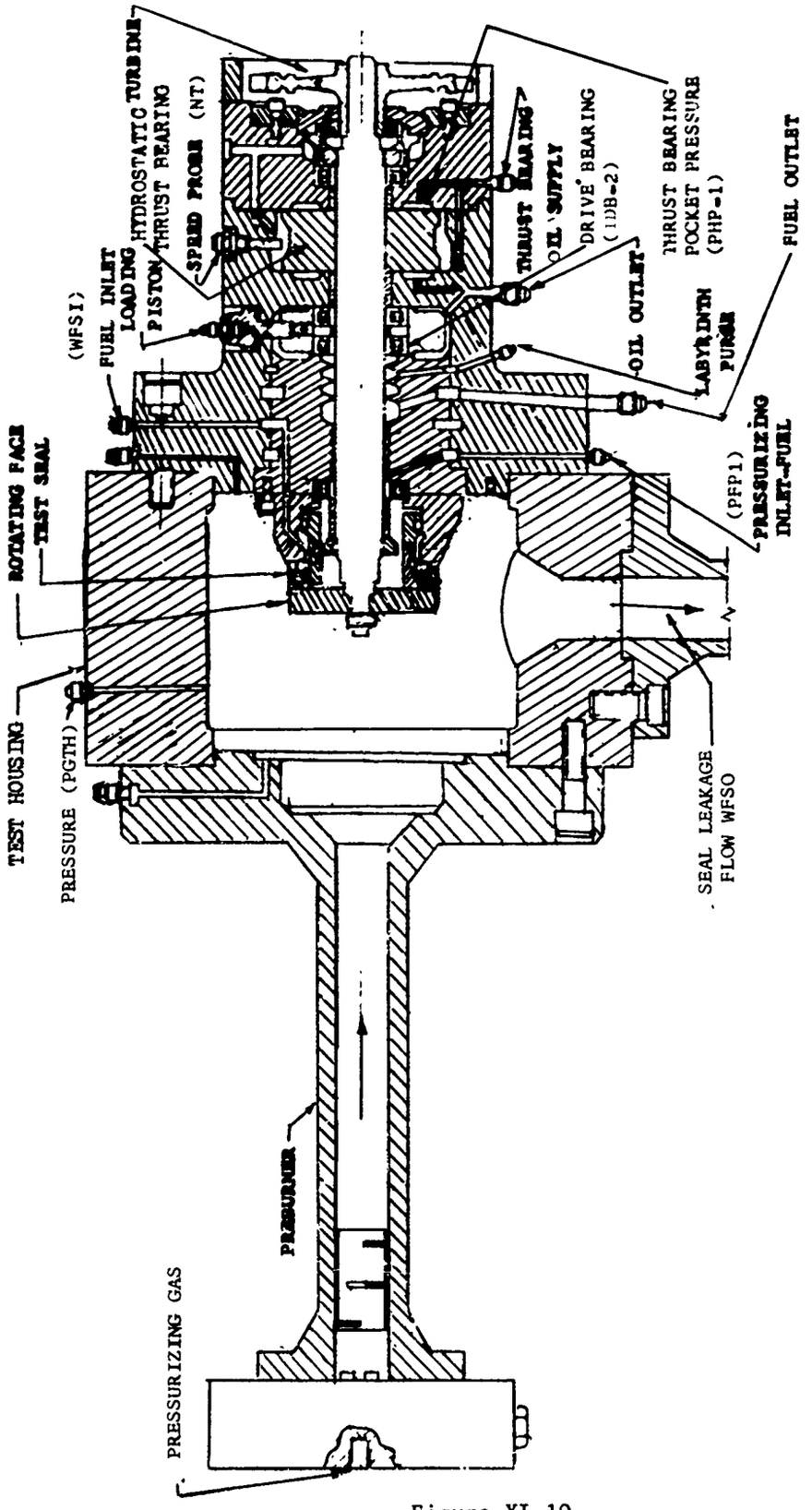

Hydrostatic Combustion-Seal Tester; Cold-Rotating AeroZINE 50 Tests

Figure XI-10

(This page is Unclassified)

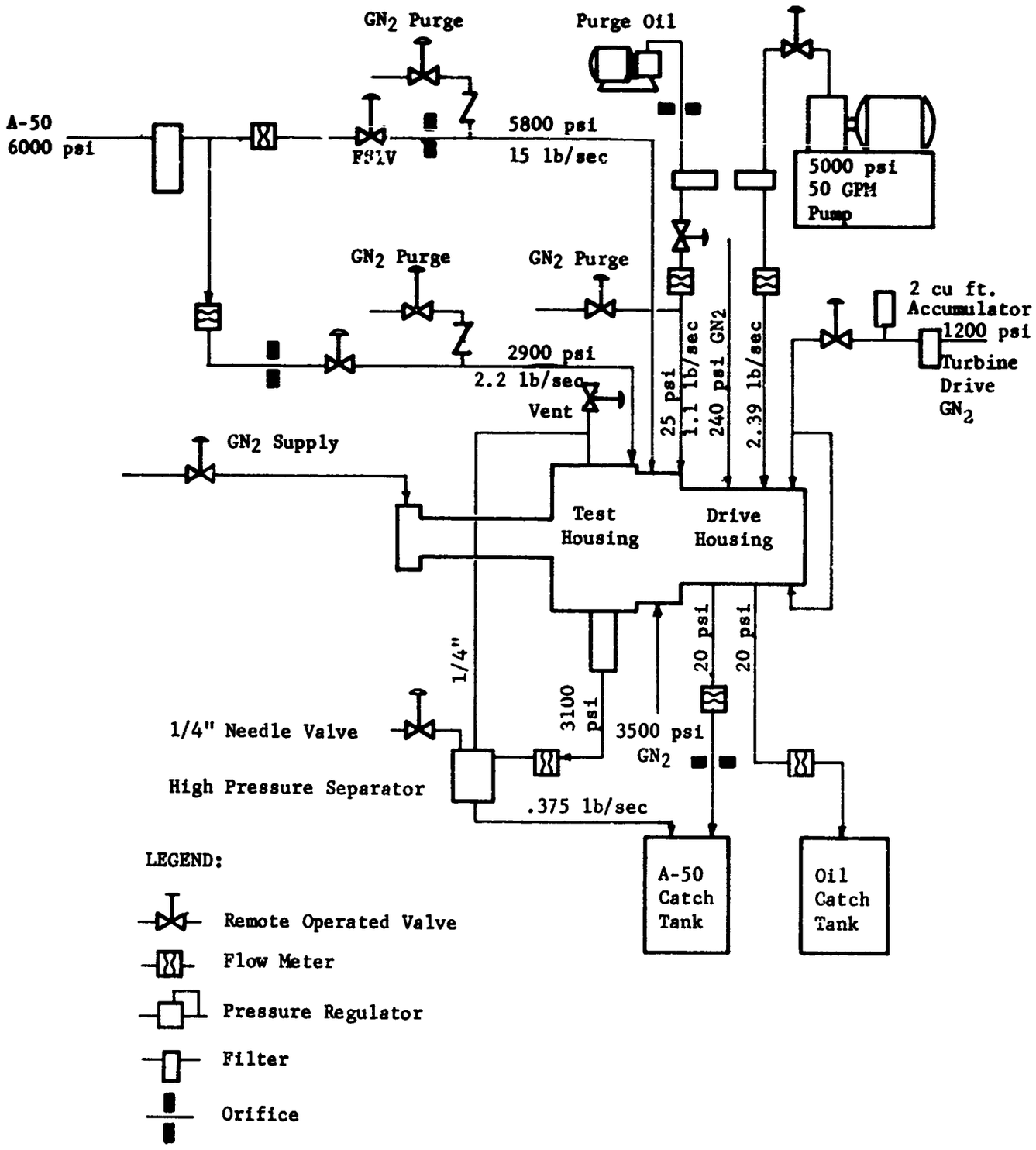

Flow Diagram, Rotating Fuel-Calibration Tests, ARES Hydrostatic Combustion Seal Program

Figure XI-11

XII.

SUCTION VALVES

A. GENERAL

1. Function

The suction valves control the flow of fuel and oxidizer from the propellant tanks to the main pump inlets of the engine module. The valves are used for positive propellant shutoff and are actuated in sequence during start and shutdown of the module. The use of metal diaphragm seals in these suction valves ensures zero leakage during long-term storage.

2. Design Philosophy

The suction valves are of the segmented-ball type to provide a spherical-seat poppet seal. The segmented-ball gate lifts off the seal and rotates completely out of the flow path in the fully open position. Since there is no shaft across the valve flow passage, flow to the main pump inlets is smooth and uninterrupted. The fuel and oxidizer valves are alike in size and design; only the oxidizer valve has a housing adapter to account for differences in fuel and oxidizer pump housing interfaces.

3. Progress

Fabrication of detail parts for two experimental suction valves, Figure XII-1, is continuing. Assembly of a suction valve for test and development is expected in April. Several housing castings for the experimental valves have been received from Aerojet's foundry and have been satisfactorily hydrotested prior to being finish-machined. Several preliminary design concepts of a prototype suction valve were studied in an effort to reduce their weight and to provide for ease of assembly. A design was selected for fabrication (Figure XII-2), and a concerted effort is being made toward producing detail drawings. Release of this prototype design is expected by 15 April 1966. All detail parts necessary for adapting a hydraulic-cylinder rack-and-pinion type rotary actuator to the suction valve have been prepared. Electro-hydraulic valves were flow-tested and calibrated, and an electrical control circuit has been designed.

B. DESIGN

1. Description

The prototype design substantially reduces the weight of the suction valve, to within the weight-requirement range for flight hardware.

The valve gate is operated and controlled by the interaction of two sets of slotted cams. One cam set is rotated by the actuator and the other

XII, B, Design (cont.)

is stationary in the body. The cam followers are attached to the valve gate. The interaction between the cams forces the cam follower and the valve-gate assembly to move down, to shear the diaphram seal, and then to rotate completely out of the fluid flow path. On the closing cycle, this same cam interaction causes the valve gate to move to the closed position and to seat on the operational seal. Final closure is similar to the motion of a poppet valve.

A working layout of the lightweight suction valve is 70% completed; detail drawings are 50% completed.

2. Stress

A stress analysis and review on the experimental suction valve was completed. Hydrotesting of valve housings was completed; all housings were found to be satisfactory.

A stress analysis is underway on the prototype design, and close liaison is being maintained between design and stress-analysis personnel to ensure that detail drawings comply with the findings.

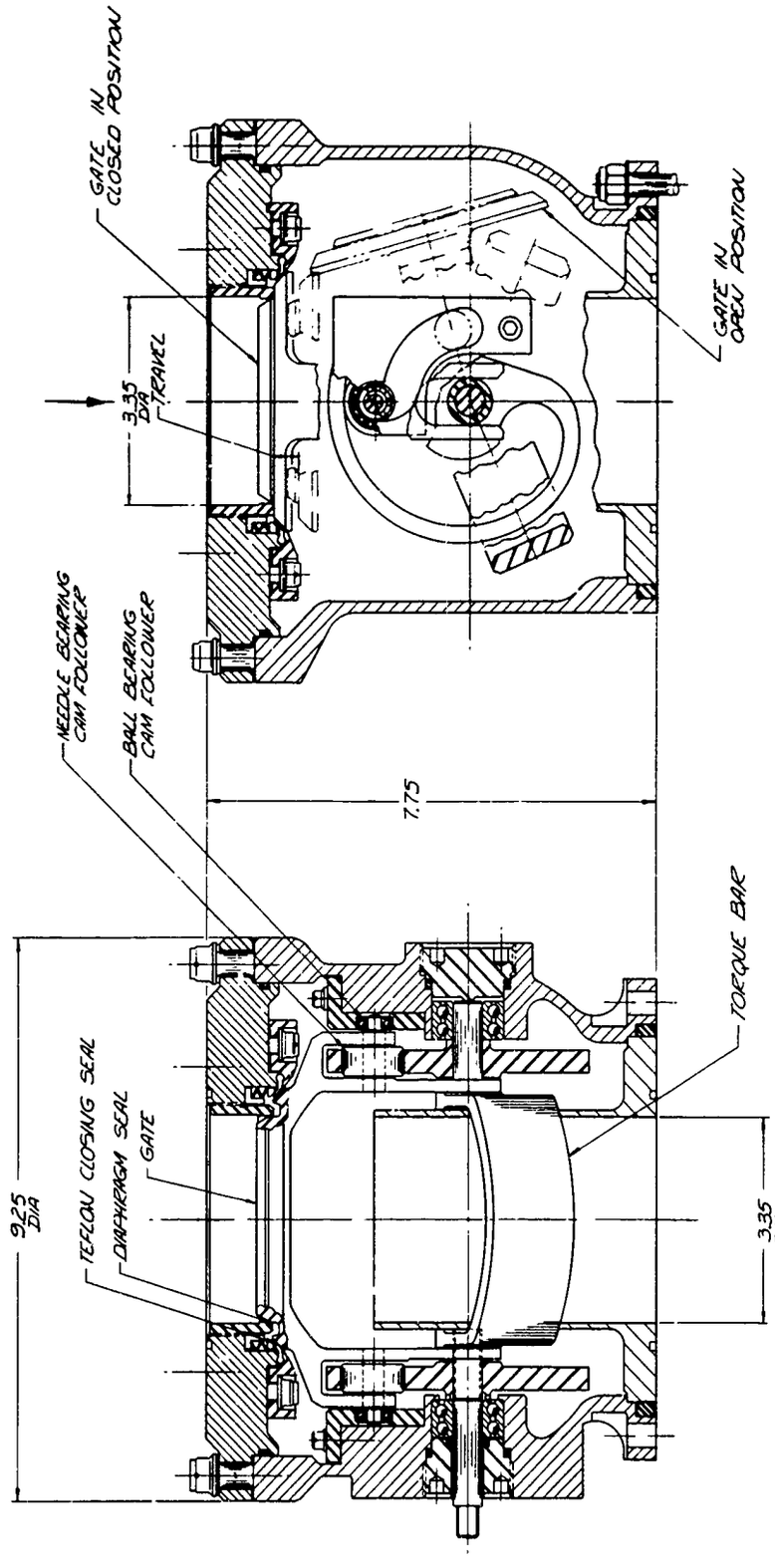

Suction-Valve Assembly, Preliminary

Figure XII-1

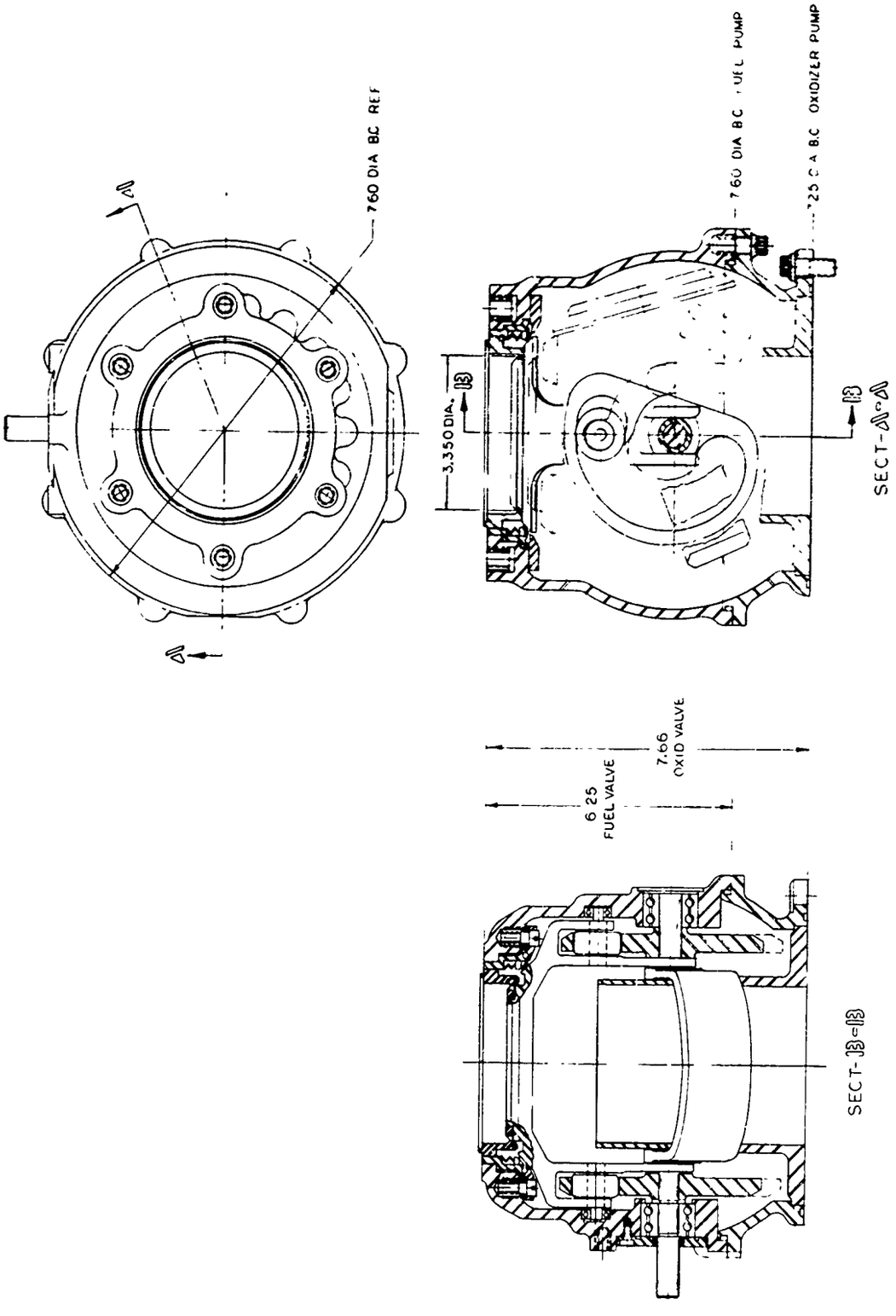

Suction Valve, Prototype

Figure XII-2

XIII.

FLOW-CONTROL VALVES

A. GENERAL

The purpose of the primary and secondary combustor fuel-flow control valves (PCFCV and SCFCV, respectively) is to control the fluid flow to these combustors during all phases of module operation. Preliminary digital-computer analyses of module performance indicated the necessity for closely coordinating the operation of the PCFCV and SCFCV, particularly during module startup and shutdown. A reliability study was completed which compared the cost versus a number of tests for four different conditions: no interlock, and mechanical, hydraulic, and electrical interlock. The choice of the type of interlock is being considered.

B. PRIMARY COMBUSTOR FUEL-CONTROL VALVE (PCFCV)

1. Design

The valve actuator chosen for initial testing will be an Aerojet-laboratory furnished linear electrohydraulic servoactuator. The proposed module-valve configuration and the proposed test valve are shown in Figure XIII-1 and -2, respectively.

2. Fabrication

Fabrication of two experimental test units was completed; the units were delivered to the frequencing laboratory for testing.

3. Test

The test setup for performing torque leak tests at a system pressure of 6000 psi was completed, and tests of the first valve were initiated. The high-pressure torque tests demonstrated the functional integrity of the valve for use in the intensifier tests of the primary combustor: the valve operated without binding at a differential pressure of 6200 psi. During leakage tests, the leakage was 1030 cm^3 of water in 10 sec, which corresponds to a water flow rate of 0.227 lb/sec. The system pressure measured at the valve inlet was 5630 psi. This low leakage is a significant indication that the valve can be used for effective module shutdown.

Flow testing of two valves was initiated. The flow-factor versus valve-position characteristics of both valves coincided with the calculated performance beyond the engine steady-state operating flow factor (K_w) of the valve. The operating K_w of the valve occurred at 67% of fully open position. Above 70%, the first test valve indicated that flow saturation occurred (see Figure XIII-3). An investigation disclosed that a choke was inadvertently caused by insufficient machining and cleaning at the meeting point of two drilled flow passages. Another choke was found in the annular flow area surrounding the inlet to the valve-orifice ports. These chokes have been removed. Figure XIII-3 shows the improvement above 70% of stroke after partial modification.

XIII, B, Primary Combustor Fuel-Control Valve (PCFCV) (cont.)

The exit passage in the valve has been enlarged to eliminate another possible choke and to extend the range of the valve. As a result, it is expected that the actual K_w values will satisfactorily meet the calculated performance.

C. SECONDARY COMBUSTOR FUEL-CONTROL VALVE (SCFCV)

1. Design

The SCFCV has been designed to provide a flow-factor versus valve-position characteristic complying with the startup and shutdown transient requirements of the digital computer model of the module. Provisions were made for interlocking the SCFCV with the PCFCV. The precision flow-control orifices ensure a closely repeatable flow factor with value position.

The saturation problem encountered in testing and PCFCV was evaluated and the necessary inlet and outlet corrections were incorporated in the SCFCV designs.

The valve will be controlled with an available existing electro-hydraulic servo actuator identical to that employed for actuation of the PCFCV.

Test valves have been designed and detailed both for high-pressure intensifier testing and for development testing in the engineering laboratories. Most of the parts have been released to fabrication. Two designs were required because the interface restrictions on the intensifier test valve were incompatible with the laboratory test facilities. The development test valve is shown in Figure XIII-4.

The module valve (Figure XIII-5), with internal control porting identical to that of the test valve, has been incorporated into the engine module assembly, and interfaces have been tentatively established.

2. Fabrication

The test-valve housing and detail parts are 50% completed. It is anticipated that development testing can be started on schedule.

---

*Flow factor, $K_w = \dfrac{\dot{W}}{\sqrt{\Delta P \times \text{Specific Gravity}}}$

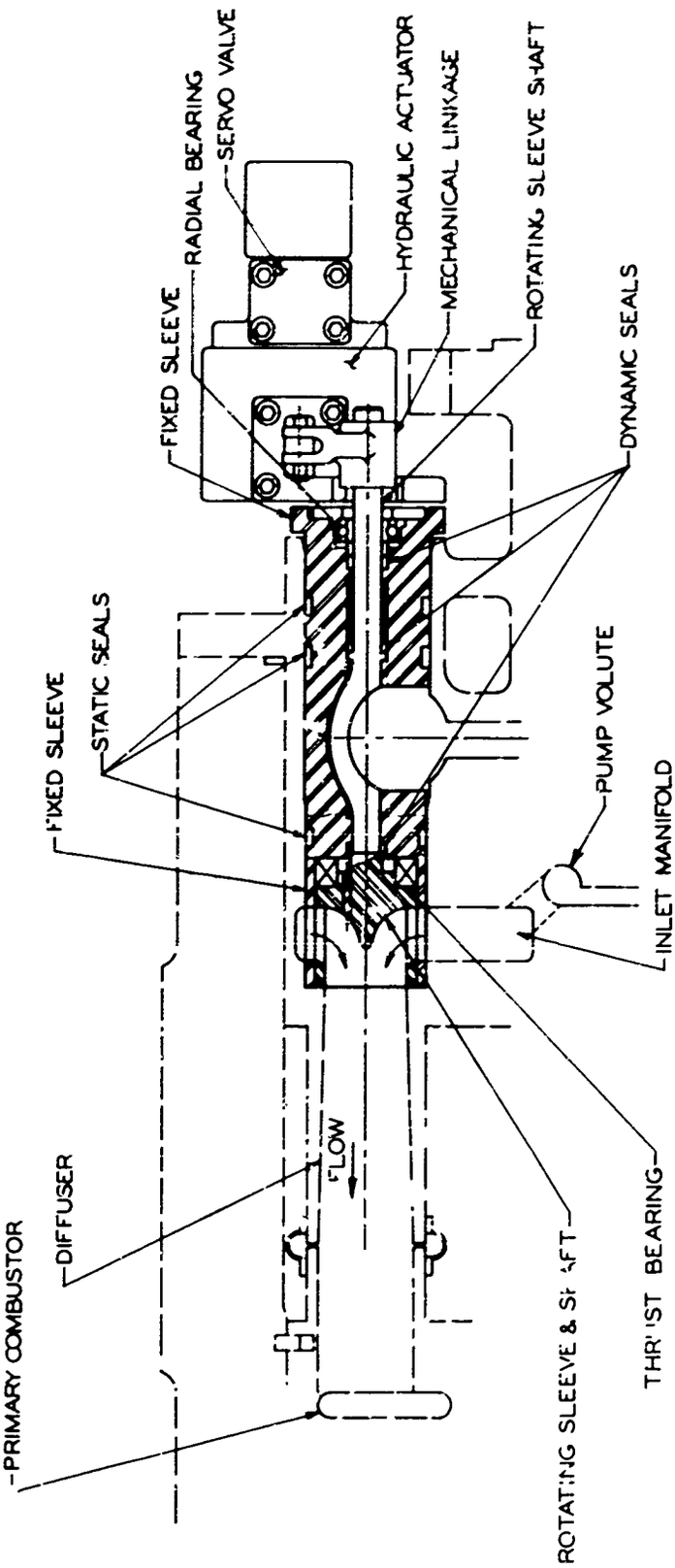

Primary Combustor Fuel Control Valve, Rotary (Module Unit)

Figure XIII-1

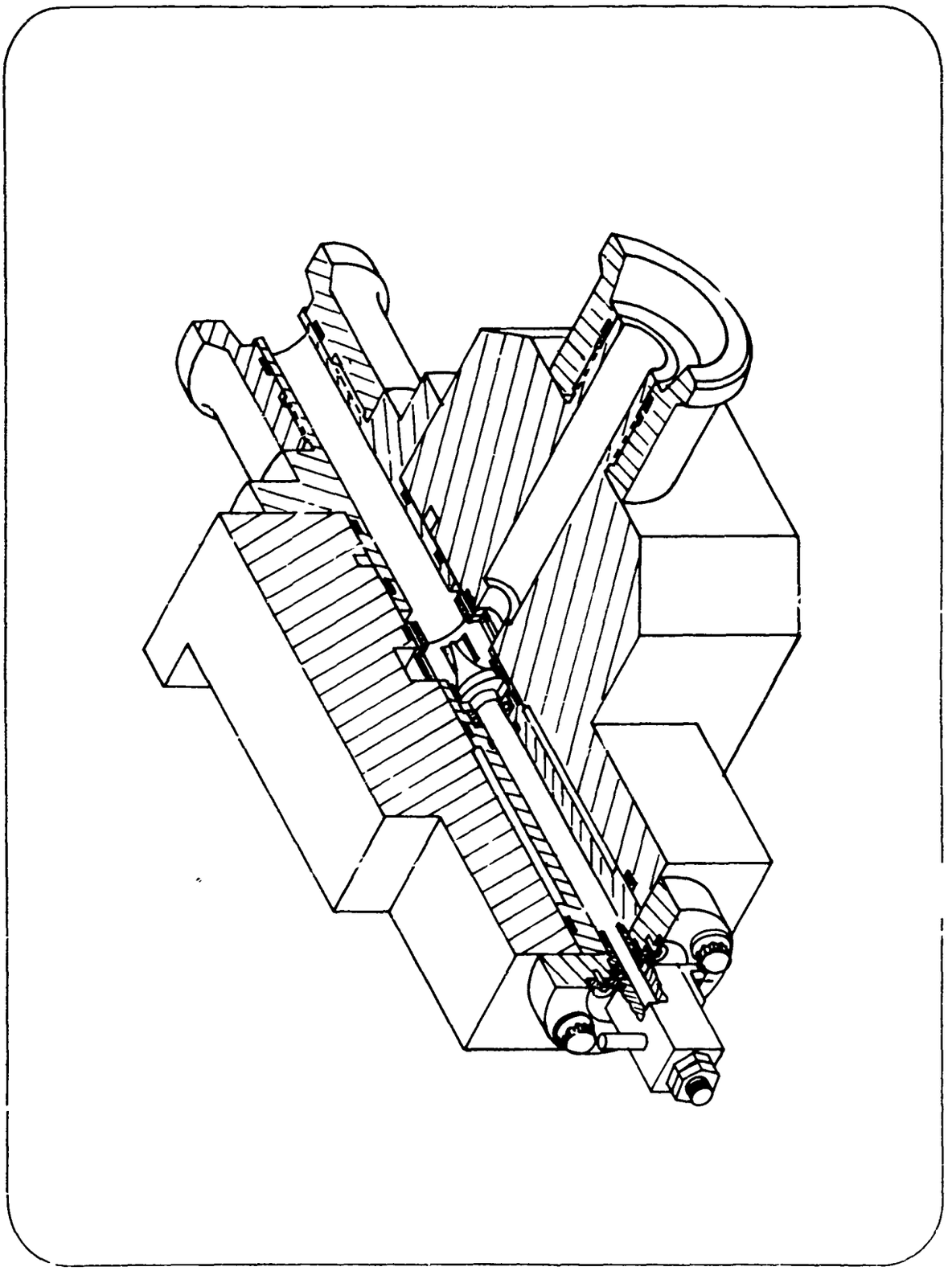

Test Valve--Primary Combustor Fuel Control

Figure XiII-2

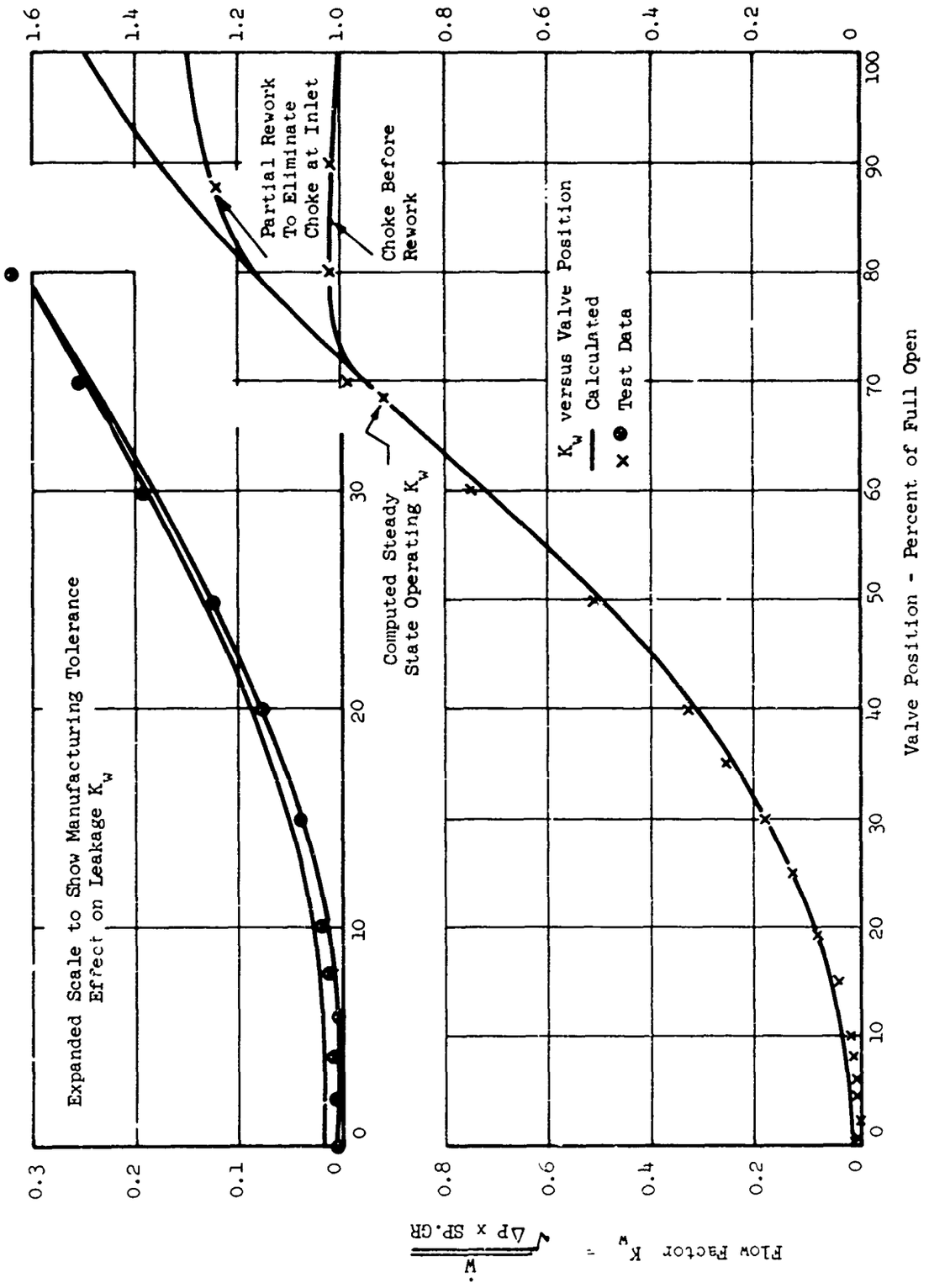

Figure XIII-3

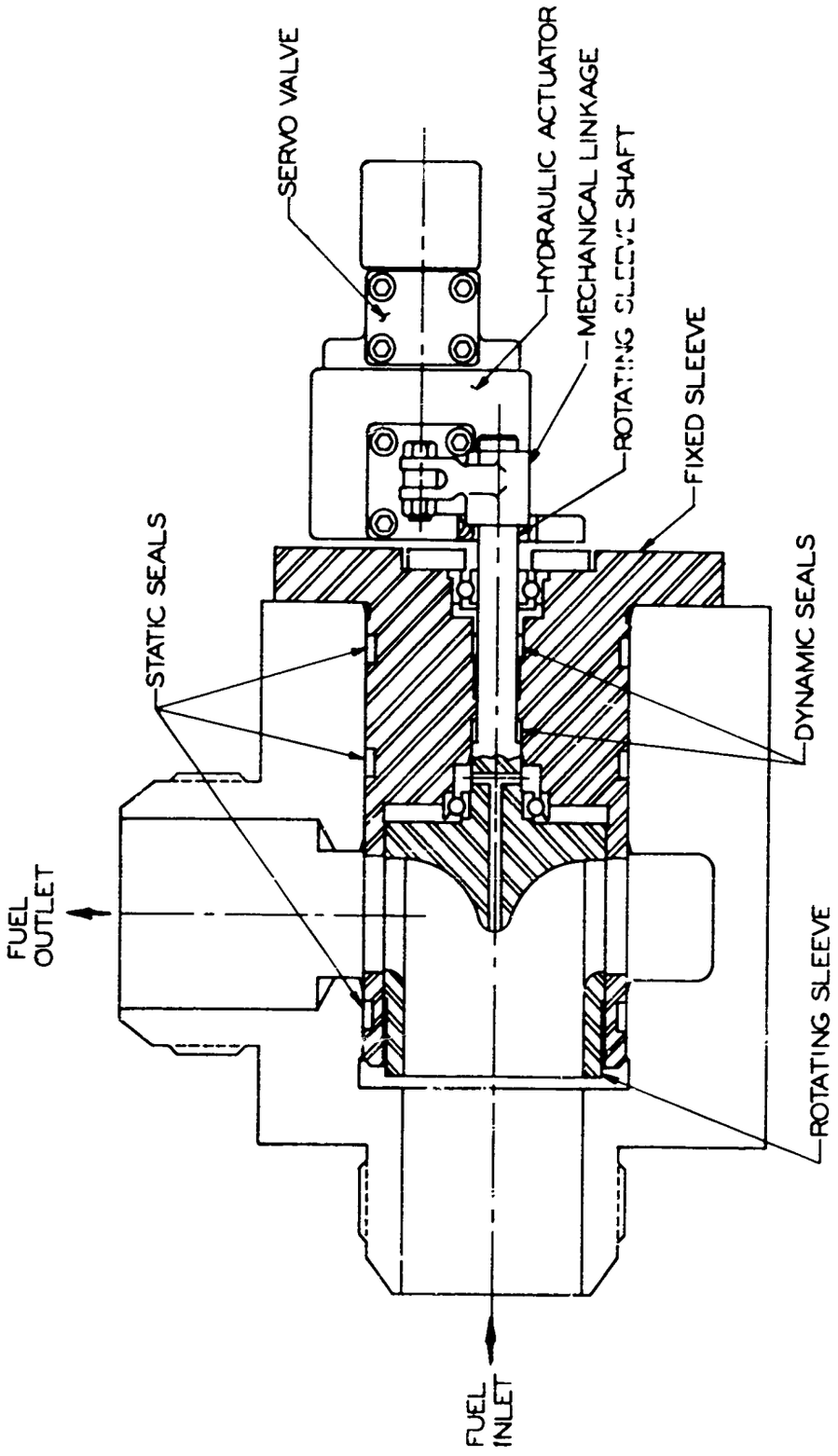

Secondary Combustor Fuel Control Valve--Rotary (Test Unit)

Figure XIII-4

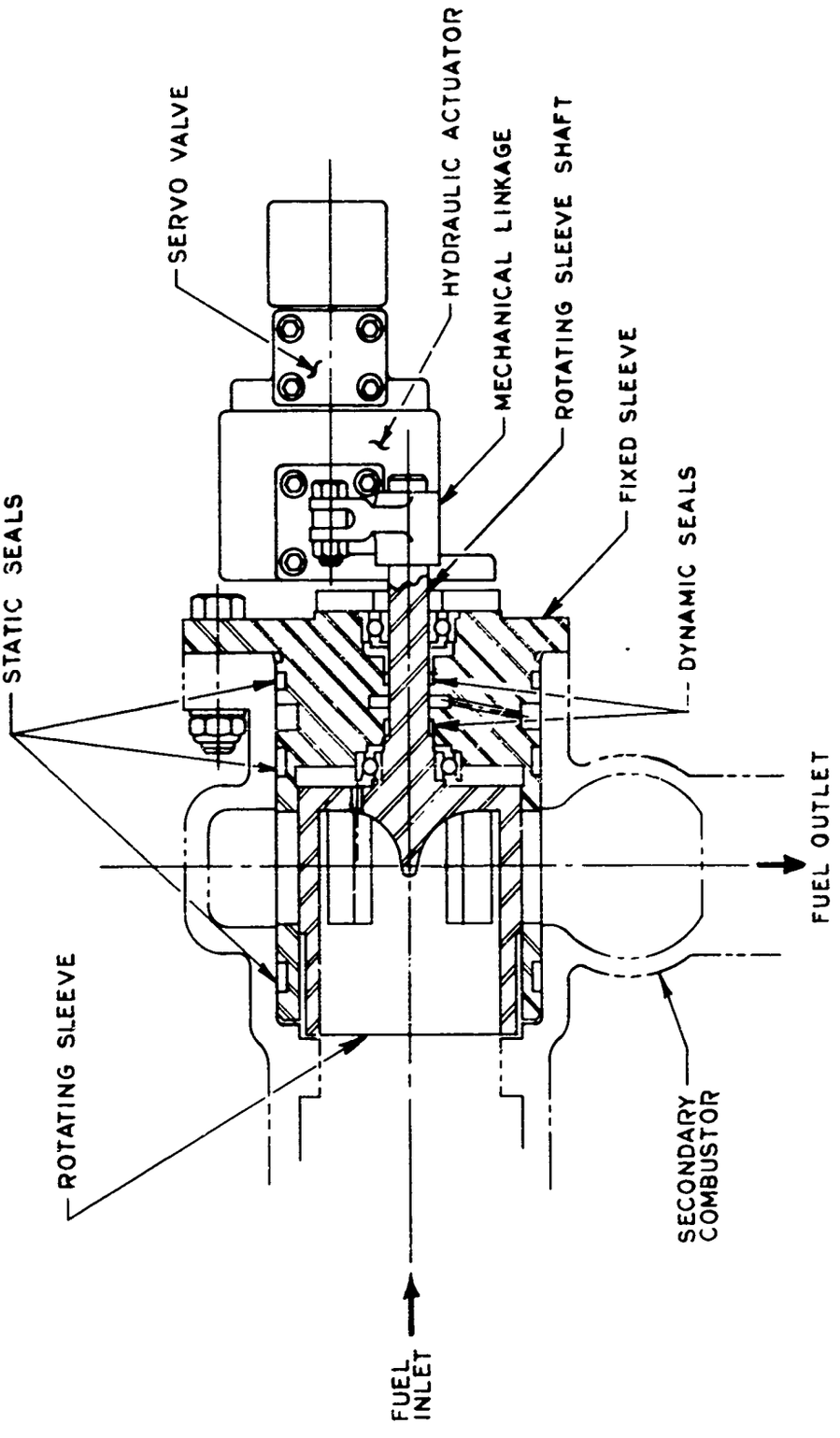

Secondary Combustor Fuel Control Valve--Rotary (Module Unit)

Figure XIII-5

XIV.

SUCTION LINES AND AUXILIARY SYSTEMS

A. GENERAL

1. Suction and Feed Lines

The suction lines provide the connection from the boost pump outlet to the suction valve inlet which in turn is mounted directly upstream of the main pump inlet. These lines are at a relatively low pressure (150 and 350 psi for the fuel and oxidizer, respectively). Conversely, the feed lines provide high-pressure propellants from the main-pump discharge to the boost-pump fluid-drive turbine inlets. These oxidizer and fuel turbine feed lines operate at main pump discharge pressures.

2. Servo-Control System

The servo-control system is intended to provide a flexible and reliable control for the primary and secondary fuel valves. Available electro-hydraulic servo actuators will be used to operate the fuel-control valves which have position-feedback to close the minor loop.

B. DESIGN

1. Suction and Feed Lines

The preliminary design analysis for sizing the suction and feed lines was completed. The sizing was based on a line length of 6 ft and on the module differential-pressure allocations shown in Figure XV-5. Tentative interfaces for the feed lines have been established.

2. Servo-Control System

An all-solid-state control system is being designed to sequentially open both the oxidizer- and the fuel-supply valves, and to provide closed-loop position control to the primary and secondary fuel valves. The solid-state approach was decided upon since it gives the highest possible flexibility of any system proposed.

This high degree of flexibility is obtained through the use of basic modules, which can be interconnected from a patch panel for a given sequence. If a different sequence is desired, only the patch cords need be changed. Flexibility is also increased by the ability to change sequence times and rates electronically, without any other modifications.

The basic modules utilized in the system consist of a NOR gate, NAND gate, flip-flop, timer, integrator, and amplifier. The preliminary circuits for the above modules have been designed and fabricated, and are presently under intensive tests. The designs will be firmed during the next report period.

XIV, B, Design (cont.)

The servo amplifier for the position-control loop is presently being designed. Initial breadboard testing demonstrated a variable-voltage gain from 1 to 100. The amplifier design will be completed and evaluated after receipt of special components now on order.

The existing electrohydraulic servoactuators, which have been integrated with the PCFCVs and SCFCVs, will become an integral part of the control system. Positional accuracy of each control valve is expected to be well within 1.0% of steady-state operating position. Additionally, the actuators have built-in fail-safe devices which will close the fuel valves in the event that either electric or hydraulic control power is lost.

XV.

PROPULSION SYSTEM

A. GENERAL

The overall objective of the propulsion-system effort is to demonstrate the engineering practicality and the performance of the ARES engine module. The Phase-I design effort will ensure that components designed for testing are compatible with engine modules for both single and clustered module applications. The module can be used either in conventional clusters of individual autonomous units or arranged to discharge through a common plug or forced-deflection type nozzle. A 20-module forced-deflection nozzle propulsion system has been defined for establishing the overall envelope requirements for the module.

B. SUMMARY

The following tasks were performed:

1. The layout of the 20-module forced-deflection (FD) nozzle propulsion system was updated.

2. The engine module layout with a Configuration-B advanced turbopump was revised, and external views of the engine module were prepared.

3. Efforts were continued to define major component interfaces.

4. Methods for mechanically interlocking the primary and secondary fuel-control valves were studied and found to be feasible.

5. A preliminary test-installation control schematic was prepared.

6. The module pressure schedule was modified, with allocated pressure-drop values being expressed in parametric form.

7. The predicted module performance versus chamber film-coolant flow rate was updated to include the revised thrust-chamber performance characteristics.

8. A revised engine operating point was established based on the predicted characteristics of the Configuration-B turbopump and on the revised prediction of secondary combustor performance characteristics.

9. A revised module flow schematic was prepared showing propellant flow values in each component for the revised operating point.

10. The mapping of engine operating parameters versus primary and secondary fuel valve positions was completed.

11. The module steady-state mathematical model was refined.

XV, Propulsion System (cont.)

C. TWENTY-MODULE PROPULSION SYSTEM

(c) A preliminary 20-module propulsion system layout, Figure XV-1, was prepared. This propulsion system incorporates modules with Configuration-B turbopumps and internal-expansion nozzles having an area ratio of 13.4:1, clustered on a FD nozzle for an overall expansion ratio of 70:1. Component envelope constraints, established from this propulsion system layout, have been incorporated in the affected component designs.

D. MODULE (ADVANCED TPA CONFIGURATION)

(u) A cross-sectional layout of the engine module, Figure XV-2, was prepared showing a Configuration-B turbopump, a secondary combustor with a characteristic length (L*) of 40 in. and capillary film-cooling tubes, and suction valves of preliminary configuration. External views of the engine module were prepared. Figure XV-3 shows the external side view of the engine module with the same orientation as that of Figure XV-2.

(u) The determination of interfaces between major components was continued. Detail drawings for the following interfaces were submitted for engineering approval: (1) thrust chamber to secondary injector, (2) turbopump to secondary injector, (3) turbopump to suction valves, (4) boost-pump turbine feed lines to oxidizer and fuel turbopump housings, and (5) boost-pump turbine feed lines to oxidizer and fuel boost-pump housings.

(u) Methods for mechanically interlocking the primary and secondary fuel-control valves as a means of ensuring their scheduled opening and closing were evaluated and found to be feasible. Mechanical interlocking is one of several methods being considered in controlling the valves during demonstration testing of the ARES module.

(u) An effort was initiated to determine the manner in which the module will be installed and tested. This effort included the preparation of a preliminary control schematic showing the module with its feed lines, hydraulic turbine lines to the boost pump, suction valves, fuel-control valves, and valve actuators. This schematic will be used to determine the requirements for component instrumentation and module controls, and the general arrangement of the controls.

(u) The module design operating pressure schedule, as shown in Figure XIV-3 of Report 10830-Q-2, was modified. Allocated passage ΔP values are now expressed in terms of K_w values where

$$K_w = \frac{\dot{W}}{\sqrt{\Delta P \times S.G.}} .$$

XV, D, Module (Advanced TPA Configuration) cont.

Figures XV-4 and -5 show the nominal design operating pressures and the allocated passage K_w values, respectively. The structural design of the module is based on the maximum operational pressure (1.21 times the values shown in Figure XV-4), and on appropriate design safety factors.

(c) A revised prediction of engine performance versus secondary combustor oxidizer film-coolant flow rate, based on test data from ICP chamber testing, was established and is shown in Figure XV-6. This figure shows the predicted specific impulse (I_s), the chamber characteristic velocity (c*), and the thrust coefficient (C_f) for a chamber having a characteristic length (L*) of 40 in. and a nozzle having an area ratio of 20:1. (The performance of the secondary combustor assembly is discussed in Section IV.)

(c) A revised engine operating point was calculated based on the allocated Kw values for the module, on the predicted performance of a Configuration-B turbopump, and on the revised performance characteristics of the thrust chamber. This predicted operating point is summarized in Figure XV-7, with the target engine specific impulse remaining at 285 sec. The allowable secondary combustor film-coolant flow rate was reduced to 21.3 lb/sec, which is about 10 lb/sec less than shown in Figure XIV-4 of Report 10830-Q-2. Operation of the engine at reduced film-coolant flow rates requires a slight increase in pump discharge pressures. These increased pump discharge pressures are compatible with the module design because they are below the design maximum operational pressure for the components involved. The module internal flow schematic, Figure XV-8, was revised to incorporate the latest internal flow-passage configurations and flow values corresponding to the revised engine operating point. This flow schematic also shows pump internal flow values, which are considered pump losses and are included in the predicted pump-efficiency values. Only those flow values shown in the schematic as entering or leaving each component are included in the module power-balance calculations for establishing the predicted operating point.

(c) Eight module-control maps were prepared, which show the steady state operating parameters of the engine as functions of the primary and secondary combustor fuel valve positions up to a thrust of 100,000 lb. A typical map, Figure XV-9, is presented in this report and shows the predicted shaft speed of the module turbopump and the mixture-ratio characteristics of the primary combustor for design and off-design steady state operation.

(u) Continuing engine-performance studies were directed toward refining the engine steady-state mathematical model. Refinements of the steady state mathematical model are discussed in Section XVI.

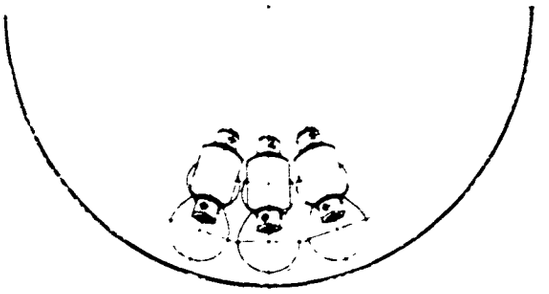

MODULE ARRANGEMENT
– TOP VIEW –

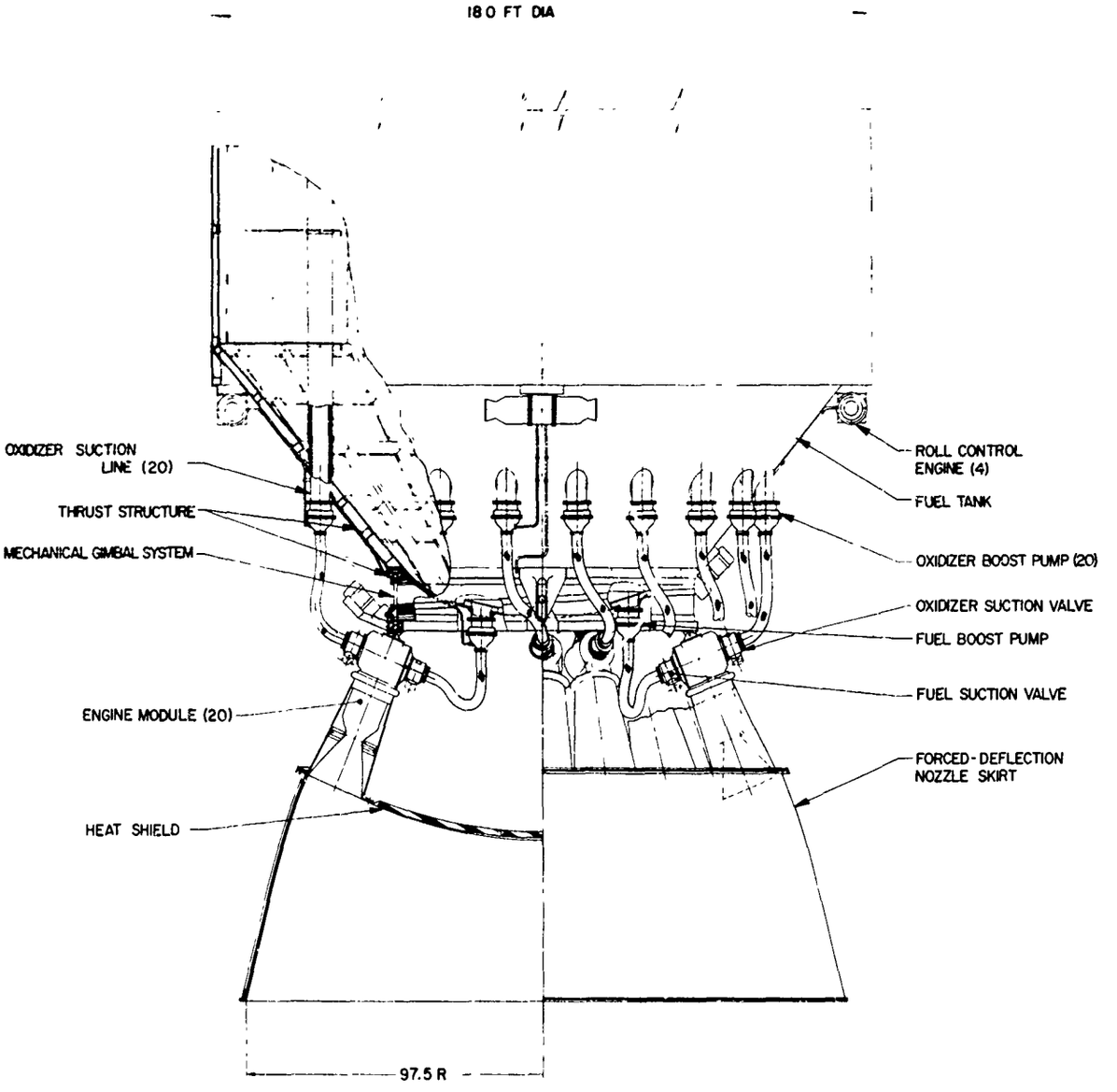

Twenty-Module Cluster, FD Nozzle

Figure XV-1
(This page is Unclassified)

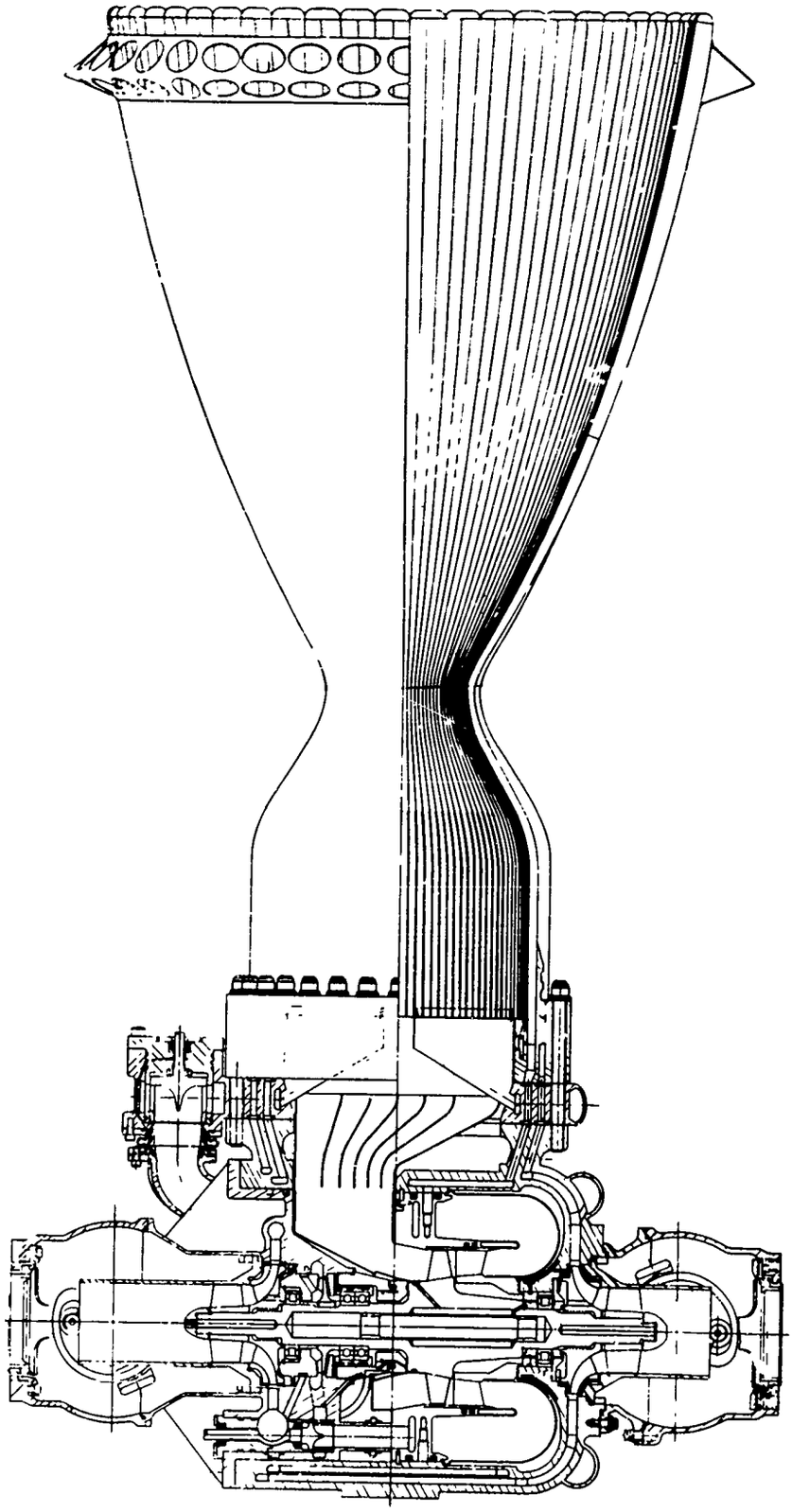

ARES Engine Module, Advanced Turbopump Configuration (u)

Figure XV-2

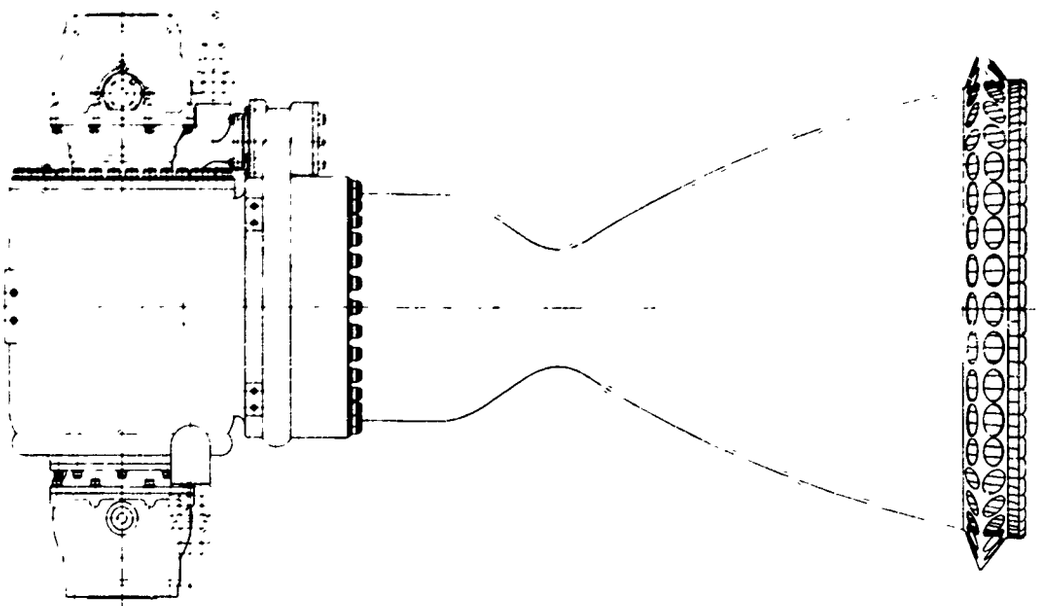

ARES Module, External Side View

Figure XV-3
(This page is Unclassified)

This pressure schedule is based on (1) allocated flow-passage, K_w, values to determine ΔP, (2) minimum allocated turbopump efficiencies, and (3) target module performance. These pressure values define target operating requirements for Phase-I design purposes, and will remain in effect unless an increase in module operating pressures becomes incompatible with existing design margins of safety.

Location	Pressure, psia*				
	Liquid Oxidizer		Hot Gas	Liquid Fuel	
Boost Pump Inlet	36.6**	75		19.5**	75
Boost Pump Discharge	310	340		170	225
Main Pump Inlet	255	295		135	190
Main Pump Discharge	6025			3750	
Boost Pump Turbine Inlet	5600			3440	
2nd Stage Fuel Pump Inlet				3600	
2nd Stage Fuel Pump Discharge				5765	
Cooling Jacket Inlet	5900				
Film Cooling Manifold	5900				
Cooling Jacket Exit	5125				
PC Injector Inlet	5000			5000	
PC Injector Face			4700		
Turbine Inlet			4575		
Turbine Exit (Blade), Static			3050		
Turbine Exit (Blade), Total			3100		
SC Injector Inlet			3010	3200	
SC Injector Face			2885		
SC Chamber (P_c)			2800		

* Total pressure unless otherwise indicated
** Corresponds to minimum NPSH per work statement

ARES Module Pressure Schedule, Advanced Turbopump Configuration (u)

Figure XV-4

	Flow Factor $K_W = \frac{\dot{W}}{\sqrt{\Delta P \times S.G.}}$ Minimum Allocated K_W	Reference ΔP, Flow and Spec. Grav. (used to establish min. allocated K_W)		
		ΔP, psi	$\dot{W}$, lb/sec	S.G.
Hydraulic Passages:				
Oxid. Suction Line	34	52.9	294.6	1.433
Oxid. Suction Valve	130	3.6	294.6	1.433
Oxid. Outer Housing Passage (Pump to Cooling Jacket)	16.8	125	213.3	1.282
Oxid. Cooling Jacket	6.8	775	213.3	1.282
Oxid. Inner Housing Passage (Cooling Jacket to PC Injector)	16.8	125	213.3	1.282
Oxid. P.C. Injector	10.9	300	213.3	1.282
Oxid. B.P. Hydraulic Turbine Line & Check Valve	1.51	450	38.3	1.433
Oxid B.P. Hydraulic Turbine Orif.	4.52	50	38.3	1.433
Fuel Suction Line	21.3	34	117.4	.9
Fuel Suction Valve	110	1.3	117.4	.9
Fuel S.C. Valve Inlet Passage	8.5	100	80.3	.9
Fuel S.C. Valve (wide open position)	7.0	-	-	-
Fuel S.C. Manifold (Valve to Inject)	8.5	100	80.3	.9
Fuel S.C. Injector	4.77	315	80.3	.9
Fuel P.C. Valve Inlet Passage	1.96	100	18.6	.9
Fuel P.C. Valve (wide open position)	1.50	-	-	-
Fuel P.C. Manifold (Valve to Inject)	2.77	50	18.6	.9
Fuel P.C. Injector	0.98	400	18.6	.9
Fuel B. P. Hydraulic Turbine Line & Check Valve	0.95	310	15.9	.9
Fuel B.P. Hydraulic Turb. Orifice	2.65	40	15.9	.9
Gas Passages:				
P.C. Injector Face to Turbine Inlet	2.02**	125	231.9	106*
Turbine Exit to S.C. Injector	3.01	90	239.6	70.7*
S.C. Gas Injector	2.60	125	239.6	68.2*
S.C. Injector Face to Plennum	$P_{Inj}/P_c = 1.03$	85		

*Spec. grav. of gas $\frac{\rho\ gas}{air} = \frac{Ps/RTs\ (av\ \ gas)}{.0808}$. **Effective K_p includes heat addition losses.

NOTES:

1. ΔP, flow, and specific gravity values are for reference only. For latest predicted pressures and flows, see current ARES Module Operating Point.
2. Pressure drop alone does not establish a firm requirement for a passage since pressure will vary with minor changes in flow, and to a lesser degree with density. The K flow factor should be used in place of ΔP as design criteria, since the measured K of a given piece of hardware will not change with operating conditions.

ARES Module Flow-Passage Design Requirements (u)

Figure XV-5

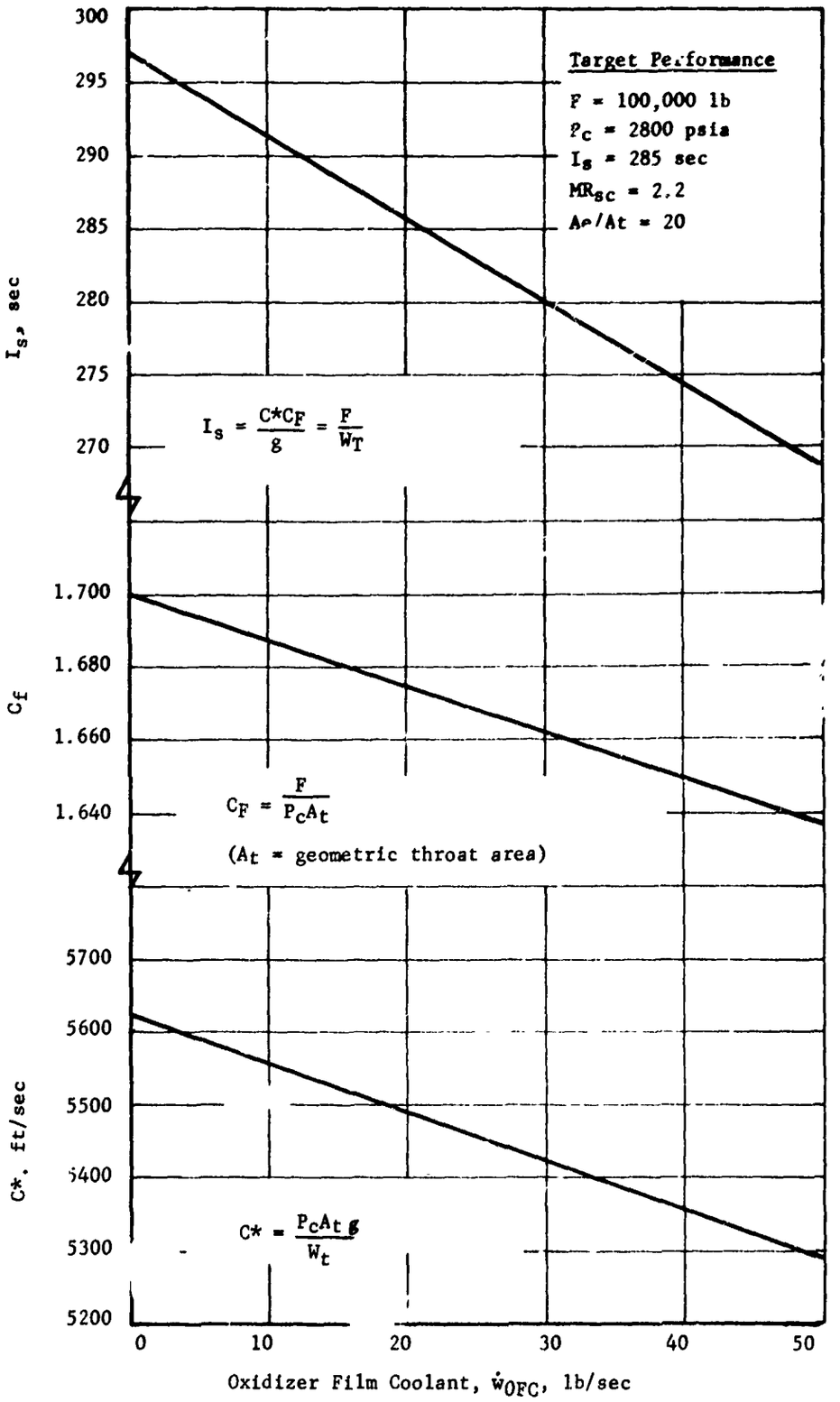

Predicted Module Performance (u)

Figure XV-6

Parameter	Symbol	Units	Value
Module Assembly			
Thrust	F	lb	100,000
Specific Impulse (Sea Level)	I_s	sec	285
Mixture Ratio, Module	M.R.	-	2.407
Total Weight Flow (1)	W_T	lb/sec	350.9
Oxidizer Weight Flow (1)	W_{OS}	lb/sec	247.9
Fuel Weight Flow (1)	W_{FS}	lb/sec	103.0
Oxidizer Suction Pressure	P_{OS}	psia	36.6
Fuel Suction Pressure	P_{FS}	psia	19.5
Oxidizer Net Positive Suction Head, Minimum	$NPSH_O$	ft	30
Fuel Net Positive Suction Head, Minimum	$NPSH_F$	ft	43
Secondary Combustor			
Chamber Pressure, Plenum	P_C	psia	2,800
Mixture Ratio, Injector	$M.R._{SC}$	-	2.2
Oxidizer Film Cooling Flow (1)	W_{OFC}	lb/sec	21.3
Primary Combustor & Turbine			
Mixture Ratio	$M.R._{PC}$	-	11.62
Turbine Inlet Total Pressure	P_{TIT}	psia	4609
Turbine Inlet Total Temperature	P_{TIT}	°F	1204
Shaft Speed	N_T	rpm	40254
Main Pumps			
Total Discharge Pressure, Oxidizer	P_{ODM}	psia	6106
Total Discharge Pressure, Fuel First Stage	P_{FDM-1}	psia	3789
Total Discharge Pressure, Fuel Second Stage	P_{FDM-2}	psia	5911
Boost Pumps			
Total Discharge Pressure, Oxidizer	P_{ODBP}	psia	310
Total Discharge Pressure, Fuel	P_{FDBP}	psia	179

(1) For complete module flows, see Module Flow Schematic, Figure XIV-8.

ARES Module Operating Po)

Figure XV-7

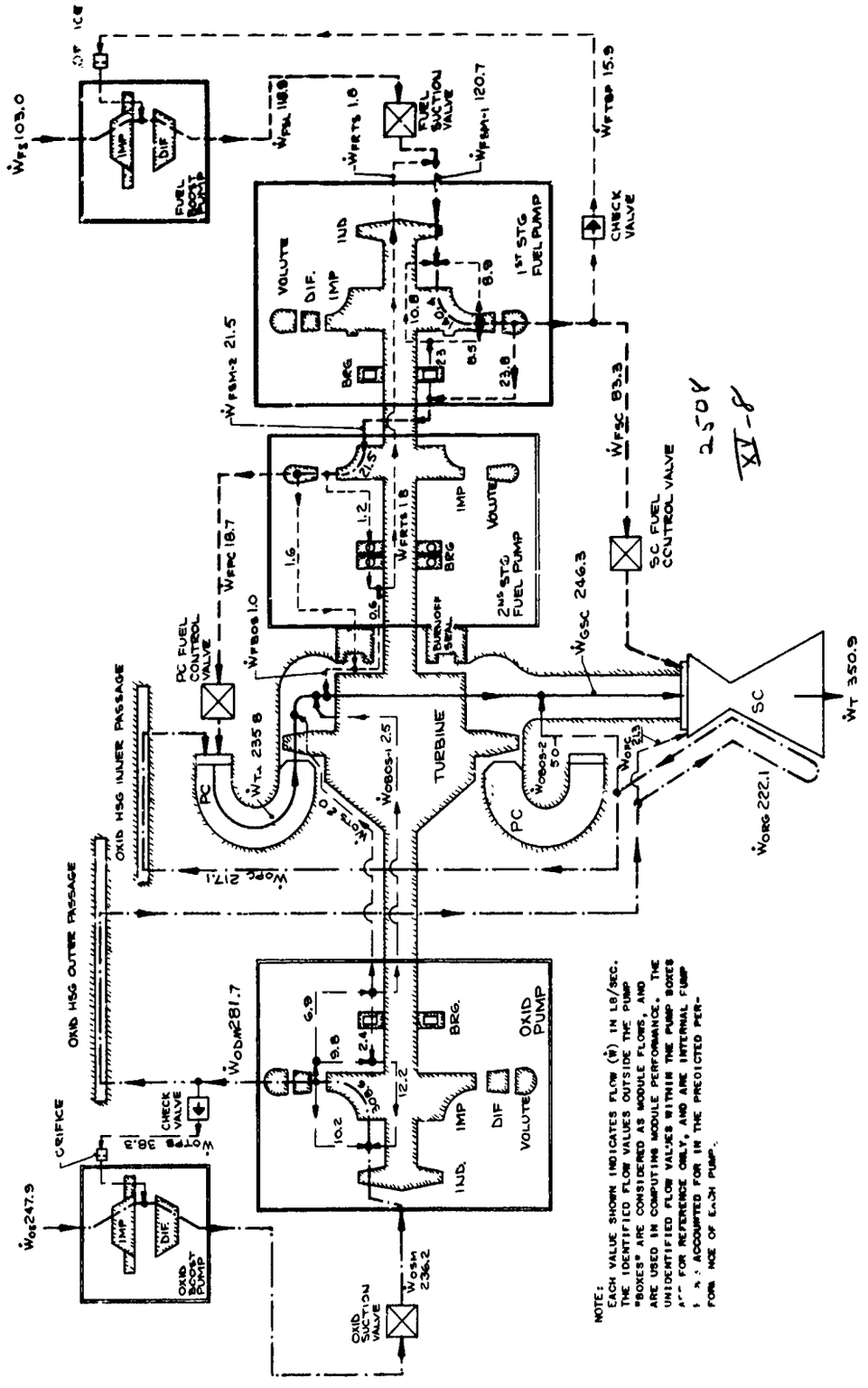

ARES System Flow Schematic (u)

Figure XV-8

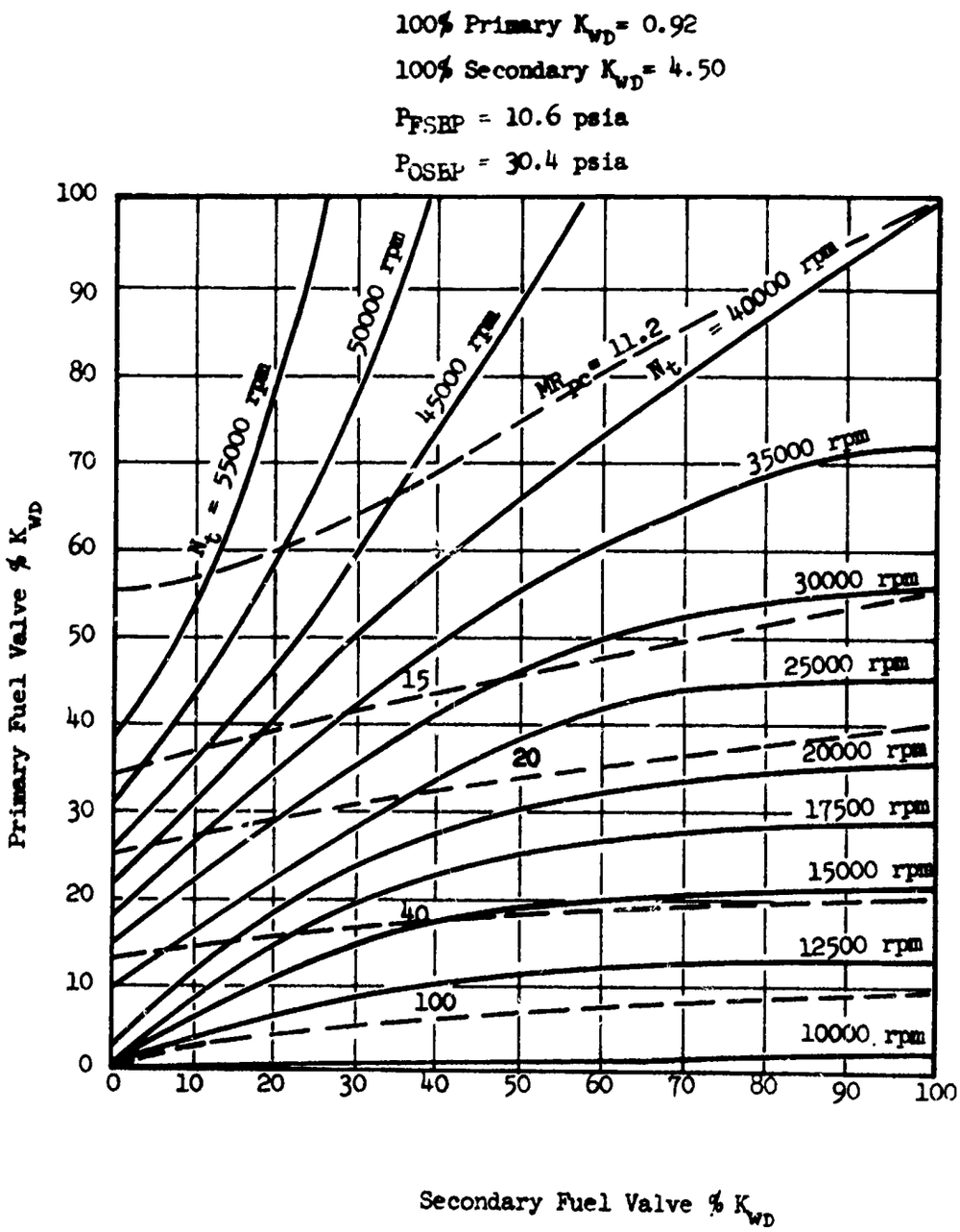

Module Control Characteristics, Turbine and Primary Combustor (u)

Figure XV-9

ENGINE ANALYTICAL MODELS

XVI.

ENGINE ANALYTICAL MODELS

A. GENERAL

Three analytical models are being developed for establishing the operating characteristics of the ARES engine and component test configurations. These three models are: (1) the steady-state program for determining the effect of system design and performance variables on engine operating point, (2) the start and shutdown transient program for establishing valve sequencing to produce smooth start and shutdown without exceeding engine design specifications (e.g., shaft acceleration rate), and (3) the low-frequency stability program to establish the dynamic characteristics of the engine for low-frequency perturbations about an operating point. These programs provide the engineering insight required to start and run the engine successfully. This is particularly necessary for a high-pressure engine where improper phasing of events during start and operation could increase component stresses to levels exceeding the design value and thus lead to failures.

The steady-state model is in operation, and only program and data maintenance has been required. The module transient model is being prepared; the models for the intensifier-fed engine have been completed. The low-frequency stability model has been completed for the intensifier-fed engines and the module model is being checked out.

B. STEADY-STATE MODEL

The module steady state mathematical model was updated. Accuracy has been improved by defining the gas turbine flow and torque characteristics as functions of speed and pressure ratio. The model is being improved further by including the effects of propellant density variations through the engine system. The steady-state model is used to establish predicted operating points, establish component requirements, and predict off-design steady-state parameters.

C. START AND SHUTDOWN TRANSIENT ANALYSIS

The major effort was directed toward completion of a transient model for the H-3 intensifier-fed engine using the new combustor subroutine, the development of a transient model for the burnoff seal tester, and the revision of the ARES module transient model. The H-3 intensifier engine system has been programed and checked out, the burnoff seal system has been programed and is being checked out, and the analytical development of the revised combustors-turbine-pump subroutine for the ARES module was completed and programing has been initiated. In addition, the revised manifold filling subroutine was completed and checked out.

The H-3 intensifier engine program uses the new waterhammer program for calculating the transmission characteristics of the hydraulic lines. New subroutines were written to simulate the dynamic characteristics of the intensifiers and the primary combustor. These subroutines contain systems of quasi-linear

XVI, C, Start and Shutdown Transient Analysis (cont.)

differential equations, which are integrated by a modified Euler approximation. In the combustor it is assumed that temperature, molecular weight, and pressure are functions of the average mixture ratio of the total propellant species residing in the chamber at any time. This differs from past models where the temperature, molecular weight, and pressure were assumed to be instantaneous functions of the injector mixture ratio. These methods are checked out and are in use for engine test simulation. These subroutines are also in use for simulation of the burnoff seal-tester. An additional subroutine was written and is being checked out for the simulation of the flow and rotational characteristics of the seal components.

In the previous module transient program, the combustors and turbopump components were separate subroutines. A convergence subroutine was used to obtain a tentative solution for the primary chamber pressure, turbine exhaust pressure, turbine speed, and secondary chamber pressure. Delays in getting useful information on engine transient behavior were frequently caused by the failure of this system of subroutines to converge on one or more of the parameters. With the exception of the pump flow rates, the convergence subroutines have been eliminated from the method of solution. Integration is obtained by using an Euler's finite-difference approximation with from two to ten successive corrections on the major variables. Convergence is still required between the pump suction and pump discharge flow because the pump performance map prohibits an explicit calculation of flow rate. The subroutine is interfaced with the liquid system by the waterhammer constants for each propellant line flowing into the primary and secondary combustors and by the waterhammer constants at the suction and discharge sides of the three main pumps.

The major differences of the new subroutine from the subroutines used to obtain the preliminary simulation are: (1) the combustion chamber propellant properties are not instantaneously a function of the incoming mixture ratio, (2) the effect of the volume between the turbine exhaust and the secondary fuel injection plane has been included, (3) the integration scheme is improved, (4) the calculation of turbine flow and torque has been replaced by the design performance curves for the turbine, and (5) the pump input has been revised to use a curve of torque as a function of speed and flow instead of the pump-efficiency curve. This avoids the discontinuity in torque at zero efficiency.

A new manifold-filling subroutine was written and checked out. The new subroutine will be added to the module simulation programs as well as the H-1 and H-3 simulation programs. The main feature of the subroutine is the distribution of the pressure drop in the lines and manifold at appropriate points. The pressure drops may be lumped at one point (entrance or exit) or may be distributed linearly as a function of the volume (cooling tubes). The last segment of volume allows some flow into the combustors prior to complete filling of the manifold. A function, $\frac{W_{out}}{W_{in}} = f\left(\frac{\text{vol filled}}{\text{vol of last section}}\right)$, will be input based on the geometry of the last section. When test data become available, this curve may be revised to better simulate actual manifold filling characteristics and, as a result, engine start characteristics.

XVI, Engine Analytical Models (cont.)

D. LOW-FREQUENCY STABILITY

The low-frequency stability analysis for the H-2 intensifier engine was completed. This engine is considered to be stable over the frequency range from 0 to 350 cps. The open-loop gain with respect to the primary combustor displays a 15-db gain margin at 255 cps, indicating that pressure oscillations originating in the primary combustor are very much attenuated when fed back to the primary. The overall open-loop gain with respect to the secondary combustor displays a 3.7-db gain margin at 260 cps and a phase-angle margin greater than 60°. The feedback gain around the secondary combustor is such that pressure oscillations are only slightly attenuated. It is therefore concluded that the system is only marginally stable since control-system experience indicates that a 6-db gain margin normally ensures a stable system. The high gain at 260 cps is attributed to a combination of a resonance in the fuel feed line from the intensifier to the branch point and to a resonance in the hot-gas duct at the same frequency.

Feed-system modifications were not required for stable operation. This conclusion has been verified by the several tests which have been conducted without any instance of unstable operation.

The design- and operating-point data for the engine module low-frequency stability model were compiled. The program for calculation of the system equation coefficients was written and checked out, and the coefficients have been calculated and checked using the design and operational data. Some revision was made to the equations which are used to represent the hydraulic line characteristics. An equivalent π circuit representation will be used rather than the second-order system originally proposed.

The program used for matrix derivation of the transfer functions has been completed and is being checked out. The program was believed to have been checked out earlier, but, during use of the program to attain transfer functions for subcomponents of the engines, an additional special case was discovered and this error has now been corrected. The subcomponent transfer functions will be obtained prior to attempting to run the entire 87th order system of equations which are used to simulate the module engine.

Two subroutines for analyzing and plotting the transfer function results are being completed and will be added to the basic program. These plotting routines will produce Bode plots and real-time response plots for a unit step input.

XVII.

NOZZLE AERODYNAMICS

A. GENERAL

Design analysis of the full-scale ARES prototype forced deflection was concluded with a detailed derivation of its estimated performance. The revised subscale nozzle-test program was accepted by the subcontractor. All aerodynamic and mechanical design of models under the revised program was completed, and cold-flow testing is underway. Performance tests of Models 1a and Model 2 without base bleed, and engine-out tests of Model 2, were completed. If the present schedule prevails, all subscale nozzle tests will be completed by the end of June.

B. SUBSCALE TEST PROGRAM

1. Program Plan

The revised subscale nozzle-test program, described in Report AFRPL-TD-66-1 (Ref 1) and submitted to the subcontractor for quote at that time, was accepted by him without change in cost. At the time of negotiation one additional item was modified; rather than test one forced-base-bleed configuration at six pressure ratios (Figure XVI-1, Reference 1), three forced-base-bleed passages will be tested at each of two pressure ratios, 25 and 1000. Results from these latter tests will be more useful for selecting an optimum ratio of secondary-to-primary mass flow than would be the case if data for only one secondary flow rate were available.

2. Accomplishments

All aerodynamic and mechanical model designs were completed, and all models except models 4 and 4a were fabricated. Model testing is well underway. Performance tests of Models 1a and Model 2, without bleed, and the engine-out tests of Model 2 (see Figures XVI-1 and XVI-2, Reference 1) were completed. However, no data are available, and analysis of results has not yet started.

C. FULL-SCALE PROTOTYPE FORCED-DEFLECTION NOZZLE, DESIGN AND PERFORMANCE

Design of the prototype forced deflection nozzle, discussed in Reference 1, was concluded with a detailed derivation of its estimated performance (Figure XVII-1). The data are presented in the form of a thrust-efficiency (C_T) versus pressure-ratio ($\lambda = P_c/P_a$) curve, and are based primarily upon cold-flow results from previous programs (Contracts AF 04(611)-8017 and -8548). Results include only the geometric decrement and do not reflect either combustion or friction losses.

XVII, C, Full-Scale Prototype Forced-Deflection Nozzle, Design and Performance (cont.)

(c) At design conditions, the factor $C_T C_D$ was calculated theoretically for both the AF 04(611)-8017 and -8548 prototype nozzles and compared with experimental results, with ambient base bleed, from the cold-flow performance-simulation Models 1 (re-run) and 11, respectively:

Contract	Theoretical $C_T C_D$	Experimental $C_T C_D$	Ratio
AF 04(611)-8017 (Model 1)	0.9926 @ λ = 2495	0.9806 @ λ = 2615	98.17
AF 04(611)-8548 (Model 11)	0.9879 @ λ = 1775	0.9764 @ λ = 1817	97.85
		Average =	98.01

Using the average value of the ratio of experimental to theoretical $C_T C_D$, 98.01, the theoretical design value of $C_T C_D$ for the ARES prototype nozzle, 0.9811, was adjusted to the expected subscale experimental value of 0.9616. Subscale-nozzle discharge coefficient of 0.9900, assumed on the basis of previous results, yielded a projected design thrust efficiency of 0.9713 for the cold-flow performance-simulation model, Model 2, with ambient base bleed. A similar technique was used to project an experimental value of design pressure ratio (1066) from that determined theoretically (1059). Since the full-scale nozzle and subscale models are designed for equality of these parameters, this is also the projected design performance of the full-scale forced-deflection configuration. The results of this technique were then compared with those that might be predicted from purely empirical data (Figures IV-31 and IV-32, Reference 2) and found to be essentially identical.

(c) Sea-level performance of the ARES prototype forced deflection nozzle was deduced from the performance data in Reference 2 by first determining the sea-level performance of cold-flow Model 2 and then extrapolating this to full-scale conditions. From Figure IV-31, Reference 2, the sea-level thrust efficiency of Model 2, with an aerodynamic area ratio of 23.68, is 0.9030 (without ambient bleed). Using the data on Figure IV-32 for the Model-2 value of $\varepsilon_v/\varepsilon_b$ = 0.6625, a thrust-efficiency increment of 0.0424 is postulated with the addition of ambient base bleed (by using the sixteen-module or annular-throat data adjusted to an aerodynamic area ratio of 23.68). The data on Figure IV-33 indicate an additional sea-level performance increment to be expected by increasing the number of modules from eight to twenty; however, the increased merging losses associated with de Laval rather than contoured-wedge modules will probably offset this increment, and the increment was not considered at this time. Extrapolating, then, the predicted subscale sea-level thrust efficiency of 0.9454, at a pressure ratio of 131, to full-scale conditions locates this value at the full-scale sea-level pressure ratio of 188 (see Reference 3, Section III,A; for a discussion of model simulation and data correlation).

(u) With full-scale sea-level and design performance now established, and considering the ideal noncompensated nozzle performance (shown as a dashed line), the remainder of the thrust-efficiency curve may be constructed by reference to any experimental curve of these parameters, such as Figure IV-35, Reference 2.

XVII, Nozzle Aerodynamics (cont.)

D. SUBSCALE MODEL DESIGN AND PERFORMANCE

1. Cold-Flow Program

Design of Models 1a, 2, and 3 was discussed in Reference 1. The remaining models, a plug nozzle and several variations of Model 2, are reviewed below.

a. Model 2a (Module-to-Skirt Flow-Merging Study)

Recalling the design of Model 2 (Section XVI,D,a, Reference 1), the skirt contour of that model was smoothly merged into the internal-expansion section (IES) contour. On Model 3, however, with its reduced module cant angle and increased base area ratio, a smooth mergence of the two contours was not possible and a sharp, zero-radius turn or compression corner joined the module cluster to the skirt. Differences in performance between these two configurations will be resolved by Model 2a, which is identical to Model 2 in every respect except that the skirt entrance angle equals the module cant angle (19.65°) rather than the module exit angle (32.13°). By experimentally isolating this effect with Models 2 and 2a, the intended results from Model 3 i.e., significance of IES area ratio changes, will not be obscured by unavoidable changes in related design parameters.

b. Model 2b (Shortened Skirt Study)

Even though forced-deflection nozzle skirts are relatively short in comparison with conventional de Laval nozzles, they are still longer, and therefore heavier, than desired. Further, the analytical tools for designing an annular throat, fully external-expansion forced-deflection nozzles have less application to the current modular configurations whose selection depends much more on empirical data. These two unrelated considerations were united during selection of the test configuration for Model 2b, whose skirt was arbitrarily shortened about 18% (to 18.147 from 22.013, nondimensionally) from that of Model 2a. This is equivalent to a theoretical design-performance reduction of 1%, and the objective of testing Model 2b is to determine if this reduction will actually occur and, if it does, whether it is as severe as predicted. All other design parameters of Models 2a and 2b are identical so that the result of arbitrarily shortening the nozzle skirt can be explicitly determined.

c. Models 2c and 2d (Cant Angle Study)

The uncertainty surrounding selection of certain modular forced-deflection nozzle design parameters, such as module cant angle, has recently been re-enforced, by evidence that, as the module throat recedes from the nozzle axis, the Prandtl-Meyer turning angle associated with the aerodynamic area ratio may not be the correct criterion for selection of IES slope. Therefore, Models 2c and 2d, with cant angles five degrees less (15°) and greater (25°), respectively, than that of Model 2a (19.65°), were selected to verify this issue. The modules

XVII, D, Subscale Model Design and Performance (cont.)

are placed relatively far from the nozzle axis and, since all other design parameters are identical except the degree of compression at module-to-skirt flow merging, the result of cant-angle variation can be deduced easily.

d. Model 2 (Forced Base Bleed)

A primary consideration in simulating forced base bleed is the selection of the secondary flow stagnation pressure. If ram air is to be the source of bleed, the vehicle trajectory and the inlet compression efficiency become significant design parameters. If base pressurization by compressor or secondary flow combustion is to be considered, complexity of the design problem is further increased. And still another aspect of the analysis is the method of introducing the secondary fluid into the base region. The relatively low level of effort to be expended in this program on this phase of nozzle performance precluded an extensive study of the interrelationship of these various design features. Rather, three secondary mass flow-ratios, (1, 3, and 5% of primary or model nozzle flow) were arbitrarily selected to provide data covering stagnation pressures from ambient static through normal-shock ram to those requiring energy addition, other than vehicle motion. This is, admittedly, a minimum effort but will provide useful data for later consideration of air-augmented nozzle configurations.

e. Models 4 and 4a

The optimum area ratio selected for the ARES prototype nozzle (Ref 4) is equally applicable to plug or forced-deflection configurations. However, an immediate limitation of the plug concept is vehicle diameter because a major portion of each module will be outside this envelope. In view of the rather arbitrary nature of this limit, the optimum area ratio was allowed to prevail since this would result in approximate equality of cold-flow model area ratios and allow the best performance comparison to date between plug and forced-deflection nozzle configurations. Prototype design did not proceed beyond this point as the overall area ratio of Models 4 and 4a was immediately equated to that of Model 1a, the forced-deflection model with contoured-wedge internal expansion sections. Design to this specification fixed the following additional model parameters:

Nozzle Area Ratio	39.59
Module Area Ratio	5.45
Module Cant Angle, °	-27.36

One further design variable was eliminated by selecting a constant IES length. Either equivalent-flow merging angle (Reference 2) or IES length could be fixed between the two models; however, since holding the flow-merging angle constant at the Model 1a value (18.90°) would result in a prohibitively long internal expansion section, the latter parameter was the one equated.

XVII, D, Subscale Model Design and Performance (cont.)

All design parameters discussed thus far are independent of plug length. The two lengths of interest in this program are the so-called 'zero-length" plug (Model 4) and a finite-length plug in which, theoretically, 97.5% of ideal vacuum thrust is realized from the plug surface. This can be achieved by a 13.18% isentropic-length plug (on a simplified flow basis), and the associated model was designated 4a. A sketch of both models is shown in Figure XVII-2.

2. Warm Flow Program

The two-dimensional warm-flow configuration was selected during the previous quarter and discussed in Reference 1. However, prior to fabrication, the configuration was modified by eliminating the IES exit gap on half of the modules to generate the most severe heating environment that could be encountered in any full-scale nozzle. A sketch of the converted model, Figure XVII-3, is included for comparison with Figure XVI-7 of Reference 1.

REFERENCES

1. Advanced Rocket Engine--Storable, Quarterly Technical Report AFRPL-TR-66-1, prepared by Aerojet-General Corporation for the United States Air Force, January 1966 (Confidential).

2. Integrated Components Program, Final Report, Technical Report AFRPL-TR-65-150, prepared by Aerojet-General Corporation for the United States Air Force, September 1965 (Confidential).

3. Design and Analysis of Altitude-Compensating Rocket Nozzles, Aerojet-General Corporation Report 8548-SR-1, December 1964 (Confidential).

4. Advanced Rocket Engine--Storable, Quarterly Technical Report AFRPL-TR-65-189, prepared by Aerojet-General Corporation for the United States Air Force, 15 October 1965 (Confidential).

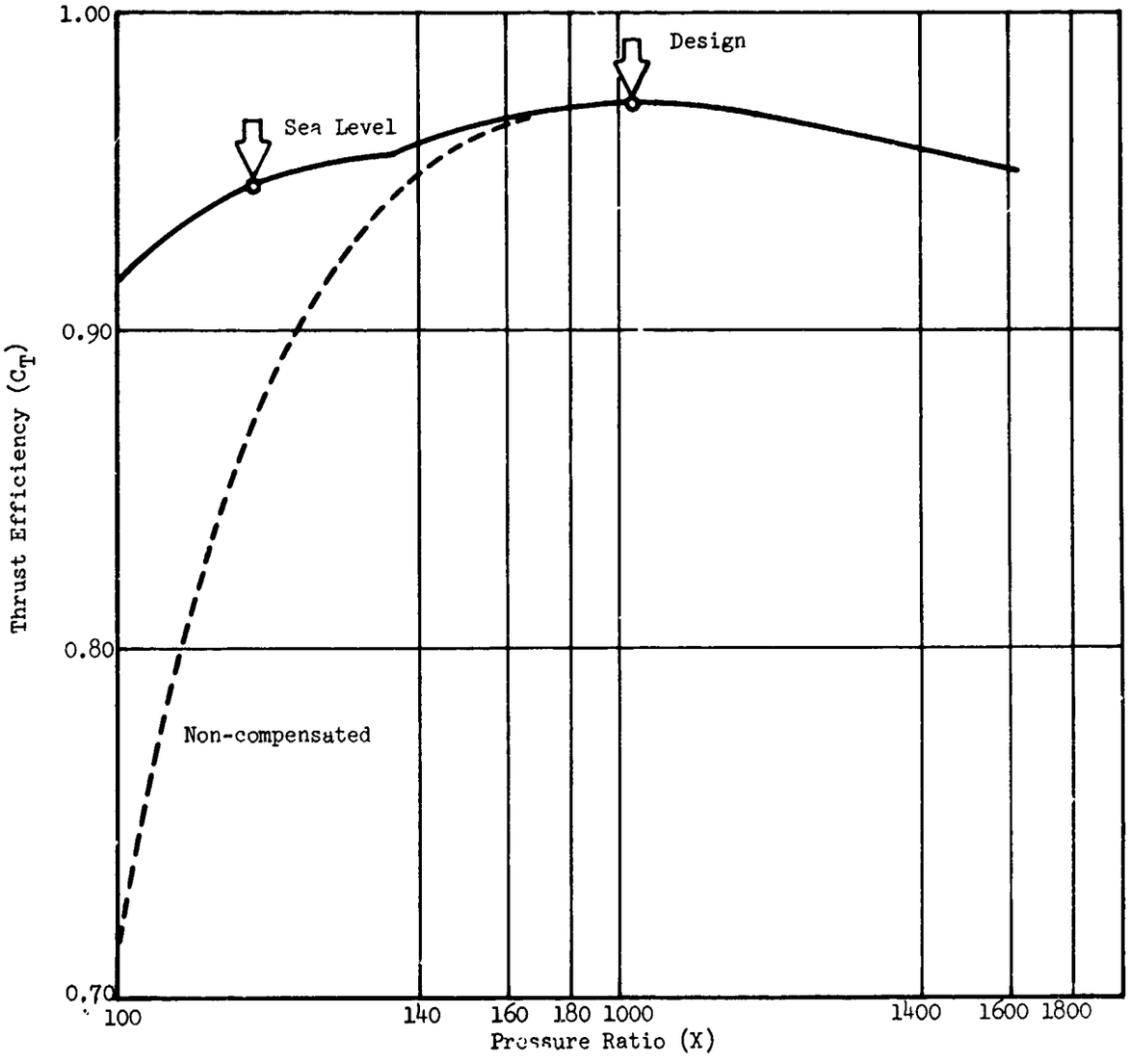

Estimated Performance of ARES Prototype Forced-Deflection Nozzle (u)

Figure XVII-1

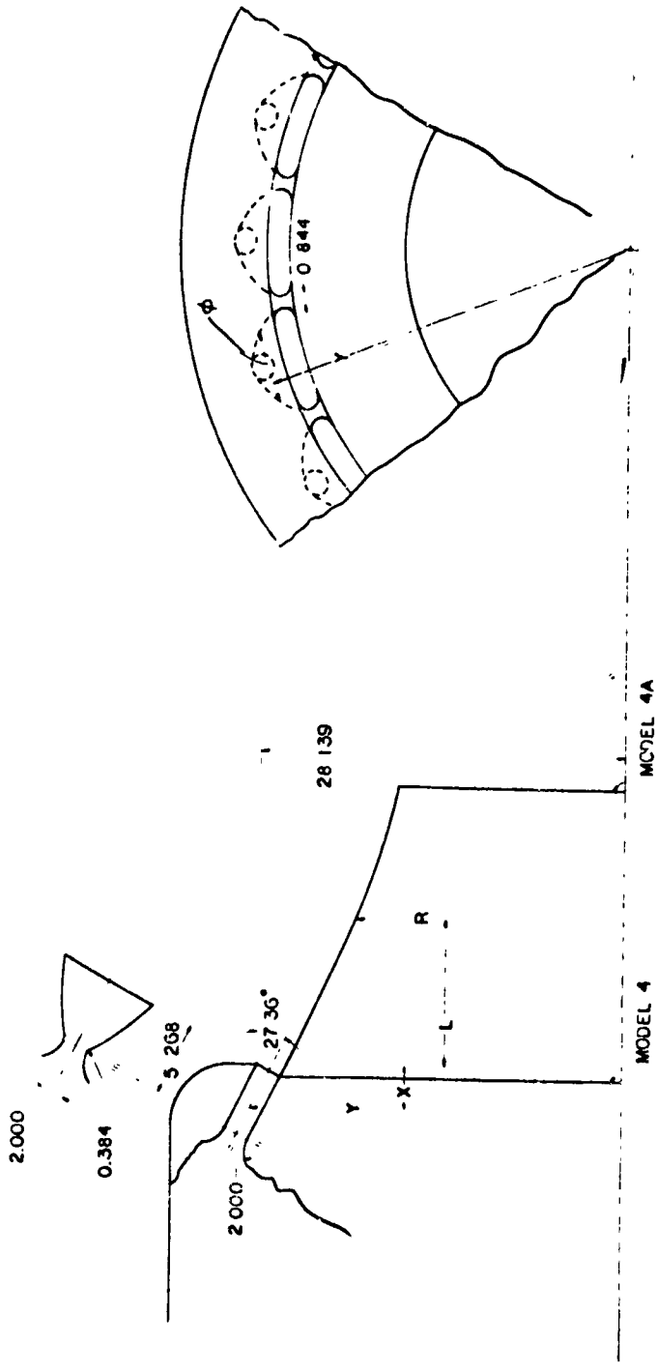

Cold-Flow Models 4 and 4a

Figure XVII-2
(This page is Unclassified)

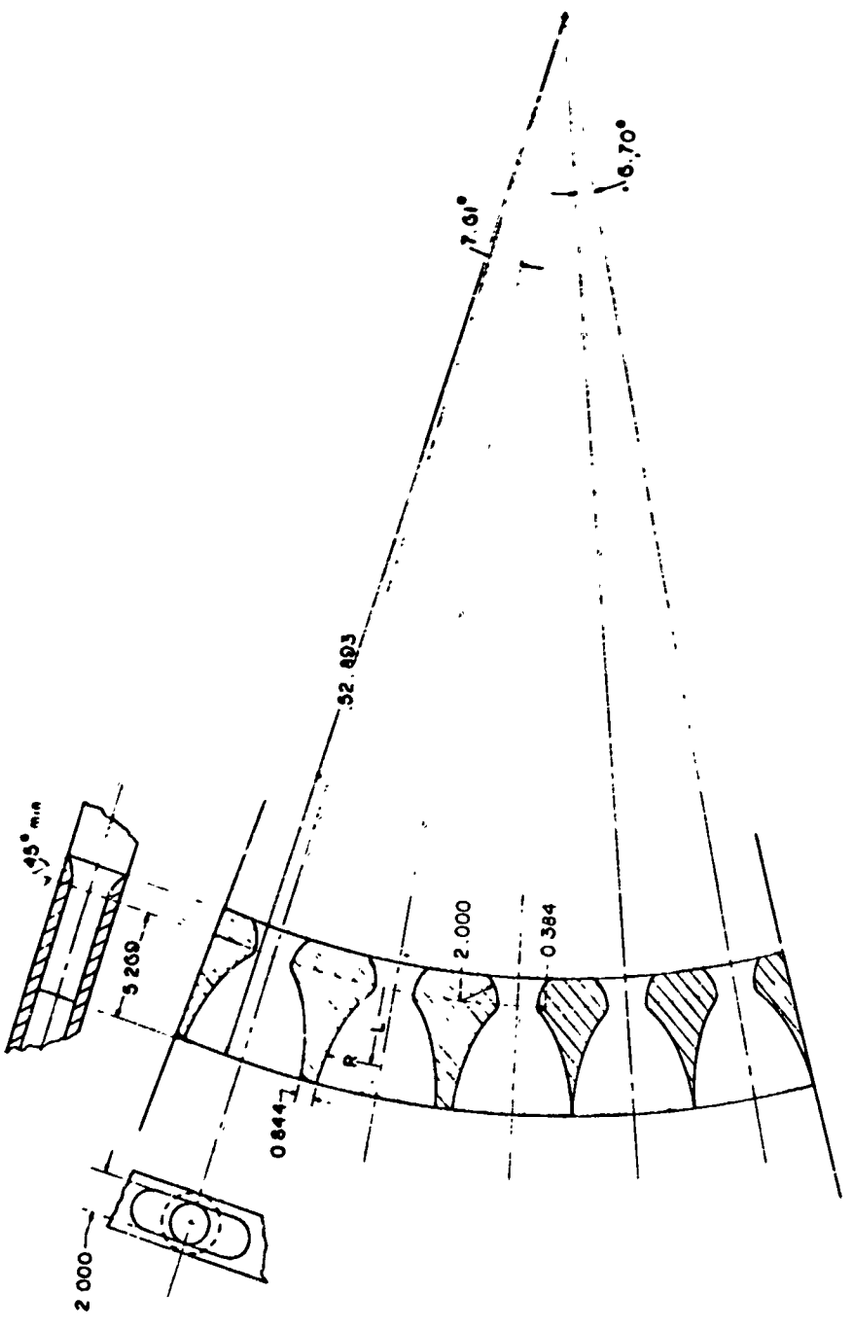

Two-Dimensional Warm-Flow Configuration--Revised

Figure XVII-3

XVIII.

AIRFLOW MODEL TESTING

A. GENERAL

The turbopump passage models to be tested in this program are briefly described in Figure XVIII-1. The planned testing order for these models is shown in the right-hand column, revised as of 30 March 1966.

Preliminary testing on the turbine inlet Model (h) was completed. Fabrication of the liquid-passage Models (a), (b), and (c) is 90% complete, and testing is scheduled for the next reporting period. The design of the turbine-exhaust Model (i) was completed, and fabrication was initiated. The design of two model turbines was completed and components are being fabricated. The assemblies will be henceforth described as Turbine Model (K), Mod I and Mod II, respectively.

Design of the backup inlet housing, Model (l), is in process, and fabrication will be initiated during the next reporting period.

B. TPA COMPONENT MODEL TESTING (AIR)

Preliminary testing of the turbine inlet Model (h) was completed on 22 February 1966 and a preliminary report issued on 4 March 1966. Preliminary data indicate that the pressure drop through the combustion zone is quite low, but that separation occurs around the center body, as shown schematically in Figure XVIII-2, leading to a considerable pitch-angle variation in the flow entering the turbine nozzles. Some modifications to the model and instrumentation techniques and locations will be made, and further tests will be conducted to establish uniform flow at the turbine entrance. Pressure loss does not appear to be a problem.

Fabrication of the oxidizer liquid-passage Models (a), (b), and (c) is 90% complete, with installation and testing scheduled for the next reporting period. These models were redeisgned to conform to the turbopump-housing Design-B configuration.

The design of the turbine exhaust model was completed, and fabrication was initiated. This model has also been designed to the latest Design-B configuration to obtain significant results for final design evaluation.

A thorough study of the turbine design for the advanced turbopump was completed and resulted in a decision to evaluate two significantly different design concepts. These will be referred to henceforth as the Mod-I and Mod-II Model (K) turbines. The Mod-I design was based upon the design criterion that the turbine should have maximum efficiency, assuming ideal operating conditions, at the design point. The Mod-II design was based upon the assumption that a simplified turbine can be designed with existing knowledge and will produce the specified performance under actual operating conditions, which may be far from the ideal.

XVIII, B, TPA Component Model Testing (Air) (cont.)

Both these designs have been completed, and fabrication of components is in process. The final scale factor for these models is 1.65.

Design of a model of the backup oxidizer turbopump inlet housing is in process; the model will be built with a scale factor of 1.4 to provide adequate space for instrumentation and to take maximum advantage of existing test-facility flow capacity.

C. INJECTOR AIRFLOW TESTING

The rebuilt Mark 125A (ICP) injector was air-flow tested. The injector was equipped with six total-pressure and two static-pressure taps located behind the injector face. These taps were to be installed in an attempt to correlate the mass-velocity distribution from hot and cold flow testing. The cold flow tests revealed no significant difference in flow distribution when tested with and without turbulators. Consequently, hot flow data would not provide any further insight into the differences between hot and cold flow distribution. No hot-flow data were obtained because the pressure taps on the injector body had to be eliminated due to leakage which could not be corrected.

Designation	Model Description	Planned Testing Order (Revised 3-30-66)
(a)	A model for the evaluation of the oxidizer liquid circuit from the discharge at the pump to the station where the regeneratively cooling tubes have a 180° bend.	2
(b)	A model for the testing of the oxidizer flow from the discharge of Model (a) to the collector ahead of the oxidizer injectors of the primary combustion chamber.	3
(c)	A transition piece, which enables the coupling of the flow passages of Models (a) and (b) to possibly evaluate the complete oxidizer circuit and the influence of the discharge conditions of Model (a) on the performance of Model (b).	4
(h)	A model of the turbine inlet passage from the injector face of the primary combustor to the exit annulus of the turbine nozzle blading.	1
(i)	A model of the turbine discharge duct from the turbine rotor exit annulus to and through the passages of the secondary injector assembly.	5
(j)	Repeat of Model (i) with a different or significantly modified secondary injector assembly configuration.	9
(k)	A 1.65-times full-size model of the turbine rotor and stator assembly installed in an existing turbine test fixture.	
	Mod I Turbine Design--a highly refined concept incorporating sharp leading edges, tapered and twisted blades, and variable blade height and chord for the purpose of achieving maximum efficiency.	7
	Mod II Turbine Design--a highly simplified concept incorporating blunt leading edges, untapered, untwisted blades of constant height and chord for the purpose of reducing fabrication complexity and providing cooling potential.	8
(l)	A model of preliminary back-up TPA pump inlet housings.	6

Summary of Mode' Configurations

Figure XVIII-1

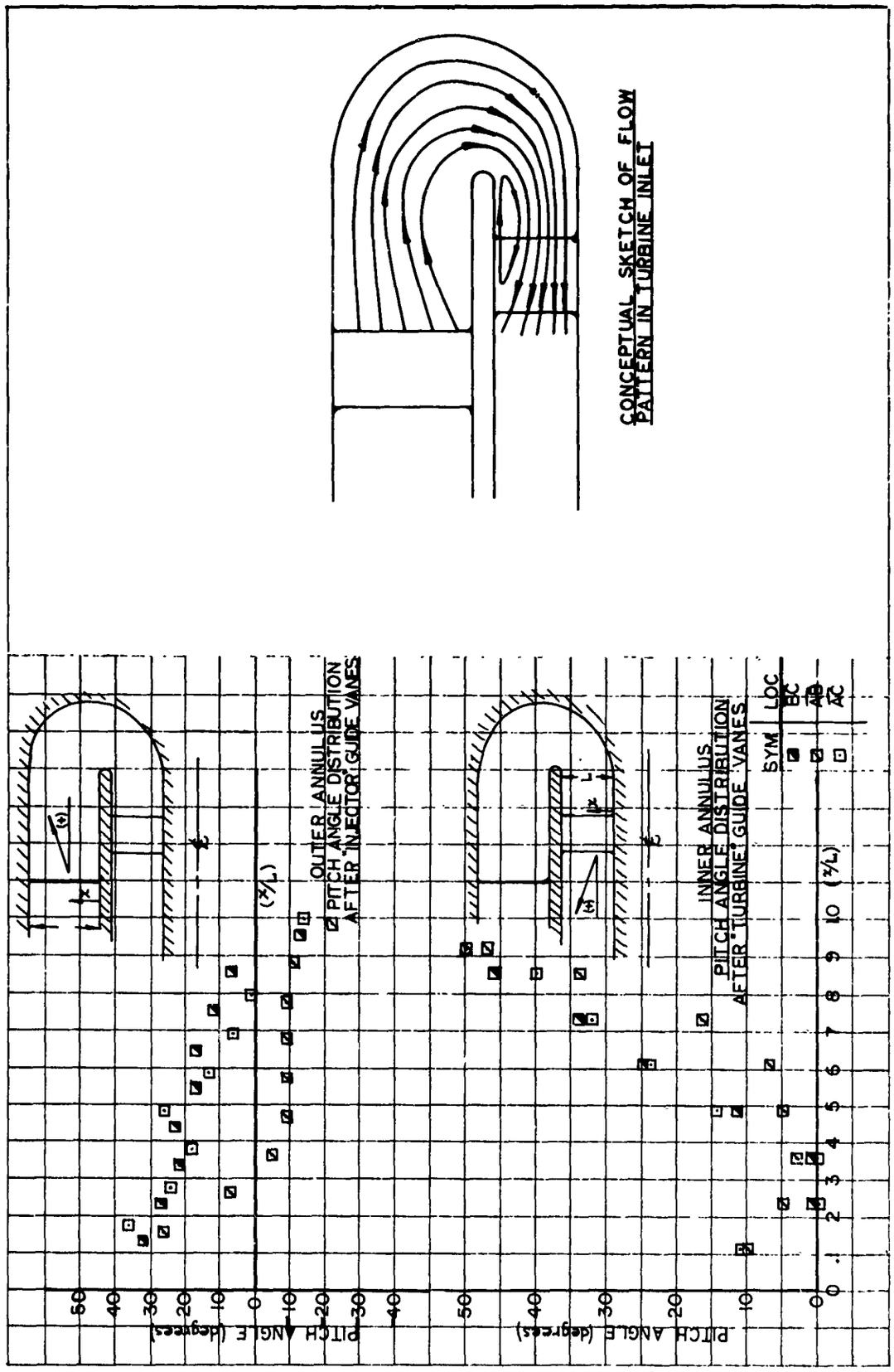

Figure XVIII-2

Preliminary Test Results, Turbine Inlet Model

XIX.

HEAT-TRANSFER ANALYSIS

A. GENERAL

The accomplishments of the heat-transfer effort during this reporting period are itemized below.

1. A characteristic length (L^*) of 40 in. was selected as optimum for the ARES chamber, based on chamber and film-cooling performance.

2. The film-cooling requirements for six versions of regeneratively cooled chambers with an L^* of 40 in. were established.

3. The capillary tube study for second-point injection was finalized, and tubes with an ID of 0.045 in. and a wall thickness of 0.005 in. were selected.

4. A parametric study of a self-cooling chamber liner was conducted to establish the feasibility of the concept.

5. The exact flow distribution to each group of washers of the transpiration-cooled chamber was determined for two conditions: a nearly uniform 1900°F wall temperature and a first-test maximum flow.

6. The evaluation of film-cooled tests and regeneratively cooled chamber tests on ICP residual hardware was completed.

7. Three efforts were initiated in the thermal-barrier program: plasma-spraying of Hastelloy-X on Inconel 718; braze-bonding of various coatings; and plasma-process improvement. The first of these efforts was completed this period.

8. Support of the component design efforts was continued including the inline and advanced TPAs, the Mark 125 injector, and the secondary injector/interface flange.

B. ARES THRUST CHAMBERS

1. Regeneratively Cooled Chambers

a. Computer Program

The completed analysis of data obtained in the test firings of ICP residual hardware (both ablative and regeneratively cooled) has precipitated a change in the "Regeneratively and Film Cooled Thrust Chamber" computer program.

XIX, B, ARES Thrust Chambers (cont.)

(u) The reference temperature for the evaluation of the convective-heat-transfer coefficients, both for gas and coolant, has been changed. These coefficients were previously referenced to the mainstream gas or film-coolant bulk temperatures, respectively. The reference temperature for the gas coefficient now is a film temperature equal to the arithmetic mean between the mainstream gas and the film coolant temperatures and for the film coefficient the reference temperature is the arithmetic mean between the film-coolant and the wall temperatures. This change has a small effect on ablative chambers or tube bundles coated with high-temperature resistant thermal barriers. The effect becomes quite pronounced in the design of uncoated tube bundles.

(u) This change in analytical techniques is reflected in all work reported for the past quarter.

b. L^* Optimization

(c) The optimum length of the ARES regeneratively cooled chamber was selected as the one which provides the highest probability of achieving the performance objectives of the ARES program. The chamber was analyzed for three L^*s (17.4, 30, and 50 in.) and for three configurations (uncoated, coated with Hastelloy X, and coated with a tungsten-base thermal coating--3% copper added to a basic 85W-12 ZrO_2 - 3 Si powder plus a nondiffused silicon topcoat). The film-cooling requirements were determined for both single-point injection (at the injector) and two-point injection (at the injector and from capillary tubes). The location of the second injection station was also varied so that the best capillary tube length could be established.

(c) The thrust-chamber parameters were based on the following average predicted test conditions: chamber pressure, 2800 psia; secondary combustor mixture ratio, 2.2; mainstream gas flow rate, 351 lb/sec; regenerative coolant flow rate, 219.2 lb/sec; and regenerative- and film-coolant inlet temperature, 90°F. The chamber heat loads were evaluated using a Dittus-Boelter correlation for the gas-side heat-transfer coefficient. This coefficient was increased by a factor to account for turbulence in the combustion zone. The factor was considered to decrease linearly with area ratio from 1.5 at the secondary injector face plane to 1.0 at the throat.

(u) The film-cooling requirements for the three chamber configurations were established as those that would limit the temperature of the outside tube wall to less than 1500°F and that of the coating surface to 2200°F for the Hastelloy X coating and to 3500°F for the tungsten coating. The temperature of 1500°F for the outside tube wall is considered maximum because the strength of Inconel 718 deteriorates above this temperature, whereas temperatures of 2200° and 3500°F are considered maximum for the respective coatings in an oxidizer-rich atmosphere.

XIX, B, ARES Thrust Chambers (cont.)

(u) A summary of the results of this study is presented in Figure XIX-1, which shows minimum film-cooling requirements for both single and two-point injection as well as the axial location of the second injection point in the latter case.

(u) These minimum film-cooling requirements are shown as a function of L* for single and two-point injection in Figures XIX-2 and 3, respectively. Figure XIX-4 presents the performance loss associated with each case. The performance loss was calculated from the following relationship

$$\% \, I_s \text{ Loss} = 0.6 \frac{W_{fc}}{W_g} \times 100$$

where W_{fc} = minimum film cooling requirement, lb/sec

W_g = mainstream gas flow rate (351 lb/sec)

(u) All performance losses other than those due to film cooling in the ARES chamber are shown as a function of L* in Figure XIX-5. This figure includes losses due to mixture-ratio distribution, combustion, nozzle friction, and nozzle geometry.

(c) The information presented in Figures XIX-4 and 5 is summarized in Figure XIX-6, which shows the effects of chamber configuration, L*, and single and two-point injection on ARES overall performance. Phase-I and Phase-II requirements of 90 and 91.6% of sea-level specific impulse, respectively, also are shown.

(c) On the basis of Figure XIX-6 the 40 L* chamber was selected as the best choice. The allowable film-coolant flow rates are 31.5 and 22.8 lb/sec for Phases I and II, respectively.

c. Capillary Tube Final Study

(u) The chamber was analyzed for three sizes of Hastelloy-X capillary tubes; inside diameters of 0.040, 0.045, and 0.050 in., each with a wall thickness of 0.005 in. The total number of these tubes is 104. Each tube was considered to extend from the injector face plane to a point five inches upstream of the throat. This location was selected although this distance is slightly greater than that associated with the minimum film-cooling requirements summarized in Figure XIX-1. The increase in total film-coolant flow resulting from this selection is small (< 1 lb/sec); the shorter capillary tube allows greater flexibility of flow rates for development testing. Additionally, the tubes end in a region of significantly lower heat flux and consequently have a greater margin of safety. A minimum film-coolant flow rate of 13.8 lb/sec is required from these tubes to cool the throat.

XIX, B, ARES Thrust Chambers (cont.)

The thrust-chamber parameters are the same as given in Section XIX,B,1,b, above.

Each tube size was analyzed for film-coolant flow rates of 13.8, 20, 30, and 40 lb/sec. Figures XIX-7, -8 and -9 present heat-flux capability as a function of velocity for the 0.040-, 0.045-, and 0.045-in.-dia tubes, respectively. The dashed lines reflect the tube heat flux at the capillary tube ends. These lines show that the heat flux is lower at the injector face for 13.8 and 20 lb/sec and at the tube exit for 30 and 40 lb/sec. The changes in heat flux for a given weight flow may be attributed to the combined effects of variations in fluid transport properties resulting from changes in pressure and temperature. A design burnout heat flux line is also shown on these figures. This line limits the film-coolant flow rates to minimum values of about 15, 19.5, and 24 lb/sec for the 0.040-, 0.045-, and 0.050-in.-dia tubes, respectively.

Figure XIX-10 presents pressure drop as a function of film-coolant flow rate for the three tube sizes. The maximum allowable pressure drop of 3100 psi limits the flow rates to about 27, 37, and 48 lb/sec for the 0.040-, 0.045-, and 0.045-in.-dia tubes, respectively.

The 0.045-in.-dia tube was selected as the best on the basis of all factors considered. This size has a capability range which encompasses the high flow rates desired for initial tests as well as the flow rate associated with the total of 31.5 lb/sec for Phase I.

Figures XIX-11 and -12 present temperature data as a function of capillary tube length for the selected geometry. The tube-wall temperatures (Figure XIX-11) indicate that Inconel 718 and possibly stainless-steel tubing would be acceptable substitutes for the Hastelloy X tubing.

The film-coolant requirements for each of six versions of the 40 L* ARES regeneratively cooled chambers are presented in Figure XIX-13.

d. Microflow Liner Parametric Study

As a possible improvement to the capillary tube cooling concept, a preliminary effort was completed to determine the feasibility of a self-cooling chamber liner consisting of small tubes or small slots. The liner should carry sufficient flow to film-cool the convergent portion of the chamber to the throat and, in so doing, to regeneratively cool itself without need of film cooling or coating.

This feasibility study was conducted for both round tubes and square slots, the results are shown in Figures XIX-14 and -15. Figure XIX-14 shows the coolant flow rate as a function of coolant velocity in the tubes for a constant inlet density of 90 lb/ft^3 and a constant length of 6 in. The coolant velocity was

determined by finding the number of tubes of each size (four are shown; 0.010 to 0.025 in.) which will fit around the circumference of the 10.5-in. chamber. All tubes used have a wall thickness of 0.0075 in. Superimposed across the curve are lines of constant pressure drop at values of 1000, 2000, and 3000 psi for a friction factor of 0.03, and of 3000 psi for a friction factor of 0.02. Finally, two lines are shown for heat loads of 20 and 25 Btu/in.^{2} sec, which correspond to the ARES chamber condition for wall temperatures of 2200°F (typical of Hastelloy X) and 1500°F (typical of Inconel 718). These lines are shown at the velocities which correspond to these heat fluxes as burnout values. By selecting Hastelloy X as a material and determining that a friction factor of 0.02 is more realistic than 0.03, an operating range can be defined by the velocity corresponding to 20 Btu/in.^{2} sec burnout heat flux on the left, by a constant pressure drop of 3000 psi across the bottom, and by the largest tube (about 0.028 in. ID) which will permit flowing the Phase I maximum requirement at or above the minimum velocity. This practical operating range is shown on Figure XIX-14.

Figure XIX-15 shows the same parameters as the previous figure but for square slots with the land between slots the same dimension as the slot itself.

Both of these curves show potential operating ranges which adequately cover the range of interest on the ARES program. Detailed heat-transfer and flow analyses of both concepts are currently being conducted and will be reported at a later date. In conjunction with these continuing studies, preliminary designs are being evaluated for fabrication feasibility. If a configuration is determined which is acceptable from both an analytical heat-transfer standpoint and from a manufacturing standpoint, a decision will be made whether to incorporate this concept into the ARES program.

2. Transpiration-Cooled Chambers

a. Coolant-Flow Requirements

The transpiration-coolant flow-rate schedules and distributions have been established for two conditions of operation, i.e., a conservative first-test flow-rate schedule and an optimized-design flow-rate schedule. The design configuration and its required flow are based on a nominal wall temperature of 1900°F, which has been established from an analytical model that will be discussed later.

The design approach is to calculate the theoretical flow requirements of the optimized conditions and to stack the platelets for achieving a flow distribution that is as close as possible to the theoretical optimum. Each pair of platelets has six relative positions available which result in six lengths of metering groove. Axial flow distribution is controlled by selecting metering groove lengths (and, hence, the pressure drop) from one of these six positions and

XIX, B, AMES Thrust Chambers (cont.)

also by selecting the coolant supply pressure for each compartment. The first test will use the platelet indexing of the design configuration, but will be made with increased coolant-flow rates which are obtained by increasing the supply pressure to all compartments to 4500 psia.

Figure XIX-16 provides a summary of flow rates associated with the platelet assemblies for both the first test and the optimized conditions. Included in this figure are flow-compartment length, platelet thickness, flow-compartment plenum pressure, the corresponding coolant flow rate, and the number and indexing position of platelets in each flow compartment. Each flow compartment is separated from the adjacent compartments by thermally instrumented platelets which are 0.021 in. thick.

b. Thermal Analysis

Transpiration-coolant flow requirements had to be established for the AMES prototype transpiration-cooled chamber without the benefit of verification with directly applicable test data. The required data are scheduled to be available in April from a company-funded IR&D program. The analytical model employed for design purposes utilizes the Hatch and Papell film-cooling model for determining the effective recovery temperature seen by the chamber wall. A factor of 1.5 was applied to the heat-transfer coefficient between the main gas stream and the coolant within the cylindrical chamber section, decreasing with the chamber diameter to a factor of 1.0 at the throat. The assumption was made that there was no coolant carryover from upstream platelets to those downstream. This means that each platelet has sufficient flow to cool itself without the aid of the upstream mass addition to the boundary layer. This is, of course, a conservative assumption which is offset to an unknown degree by the possible chemical reaction of the oxidizer coolant within the boundary layer. The equilibrium reaction of $N_2O_4 \rightleftharpoons 2NO_2$ was also assumed, as well as fully established laminar flow within the platelets.

The effective recovery temperature determined by means of the Hatch and Papell film-cooling model provides a boundary condition for the solution of the one-dimensional or fin-type conduction-convection problem, whose solution takes the form:

$$\frac{T_w - T_c}{T_{FR} - T_c} = \frac{\text{Sinh}\left[\frac{\beta}{2\gamma} N (\bar{\delta} - \bar{x})\right] + N \cosh\left[\frac{\beta}{2\gamma} N (\bar{\delta} - \bar{x})\right]}{(1 + 2\gamma)\,\text{Sinh}\left(\frac{\beta}{2\gamma} N \bar{\delta}\right) + N \cosh\left(\frac{\beta}{2\gamma} N \bar{\delta}\right)} \; e^{\frac{\beta \bar{x}}{2\gamma}}$$

XIX, B, ARES Thrust Chambers (cont.)

where:

T_w = gas-side wall temperature

T_c = initial coolant temperature

T_{FR} = average effective recovery temperature

$\beta = \dfrac{2h_L K_m}{h_g^2 \, l}$

$\gamma = \dfrac{G \, C_c \, d}{h_g \, l}$

$\bar{\delta} = \dfrac{h_g \, \delta}{K_m}$

$\bar{x} = \dfrac{h_g}{K_m}$

$N = \sqrt{1 + 4 \dfrac{\gamma^2}{\beta}}$

h_L = coolant convection coefficient

h_g = gas-side convection coefficient

K_m = metal thermal conductivity

l = platelet thickness

d = coolant channel thickness

C_c = coolant specific heat

G = coolant mass velocity

δ = depth of finite platelet

x = distance from gas-side surface

XIX, B, ARES Thrust Chambers (cont.)

c. Hydraulic Analysis

The nominal flow rates are well within the laminar flow regime and are assumed to be fully established, making the pressure drop per unit length proportional to the mass flow through the channel:

$$\frac{\Delta P}{L} = \frac{\mu \dot{W}}{\rho g_c} \quad \frac{12}{ab^3 [4/3 - 0.836\ b/a]}$$

where:

ΔP = pressure drop, psi

L = channel length, in.

μ = coolant viscosity, lbm/ft sec

$\dot{W}$ = coolant mass flow, lbm/sec

ρ = coolant density, lbm/ft^3

g_c = gravitational constant, lbm ft/sec^2 lbf

a = channel half-width, in.

b = channel half-height, in.

The entrance loss was taken as 1.3 times the velocity head and the exit loss was taken as 1.0 times the velocity head.

C. ICP RESIDUAL HARDWARE

This study examined the validity of the analytical model which is presently being used to determine the cooling requirements for the ARES thrust chamber. Experimental temperature data from five test firings of the ICP Sector Engine were compared to the analytical predictions.

Figures XIX-17, -18, and -19 compare predicted and experimental wall temperatures for film-cooled ablative-chamber Tests 1.2-07-WAM-009, -010, and -011. The predicted wall temperatures shown in the above-mentioned figures were based on a "Bartz factor" of 1.5 at the point of injection scaled to 1.0 at the throat. This value of the "Bartz factor" was chosen for this comparison as it has been the basis of all design work on the ARES Program. As may be seen from the figures, and as was intended, this value of the "Bartz factor" produces reasonably close, but conservative, predictions for thrust-chamber wall temperatures. The "Bartz factor"

XIX, C, ICP Residual Hardware (cont.)

which most closely approximates measured data was found to be 1.0 at the injector face scaled to 1.2 at the throat. However, for clarity, this curve has been omitted from these figures.

In Tests 1.2-08-WAM-002 and -003, both film cooling and regenerative cooling techniques were employed. Since wall temperatures were not available, the comparison in these tests was made between predicted and measured values of regenerative coolant temperature. As in Tests 1.2-07-WAM-009, -010, and -011, the predicted temperatures are based on a "Bartz factor" of 1.5 at the injector scaled to 1.0 at the throat. Figures XIX-20 and -21 show regenerative coolant temperature versus axial distance from the secondary injector for Tests -002 and -003, respectively. Both tests were conducted using single-pass tube bundles in which the regenerative coolant is passed countercurrent to the main gas flow.

In Test -002 film coolant was injected only at the face of the secondary injector. In Test -003 film coolant was injected at the face of the secondary injector and, through 0.058-in.-OD capillary tubes, at a point 12.25 in. (measured axially) downstream of the injector. The capillary tubes were located in the valleys between regenerative coolant tubes. Since the capillary tubes greatly shielded the coolant tubes from the hot combustion gases, they were assumed to absorb 83% of the heat which would have, in their absence, been absorbed by the regenerative coolant. The predicted temperature of the regenerative coolant was, therefore, reduced based on this assumption.

The placement of the capillary tubes necessitated an additional arbitrary assumption. In all previous film-cooling tests the film cooling effectiveness (η) was assumed to be constant downstream of the throat, based on earlier test data. However, this assumption would be unrealistic for Test -003 since film coolant was introduced from the capillary tubes only one inch from the throat. Therefore, for Test -003 only, constant film-cooling effectiveness (η) was assumed to begin at a point somewhat downstream of the throat. This point occurs at a location where the predicted temperature of the film downstream of the throat is equal to the predicted temperature of the film at the throat in Test -002.

In Test -002 an oxidizer leakage of about 8 lb/sec occurred in the chamber prior to the data period. This leakage rate was not included in either the regenerative or film-coolant flow rates used for predicting temperatures.

The predicted temperature rise of the regenerative coolant agreed well with the measured value for Test -003, as may be seen from Figure XIX-21. However, in Test -002 the predicted temperature rise was 7° less than measured. This discrepancy may be attributed to a loss of coating at several locations in the throat region where the heat flux is maximum. In addition, the film cooling effectiveness (η) may have been reduced due to a local loss of coating near the injector face. This loss of coating resulted in a severe (0.056 in.) discontinuity on the wall near the film-coolant tubes, possibly causing increased mixing of the coolant with the mainstream gases.

XIX, C, ICP Residual Hardware (cont.)

(u) The backside thermocouple data for both tests show considerable scatter and are, therefore, of questionable value.

(c) The specific test parameters which were considered for calculations of the predicted performance have been tabulated for each test in Figure XIX-22. The stagnation temperature of the combustion gases was calculated for each test based on injector mixture ratio, chamber pressure, and combustion efficiency. The combustion efficiency associated with the Mark 125 injector, used in all five tests, was taken as 94.8%. This value was obtained from Test -012, which was uncooled. The stagnation temperature of the combustion gases was then calculated for each test assuming a direct proportionality with the square of combustion efficiency.

D. THERMAL-BARRIER DEVELOPMENT

1. Summary

(u) Three phases of laboratory investigation were initiated:

1. Evaluation of plasma-sprayed Hastelloy X,
2. Evaluation of braze bonding,
3. Plasma process improvement.

(u) The first task was completed and is discussed in paragraph D,2, below.

(u) Sixteen braze-bonding disc type specimens were sprayed and ten of these were heat-treated for 2 hr at 1730 ± 10°F to flow the NICORO 80 braze alloy and to react the silicon topcoat with the tungsten-based thermal barrier. Five specimens were heat-treated in dry hydrogen and five in a vacuum. One of the specimens heat-treated in hydrogen and four of the specimens heat-treated in a vacuum appeared to be well bonded. Thermal shock and oxidation tests will be used to evaluate these specimens and others of the same composition which were not heat treated.

(u) Four specimens consisting of three tubes each were sprayed with blends of Hastelloy X and 5% Nicoro 80, and two of these were brazed for 20 min at 1730°F in dry hydrogen. Thermal-shock tests of "as-sprayed" and of heat-treated specimens will be made in April.

(u) Designs were completed and fabrication initiated for plasma-process improvements involving tungsten shroud nozzles, axial powder injection techniques, and a nitrogen blast adapter to reduce overspray contamination.

XIX, D, Thermal-Barrier Development (cont.)

2. Sprayed Hastelloy X Test Results

a. Investigation

Three thermal-shock specimens were coated with 0.010 in. of Hastelloy X. The thermal-shock specimens consist of three tubes of Inconel 718 brazed together with water adapters at each end. The tubes are 9.5 in. long, have an OD of 0.25 in., and are 0.014 in. thick.

Thermal shock tests were conducted with water cooling and a plasma-arc heat source. The test procedure was to adjust the heat flux to a desired value on a water-cooled calorimeter and to rotate the specimen in and out of the flame at 20-sec intervals in the heating cycle until a failure occurred.

The test results are summarized in Figure XIX-23. The first specimen tested, No. 180, failed in the first cycle due to a burnout caused by insufficient availability of water cooling.

Two positions on the second specimen, No. 178, were tested. At one position, 178-1, a small area of coating on the center tube spalled and melted in the fourth cycle. The second position, 178-2, burned out in the first cycle. The appearance of the burnout is shown in Figures XIX-24. Several small pinholes, a dark stain in the liquid side, and wall thinning occurred in a remarkable similarity to burnouts observed on chambers.

Three positions were tested on Specimen 179 with the heat flux lowered slightly to eliminate the burnout problem. Failures occurred in two to seven cycles as listed in Figure XIX-23. The microstructure of a failed area on Specimen 179-3 is shown in Figure XIX-25. The thermal-shock failure definitely originates in the bond zone. The sprayed Hastelloy X has very little porosity, which is exceptionally good for sprayed material.

b. Summary of Results

The thermal shock resistance of plasma-sprayed Hastelloy X on Inconel 718 tubing was found to be insufficient for use in the ARES chamber. Spalling type thermal-shock failures occurred between two to seven 20-sec cycles due to insufficient adherence. Apparently, the bond between Hastelloy X and Inconel 718 is mechanical, whereas the bond between tungsten and Inconel 718 is a diffusion type which accounts for the superior results with tungsten-based coatings.

Metallographic examination of the plasma-sprayed Hastelloy X showed that thermal shock failures initiated at the bond zone and that the sprayed material had very little porosity. Braze-bonding studies of sprayed Hastelloy X using 5% Nicoro 80 and a furnace treatment at 1730°F have been initiated.

XIX, Heat-Transfer Analysis (cont.)

E. COMPONENT DESIGN SUPPORT

1. Inline TPA

This section presents the results of a preliminary analysis which was conducted to predict maximum wall temperatures, for steady-state operation, at several critical points in the primary combustor of the inline TPA. Since the final design had not yet been established, it was agreed that the temperatures should be estimated based on either one-dimensional or radial heat flow and that a more rigorous analysis would subsequently be performed on the final design if necessary.

Temperatures were calculated at five locations along the housing wall. These locations are specified in the sketch of Figure XIX-26 as A, B, C, D, and E. Tabulated below are the calculated wall surface temperatures along with some of the more important parameters on which the calculations were based.

Location	Surface Temperature, °F	Gas Velocity, ft/sec	Gas Heat-Transfer Coefficient, Btu/ft^2-hr-°R	Material Thickness, in.	Method of Analysis
A	431	3	147	---	2-Dim
B	270	1	39	0.41	1-Dim
C	438	1	39	0.8	1-Dim
D	400	<1	20	1.5	1-Dim
E	425	<1	20	1.25	Radial

The gas-side heat-transfer coefficients were based on estimates of the gas velocity between the housing wall and a protective metal liner. The liner contained small slots in the vicinity of the injector to equalize the pressure on both sides. However, since there was no downstream outlet for the gases, the velocities in this region were assumed to be very small. Downstream of the slots (Points B and C) the velocity was assumed equal to 1 ft/sec. At Points D and E, near the stator, the heat-transfer coefficients used in the analysis were between those based on a velocity of 1 ft/sec and those based on free convection. The temperature of the gas adjacent to the wall was assumed equal to 1500°F in all cases.

The resistance to heat flow on the liquid side was negligible compared to the overall resistance across the wall. Therefore, the liquid-side temperatures were essentially equal to the liquid temperature, which was assumed constant at 70°F.

XIX, E, Component Design Support (cont.)

The resistance of the metal to heat flow was based on a conductivity of 2.04×10^{-4} Btu/in.-sec°R, which is representative of Inconel 718.

In the cylindrical section of the primary combustor, Point A, the conduction problem was solved by using a two-dimensional analysis which is considered to be accurate for this geometry.

At Points B, C, and D the wall surface temperatures were calculated using one-dimensional heat-flow approximation. This assumption is reasonable at Point B and, therefore, the temperature calculated at this point should be accurate. The temperature at Point C must be considered somewhat optimistic due to the additional heating at the adjacent corner. At Point D a number of effects must be considered in evaluating the accuracy of the predicted temperature. However, it is believed that the "inside corner effect' at this point will predominate, and, thus, the predicted temperature will be slightly conservative. Also, it should be noted that the four coolant passages, indicated by (1) in Figure XIX-26 have been ignored.

At Point E, just upstream of the stator, the temperature was calculated assuming radial heat flow. This assumption is considered to be slightly conservative since the effect of nearby coolant passages has been ignored.

Calculations were also performed to estimate the temperature rise in the N_2O_4 flowing along the shaft. Assuming a flow rate of 5 gpm, it is estimated that the temperature of the N_2O_4 would rise only four degrees between the pump outlet and the radial bearings. The maximum heating of the N_2O_4 will occur adjacent to the nozzle block. Here it is estimated that the temperature of the fluid will rise a maximum of 30 degrees, again assuming a flow rate of 5 gpm.

2. Advanced TPA

A heat-transfer analysis was conducted to determine the temperature distribution in the B-design turbine shaft during steady state operation. The results are presented in Figures VI-9 and VI-10 in the form of isothermal lines, for expansion-slot depths of 0.30 in. and 0.58 in., respectively.

The boundary conditions used in the analysis are specified schematically in Figure XIX-27. Unless otherwise specified, all heat-transfer coefficients were calculated using the Colburn equation:

$$h = \frac{0.027k}{D_H} Re^{.8} \quad Pr^{.4}$$

where k = thermal conductivity

D_H = hydraulic diameter

Re = Reynolds number

Pr = Prandtl number

XIX, E, Component Design Support (cont.)

The transport properties were evaluated at the average temperature between the free stream and the surface. The surface of the shaft and of the hub upstream of the blades was assumed to be cooled by N_2O_4 at a constant temperature of 70°F. Similarly, the shaft on the downstream side of the blades was assumed to be cooled by AeroZINE 50 at a temperature of 100°F. The heat-transfer coefficients along these surfaces were calculated by assuming that the relative velocities between the liquid and the shaft are equal to one-half the tangential velocity of the shaft.

Six holes drilled parallel to the shaft axis feed N_2O_4 through an annular slot (Section B-B in Figure VI-9) to the burnoff seal. The cooling effect of the six holes (shown as dotted lines in Figure XIX-27) has been neglected for this analysis. The heat-transfer coefficients in the annular passages between the end of the six holes and the burnoff seal were calculated based on a flow rate of 12.7 gpm. The temperature of the N_2O_4 in this region was again assumed constant at 70°F.

Another annular slot is located just downstream of the blades. The purpose of this slot is to reduce the thermal stresses induced in the hub near the gas surface and thus to minimize distortion of the hydrostatic-seal running surface. The heat-transfer coefficient within the slot was calculated based on an assumed gas velocity of 20 ft/sec, which is considered conservative. The temperature of the gas in the slot was taken as 1360°F.

The heat transferred to the hub was accounted for by calculating a single composite heat-transfer coefficient which included both convection between the gas and the hub and conduction between the blades and the hub.

The convective coefficient was calculated based on an average velocity of 699 ft/sec relative to the hub surface using the Colburn equation. The conductive heat-transfer coefficient at the hub surface was calculated from the following equation:

$$h_{cond} = km \left[\frac{1 - \frac{km - h}{km + h} e^{-2mL}}{1 + \frac{km - h}{km + h} e^{-2mL}} \right]$$

and $m = \sqrt{\frac{hC}{kA}}$

where k = thermal conductivity of the blades

h = convective heat-transfer coefficient between the gas and the blades

L = radial length of the blades

C = blade circumference at a cross section

A = blade cross-sectional area

XIX, E, Component Design Support (cont.)

The preceding equation is based on the following assumptions:

a. No temperature gradient in the blades parallel to the axis of the shaft.

b. The ratio of circumference to area at any cross-section is a constant.

The first assumption is considered to be valid for steady-state operation, within the required limits of accuracy of the analysis. However, regarding the second assumption, the ratio of blade circumference to cross-sectional area decreases with radial distance from the hub. To compensate for this discrepancy and to give conservative temperatures, the above ratio was evaluated at one-fourth of the distance between the blade root and the tip.

The average heat-transfer coefficient between the gas and the blade surface was taken as 6020 Btu/ft-hr-°R. This value was calculated for a previous heat-transfer analysis of the A-design.

Having obtained the convective and conductive coefficients at the hub surface, a composite coefficient was then calculated to be 4380 Btu/ft^2-hr-°R based on the relative areas to which they applied:

$$h_{comp} = \frac{1}{A_{hub}} \left(h_{conv}A_{conv} + h_{cond}A_{cond}\right)$$

where h_{comp} = composite heat-transfer coefficient at the hub surface

A_{hub} = total surface area of hub

h_{conv} = convective heat-transfer coefficient between the gas and the exposed surface of the hub

h_{cond} = conductive heat-transfer coefficient, evaluated at the hub surface, between the blades and the hub

A_{conv} = surface area of the hub exposed to the gas

A_{cond} = surface area of the hub occupied by the blade

The driving-force temperature at the hub surface was taken as 1360°F based on a stagnation temperature at the injector of 1500°F.

The inside surface of the hollow shaft was assumed to be an adiabatic boundary. This assumption is justified since only free convection will occur at this surface.

XIX, E, Component Design Support (cont.)

The conduction problem was solved using the thermal analyzer computer program. The blades and the shaft were considered to be integral with a constant thermal conductivity of 14.0 Btu/ft-hr-°R.

As may be seen from the temperature distribution plots of Figures VI-9 and VI-10, significant heating of the shaft occurs only in the hub area due to the cooling effect of the N_2O_4 or AeroZINE 50 flowing along the shaft. The heat-transfer coefficients in this area are very large as a result of large relative velocities between the shaft and the fluids. The region of the hub just downstream of Section B-B in Figure VI-9 remains almost at ambient temperature since the design is isolated from the source of heat by an annular cooling passage.

At the surface of the hub the temperatures very closely approach the recovery temperature of the gas on the blades. A very high temperature gradient exists at the upstream extremity of the hub where the N_2O_4 coolar meets the mainstream gas. A similar high temperature gradient at the downstream end of the hub is avoided by the insulating effect of the expansion slot.

Of primary interest in this analysis are the temperatures near the bottom of the expansion slot, which are necessary to evaluate the stress concentration in this area. Increasing the depth of the slot may somewhat alleviate this problem by placing the region of high stress concentration in an area of generally lower temperatures.

3. Mark 125 Injector Vane

An analysis was performed on a Mark 125 injector vane to determine the temperature distribution for the purpose of a stress analysis. Figure XIX-28 shows the section of the analyzed vane. The temperatures calculated at Station 1 were based on radial heat flow, with the gas-side heat-transfer coefficient varying around the periphery as in flow across a cylinder. The temperatures at Station 4 were calculated by a two-dimensional thermal analyzer using finite differences. The temperature at Station 6 was taken equal to the gas temperature whereas those at Stations 2, 3, and 5 are interpolations. The effect of the mass below the primary fluid channel was neglected due to the presence of the large number of cooling passages; however, the temperatures in View B are slightly optimistic due to this assumption. In no case will they exceed the values in View A.

4. Secondary Injector/Interface Flange

The temperature predictions presented in this paragraph are based on a free-stream gas temperature of 1118°F, an N_2O_4 coolant temperature in the up-flow passage of 200°F, an N_2O_4 temperature in the film-coolant annulus of 70°F, and an AeroZINE 50 temperature of 70°F. One-dimensional flow has been assumed with the regenerative-coolant passage considered to be an annulus. Gas-side velocities range from 103 to 82 ft/sec.

XIX, E, Component Design Support (cont.)

A detailed two-dimensional analysis, performed on the "Thermal Analyzer" computer program, was made for one station and verifies the accuracy of the one-dimensional assumption.

The wall temperatures for the gas side (denoted by • in Figure XIX-29) and the liquid side (denoted by ◉) are summarized below:

Station	Gas-Side Wall Temperature, °F	Liquid-Side Wall Temperature, °F
1	1030	217
2	810	151
3	935	226
4	870	255
5	886	248
6	776	430

The station locations are identified in Figure XIX-29.

	Uncoated			Hastelloy X Coated			Tungsten Coated		
Surface Temperature Limits, °F									
Outside tube wall		1500			1500			1500	
Coating surface					2200			3500	
Characteristic Length (L*), in.	17.4	30	50	17.4	30	50	17.4	30	50
Minimum Film-Cooling Requirements, lb/sec									
Single-point injection	20.6	31.0	46.0	16.0	24.0	35.2	7.2	10.7	16.2
Two-point injection	14.0	17.9	21.0	11.0	13.4	16.6	5.4	5.8	8.4
Injector face plane	4.0	6.1	6.4	4.2	4.2	6.0	2.4	2.4	4.2
Capillary tubes	10.0	11.8	14.6	7.3	9.2	10.6	3.0	3.4	4.2
Axial Location of Second Injection Point (Distance from Throat), in.	3.75	4.25	5.25	3.50	4.00	5.00	3.00	3.50	4.25

Figure XIX-1 Film-Cooling Requirements for ARES Chambers (u)

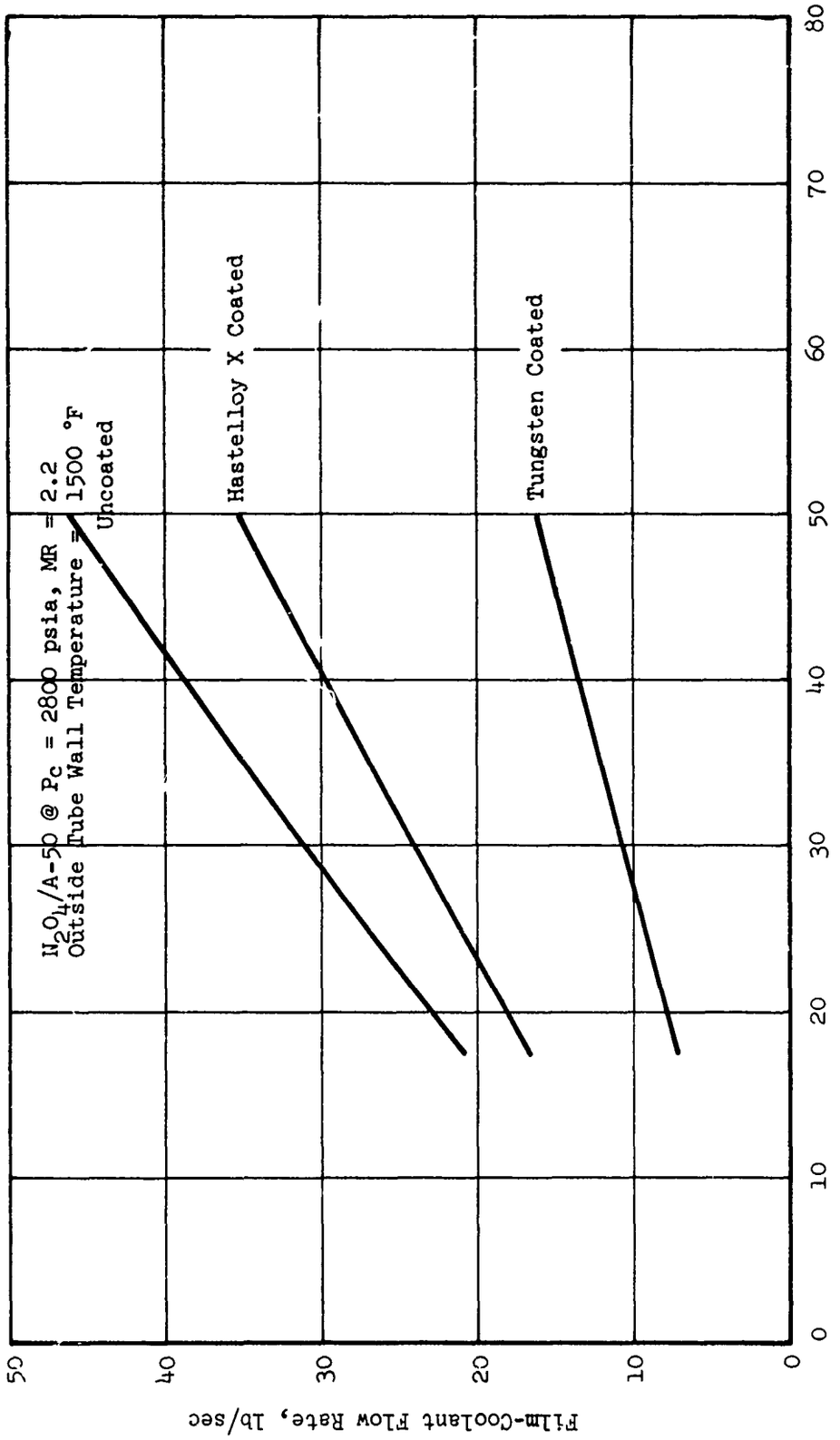

Minimum Film-Cooling Requirements for ARES Chambers with Single-Point Injection (u)

Figure XIX-2

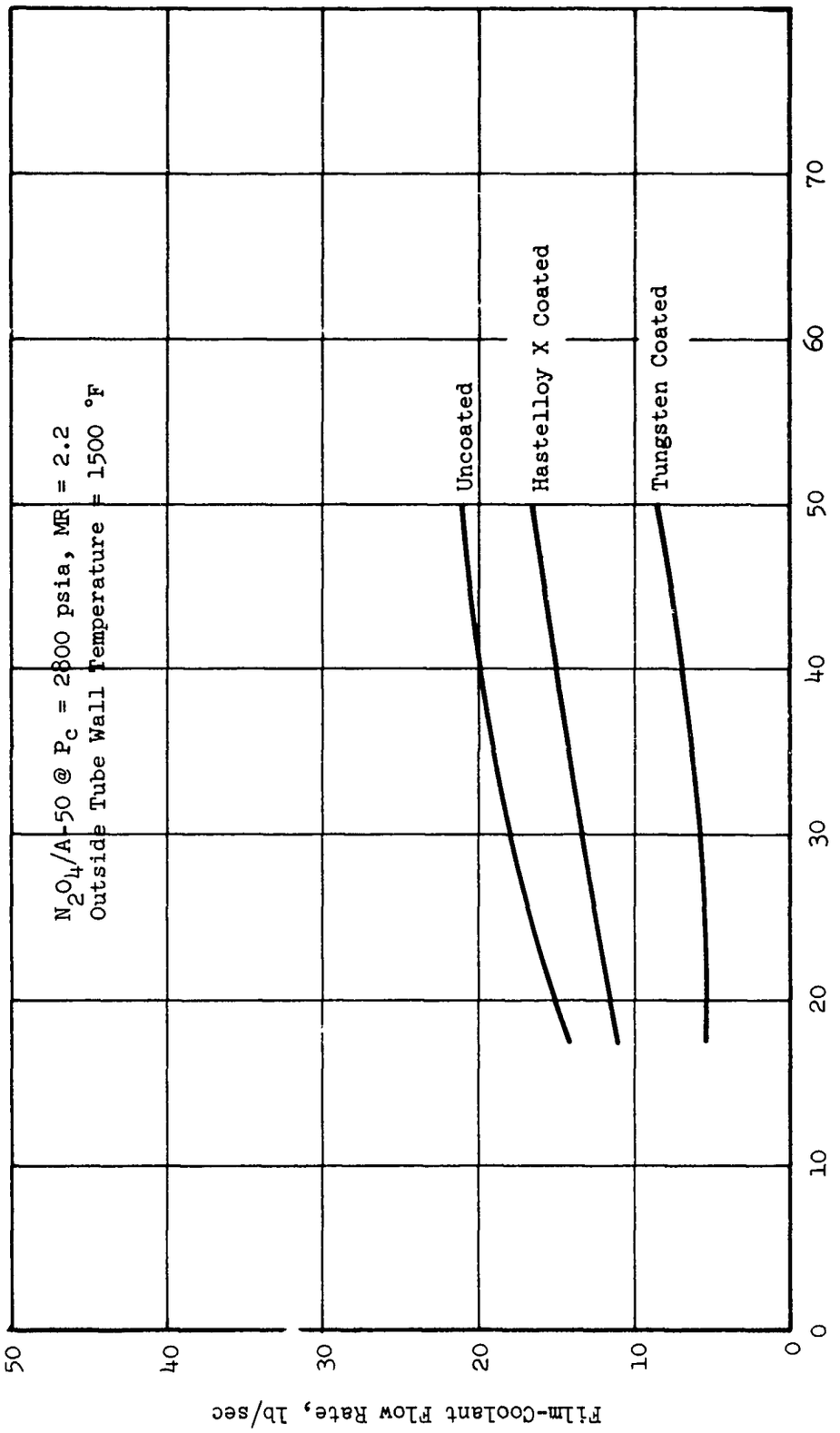

Minimum Film-Cooling Requirements for ARES Chambers with Two-Point Injection (u)

Figure XIX-3

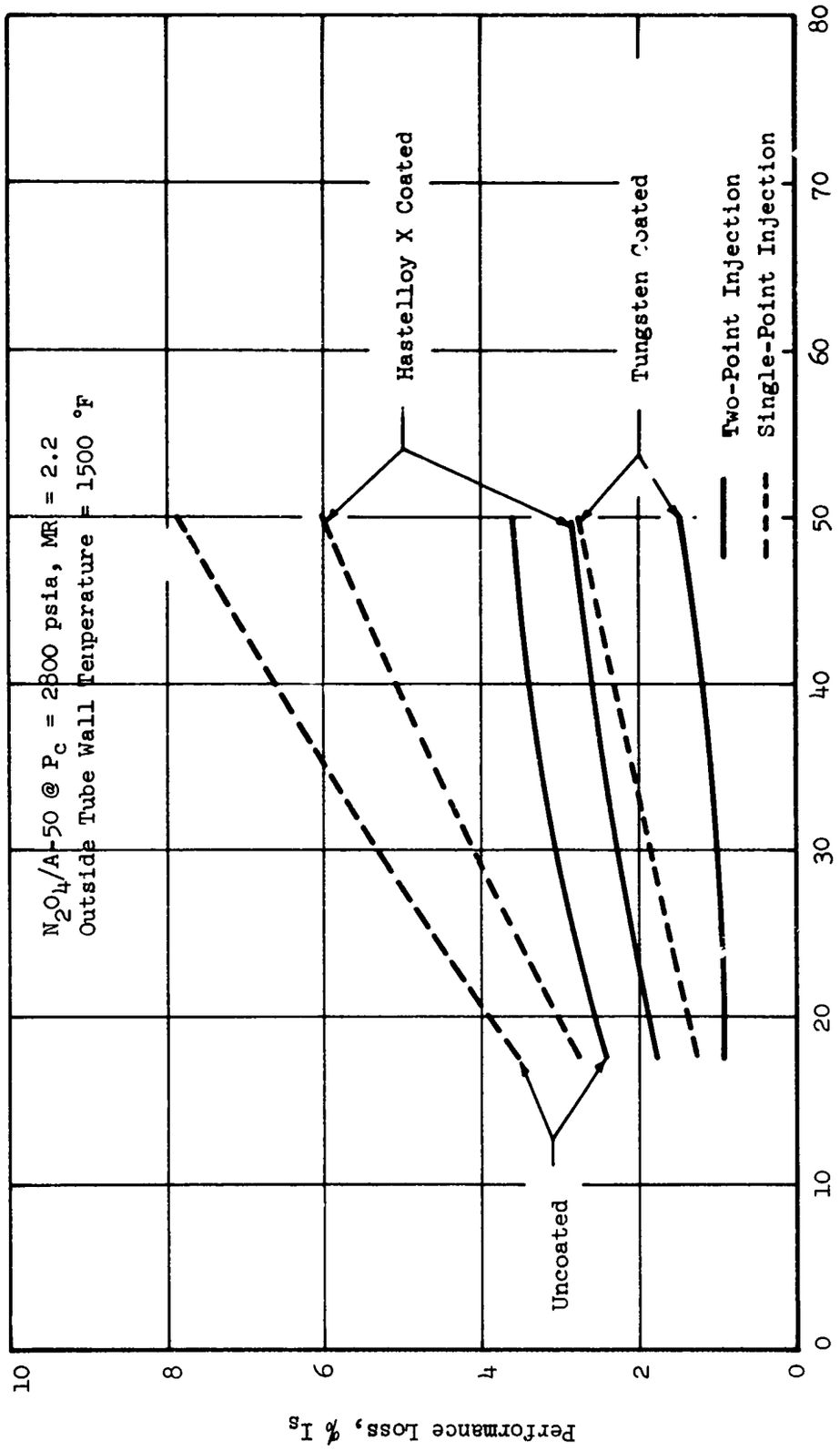

Minimum Performance Loss Due to Film-Cooling the ARES Chamber (u)

Figure XIX-4

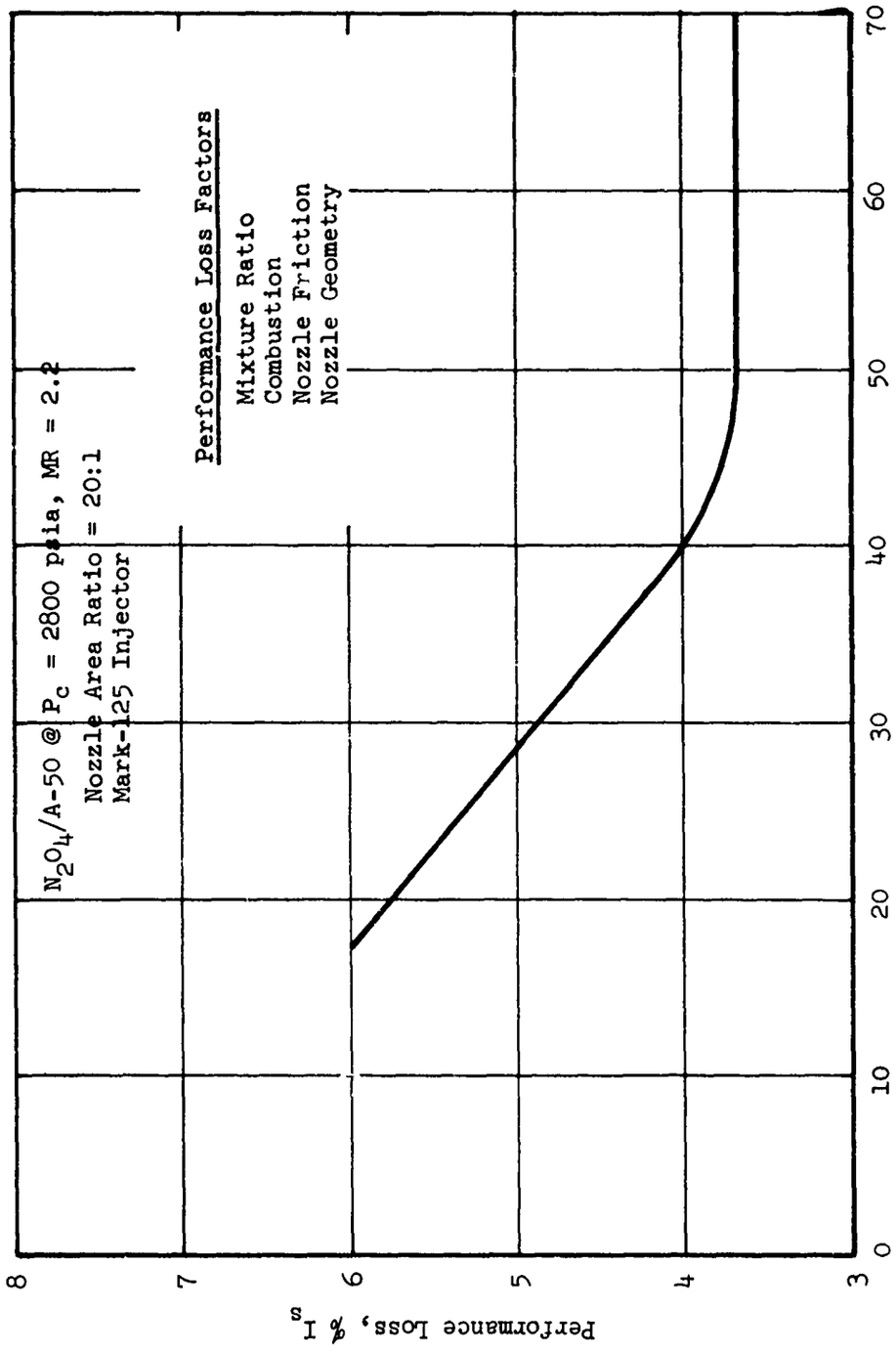

Performance Losses in ARES Chambers (u)

Figure XIX-5

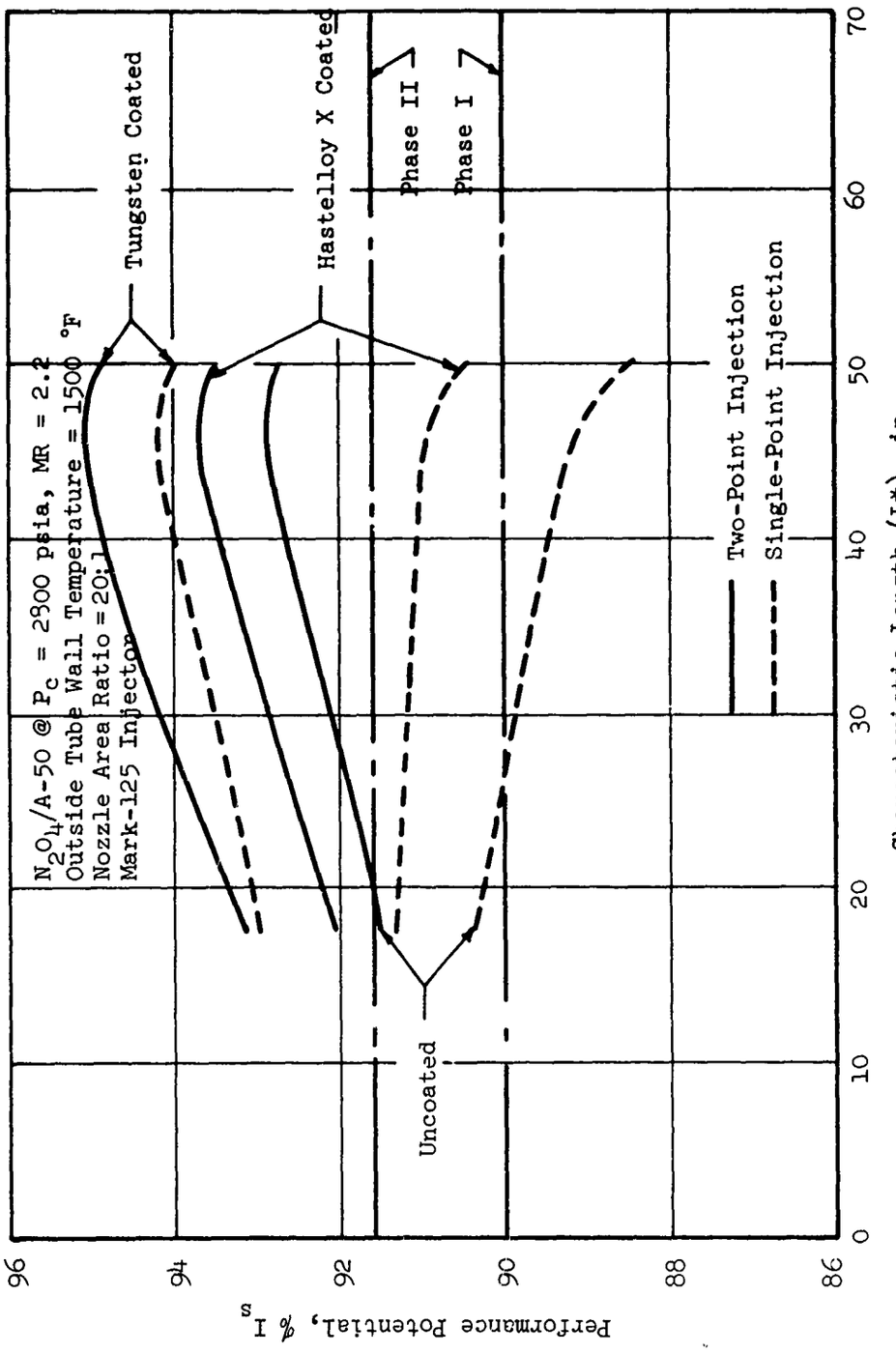

Performance Potential in ARES Chamber (u)

Figure XIX-6

	Uncoated	Hastelloy X Coated	Tungsten Coated
Surface Temperature Limits, °F			
Outside tube wall	1500	1500	1500
Coating surface		2200	3500
Film-Cooling Requirements, lb/sec			
Single-point injection	38.6	29.7	13.5
Two-point injection	20.4	16.0	8.0
Injector face plane	6.6	5.3	3.0
Capillary tubes (5 in. from throat)	13.8	10.7	5.0

Film-Cooling Requirements for ARES 40-in. L* Regeneratively Cooled Chamber (u)

Figure XIX-7

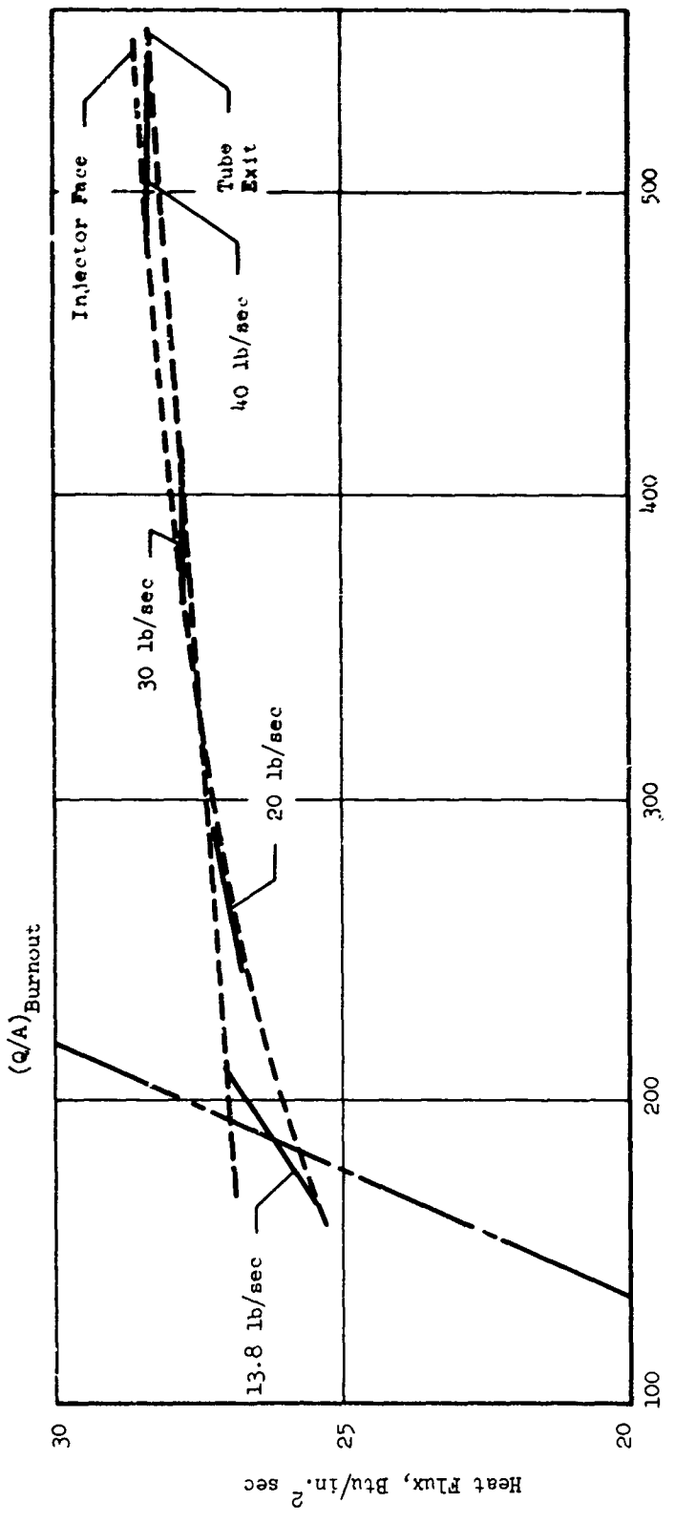

ARES Uncoated Capillary Tube Heat-Flux Capability (Based on Outside Surface Area), 0.040 in. ID

Figure XIX-8
(This page is Unclassified)

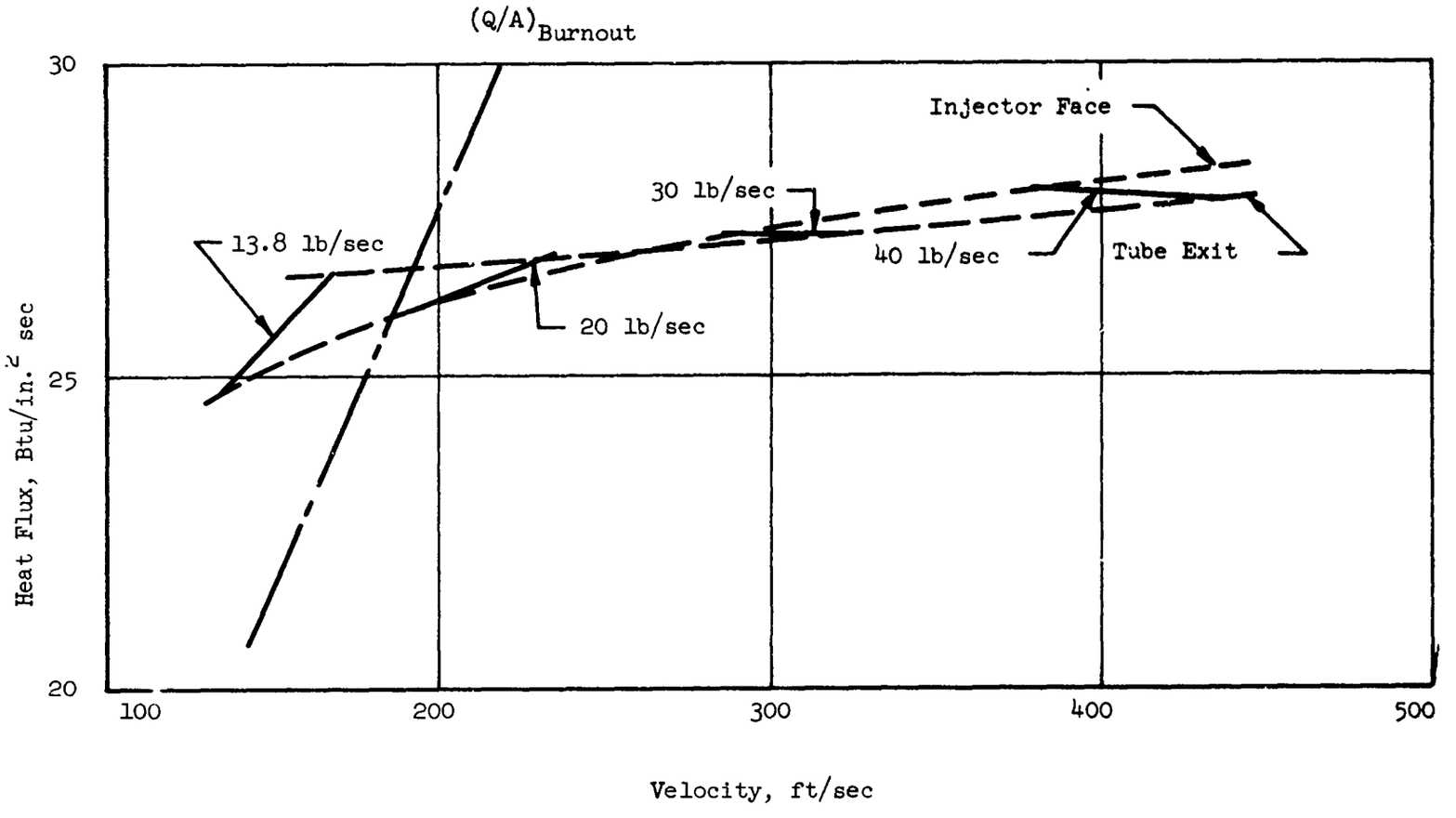

Tube Inside Diameter = 0.045 in.
Tube Wall Thickness = 0.005 in.

ARES Uncoated Capillary Tube Heat-Flux Capability (Based on Outside Surface Area), 0.045 in. ID

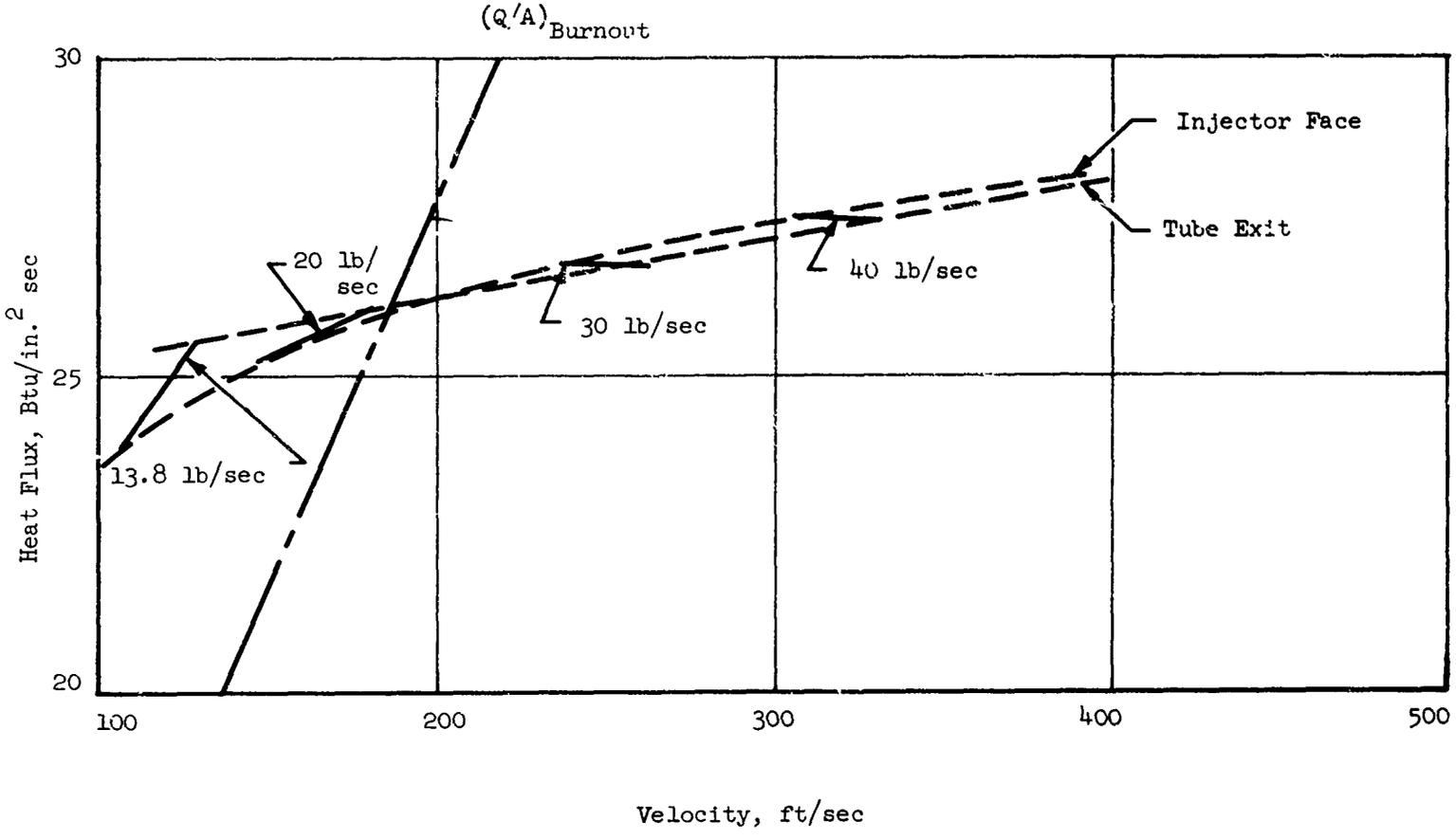

Figure XIX-10

Tube Inside Diameter = 0.050 in.
Tube Wall Thickness = 0.005 in.

ARES Uncoated Capillary Tube Heat-Flux Capability (Based on Outside Surface Area), 0.050 in. ID

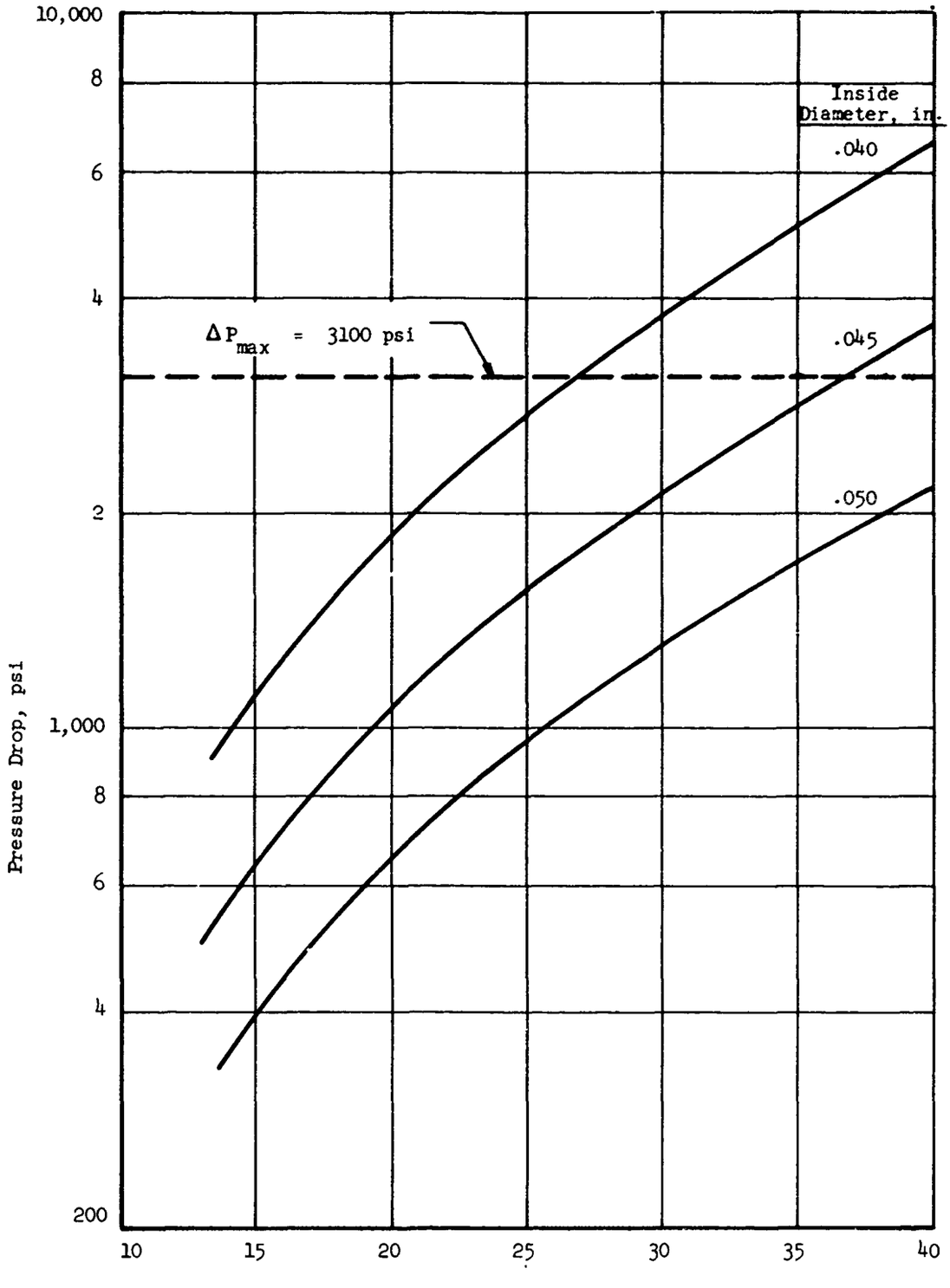

Pressure Drop in Capillary Tubes

Figure XIX-11

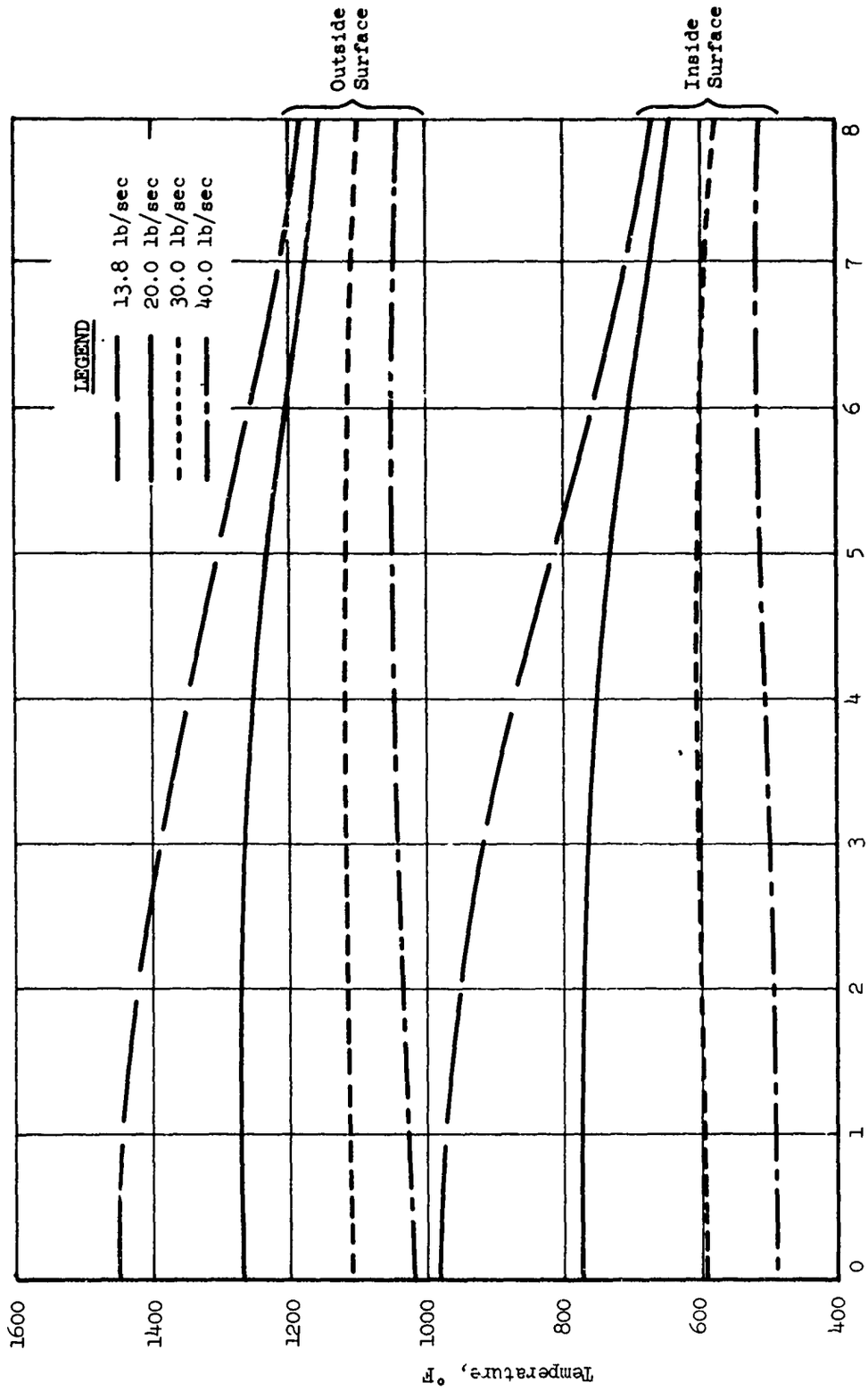

ARES Capillary Tube Wall Temperatures

Figure XIX-12

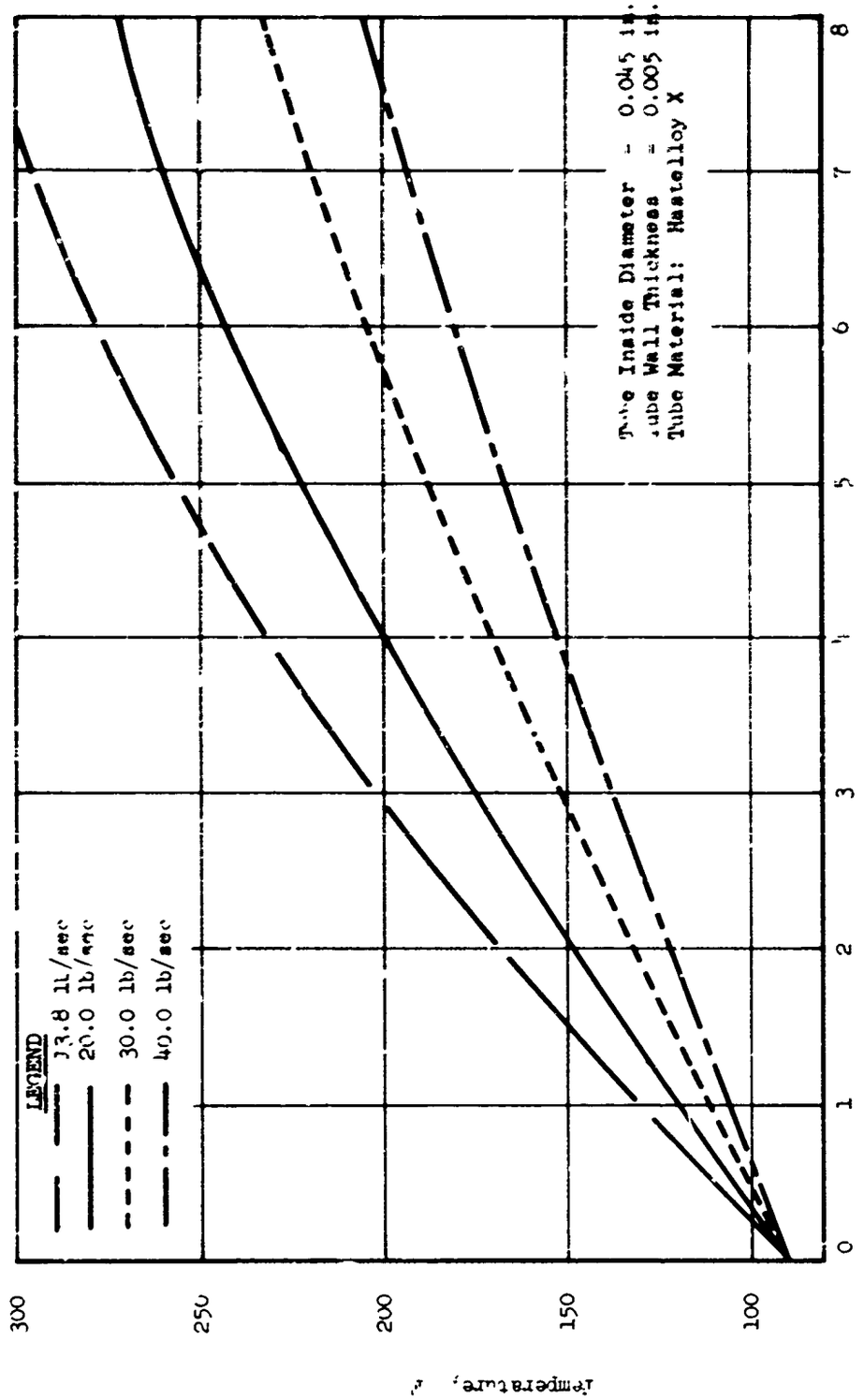

Film-Coolant Temperature in ARES Capillary Tubes

Figure XIX-13

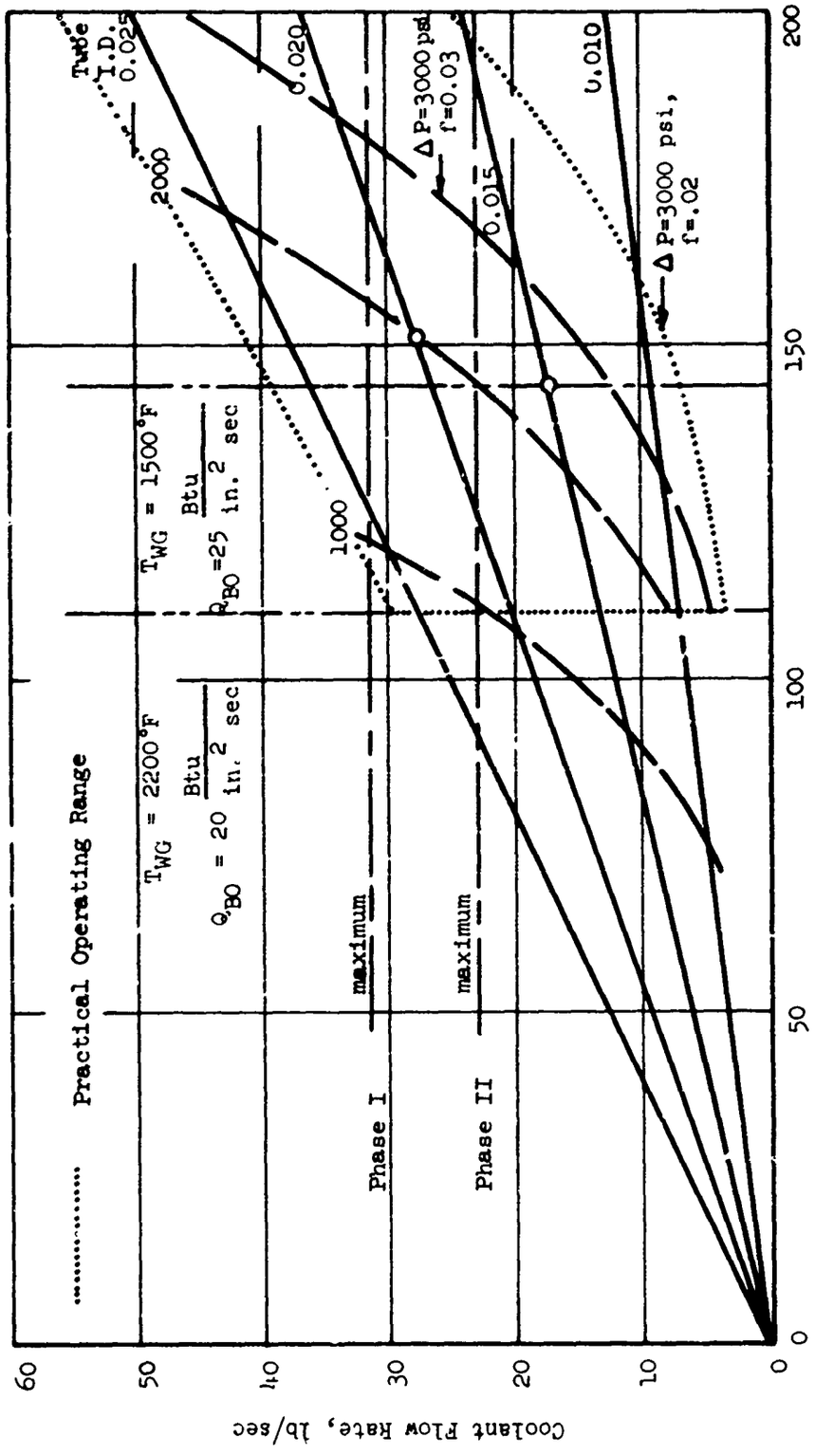

Microflow Liner, Parametric Study, Round Tubes

Figure XIX-14

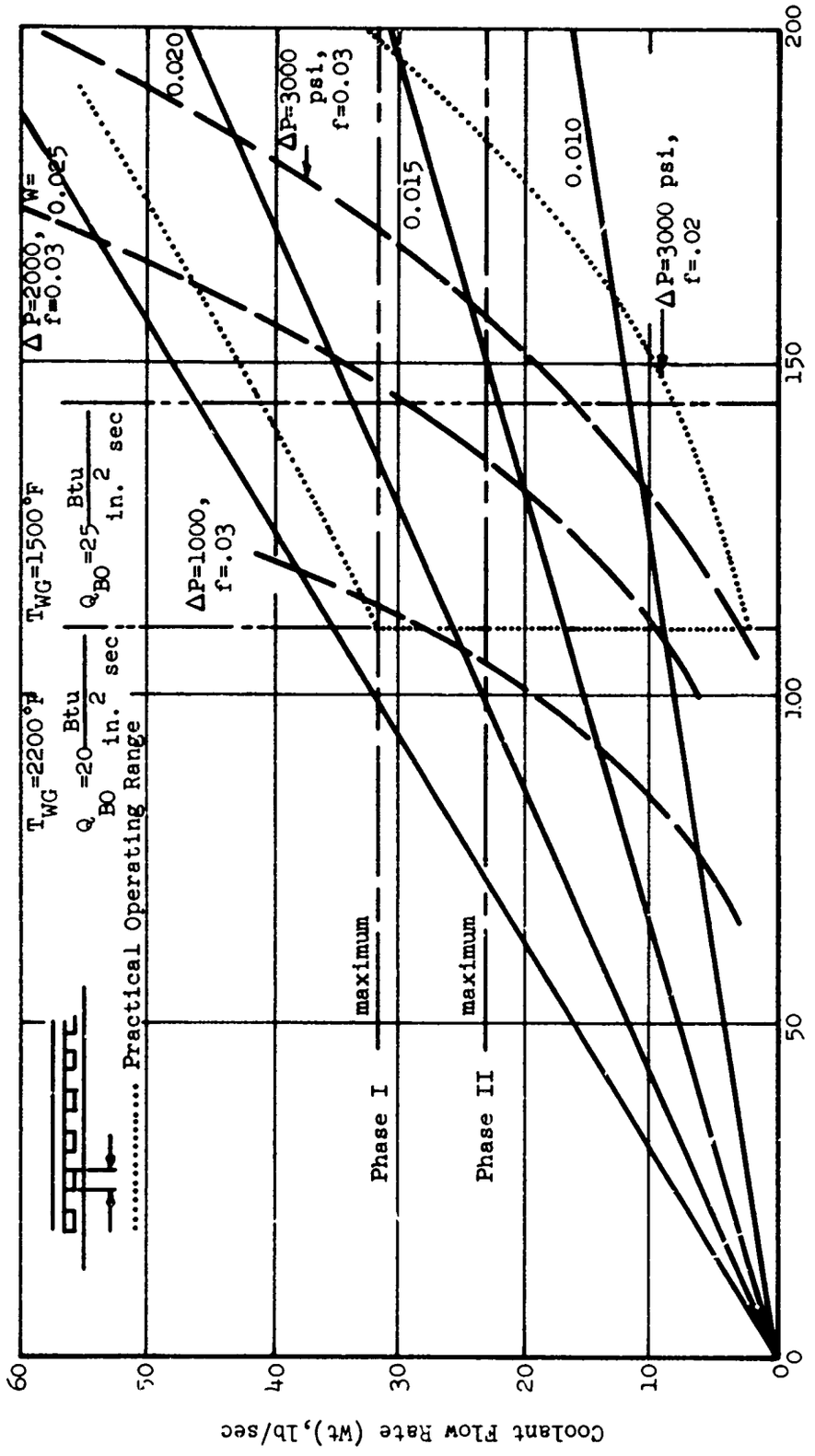

Figure XIX-15

Microflow Liner, Parametric Study, Square Slots

CHAMBER COMPARTMENT NUMBER

ITEM	1	2	3	4	5	6	7	8	9	10	11	12	TOTAL
Compartment Length (in.)	0.986	2.331	2.331	1.680	1.932	2.035	1.133	0.481	0.528	0.781	1.375	2.289	
Platelet Thickness (in.)	0.021	0.021	0.021	0.021	0.021	0.011	0.011	0.011	0.011	0.011	0.011	0.021	
Plenum Pressure (psia)	3320	3320	3320	3370	3890	3515	3400	3080	3000	2480	1525	1490	
Weight Flow for 1900°F Nominal Wall Temp., lb/sec.	0.60	1.41	1.41	1.11	2.06	1.90	1.30	0.65	0.69	0.95	1.11	1.65	14.84
Maximum Weight Flow (Plenum Pressure 4500 psia)	1.83	4.24	4.24	3.10	3.10	3.73	2.28	1.28	1.28	1.99	3.79	3.90	34.76
Platelet Indexing Position & Number of Platelets	1 47	1 111	1 111	1 80	4 15	1 103	1 13	1 22	2 24	1 6	1 22	1 27	
					3 18	2 82	2 69	2 22	3 12	2 10	2 17	2 14	
					2 31		3 21		4 12	3 13	3 16	3 19	
					1 28					4 14	4 15	4 13	
										5 11	5 12	5 11	
										6 14	6 43	6 25	

Transpiration-Cooled Chamber Coolant--Flow Distribution

Figure XIX-16

Report 10830-Q-3

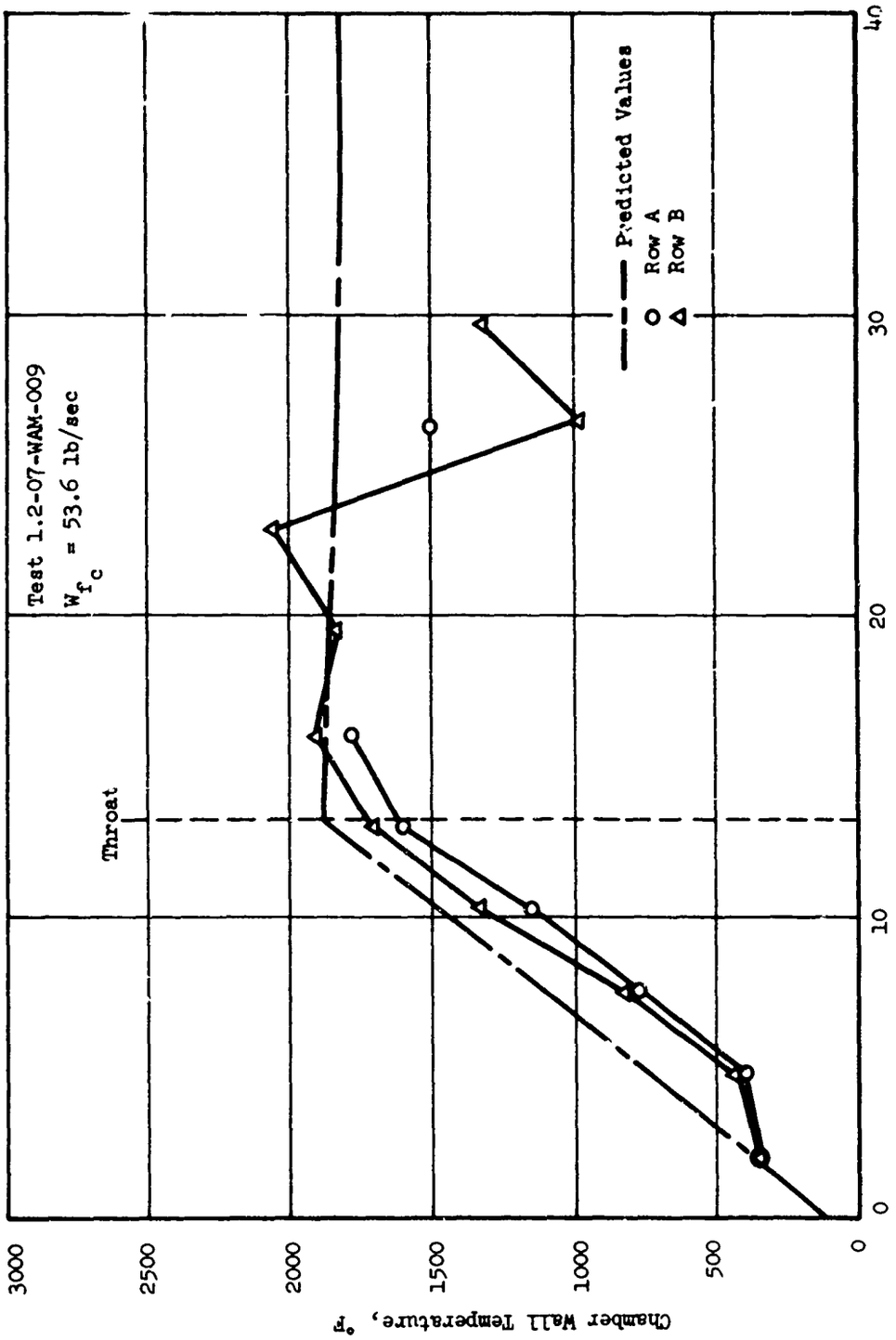

Film-Cooled Test Data, Test 1.2-07-WAM-009

Figure XIX-17

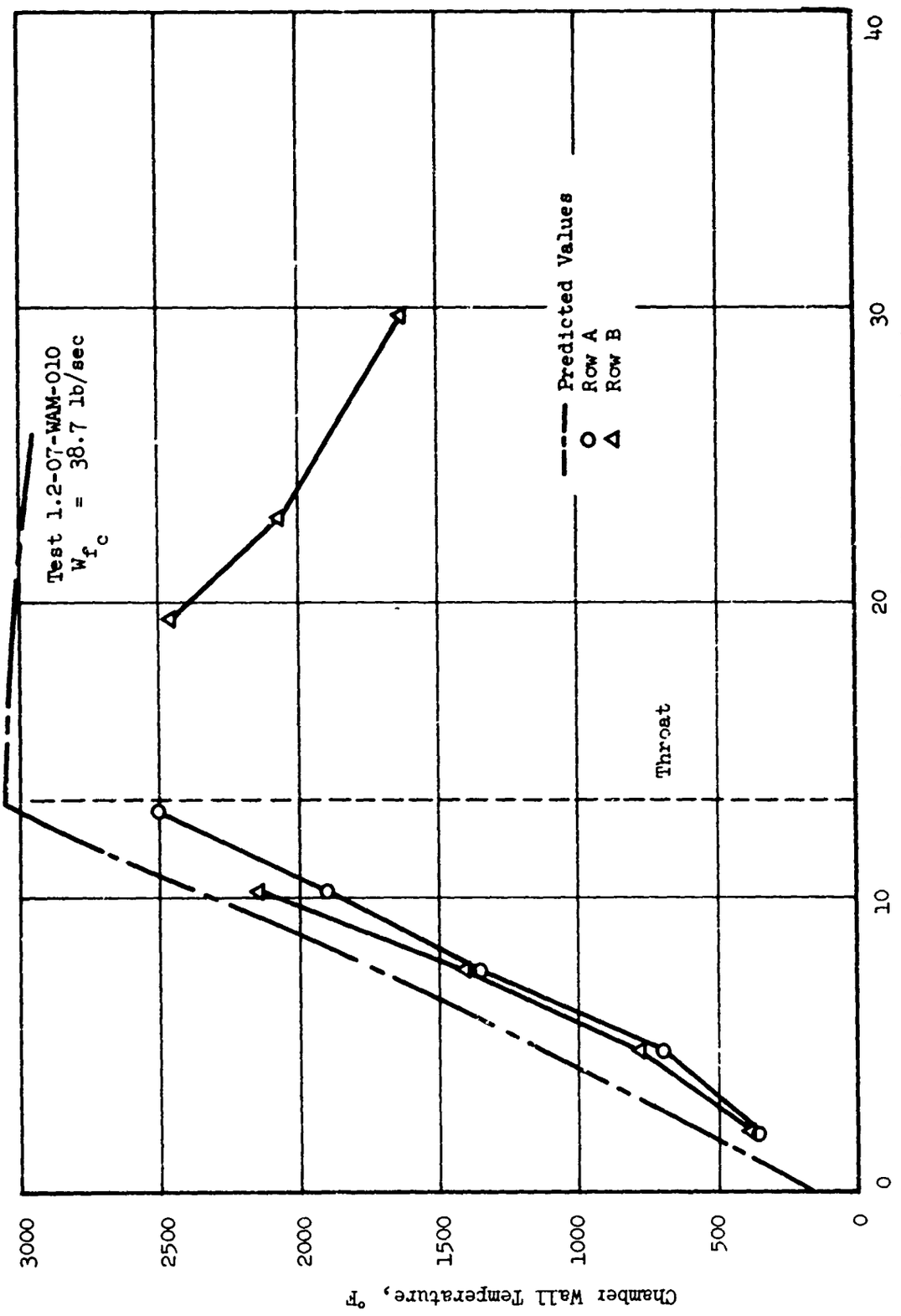

Film-Cooled Test Data, Test 1.2-07-WAM-010

Figure XIX-18

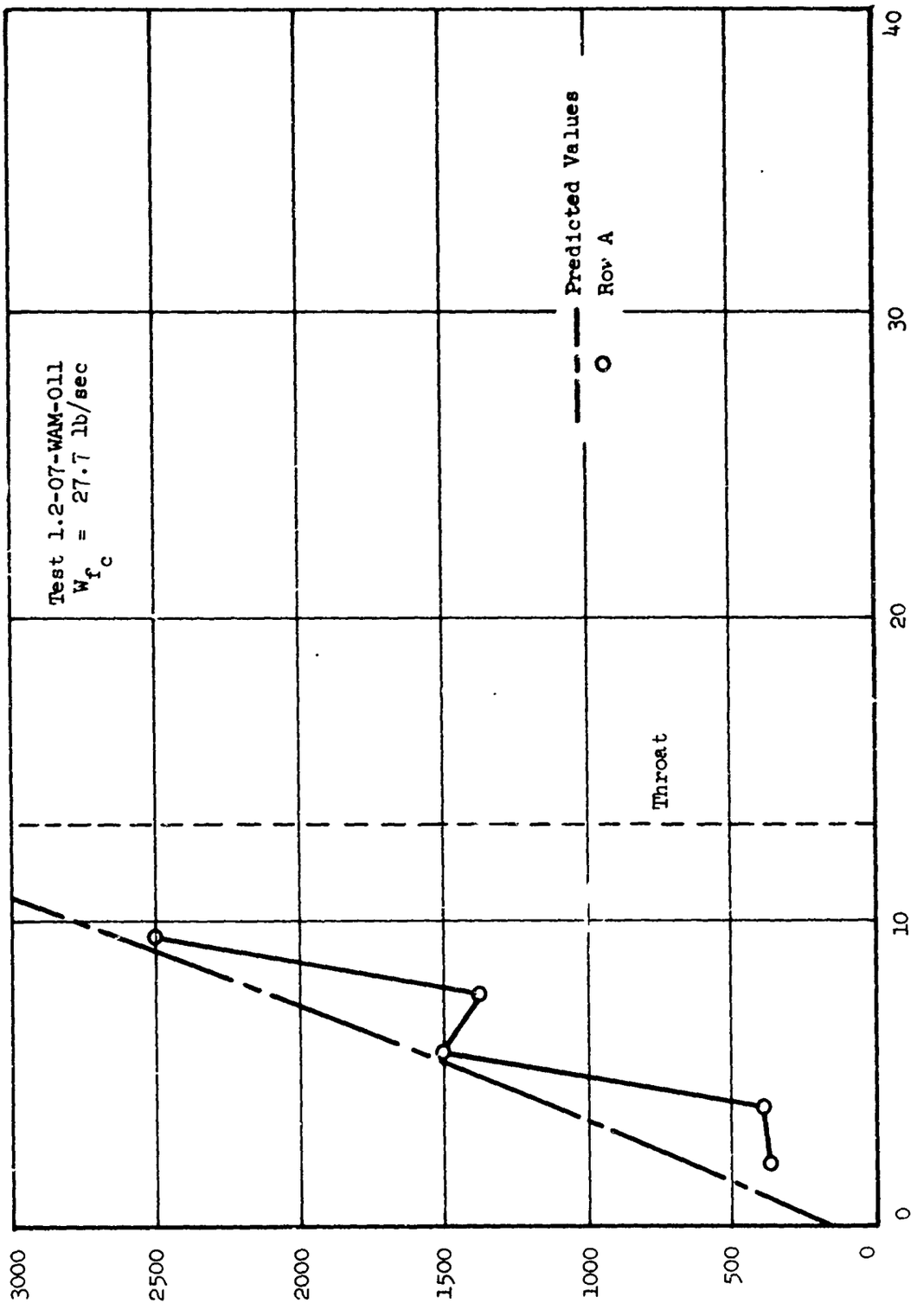

Film-Cooled Test Data, Test 1.2-07-WAM-011

Figure XIX-19

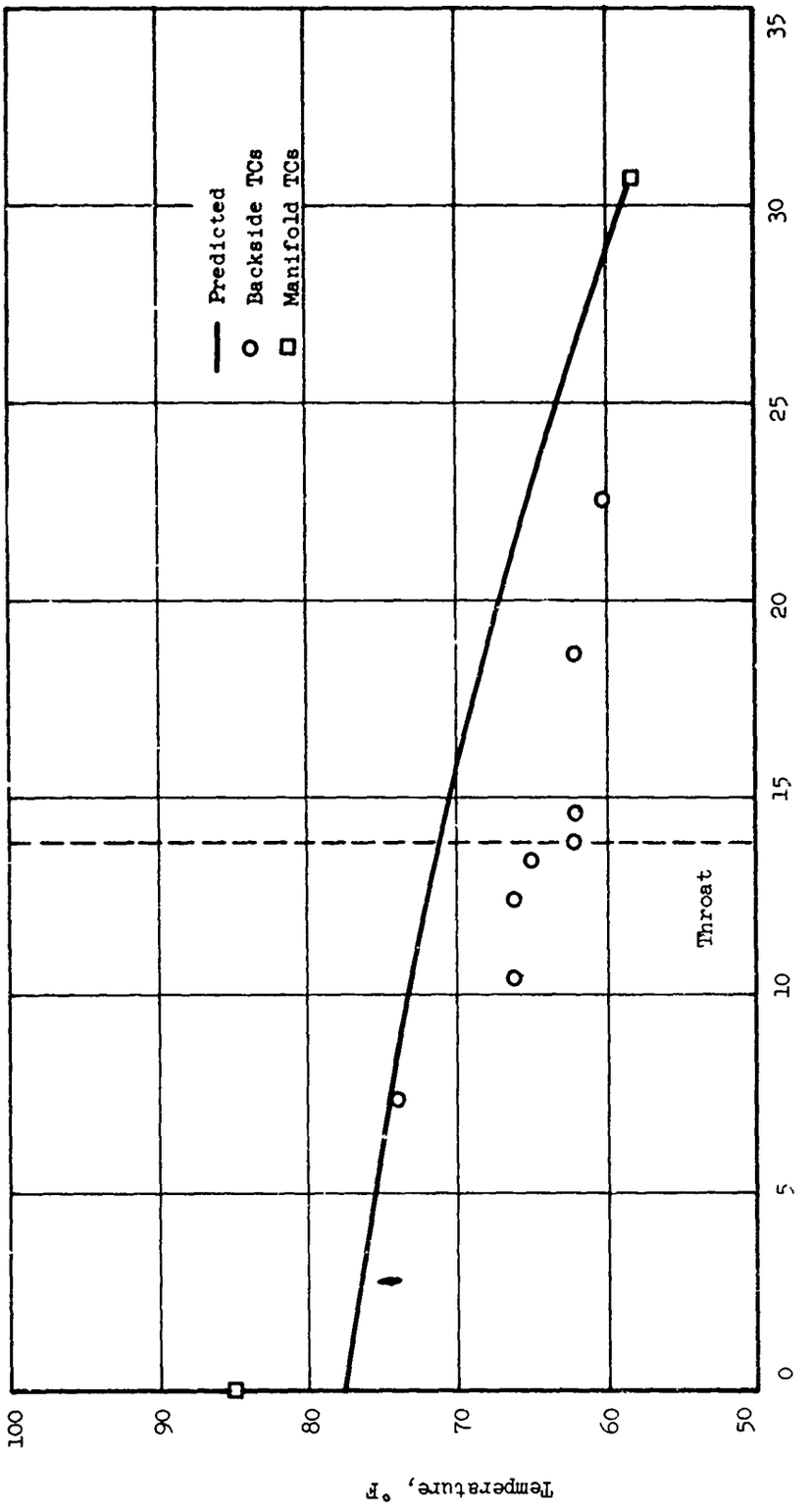

Regenerative Coolant Bulk Temperature, Test 1.2-08-WAM-002

Figure XIX-20

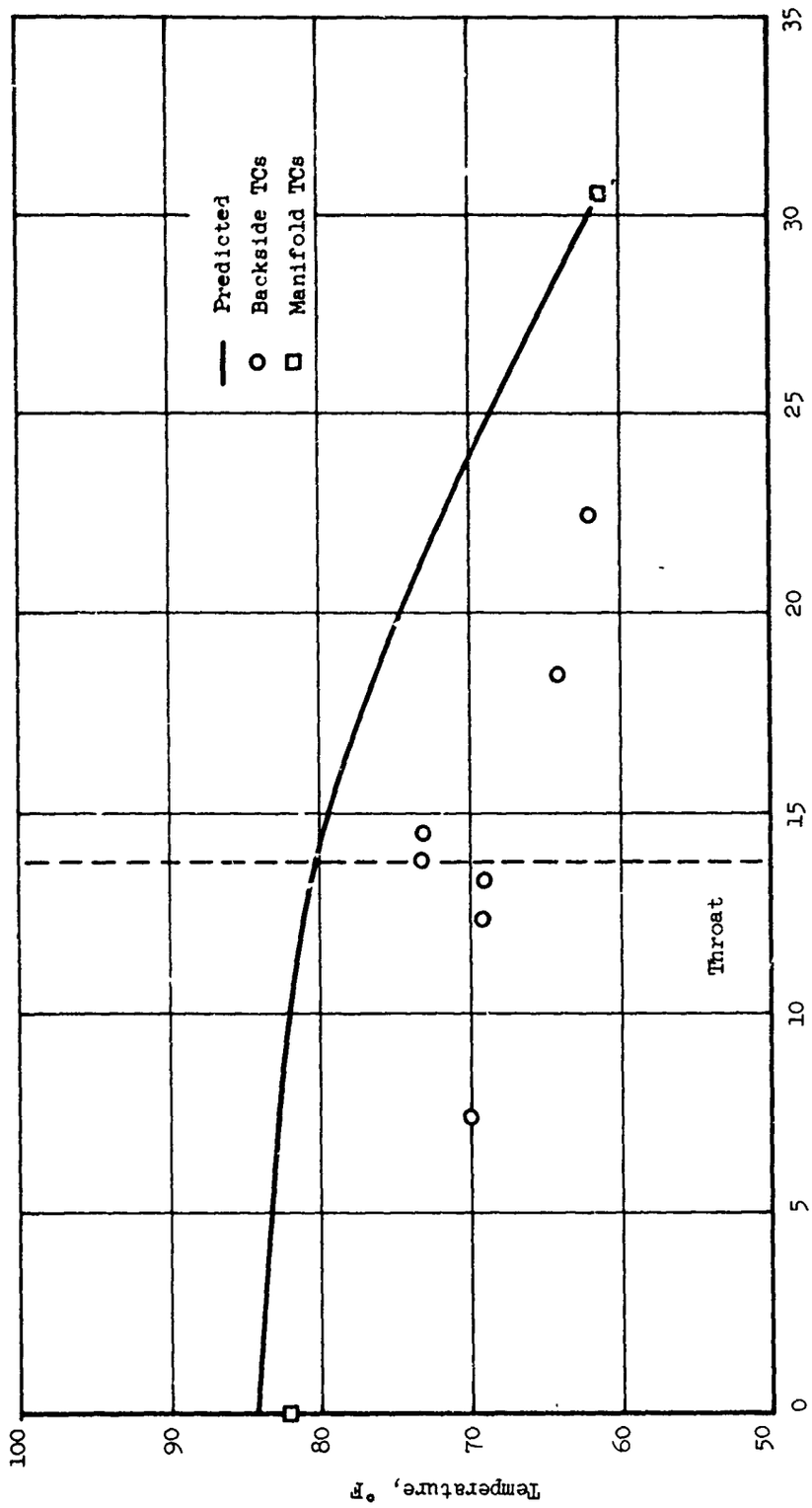

Regenerative Coolant Bulk Temperature, Test 1.2-08-WAM-003

Figure XIX-21

Test No.	Coating Thickness in.	Coating Cond. B/in.-sec°R	Wall Thickness in.	Wall Cond. B/in.-sec°R	W_{REG} lb/sec	$W_{Main\ Stream}$ lb/sec	w_{f_c} lb/sec	X_{f_c} in.	Inlet Vel. (fc) ft/sec	Inlet Temp (fc) °R	T (Mainstream) °R
1.2-07-WAM -009	-	-	-	-	-	303.6	53.6	0	410.	545.	5500.
1.2-07-WAM -010	-	-	-	-	-	351.3	38.7	0	410.	545.	5540.
1.2-07-WAM -011	-	-	-	-	-	312.6	27.7	0	410.	545.	5460.
1.2-08-WAM -002	.056	.00016	.012-.02	.00026	193.5	272.4	49.5		346.	518.	5478.
1.2-08-WAM -003	.025	.00012	.012-.020	.00026	202.0	275.5	24.	0	476.	521.	5407.
*	.025	.00012	.004	.00026	16.	275.5	16	12.25	187.	581.	

Figure XIX-22

Test Parameters on Which Predictions are Based

Specimen No.	Heat Flux, Btu/in.^{2}-sec	Estimated Temperature, °F		Number of 20 Sec Cycles To Spall
		Interface	Hastelloy X Gas Side	
180	16.7	1350	2020	(Burned out*)
178-1	13	1150	1660	4
178-2	17.5	1380	2080	(Burned out*)
179-1	14.2	1210	1780	6
179-2	13.2	1160	1690	5
179-3	13.7	1180	1730	2 Left Tube 7 Center Tube

*Burned out because insufficient water cooling available.

Hastelloy-X Thermal-Shock Test Results

Detail A - Coated Side

Detail B - Liquid Side

Closeup View of Specimen 178-2

Figure XIX-24

Microstructure of Specimen 179-3 (100X)

Figure XIX-25

Microstructure of Specimen 179-3 (100X)

Figure XIX-25

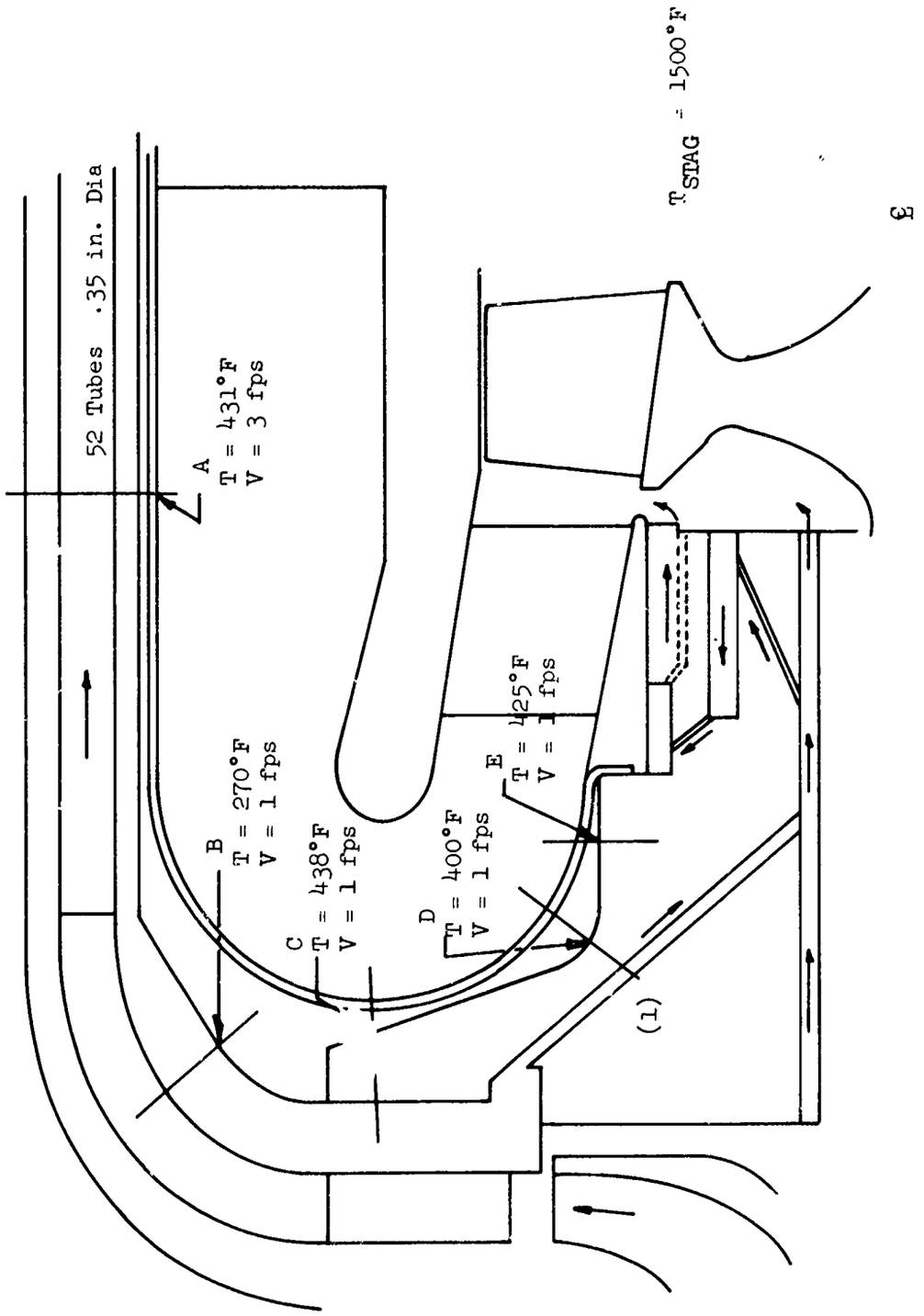

Inline Primary Combustion Chamber

Figure XIX-26

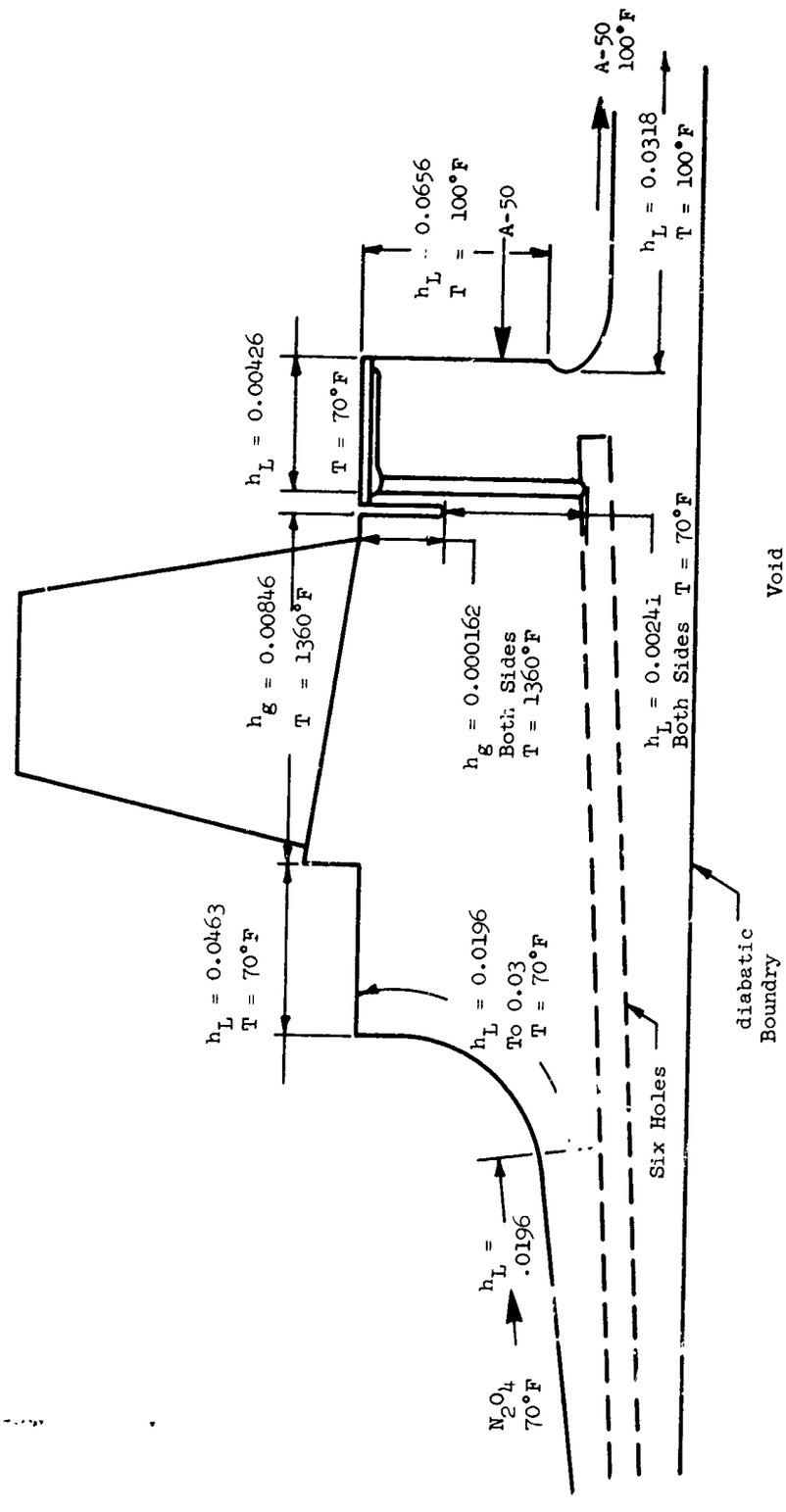

Boundary Conditions for Advanced TPA B-Design Rotor

Figure XIX-27

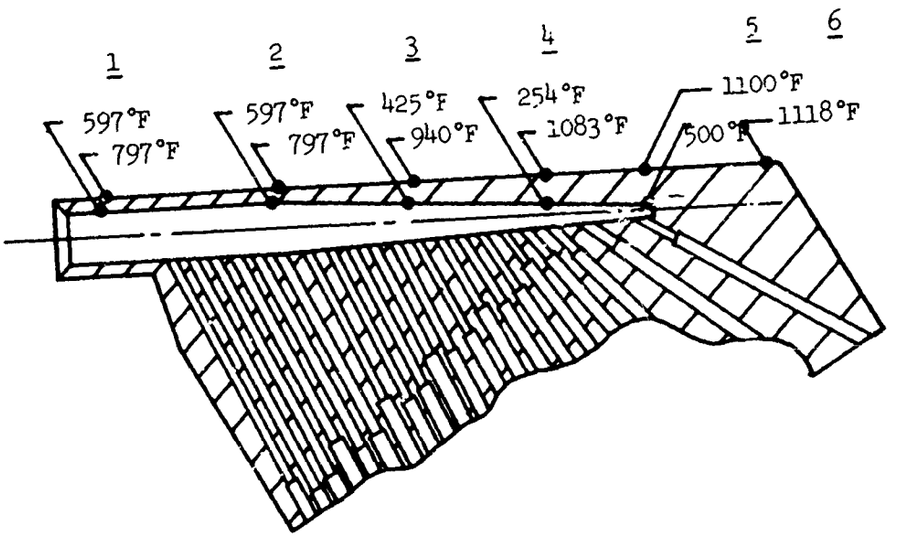

VIEW 'A'

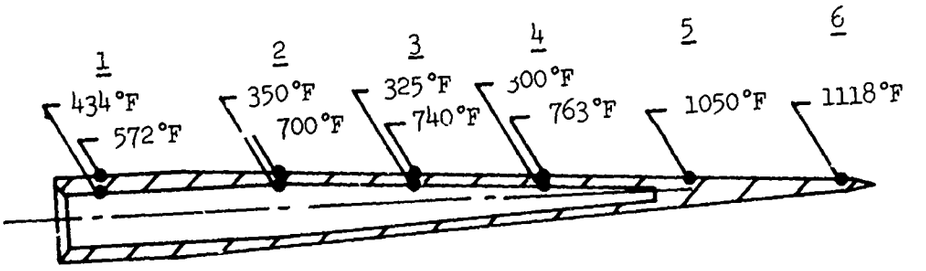

VIEW 'B'

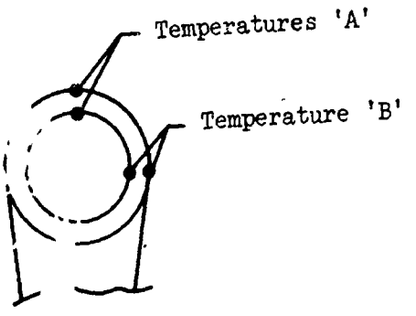

Typical Section

1. Gas Temperature = 1118°F
2. Liquid Temperature = 70°F

Mark 125 Injector Vane

Figure XIX-28

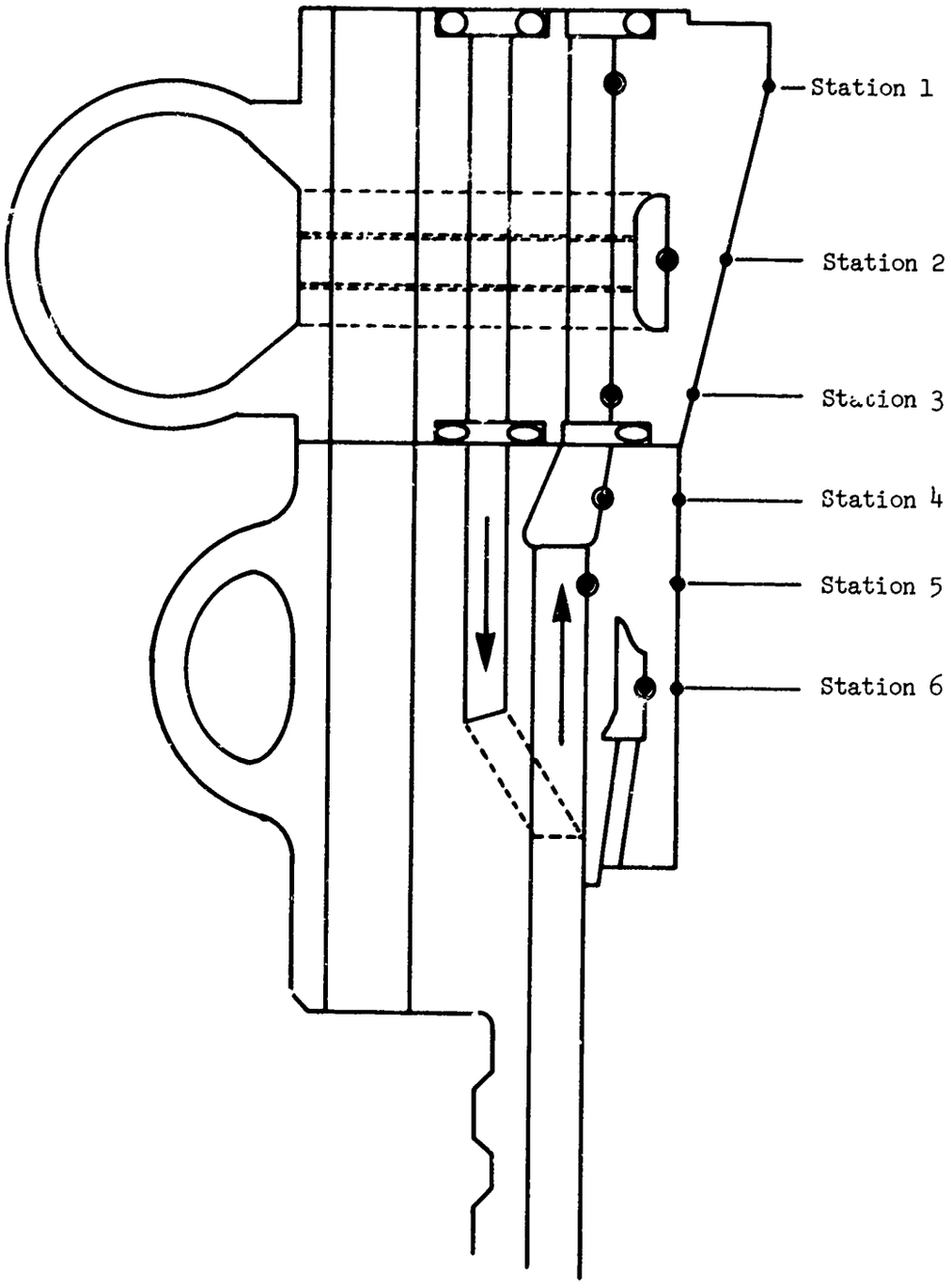

Regeneratively Cooled Combusti. Chamber 1, condary
Injector/Interfac• Flange

Figure XIX-29

XX.

RELIABILITY

A. GENERAL

The reliability engineering tasks during Phase I are design review and reliability prediction. Design review includes modes-of-failure analyses, test-plan review, test-data review, and maintainability analyses. Reliability prediction includes the prediction of component and module reliabilities.

Primary attention was given to the modes-of-failure analyses which are the basis for design-review recommendations during this critical component development phase of the program.

B. MODES-OF-FAILURE ANALYSIS (MOFA)

Various methods for interlocking the fuel-control valves were studied on the basis of MOFA results for start and shutdown transients. The effects of electrical, hydraulic, and mechanical interlock concepts on overall program cost and program time were compared. Controls flexibility and reliability, along with expected hardware costs, were considered as factors affecting program cost. This study will be completed during the next reporting period.

The potential reliability of various interpropellant seal concepts was compared. The alternatives evaluated were:

1. For the advanced TPA: the hydrostatic combustion seal, the liquid-purged seal, and the gas-purged seal.

2. For the in-line TPA: the liquid-purged seal, the gas-purged seal, and the rubbing-contact seal.

Assuming equal reliability growth rates, it was concluded that in the first fabricated unit of the advanced TPA both purged seals would offer a higher potential reliability than the combustion seal, and that in the in-line TPA the rubbing-contact seal would offer a higher reliability potential than either of the purged seals. This higher reliability of purged and rubbing-contact seals is due primarily to the extensive experience gained throughout the industry with this type of seal. However, with a sufficiently steep reliability growth rate, the combustion seal could overcome its initial reliability handicap and attain, or even surpass, the ultimate reliability level of the purged seal. (The analysis did not include factors such as cost, weight, maintenance, or versatility.)

A study was initiated to evaluate all module failure modes that could occur during the start and shutdown transients due to failures of components other than valves. (Start and shutdown failure modes caused by valves were evaluated earlier.) The detailed component MOFAs completed to date will provide a basis for this new study.

XX. B, Modes-of-Failure Analysis (MOFA) (cont.)

The method of explosively welding the regenerative-coolant tubes to the TCA flange was reviewed for reliability. Test welds were made at Aerojet's Downey facility and will be inspected early in April.

C. TEST-PLAN REVIEW

A thorough review of the entire modular-hardware TCA test plan will be made to ensure adequate data for posttest analysis at minimum cost.

D. TEST-DATA REVIEW

A review of test data documentation will be made to ensure adequate appraisal of performance achieved and attainable, and of causes of failures.

E. MAINTAINABILITY ANALYSIS

The study to evaluate the maintainability of developmental hardware and the acceptance of production engines without acceptance firings was continued. Completion of the study is scheduled for the end of June 1966.

F. RELIABILITY PREDICTION--COMPONENTS

Data from various Titan and Integrated Components Programs were accumulated, and sufficient MOFAs for ARES components were completed to provide a basis for initial component-reliability predictions. The initial predictions will be completed during the next reporting period.

G. RELIABILITY PREDICTION--MODULE

The initial prediction of module reliability based on predicted component reliabilities will be made during the next reporting period.

Unclassified
Security Classification

DOCUMENT CONTROL DATA - R&D
(Security classification of title, body of abstract and indexing annotation must be entered when the overall report is classified)

1 ORIGINATING ACTIVITY (Corporate author) Aerojet-General Corporation P.O. Box 1947, Sacramento, California	2a REPORT SECURITY CLASSIFICATION Confidential 2b GROUP Four

3 REPORT TITLE

ADVANCED ROCKET ENGINE--STORABLE

4 DESCRIPTIVE NOTES (Type of report and inclusive dates)
Quarterly Technical Report (January through March 1966)

5 AUTHOR(S) (Last name, first name, initial)
Aerojet-General Corporation
Advanced Storable Rocket Engine Division

6 REPORT DATE April 1966	7a TOTAL NO OF PAGES 257	7b NO OF REFS 4
8a CONTRACT OR GRANT NO AF 04(611)-10830 b PROJECT NO c d	9a ORIGINATOR'S REPORT NUMBER(S) Aerojet Report 10830-Q-3 9b OTHER REPORT NO(S) (Any other numbers that may be assigned this report) AFRPL-TR-66-82	

10 AVAILABILITY/LIMITATION NOTICES

11 SUPPLEMENTARY NOTES	12 SPONSORING MILITARY ACTIVITY AFRPL, Research and Technology Division, Edwards AFB, Calif.

13 ABSTRACT

The objective of the ARES (Advanced Rocket Engine, Storable) program is to demonstrate the engineering practicality and the performance characteristics of an advanced storable propellant modular engine embodying high chamber pressure and the staged-combustion cycle. This third quarterly report describes the technical accomplishments of the reporting period. Generally, the period was characterized as one in which many analyses and designs were completed, fabrication of many components was completed, and testing accelerated. The most noteworthy accomplishment was the successful hot firing of two different modular injectors using the intensifier test system.

DD FORM 1 JAN 64 1473

Unclassified
Security Classification

AFSCR 80-20

Unclassified
Security Classification

14 KEY WORDS	LINK A		LINK B		LINK C	
	ROLE	WT	ROLE	WT	ROLE	WT

INSTRUCTIONS

1. ORIGINATING ACTIVITY: Enter the name and address of the contractor, subcontractor, grantee, Department of Defense activity or other organization *(corporate author)* issuing the report.

2a. REPORT SECURITY CLASSIFICATION: Enter the overall security classification of the report. Indicate whether "Restricted Data" is included. Marking is to be in accordance with appropriate security regulations.

2b. GROUP. Automatic downgrading is specified in DoD Directive 5200.10 and Armed Forces Industrial Manual. Enter the group number. Also, when applicable, show that optional markings have been used for Group 3 and Group 4 as authorized.

3. REPORT TITLE: Enter the complete report title in all capital letters. Titles in all cases should be unclassified. If a meaningful title cannot be selected without classification, show title classification in all capitals in parenthesis immediately following the title.

4. DESCRIPTIVE NOTES: If appropriate, enter the type of report, e.g., interim, progress, summary, annual, or final. Give the inclusive dates when a specific reporting period is covered.

5. AUTHOR(S): Enter the name(s) of author(s) as shown on or in the report. Enter last name, first name, middle initial. If military, show rank and branch of service. The name of the principal author is an absolute minimum requirement.

6. REPORT DATE. Enter the date of the report as day, month, year, or month, year. If more than one date appears on the report, use date of publication.

7a. TOTAL NUMBER OF PAGES: The total page count should follow normal pagination procedures, i.e., enter the number of pages containing information.

7b. NUMBER OF REFERENCES: Enter the total number of references cited in the report.

8a. CONTRACT OR GRANT NUMBER: If appropriate, enter the applicable number of the contract or grant under which the report was written.

8b, 8c, & 8d. PROJECT NUMBER. Enter the appropriate military department identification, such as project number, subproject number, system numbers, task number, etc.

9a. ORIGINATOR'S REPORT NUMBER(S): Enter the official report number by which the document will be identified and controlled by the originating activity. This number must be unique to this report.

9b. OTHER REPORT NUMBER(S): If the report has been assigned any other report numbers *(either by the originator or by the sponsor)*, also enter this number(s).

10. AVAILABILITY/LIMITATION NOTICES: Enter any limitations on further dissemination of the report, other than those imposed by security classification, using standard statements such as:

(1) "Qualified requesters may obtain copies of this report from DDC."

(2) "Foreign announcement and dissemination of this report by DDC is not authorized."

(3) "U. S. Government agencies may obtain copies of this report directly from DDC. Other qualified DDC users shall request through _____."

(4) "U. S. military agencies may obtain copies of this report directly from DDC. Other qualified users shall request through _____."

(5) "All distribution of this report is controlled. Qualified DDC users shall request through _____."

If the report has been furnished to the Office of Technical Services, Department of Commerce, for sale to the public, indicate this fact and enter the price, if known.

11. SUPPLEMENTARY NOTES: Use for additional explanatory notes.

12. SPONSORING MILITARY ACTIVITY: Enter the name of the departmental project office or laboratory sponsoring *(paying for)* the research and development. Include address.

13. ABSTRACT: Enter an abstract giving a brief and factual summary of the document indicative of the report, even though it may also appear elsewhere in the body of the technical report. If additional space is required, a continuation sheet shall be attached.

It is highly desirable that the abstract of classified reports be unclassified. Each paragraph of the abstract shall end with an indication of the military security classification of the information in the paragraph, represented as *(TS), (S), (C), or (U)*

There is no limitation on the length of the abstract. However, the suggested length is from 150 to 225 words.

14. KEY WORDS: Key words are technically meaningful terms or short phrases that characterize a report and may be used as index entries for cataloging the report. Key words must be selected so that no security classification is required. Identifiers, such as equipment model designation, trade name, military project code name, geographic location, may be used as key words but will be followed by an indication of technical context. The assignment of links, rules, and weights is optional

Unclassified
Security Classification